11-2-2016 12:00 AM

Multi-Nuclear Magnetic Resonance Imaging of Obstructive Lung Disease

Khadija Sheikh
The University of Western Ontario

Supervisor
Dr. Grace Parraga
The University of Western Ontario

Graduate Program in Medical Biophysics
A thesis submitted in partial fulfillment of the requirements for the degree in Doctor of Philosophy

Abstract

Obstructive lung diseases such as chronic-obstructive-lung-disease (COPD), bronchiectasis, and asthma are characterized by airflow obstruction. They affect over six million Canadians costing the economy $12 billion/year. Despite decades of research, therapies that modify obstructive-lung-disease progression and control are lacking because patient diagnosis, monitoring, and response to therapy are currently made using airflow measurements that may conceal the independent contributions of underlying pathologies. One goal of obstructive-lung-disease research is to develop ways to identify patients with specific underlying pathological phenotypes to improve patient care and outcomes. Thoracic computed-tomography (CT) and magnetic-resonance-imaging (MRI) provide ways to regionally identify the underlying pathologies associated with obstructive-lung-disease, and offer quantitative biomarkers of obstructive-lung-disease (e.g. lung-density, airway dimensions, ventilation abnormalities, and lung microstructure). As the first step to identify patients with specific underlying pathological phenotypes, it is important to understand the physiological and clinical consequences of these imaging derived measurements. Accordingly, our objective was to evaluate lung structure and function using multi-nuclear pulmonary MRI in aging and obstructive-lung-disease to provide a better understanding of MR-derived biomarkers. In older never-smokers, the majority of subjects had ^{3}He MR ventilation abnormalities that were not responsive to bronchodilation. ^{3}He ventilation abnormalities were related to airflow obstruction and airways resistance, but not occupational exposure or exercise limitation. We then developed and evaluated ultra-short-echo-time MRI in COPD subjects with and without bronchiectasis. This work demonstrated that ultra-short-echo-time MR-derived measurements were reproducible and significantly related to CT tissue-density measurements. In the COPD subjects with bronchiectasis, ultra-short-echo-time signal-intensity was related to airway measurements. In COPD subjects without bronchiectasis, ultra-short-echo-time signal-intensity was related to the severity of emphysema. Finally, based on the ultra-short-echo-time MR biomarkers developed in patients with COPD and bronchiectasis, patients that share some of the airway and inflammatory features common in asthmatics, we produced ultra-short-echo-time MR measurements in asthma. These measurements not only provided similar information as CT, but also information about regional ventilation deficits. These results demonstrated that

ultra-short-echo-time MR biomarkers may reflect ventilation heterogeneity and/or gas-trapping in asthma. These important findings indicate that multi-nuclear pulmonary MRI has the potential to quantitatively evaluate the different pathologies of obstructive-lung-disease.

Keywords

Aging, Obstructive Lung Disease, Chronic Obstructive Pulmonary Disease, Asthma, Bronchiectasis, X-ray Computed Tomography, Magnetic Resonance Imaging, Hyperpolarized ^{3}He, Hyperpolarized ^{129}Xe, Ultra-short echo time, Pulmonary Imaging, Imaging Biomarkers

Co-Authorship Statement

The following thesis contains three manuscripts. Two manuscripts have been published in scientific journals and one manuscript has been submitted for publication. As the first author of these peer-reviewed manuscripts, I was a significant contributor to all aspects of the studies as well as the manuscript preparation and submission. Specific tasks included: contributing to the study design and subject recruitment, organization and management of study visits, the development of the proton MRI acquisition and reconstruction protocols, acquisition of pulmonary function and noble gas MRI data. Following data acquisition, tasks included: database organization, statistical analysis and interpretation, image analysis, clinical/physiological interpretation of the data, drafting and final approval of the manuscripts. Dr. Grace Parraga, as the principal investigator and supervisor, provided ongoing guidance and was responsible for study conception and experimental design, data analysis and interpretation, drafting and final revisions and approval of the manuscripts. She was also the guarantor of integrity of the data as well as responsible for Good Clinical Practice. The management of study visits and acquisition of pulmonary function data was performed under the supervision of Sandra Blamires. Polarization of the ^{3}He and ^{129}Xe gases was performed by Andrew Wheatley, David Tessier, and Dante PI Capaldi. MRI acquisition was performed by Trevor Szekeres, Heather Biernaski, and David Reese. Listed below are the specific contributions for all other co-authors for each manuscript contained in this thesis.

Chapter 2 is an original research article entitled "Pulmonary Ventilation Defects in Older Never-Smokers" and was published in the *Journal of Applied Physiology* in 2014. This manuscript was co-authored by Khadija Sheikh, Gregory A Paulin, Sarah Svenningsen, Miranda Kirby, Nigel AM Paterson, David G McCormack, and Grace Parraga. As the first author of this work, I was a significant contributor to all aspects of the studies as well as the manuscript preparation and submission. Specific tasks included: experimental design, recruitment of all subjects, organization and management of study visits, acquisition of pulmonary function and noble gas MRI data, database organization, statistical analysis and interpretation, image analysis, clinical/physiological interpretation of the data, and drafting and final approval of the manuscript. Gregory Paulin and Sarah Svenningsen assisted with the recruitment of study participants, acquisition of data, statistical analysis, and interpretation.

Miranda Kirby assisted with the statistical analysis and data interpretation. Nigel AM Paterson and David G McCormack were responsible for clinical/physiological interpretation of the data.

Chapter 3 is an original research article entitled "Ultra-Short Echo Time Pulmonary Magnetic Resonance Imaging: Evaluation and Reproducibility in COPD Subjects with and without Bronchiectasis" and was published in the *Journal of Magnetic Resonance Imaging* in 2014. This manuscript was co-authored by Weijing Ma, Khadija Sheikh, Sarah Svenningsen, Damien Pike, Fumin Guo, Roya Etemad-Rezai, Jonathon A Leipsic, Harvey O Coxson, David G McCormack, and Grace Parraga. As the second author of this work, I was a significant contributor to all aspects of the studies as well as the manuscript preparation and submission. Specific tasks included: developing the ultra-short echo time MR acquisition protocol, experimental design of the reproducibility study, assistance with all study visits, acquisition of MRI data, database organization, statistical analysis and interpretation, image analysis, clinical/physiological interpretation of the data, and drafting and final approval of the manuscript. Weijing Ma assisted with the acquisition of data, MR image analysis, and drafting the manuscript. Sarah Svenningsen and Damien Pike assisted with the acquisition of data and CT analysis. Fumin Guo assisted with the MR image analysis. Roya Etemad-Rezai provided clinical expertise and aided in interpretation of the CT images. Jonathon A Leipsic assisted with the interpretation of the CT data. Harvey O Coxson assisted with the interpretation of MRI and CT data. David G McCormack was responsible for clinical/physiological interpretation of the data

Chapter 4 is an original research article entitled "Ultra-short Echo Time Magnetic Resonance Imaging Biomarkers of Asthma" and has been accepted to the journal the *Journal of Magnetic Resonance Imaging* (JMRI-16-0866R1) and is currently *e-pub ahead of print*. This manuscript was co-authored by Khadija Sheikh, Fumin Guo, Dante PI Capaldi, Alexei Ouriadov, Rachel L Eddy, Sarah Svenningsen, and Grace Parraga. As the first author of this work, I was a significant contributor to all aspects of the studies as well as the manuscript preparation and submission. Specific tasks included: developing the whole lung ultra-short echo time MR acquisition protocol, experimental design, assistance with all study visits, acquisition of MRI data, database organization, statistical analysis and interpretation, image analysis, clinical/physiological interpretation of the data, drafting and approving the final version of the manuscript. Fumin Guo contributed to the development of the image analysis tools and

assisted with data analysis. Alexei Ouriadov and Dante PI Capaldi assisted with the development of the image acquisition methods and the interpretation of the data. Rachel L Eddy and Sarah Svenningsen assisted with the data acquisition and interpretation of the data.

To the study participants:
For showing me perseverance.

Acknowledgments

First and foremost, I would like to thank my supervisor Dr. Grace Parraga. I am appreciative for all of the opportunities you have given me to work with the clinical staff, perform study visits, and encouraging me to pursue local and global collaborations. Thank-you for challenging me and pushing me much further than I thought possible. Your belief in my abilities and emphasis on teamwork and productivity has pushed me to excel and for this I am very grateful. The guidance, wisdom, and knowledge you have given me during my graduate career is invaluable and I intend to apply it all during my future endeavours. Thank-you for reminding me that graduate school is a marathon and not a sprint.

To the Department of Medical Biophysics: it takes a village to raise a graduate student. Thank-you for providing me with endless opportunities to grow both professionally and personally. To Dr. Dan Goldman: thank-you for your guidance during my first few years of graduate school. To Wendy Hough: thank-you for always being available to answer my questions regarding my study plan and scholarship applications. To Dr. Jerry Battista and Dr. Rob Stodilka: thank-you for providing me with CAMPEP guidance these past four years.

I would also like to thank my advisory committee: Dr. Aaron Fenster, Dr. Terence Peters, and Dr. Nigel Paterson. To Dr. Fenster, I am thankful for the professional mentorship, guidance and support that you have provided. To Dr. Peters, thank-you for being engaged in my research, your guidance and criticisms have been imperative to my development as a researcher and communicator. To Dr. Paterson, thank-you for providing invaluable clinical and physiological insight into our research.

To the Parraga lab staff: Trevor, Dave, Sandra, Lyndsey, Andrew, and Alexei. To Trevor and Dave, your enthusiasm during the UTE MRI project was unbelievable and very motivating. I cannot thank-you enough for all you have taught me and your positive responses to our lengthy scans. To Sandra, thank-you for your guidance during patient visits. To Andrew, thank-you for always achieving superb polarization, and for training me to excel in high stress situations. To Alexei, I would like to thank-you for your guidance and willingness to help me with the UTE MRI project. To Lyndsey, thank-you for teaching me about patient care, sharing your clinical expertise, and being a great listener and friend. I will miss our lunch chats.

To my lab mates and friends; you have made the past four years very memorable. To Sarah: I could not have asked for a better role model or friend. Thank-you for inspiring me to be assertive, ambitious, and most importantly compassionate to our study participants. To Dante: you were always there pushing me through the challenges of graduate school and laughing with me during the memorable moments. Thank-you for believing in me. I look forward to watching you excel in all your future endeavors. To Miranda: thank-you for being a great role model and for all you have taught me. To Tamas: I am grateful to our friendship and your meticulous eye while reviewing papers and talks. To Greg: thank-you for encouraging me to become a better communicator and enduring our first manuscript submission together. To Damien: thank-you for your positive outlook on the challenges we faced in the past four years. To Fumin: thank-you for our evening chats on lung physiology and imaging physics. To Eric and Rachel: you made my last year of grad school a memorable one, especially with our weekly Thursday night adventures. I wish you both the best in your future aspirations. To Heather: thank-you for the coffee and tea breaks. To Anurag: thanks for letting me pick your brain about medicine and respirology related things. Thank-you to my other fellow lab mates past and present: Nikhil, thank-you for the chats in the dark room through those long days of segmentation; Amir, thank-you for your ongoing career mentorship and guidance; Megan, thank-you for the fun coffee breaks and laughs; Nanxi, it was a pleasure working alongside you; and Emma, thank-you for always offering a positive outlook on life.

Most importantly, I would like to thank my family, Mark, and my friends. I am indebted to you for your support, patience, and love. To my parents: thank-you for teaching me to persevere and giving me the chance to pursue my dreams. Mustafa, thank-you for encouraging me to learn MATLAB and always believing in me. Mark, thank-you for being by my side during this journey. I could not have succeeded without you.

Finally, I would like to express my gratitude to the various sources of funding that I have received over the past four years. I acknowledge funding support from the Natural Sciences and Engineering Research Council of Canada, the Canadian Institutes of Health Research Strategic Training Program in Vascular Research, the Ontario Graduate Scholarship, and the Schulich School of Medicine and Dentistry.

Table of Contents

List of Tables

List of Figures

List of Appendices

List of Abbreviations

AATD	Alpha-1 Antitrypsin Deficiency
ADC	Apparent Diffusion Coefficient
ANOVA	Analysis of Variance
ATS	American Thoracic Society
BMI	Body Mass Index
BOLD	Burden of Obstructive Lung Disease
BPD	Bronchopulmonary Dysplasia
BSA	Body Surface Area
BW	Bandwidth
CF	Cystic Fibrosis
CI	Confidence Interval
CO	Carbon Monoxide
COPD	Chronic Obstructive Pulmonary Disease
COV	Coefficient of Variation
CPET	Cardiopulmonary Exercise Testing
C_R	Normalized Contrast-to-Noise Ratio
CT	Computed Tomography
CTS	Canadian Thoracic Society
DI	Deep Inspiration
DL_{CO}	Diffusing Capacity of the Lung for Carbon Monoxide
DW	Diffusion Weighted
ERS	European Respiratory Society
ERV	Expiratory Reserve Volume
FD MRI	Fourier Decomposition Magnetic Resonance Imaging
FE	Full Expiration
FEV_1	Forced Expiratory Volume in 1 second
FGRE	Fast Gradient Recalled Echo
FI	Full Inspiration
FOV	Field of View
FRC	Functional Residual Capacity
FVC	Forced Vital Capacity
G	Gradient amplitude
GOLD	Global Initiative for Chronic Obstructive Lung Disease
GOLD-U	GOLD-Unclassified
^1H	Proton
^3He	Helium-3
HIPAA	Health Insurance Portability and Accountability Act
HU	Hounsfield Unit
HU_{15}	15th Percentile of the frequency distribution of Hounsfield Units
IC	Inspiratory Capacity
ICC	Interclass Correlation Coefficient
IRV	Inspiratory Reserve Volume
LA	Lumen Area
MIP	Maximum Inspiratory Pressure
MRI	Magnetic Resonance Imaging
mSv	Millisieverts

N_2	Nitrogen
NDW	Non-Diffusion Weighted
NEX	Number of Excitations
PA	Posterior-anterior
Pi10	Airway Wall Thickness at an Internal Perimeter of 10mm
PIPEDA	Personal Information Protection and Accountability Act
PVV	Percent Ventilated Volume
RA_{950}	Relative Area under -950 HU
Raw	Airways Resistance
RER	Respiratory Exchange Ratio
RF	Radiofrequency
ROI	Region of Interest
RV	Residual Volume
SaO_2	Arterial Oxygen Saturation
SD	Standard Deviation
SDD	Smallest Detectable Difference
SI	Signal Intensity
SI	Superior-Inferior
SI_{15}	15th Percentile of the frequency distribution of signal intensity
SNR	Signal-to-noise Ratio
SPECT	Single Positron Emission Computed Tomography
S_R	Apparent Signal-to-Noise Ratio
STPD	Standard Temperature Pressure and Dry
T_1	Spin-Lattice Relaxation Time (a.k.a. longitudinal relaxation time)
T_2	Spin-Spin Relaxation Time (a.k.a. transverse relaxation time)
TCV	Thoracic Cavity Volume
TLC	Total Lung Capacity
TE	Echo Time
TR	Repetition Time
UTE	Ultra-short Echo Time
VC	Vital Capacity
VDP	Ventilation Defect Percent
VDV	Ventilation Defect Volume
VDV_{Per}	Ventilation Defect Volume of Peripheral Lung
VDV_{WL}	Ventilation Defect Volume of Whole Lung
V_E	Minute Ventilation
VO_2	Oxygen Uptake
V_T	Tidal Volume
VV	Ventilation Volume
WA%	Wall Area Percent
^{129}Xe	Xenon-129

CHAPTER 1

1 INTRODUCTION

Obstructive Lung Diseases are chronic and heterogeneous diseases characterized by the obstruction of the airways resulting from inflammatory processes. Chronic obstructive pulmonary disease (COPD) and asthma are the most common obstructive lung diseases. COPD is characterized by persistent airflow limitation that is usually progressive and associated with an enhanced response of the lungs due to noxious particles or gases,[1] whereas asthma is a chronic inflammatory disorder characterized by airway hyper-responsiveness and inflammation.[2]

1.1 The Burden of Obstructive Lung Disease

According to the World Health Organization's estimates, 300 million people suffer from obstructive lung disease (i.e. chronic obstructive pulmonary disease [COPD]: n=64 million[3] and asthma: n=235 million[4]). All respiratory diseases including asthma and COPD accounted for the 4th leading cause of death worldwide (**Figure 1-1**).[5] However, looking at all diseases individually, COPD was the 3rd leading cause of death worldwide (n=3.1 million), behind ischaemic heart disease (n=7.4 million) and stroke (n=6.7 million), but just above lower respiratory infections (n=3.0 million). Unfortunately, asthma also accounted for 386,318 deaths.

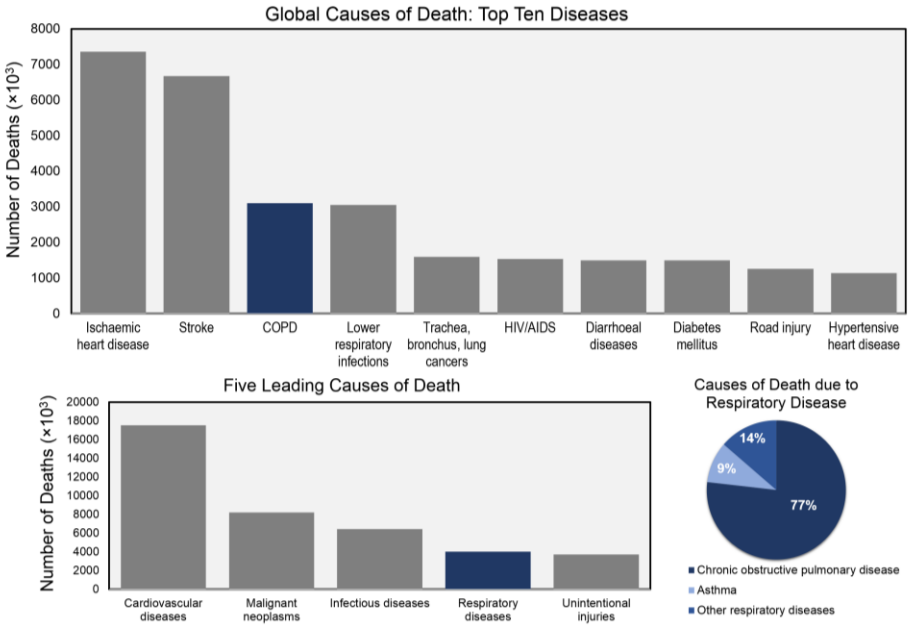

Figure 1-1 Proportion of deaths due to respiratory disease

Above: Number of disease specific deaths. Below: Left-Top five leading causes of death. Right-proportion of causes of death due to respiratory diseases: 1) COPD (n= 3,104,330), 2) Other respiratory diseases (n=551,425), and, 3) Asthma (n=386,318).

In 2014, Statistics Canada reported that over 3 million people were affected by COPD (n=804,043) and asthma (n=2,448,817).[6] Obstructive lung disease also accounted for the most number of hospitalizations, surpassing the number of hospitalizations due to angina, heart failure, and diabetes in 2007 (as shown in **Figure 1-2**). Although, COPD accounted for the number one reason for hospitalizations (and remained the leading cause of emergency department visits in 2014), asthma was the most common cause of hospitalizations among children.[7-9]

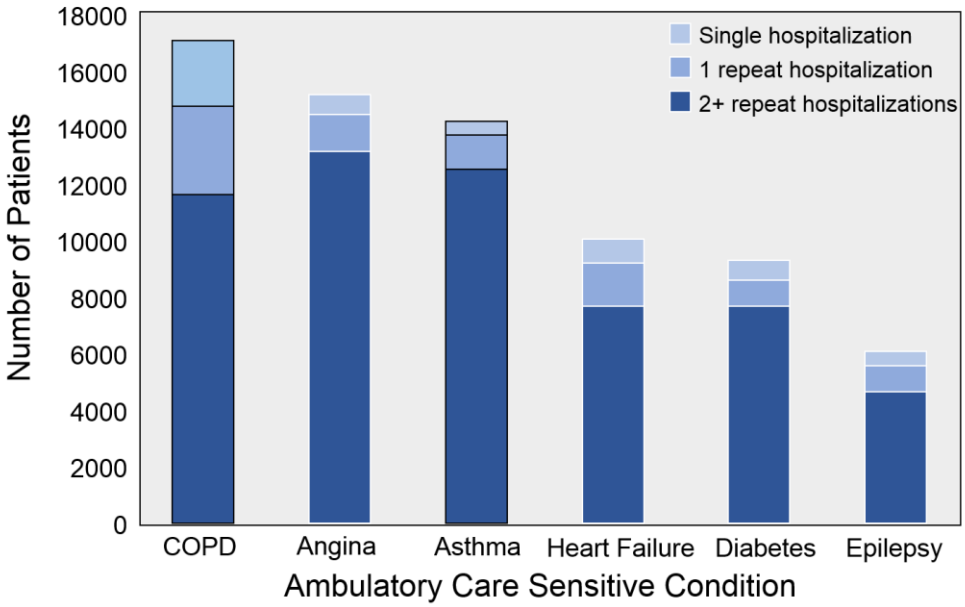

Figure 1-2 Repeat Hospitalizations by Condition at First Admission
This graph shows the number of patients (outside Quebec) with a single hospitalization, one repeat hospitalization, and two or more repeat hospitalizations by Ambulatory Care Sensitive Condition at first admission. Adapted from the Canadian Institute for Health Information's (CIHI) publication.[10]

In Ontario, from the years 2002 to 2011, 722,494 individuals were identified as having COPD. The prevalence rate for COPD in Southwestern Ontario was significantly higher than the provincial average of 103 per 1000 population aged 35 years and older.[11] In 2015, asthma statistics reported by the Ontario Asthma Surveillance Information System, and data provided by the Institute for Clinical Evaluative Sciences demonstrated that there were about 2 million individuals living with asthma in Ontario.[12,13] In terms of healthcare

service use, in Southwestern Ontario, from 2003-2013 the average emergency department visit rate was greater than 2.4 per 1000 asthma prevalence.[14] Evidently, obstructive lung disease is a health and economic challenge in Ontario. To give some perspective, in 2011 the total projected expenses for the Government of Ontario was $124 billion and the direct and indirect costs for COPD and asthma were over $5 billion.[15]

Despite these alarming statistics, therapies that modify obstructive lung disease outcomes are still lacking and perhaps it is because of our reliance on pulmonary function test measurements.[1] While these measurements provide a reproducible and easy method to evaluate lung function, they can hide the different underlying components of obstructive lung disease and do not provide any regional information. Accordingly, one goal of obstructive lung disease research is to develop methods to identify obstructive lung disease patients with specific underlying pathological phenotypes with the hope that this will improve patient care and outcomes.

Pulmonary magnetic resonance imaging (MRI), with and without the use of inhaled contrast agents, is an emerging technique that not only provides a way to quantify lung structure and function *in-vivo*, but also provides spatial information. However, before these methods can be translated to clinic, a strong understanding of the different MR imaging biomarkers is needed, more specifically, their clinical consequences and structural determinants. Equipped with such knowledge, there is potential to use these measurements to phenotype patients with obstructive lung disease to better guide and individualize therapies. This thesis focuses on the development and application of novel quantitative measurements of lung structure and function derived from hyperpolarized noble gas MRI and non-contrast enhanced ultra-short echo time (UTE) MRI. These measurements were evaluated in older never-smokers and subjects with obstructive lung disease (COPD and asthma). In order to validate and understand imaging biomarkers aimed at quantifying lung function in obstructive lung disease, imaging measurements must first be understood in healthy lung aging. These measurements can then be extended to evaluate lung function in the context of obstructive lung disease, and more specifically, COPD and asthma.

In this Chapter, the relevant background knowledge necessary to understand and motivate the original research presented in Chapters 2 to 4 will be summarized. It will begin with a general overview of the respiratory system's structural and functional responsibilities while addressing the current understanding of normal lung aging **(1.2)**. The pathophysiology and underlying disease mechanisms of obstructive lung disease (i.e. COPD and asthma) will be addressed next **(1.3)** and followed by the standard clinical measurements of obstructive lung disease **(1.4)**. The benefits and limitations of currently available imaging methods will then be discussed with respect to imaging biomarkers and the different pathophysiology they probe **(1.5)**. Novel multi-nuclear MRI methods for pulmonary imaging will then be discussed **(1.6)**. Finally, the specific hypotheses and objectives of this thesis will be introduced **(1.7)**.

1.2 Lung Structure and Function

The respiratory system is responsible for the exchange of oxygen and carbon dioxide between the cells of the body and the external environment. In humans, the respiratory system includes the oral and nasal cavities, two lungs, the conducting airways, the chest wall structures, diaphragm, and the central nervous system responsible for controlling the muscles of respiration.[16] The primary function of this system is to move oxygen from the environment into the blood and to move carbon dioxide out of the blood and back into the environment. The oxygen is used for cellular metabolism and the carbon dioxide waste that is produced by cellular metabolism is eliminated. This process is called "gas exchange".[16] This section will begin with a discussion on the process by which air moves from the environment into our body through the conducting and respiratory zones.

1.2.1 The Airways: Conducting and Respiratory Zones

The conducting zone is responsible for leading air from the external environment to the exchange surface of the lung. During inspiration, air enters the upper respiratory tract through the oral or nasal cavities and passes through the pharynx, larynx, and then into the trachea. The trachea is a hollow tube held open by cartilage rings and extends down into the thorax where it branches into the primary bronchi.[17] Each bronchus feeds into the left and right lung. Within the lung, the bronchi continue to divide while progressively

decreasing in diameter (**Figure 1-3**). Similar to the trachea, the bronchi are supported by cartilage. The smallest bronchi branch to become bronchioles, which are small collapsible airways with smooth muscle walls. The bronchioles are histologically different from the bronchi because they are not supported by cartilage.

As shown in **Figure 1-3**, the last seven generations of the airway tree make up the respiratory zone.[16] The respiratory zone contains air passages with alveoli which facilitate gas exchange. The bronchioles continue to branch until the respiratory bronchioles form a transition between the airways and the exchange epithelium of the lung. The diameter of the bronchioles decreases progressively the further they are from the trachea and consequently their number and the total cross section increases.[16,17] The respiratory zone makes up most of the volume in the lung, accounting for 2.5 to 3 liters at rest.

The upper airways and bronchi are involved in conditioning the air before it reaches the alveoli. There are three main components to air conditioning: the air is heated to body temperature, water vapour is added to ensure the air reaches 100% humidity, and foreign material is filtered out.[17] The air entering the human body needs to be heated to body temperature (37°C) and moistened to ensure that the core body temperature does not change and the cold air does not damage or dry out the alveoli. The air is heated and moistened by the water evaporating from the mucosal lining of the airways. The trachea and bronchi are lined with ciliated epithelium. A sticky layer of mucus floats over cilia to trap particles larger than 2μm. The cilia beat upward to move mucus toward the pharynx and once the mucus reaches the pharynx, it can be expectorated or swallowed.[17]

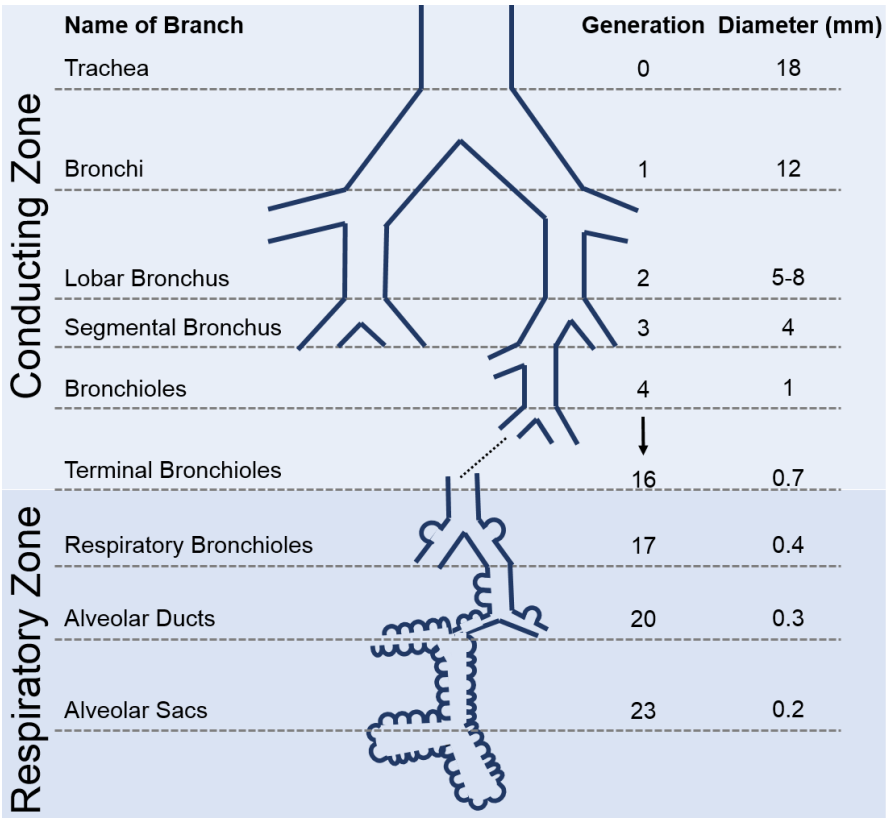

Figure 1-3 Schematic of the human airways
Generations 0 to 16 make up the conducting zone and the last 7 make up the respiratory zone. The conducting zone is responsible for guiding air into the gas exchanging regions of the lung. The respiratory zone is where gas exchange occurs. Adapted from West, JB, Respiratory Physiology: The Essentials, Ninth Edition.[16]

1.2.2 The Alveoli: Site of Gas Exchange

The alveoli line the respiratory bronchioles, alveolar ducts, and alveolar sacs, thus making up the majority of lung tissue. The average adult lung has 480 million alveoli[18] with each alveolus being about 1/3mm in diameter.[16] Their main function is to exchange gas between themselves and the blood via simple diffusion (i.e. from high partial pressure to low partial pressure). Two cells make up the epithelium of the alveoli (Type I: thin alveolar cells to allow for gas diffusion, and, Type II: thicker alveolar cells that produce surfactant to aid the lungs in expanding). The walls of the alveoli are thin (approximately 0.2μm)[19] without any muscle and surrounded by capillaries to ensure rapid gas exchange. The surface area of the alveoli in contact with capillaries is approximately $70m^2$.[20]

1.2.3 Ventilation and Diffusion

Ventilation is the bulk flow exchange of air between the environment and the alveoli.[17] During a normal breath, about 500mL of air is inspired (at a rate of 1L/s) and the volume of the thoracic cavity increases while the pressure decreases, thus drawing air in. The mechanism for this is partly due to the diaphragm contracting and descending and the intercostal muscles raising the ribs and increasing the cross-sectional area of the thorax.[17] The rate and force of inspiration and expiration depends on the respiratory system compliance. Compliance is the change in volume relative to the change in pressure. Once air reaches the terminal bronchioles, the air is drawn in by bulk flow (i.e. due to a pressure gradient). Finally, when air is in the respiratory bronchioles, the forward velocity of the air decreases and the mechanism of ventilation becomes diffusion.

Expiration is a passive process during quiet breathing. The average healthy adult exhales 500mL of air at 15 breaths/min—meaning that each minute 7500mL of air has been exhaled. This is known as *total ventilation*.[16] The amount of air that is inhaled is slightly more than what is exhaled because more oxygen is taken in than carbon dioxide is given out. It should also be noted that not all of the 500mL of gas that is inhaled reaches the alveoli. About 150mL of the 500mL of gas that is inhaled comprises "dead space" and is the same volume as that of the conducting airways. The volume of new gas that enters the respiratory zone each minute is thus 5250mL and this is called *alveolar ventilation*.[16]

Once air has entered the alveoli from the atmosphere, the gas is transferred across the blood-gas barrier by a process called *diffusion*. The process of diffusion through tissues can be described by Fick's law: *the rate of transfer of gas through a sheet of tissue is proportional to the tissue area and the difference in gas partial pressure between the two sides, and inversely proportional to the tissue thickness*.[21]

The pulmonary arteries follow the airways as far as the terminal bronchioles and then supply the capillary bed in the walls of the alveoli. The partial pressure of oxygen (P_{O2}) in a red blood cell entering a capillary is normally 40 mmHg and across the blood-gas barrier the pressure increases to 100 mmHg.[16] Blood takes in oxygen from the alveolar air space

provided that the oxygen there is greater than in the blood. Oxygen then diffuses across the alveolar walls into the blood down the concentration gradient.

1.3 Pathophysiology of Obstructive Lung Disease

Obstructive lung disease is characterized by persistent airflow limitation. Increased resistance to airflow can be caused by conditions inside the lumen, the airway wall, or the peribronchial region (i.e. the region outside the airway). The airway lumen may be partially occluded by excessive secretions (as in chronic bronchitis), acutely due to pulmonary edema, or localized due to the inhalation of foreign particles. The airway wall may be contracted due to the airway smooth muscle (as in asthma), or inflamed (as in bronchitis and asthma). There may be hyperinflation due to gas-trapping (i.e. abnormal retention of air) caused by mucus plugging of the segmental, subsegmental, and smaller conducting airways. In the peribronchial region, the lung parenchyma may become destroyed (i.e. emphysema), the bronchus may become compressed locally by an enlarged lymph node, and peribronchial edema could case narrowing. Before addressing the pathophysiology of obstructive lung disease, the physiology of aging will be briefly discussed.

1.3.1 The Aging Lung

Aging is a progressive phenomenon that occurs in each and every individual. In order to appreciate and recognize obstructive lung disease, it is essential to understand the age-related changes involving the lung in the absence of disease. Physiological and immunological changes with aging influence the presentation of disease, responses to treatment, and possible complications.

Aging of the lung can be classified into a growth phase, maturation phase, a plateau phase, and a decline phase. The major physiological changes of the aging lung during the decline phase are: 1) loss of elastic recoil, 2) decrease of chest wall compliance, 3) change in the shape and structure of the lung, and, 4) decrease in respiratory muscle strength.[22]

Similar to an elastic band, the lungs experience elastic recoil during inspiration and expiration. Elastic recoil is the rebound of the lungs after being stretched during

inspiration. The lungs have elastic fibers (elastin), collagen, smooth muscle, pulmonary blood, and bronchial mucus which all have elastic properties and contribute to elastic recoil. As the lung increases in volume, the elastic recoil also increases. Although the decrease in elastic recoil in the lung is not completely understood, some studies have demonstrated that reduced elastic recoil and diffusing capacity of the lung (a measure of the transfer of gas from the lungs to the surrounding blood vessels) is a result of stress relaxation of elastin-fibers as evidenced by an apparent increase in thickness along with the appearance of more loosely associated fibers.[23] A disruption in collagen fibers leading to an increase in intermolecular crosslinks has also been hypothesized to explain diminished elastic recoil with age.[24] Currently, there is limited and conflicting evidence to support this theory.

The chest wall also stiffens with age leading to a decrease in chest wall compliance. This is due to structural changes of the lung such as the decalcification of the ribs, calcification of the costal cartilage, changes in rib-vertebral articulations, changes in the shape of the chest, and narrowing of the intervertebral disk space.[25] Other structural changes that contribute to decreased chest wall compliance are kyphotic curvature of the spine and deformation of the diaphragm leading to a reduction in its force generating capabilities.[26] Taken together, all these structural changes lead to the decreased respiratory system compliance which ultimately increase the work of breathing.

The fine structures of the lung also undergo changes with age. The degeneration of the elastic fibers around the alveolar duct results in airspace enlargement which leads to a reduction of airspace wall surface per unit volume of lung tissue.[22,27] Reduction in supporting tissue results in premature closure of small airways during normal breathing. There is also calcification of bronchial cartilage. These changes result in an increase in anatomic dead space, gas-trapping, and hyperinflation.[28]

Lastly, muscle strength and endurance decrease with age. The thoracic diaphragm, a sheet of internal skeletal muscle extending across the bottom of the thoracic cavity, is the most important respiratory muscle and plays a vital role in inspiration. Maximum inspiratory pressure is an index of diaphragm muscle strength and is measured using a mechanical

pressure gauge with a closed valve at the mouth during an inspiration. A decline in this measurement is indicative of impaired ventilation and impaired clearance of airway secretions. Studies have demonstrated that maximum inspiratory pressure is higher in men than in women and decreases with age.[29,30] Reduced maximum inspiratory pressure and decreased diaphragm muscle strength may be due to age-related muscle atrophy and decrease in fast twitch muscle fibers that are responsible for generating higher peak tensions. The age related changes to the lungs are reflected in clinical measurements of lung function which will be discussed in **Chapter 1.4**.

1.3.2 Obstructive Lung Disease: Airways Disease in Asthma and COPD

Airway disease in obstructive lung disease (i.e. asthma and COPD) is characterized by an inflammatory process of the airways that can lead to airflow limitation. Airflow limitation is mostly reversible in asthma and is mostly irreversible in COPD. The natural progression of asthma and COPD are different. Asthma begins in childhood[31,32] and has been associated with allergic diathesis and environmental factors in modern affluent countries.[33,34] The onset of COPD is attributed to the total burden of toxic gases and particles that a person inhales during his or her lifetime.[35,36] The smoking of tobacco products is the major risk factor for the development of COPD.[37,38]

Asthma

Asthma is a chronic disease confined to the airways characterized by airway hyper-responsiveness (i.e. increased responsiveness of the airways to stimuli), airway inflammation and narrowing. Histopathological studies have demonstrated that asthma affects the central and peripheral airways.[39] This process involves cellular changes (infiltration of inflammatory cells such as eosinophils and lymphocytes) and structural changes (such as thickened airway walls). **Figure 1-4** shows a bronchiole of a subject who died during an asthma attack. There is a luminal occlusion caused by muscle constriction, airway wall thickening, increased smooth muscle mass, and a marked inflammatory response in the airway wall which is characterized by eosinophils.[40]

Airway inflammation is a multi-cellular process which involves eosinophils, CD4 T-lymphocytes, and mast cells. Eosinophils are the most striking cellular feature of asthma.

Distribution of eosinophils varies between the small and large airways. In the small airways, most eosinophils are in the outer section of the airway wall (between the smooth muscle and the alveolar attachments). The increased density of eosinophils in the outer airway promotes airway constriction by decreasing the tethering forces of the parenchyma in the airway wall. In the larger airways, eosinophils are mostly located in the inner section of the airway wall (between the smooth muscle and the basement membrane).[41] The increased density of eosinophils in the inner airway wall promotes constriction by increasing the effect of bronchial smooth muscle shortening.

The structural changes that accompany asthmatic airways are increased smooth muscle mass, mucous gland hypertrophy, and bronchial wall edema. These all lead to a thickened airway wall which contribute to airflow limitation resulting from the increased airways resistance. The increase in smooth muscle mass is induced by inflammatory mediators, cytokines, and growth factors. Further enhancing this flow limitation is the increased amount of mucous and inflammatory exudate. They not only block airways, but can increase surface tension which can lead to airway closure. The excess production of mucous is not only due to the hypertrophy of mucous glands, but also resultant of hyperplasia of goblet cells.

Taken together, these cellular and structural changes of the airways can obstruct airflow in the large and small airways, thus affecting ventilation or leading to an abnormal retention of air at expiration (i.e. gas-trapping).

Chronic Obstructive Pulmonary Disease

In COPD, airways disease can present itself as chronic bronchitis. This is characterized by airway inflammation and excessive mucous production. The inflammation associated with chronic bronchitis is located in the epithelium of the central airways (airways with a diameter larger than 4mm) and extends along the gland ducts into the mucous-producing glands.[42-44] There is hypertrophy of the mucous glands in the large bronchi and chronic inflammation in the small airways. Excessive mucous is found in the airways and can obstruct them.

The major site of obstruction in COPD is found in the smaller conducting airways (less than 2mm in diameter). The small airways are spread out between the fourth and 14th generation of airway branching. The increase in the number of airways with respect to the branching increases their total cross sectional area and decreases their resistance. In the healthy lung, about three quarters of the total airway resistance is from the large airways (i.e. diameter greater than 2mm) and the rest is from the small airways. The airways below the larynx account for half of the total resistance measured at the mouth, and the smaller conducting airways only account for 10–15% of total airway resistance. For this reason, the smaller conducting airways are the lungs' silent zone.[45] This means that the disease may accumulate for many years without being detected.

The structural and physiological components responsible for the increase in peripheral airway (small conducting airway) resistance include: the destruction of alveolar support of the peripheral airways,[46] loss of elastic recoil in the parenchyma that support the airways,[47] a decrease in the elastic force available to drive flow out of the lung,[48] and structural narrowing of the airway lumen because of inflammatory processes.[49] **Figure 1-4** shows a representative small airway of a subject with COPD. The airway is inflamed with a thickened wall in which the lumen is partly filled with an inflammatory exudate of mucous and cells. Similar to asthma, these changes can lead to ventilation abnormalities and the retention of air, i.e. gas-trapping.

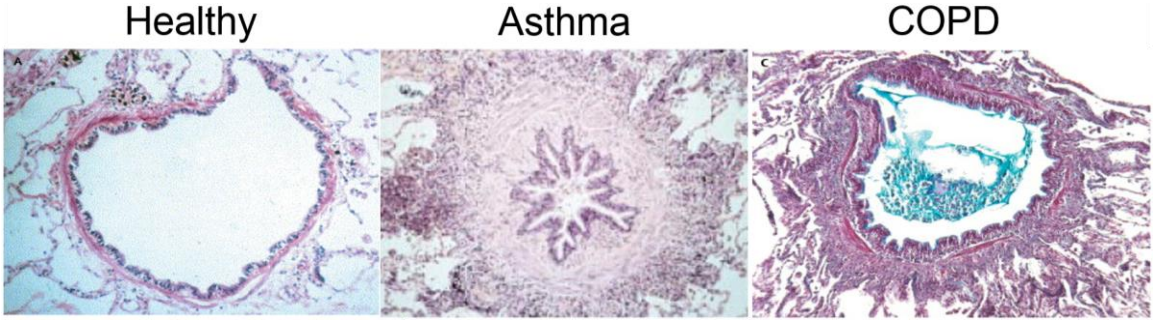

Figure 1-4 Small airway pathology in health, asthma, and COPD
From left to right: *Healthy*: normal small airway, *Asthma*: luminal occlusion resulting from muscle constriction, thickening of the airway wall, increased smooth muscle mass, and an increased inflammatory process in the airway wall (mainly characterized by eosinophils), *COPD*: inflamed airway with thickened wall in which lumen is partly filled with an inflammatory exudate.
Adapted from Hogg JC, Lancet (2004)[43] and Saetta M et al. Eur Respir J (2001).[40]

1.3.3 Obstructive Lung Disease: Emphysema

Emphysema is defined as "the enlargement of air spaces distal to the terminal bronchiole, accompanied by the destruction of their walls and without obvious fibrosis."[50,51] This destruction reduces the expiratory flow because of the reduced elastic recoil force available to expire the air out of the lung. **Figure 1-5** shows a typical appearance of histology of a healthy subject and a subject with emphysema. The emphysematous lung has loss of alveolar walls and the small airways are reduced in number in comparison to the healthy subject.

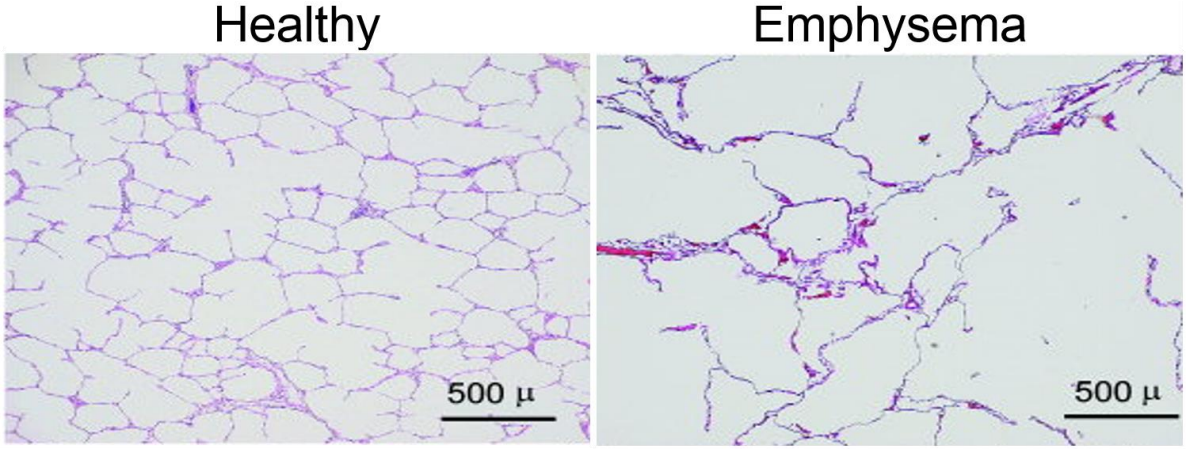

Figure 1-5 Parenchymal pathology in healthy and COPD subject.
Adapted from Wood et al.

There are two major types of emphysema: centriacinar and panacinar. These classifications are based on where the destruction occurs in the acinus. Centriacinar emphysema is more prominent in smokers and is confined to the destruction of the central part of the lobule and does not affect the peripheral alveolar ducts or alveoli. It initially affects the upper lobes and spreads down the lung as the disease progresses. Panacinar emphysema affects the entire lobule and is more common in the lower lobes.[52]

It is interesting to note that only 40% of smokers develop emphysema and only 15% develop airflow limitation.[43] Smokers who develop emphysema have an increased number of macrophages, neutrophils, T-lymphocytes, and eosinophils in their lungs compared to those smokers who do not develop emphysema.[44,53-55]

1.4 Clinical Measurements of Lung Function

There are several methods that can be used to evaluate lung function in patients with obstructive lung disease. Here, two clinically available methods for testing lung function are discussed: pulmonary function testing and cardiopulmonary exercise testing (CPET). Pulmonary function testing is the first method of choice to evaluate lung function at a physician's clinic. These measurements are made at the mouth that provide global lung function and lung volume measurements. These tests can be used to evaluate forced expiration, lung volumes, diffusion, and airways resistance. CPET is another method that can be used to test exercise responses that involve the respiratory, cardiovascular, skeletal muscle, and neuropsychological systems that cannot be adequately reflected by evaluating one organ system. The use of CPET stems from the fact that resting pulmonary and cardiac testing cannot reliably predict exercise performance and functional capacity. Although pulmonary function testing is more commonly used clinically, CPET should be considered when specific questions remain unanswered.

1.4.1 Pulmonary Function Testing

Pulmonary function testing can be divided into spirometry, plethysmography, and single breath carbon monoxide diffusing capacity. Spirometry measures the volume of air that is inhaled or exhaled as a function of time. The primary signal measured using spirometry is volume or flow. Plethysmography allows for the measurement of lung volumes (i.e. the volume of air in the lungs).

Figure 1-6 shows a spirometer which is a mouthpiece attached to a small machine that allows for the measurement of volume inhaled or exhaled. The plot beside the spirometer is the volume of air inspired as a function of time. The two most important measurements obtained from spirometry are the forced expiratory volume (FEV) and the forced vital capacity (FVC). FEV_1 is maximum volume of air expired in one second after a full inspiration. FVC is the maximum volume of air that can be expired when the patient exhales as forcefully and quickly as possible after a maximum inspiration.[56]

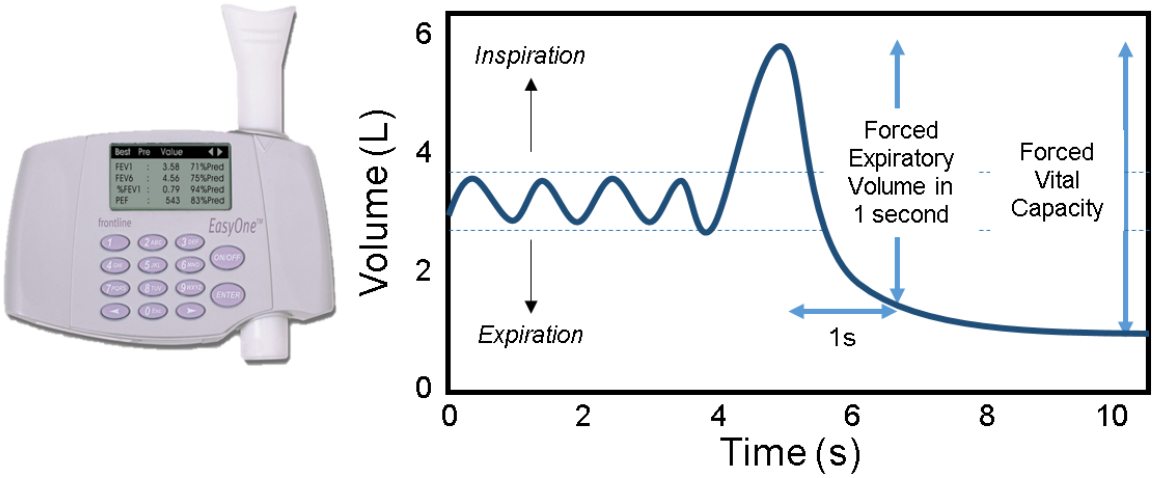

Figure 1-6 Pulmonary Function Testing: Spirometry
Shown above is a hand held spirometer and a sample airflow curve measured by the spirometer.

Figure 1-7 shows a plethysmograph which is an air-tight box that patients sit in to perform lung function tests. The plot shown on the right is an example airflow curve of volume inspired as a function of time. The main measurements obtained using plethysmography are: functional residual capacity (FRC), residual volume (RV), tidal volume (V_T), inspiratory capacity (IC), vital capacity (VC), and total lung capacity (TLC).[57] The FRC is the volume of air present in the lung at the end of a passive expiration. The maximum volume of gas that can be inspired from FRC is the IC. RV is the volume of air remaining in the lung after a maximum expiration. The volume of gas displaced between passive and inhalation and expiration during the respiratory cycle is the V_T. The VC is the volume change at the mouth between the positions of full inspiration and complete expiration. Finally, TLC is the volume of gas in the lungs after a maximum inspiration.[57]

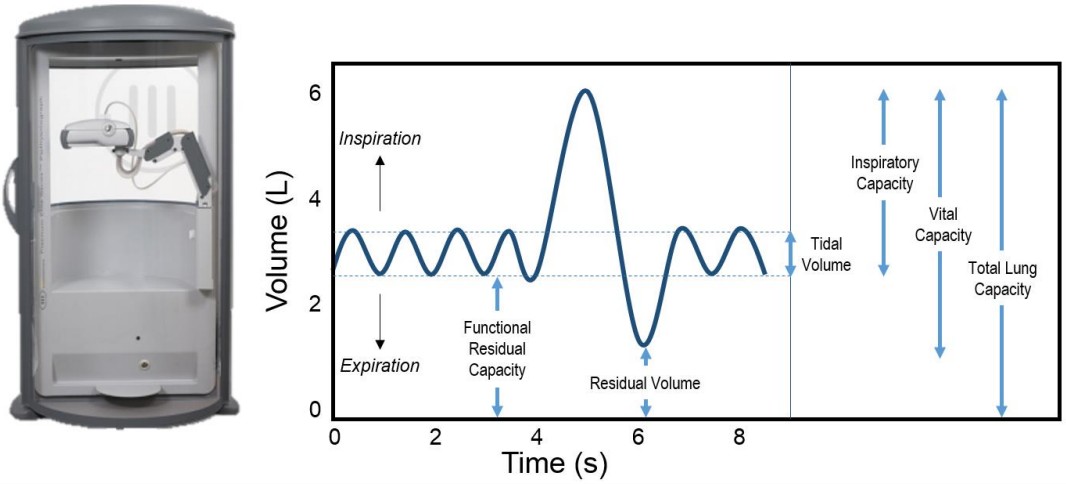

Figure 1-7 Pulmonary Function Testing: Plethysmography
Above: a whole body plethysmograph and a sample airflow curve used to determine lung volumes.

The diffusing capacity of the lung for carbon monoxide (DL_{CO}) can also be determined using pulmonary function tests and provides an indirect measure of diffusion of gases across the alveolar membrane into the blood.[58] DL_{CO} is measured when the subject exhales to RV and then performs a maximum inhalation to TLC. The subject inhales a gas mixture that contains a very low concentration of carbon monoxide (CO) (0.3%) and helium (10%) with air. The subject then holds his/her breath for 8 seconds before exhalation. The exhaled gas is collected and analyzed. The gas first exhaled is discarded as it represents the anatomic dead space volume and is defined as the product of 2.2ml and the body weight in kilograms. The remaining volume is analyzed by comparing the exhaled concentrations of CO and helium to the inspired concentrations to determine the amount of CO diffusing across the alveolar membrane. The capacity of the lung to exchange gas across the alveolar-capillary interface is determined by its structural (e.g. lung gas volume, path length for diffusion, thickness and area of the alveolar capillary membrane, etc.) and functional (e.g. levels of ventilation, composition of the alveolar gas, diffusion characteristics of the membrane, the concentration and binding properties of haemoglobin in the alveolar capillaries, etc.) properties. Flow rates, lung volumes, and DL_{CO} are expressed as a percent of predicted value ($\%_{pred}$). These measurements are dependent on age, sex, height, and ethnicity.[59]

Aging

The underlying structural changes that occur in the aging lung lead to changes in lung function, including dynamic flow rates, static lung volumes, and alveolar gas exchange rates. The current understanding of lung function decline over age stems from work done by Fletcher et al. in 1977. This work showed a continuous decline in FEV_1 at a rate of roughly 42 ml/year beginning between the ages of 25 and 30 (**Figure 1-8**).[38] FVC has also been shown to steadily decrease to approximately 75% of the corresponding peak-value. Together, with the age-related changes in FEV_1, this results in an overall decrease in the FEV_1/FVC ratio (approximately 70-75% of peak value) by the age of 70, as FEV_1 declines more rapidly than FVC. In terms of lung volumes, RV, RV/TLC, and FRC (due to increased lung compliance) decrease, while TLC shows no change with age.[26,28] The increase in RV that occurs with age is likely due to the decreased strength of the expiratory muscles and the tendency of the small airways to collapse. There is also an increase in anatomic dead space that occurs during aging and this is thought to be due to calcification of the bronchial cartilage.[28] Finally, studies have also suggested that there is a decline in DL_{CO} with age, corrected for alveolar volume. The reported decrease in DL_{CO} correlates well with the decrease in internal surface area of the lung.[60]

It should be noted that although elderly subjects have sufficient lung function for their normal day-to-day lives,[61] these age-related changes increase the risk of breathlessness and respiratory failure when compromised. And although the changes associated with aging are histologically different from COPD-related changes to the lung parenchyma, they result in similar changes in lung compliance and function. A consequence of the reduction in supporting tissues (as mentioned above) around the airways is the tendency of the smaller airways to collapse.

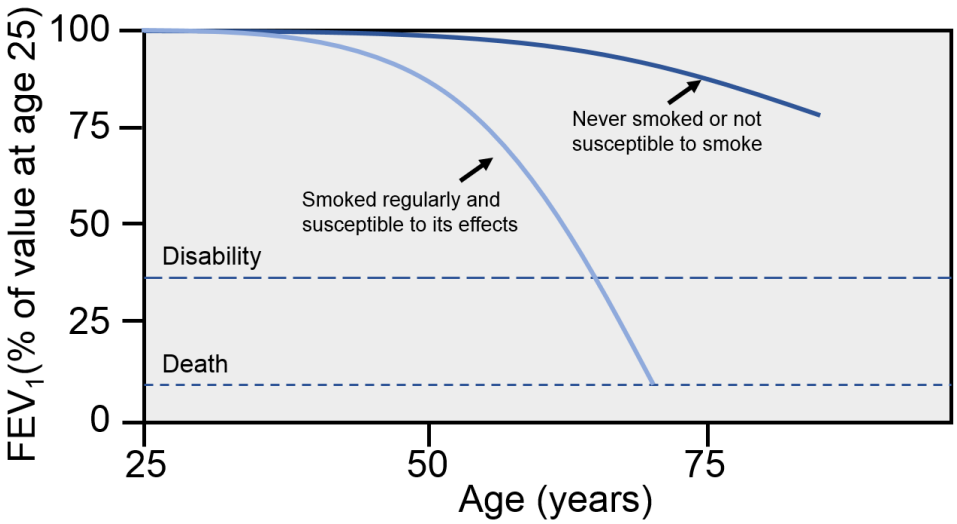

Figure 1-8 Pulmonary function decline in aging in health and disease.
Plot of FEV_1 over time in non-smokers and smokers not susceptible to smoke and smokers that are susceptible to effects of smoking (with the risk of smokers developing airflow obstruction being 25%[62]). Adapted from Fletcher *et al*.[38]

Obstructive Lung Disease

Most of the pulmonary function features of obstructive lung disease stem from the pathologic features discussed above. In asthma, especially during a lung attack, measurements of expiratory flow are reduced (i.e. FEV_1 and FEV_1/FVC). The FVC is also reduced because the airways prematurely close during forced expiration. Static lung volumes are also increased (such as FRC and TLC) during asthma attacks. The increase in RV is caused by premature airway closure during a full expiration which can be a result of increased smooth muscle, edema, or inflammation of airways. This may be indicative of gas-trapping. In COPD, FEV_1, FVC, and FEV_1/FVC are all reduced. These measurements reflect airway obstruction, whether it is caused by excessive mucous in the lumen, thickening of the airway wall by inflammation, or by the loss of radial traction. FVC is reduced because the airways close prematurely during expiration at an abnormally high lung volume and this can also increase RV. In patients with emphysema, TLC, RV/TLC, and FRC are also increased resulting from the loss of elastic recoil. A decrease in IC can be indicative of hyperinflation. A decline in DL_{CO} is measured in patients with COPD, reflective of the loss in alveolar surface area.[63]

Pulmonary function test measurements remain the gold standard for the diagnosis and monitoring treatment of obstructive lung disease. These measurements evaluate the lung on a global basis and lack the ability to detect functional changes in the distal lung.[45] These measurements are also dependent on patient effort.[56]

1.4.2 Cardiopulmonary Exercise Testing

Cardiopulmonary exercise testing (CPET) is used to evaluate a combination of exercise responses involving multiple body systems (i.e. respiratory, cardiovascular, neuropsychological, and skeletal muscle systems). CPET allows for the evaluation of submaximal and peak exercise responses while providing an objective measurement of functional capacity and impairment.[64] Studies have shown that measurements of exercise intolerance, functional capacity and impairment[65] correlate better with overall health status than resting lung function measurements.[64] CPET can be performed using two methods involving either a treadmill or a cycle ergometer. In addition to measuring respiratory gas exchange (e.g. respiratory exchange ratio [RER]), oxygen uptake (VO_2), carbon dioxide output (VCO_2), minute ventilation (V_E), heart rate, and blood pressure can also be evaluated. Two different types of gas analyzers can be used to determine the O_2 and CO_2 concentrations: a mass spectrometer (this is considered the "gold standard") which analyzes all gases (CO_2, O_2, N_2), and separate mass spectroscopy analyzers for CO_2 and O_2. Exercise testing in patients with obstructive lung disease is clinically useful in relating symptoms to exercise limitation, especially when exertional symptoms are disproportionate to resting pulmonary function test measurements.

1.5 Imaging Measurements of Lung Structure and Function

While pulmonary function testing and CPET measurements provide global measurements of lung function, they do not expose underlying pathologies of lung disease, have been shown to be poor predictors of mortality[66] and are insensitive to disease onset, progression, and treatment response.[67] These limitations have motivated researchers to investigate methods that provide biomarkers sensitive to regional structural and functional changes, and sensitive to the heterogeneity of lung disease. Thoracic imaging is a potential method that allows for the regional evaluation of obstructive lung disease and provides quantitative

measurements of lung disease. Thus far, imaging methods such as chest x-ray, thoracic computed tomography (CT), single photon emission computed tomography (SPECT), and positron emission tomography (PET), have played a role in the visualization of pulmonary structure and function in obstructive lung disease and will be discussed in this section.

1.5.1 Chest X-ray

The discovery of x-rays was made in 1895 by a German physicist, Wilhelm Röntgen. Today, x-rays are widely used in for diagnostics because of the short acquisition time, low cost, and low radiation dose. A typical dose associated with a chest radiograph is approximately 0.01mSv[68] which is less than a percent of the annual background radiation (2-3mSv/year).[68] Radiographs (or x-ray images) are shadows created when all or part of a beam of x-rays are attenuated by part of the body. The x-rays that are not absorbed by the body are absorbed by a detector and this results in a projection of the objects in the path of the x-ray beam. Essentially, the resulting image is an overlap or superposition of all structures in the path of the x-ray leading to a loss of depth information.

Image contrast is thus dependent on the mass attenuation coefficient of the tissue which varies with photon energy, atomic number, and mass density of the absorbing material. Thus, a bony structure, is highly attenuating (i.e. absorbs many x-rays) and appears white on an x-ray image. On the other hand, a low attenuating structure, such as the lung, absorbs fewer x-rays and thus appears black on a radiograph. **Figure 1-9** shows a chest radiograph of a healthy volunteer. The lungs appear dark and the ribs, scapula, and spine appear white, which is consistent with the notion that bony structures attenuate x-rays more than soft tissues such as the lung.

Radiographic abnormalities in patients with obstructive lung disease have previously been studied. In asthma, the most common radiographic findings include: hyperinflation and abnormalities of the airways.[69,70] On a frontal radiograph, similar to what is shown in **Figure 1-9**, hyperinflation is seen as an increase in the length of the lung, a depression of the diaphragm, and a decrease in the transverse cardiac diameter. Airway abnormalities of the large airways are also visible on a frontal radiograph, more specifically, bronchial wall thickening. In patients with emphysema, a chest radiograph is mostly useful at detecting

moderate-to-severe emphysema.[52] The key features on a radiograph in a patient with emphysema are hyperinflation and abnormalities of the small vessels.[71] The radiographic signs of hyperinflation in emphysema (**Figure 1-9**) are no different than what is observed in asthma (i.e. elongated lung, depressed diaphragm, and change in the cardiac silhouette).

Radiographic findings in asthma, such as bronchial wall thickening have been shown to be signs of an asthmatic exacerbation.[72,73] Bronchial wall thickening in asthma has also been qualitatively evaluated in asthma using chest radiographs and compared with healthy controls.[74] This work has demonstrated that wall thickening measured using chest x-rays is greater in asthmatics than in healthy volunteers.[74] In patients with COPD, as stated before, only moderate-to-severe emphysema is detectable on radiographs. The limited work that has been done in COPD using planar x-rays, has demonstrated that emphysema severity (evaluated using chest x-rays) is related to pulmonary function test measurements.[75]

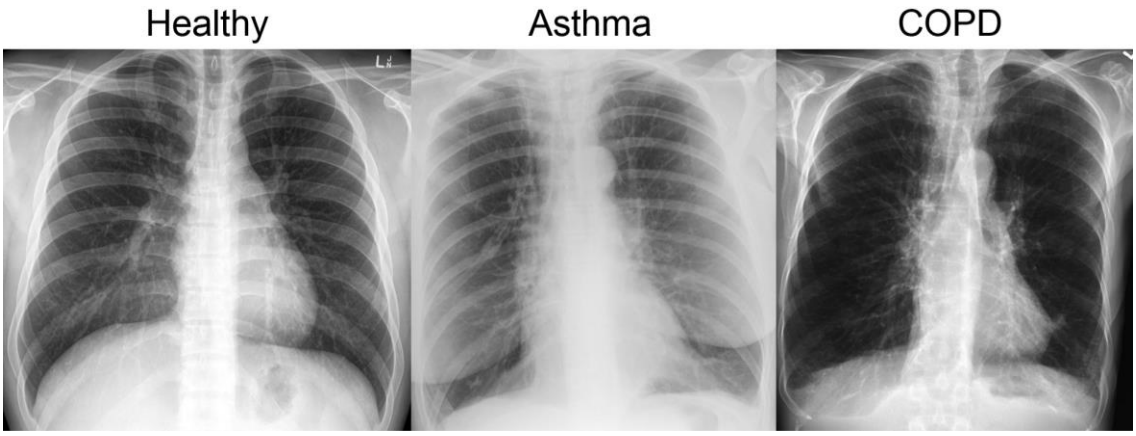

Figure 1-9 Representative posterior-anterior chest radiograph of a healthy volunteer, an asthmatic subject, and subject with COPD.
In asthma, the lungs appear hyperlucent, the diaphragm is flattened indicative of hyperinflation, and more than six anterior ribs are in the mid-clavicular line at the lung diaphragm level. In COPD, the lungs are hyperinflated (consistent with a flat diaphragm and secondary to emphysema), the retrosternal airspace is enlarged, and the pulmonary arteries are protruding (consistent with pulmonary hypertension).
Healthy case courtesy of Dr. Frank Gaillard, Radiopaedia.org, rID: 8090. Asthma case courtesy of Dr. Ian Bickle, Radiopaedia.org, rID: 33470. COPD case courtesy of Dr. Mai-Lan Ho, Radiopaedia.org, rID: 6452.

1.5.2 X-ray Computed Tomography

The limitations of a planar chest x-ray, including the loss of depth information and poor contrast, for the evaluation of obstructive lung disease has been recognized for some while. In the 1970s, radiography (the science of medical x-ray images) was revolutionized with the introduction of x-ray CT. Over the past few years, CT has become the imaging modality of choice for the lung because it provides subtle differences in lung parenchymal density and eliminates the anatomical superposition present in chest x-rays.[76,77] Furthermore, high resolution CT allows for the assessment of emphysema and airways disease using quantitative indices.[78]

During a CT scan, a series of x-ray projections are collected from different regions of the body. These projections are created by an x-ray source which is detected by a series of detectors that lie opposite to one another. Each voxel in a CT image represents a relative measurement of tissue density based on the attenuation coefficient of water:

Equation 1-1

$$Hounsfield\ Unit = \left(\frac{\mu_{tissue} - \mu_{water}}{\mu_{water}}\right) 1000\ [HU]$$

where μ_{water} and μ_{tissue} are the linear attenuation coefficients of water and tissue, respectively. The Hounsfield Unit (HU) scale is a standard scale that represents densities within the tissue being scanned. The scale is based off of water which has a Hounsfield value of 0HU. Tissues or substances with higher densities have higher Hounsfield numbers compared to those with lower densities. A soft tissue such as the liver would have a Hounsfield value between 30-50HU, blood around 80HU, and bone around 1500-4000HU.[79] A tissue with low density such as the lung would have a Hounsfield value between -1000HU to -525HU. The dose associated with a typical chest CT is approximately 7-8mSv.[80] Depending on where an individual lives, this is equivalent to about 4 years of natural background radiation or 400 chest x-rays. It should be noted, low dose and ultra-low-dose CT acquisitions[81] are becoming achievable with new image reconstruction techniques where doses on the order of 0.1mSv have been observed. These methods have yet to be implemented in clinic.[82]

Airway Disease

Airway disease in patients with obstructive lung disease presents with varying diagnoses and symptoms as discussed above. The key features of airways disease seen on CT include: mosaic attenuation patterns, mucous plugging, atelectasis, bronchiectasis, and bronchial wall thickening. The small airways (diameter less than 2mm) cannot be directly evaluated using CT because of spatial resolution limitations. As a result the small airways, as shown in **Figure 1-10**, in obstructive lung disease are reflected by gas-trapping, more specifically the mosaic attenuation pattern. A typical mosaic pattern results when the distribution of these areas of decreased attenuation is patchy, which is often the case in gas-trapping, and when the surrounding normal lung areas show increased lung density resulting from compensatory hyper-perfusion. Gas-trapping is best visualized on expiratory CT. The extent of gas-trapping can be estimated using computerized and automated analysis. In this analysis the CT density histogram of all Hounsfield unit values is evaluated using a number of HU threshold to generate the relative area of the lung occupied by attenuation values lower than specific threshold (e.g. relative area under -856HU [RA_{856}] at full expiration to evaluate gas-trapping[83]).

Large airway abnormalities, such as bronchiectasis and bronchial wall thickening, are frequent findings in patients with obstructive lung disease. Bronchiectasis is reflected by bronchial dilation where the diameter of the bronchus is approximately 1.5 times greater than the corresponding artery. In **Figure 1-10**, the yellow arrows in the axial slice indicate cylindrical bronchiectasis, whereas the arrows in the coronal view show a signet ring and varicose bronchiectasis. Bronchial wall thickening appears like a donut, where the edge of the airway wall is thicker and the centre contains air.

Airway dimensions can be quantified using CT and this is helpful in obstructive lung disease to provide an understanding of bronchial inflammation and remodeling. Currently, there is software available (e.g. Pulmonary Workstation V.2.0 [VIDA Diagnostics, Coralville, Iowa, USA]) for the reconstruction of airways from volumetric datasets. These software allow for the quantification of luminal diameter and wall thickness to the fifth-sixth airway generation. Indices for evaluating airway dimensions include: bronchial

luminal area (LA), bronchial wall thickness and area (or percent, where the wall area in normalized to the outer wall area [WA%]), and total bronchial area.

In patients with asthma, CT bronchial wall thickness measurements are greater than healthy controls[84] and have been shown to be associated with airflow obstruction.[85,86] Decreased lung density has been shown to be related to pulmonary function test measurements of gas-trapping (e.g. RV) and airflow obstruction (e.g. FEV_1).[87,88] Furthermore, CT measurements of gas-trapping have been shown to be associated with increased number of asthma related hospitalizations and intensive care unit visits.[83]

Airway wall measurements in patients with COPD have been associated with histology,[89] frequency of exacerbation,[90] and dyspnea.[91] Wall area measurements have also been shown to be correlated with the FEV_1/FVC, and RV/TLC, but not DL_{CO}.[92] COPD patients with a clinical diagnosis of chronic bronchitis have also been shown to have thicker airway walls (measured using CT) than those without chronic bronchitis.[93] Recent work showed that quantitative CT measures of airway thickness in COPD patients were greater in those with bronchodilator responsiveness.[94]

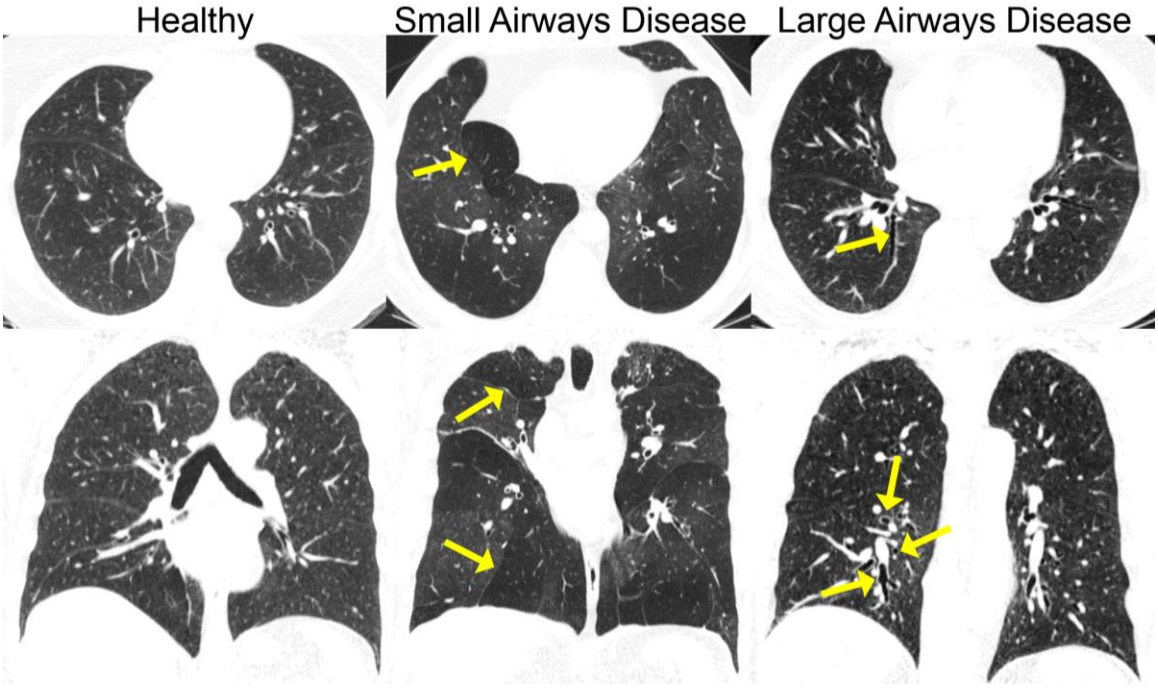

Figure 1-10 Axial and coronal x-ray CT images of representative subjects. Subjects shown in health, with small airways disease, and large airways disease.

Emphysema

The evaluation of emphysema using CT has been done for the past three decades. The earliest studies evaluating emphysema noted the key feature of emphysema was the decrease of lung density.[95] Other radiological signs of emphysema include focal areas of low attenuation, no definable wall, upper zone predominance, no obvious fibrosis, vascular pruning and distortion, and bullae.[96]

The CT image is essentially a densitometric map of the lung, where each pixel corresponds to a Hounsfield Unit value representing tissue density. The evaluation of emphysema has evolved from visual scoring systems which are subject to high inter- and intra-user variability[97] to less biased quantitative methods. Emphysema can now be estimated using computerized and automated analysis. In this analysis the CT density histogram of all Hounsfield unit values is evaluated using a number of HU threshold to generate the relative area of the lung occupied by attenuation values lower than specific threshold (**Figure 1-11**) and percentiles (e.g. relative area under -950HU [RA_{950}] or the lowest 15^{th} percentile [HU_{15}] at inspiration to evaluate emphysema). These values have been shown to correlate well with manual radiologists' emphysema scores,[98] pulmonary function test measurements,[99] and with histology.[100] Limitations with single threshold methods include the over or under-estimation of emphysema, where a lower threshold differentiates more severe emphysematous regions[101] disregarding regions with mild tissue destruction and a higher threshold identifies mild emphysematous regions.[102] Consequently, methods that diverge from single threshold measurements have emerged. An example of this is an automated evaluation of the CT density histogram using principal component analysis that has been used to generate a principal component score based on each frequency–HU pair. This measurement was strongly related to pulmonary function tests and expert radiologist emphysema scores.[103]

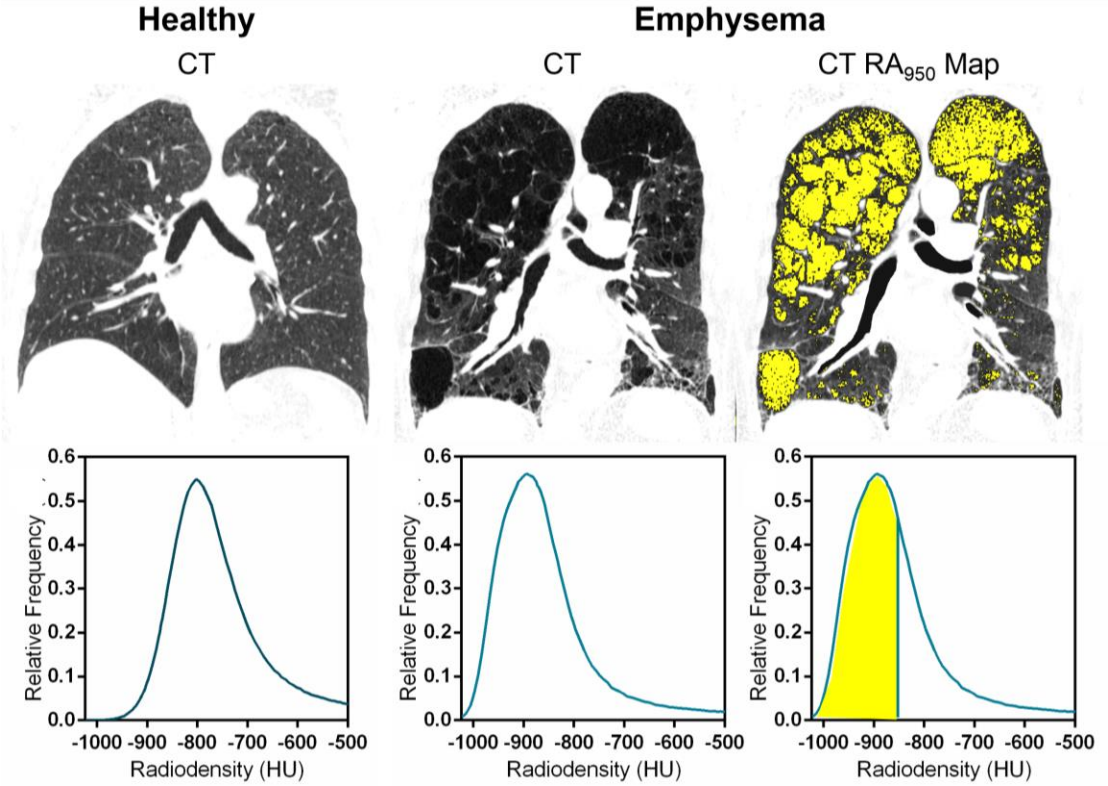

Figure 1-11 Representative CT images and corresponding frequency distribution of radiodensity shown below for healthy and emphysematous lungs.
The regions below -950HU are shown in yellow.

Another commonly used measurement of emphysema is the percentage of lower attenuation areas (LAA%). The LAA% expresses the emphysema volume as a proportion of total lung volume measured by CT and has been shown to be associated with pulmonary function test measurements,[104] frequency of COPD exacerbations,[90] and quality of life scores.[105]

It should be noted that the use of CT for pulmonary applications, especially for serial and/or longitudinal studies or pediatric applications, is limited due to the potential risks related to radiation doses stemming from the ionizing x-ray radiation (the radiation that displaces electrons from atoms or molecules and produces ions).[106] However, thoracic x-ray CT provides a wealth of structural pulmonary information, where each voxel in the resulting CT image provides a physical unit of tissue density.

1.5.3 Nuclear Medicine

In comparison to CT imaging methods that are based on the relative absorbance of x-rays, nuclear medicine techniques utilise tracers that emit radiation. These methods involve intravenous injection of radioisotopes to the pulmonary vasculature or inhalation to the peripheral airspaces, thus giving functional images of ventilation and perfusion.

Single Photon Emission Computed Tomography

Three-dimensional SPECT has been clinically available for 30 years, having mainly been used for myocardium, brain, and liver imaging. The technique has also been applied in lung scintigraphy, especially for the assessment of pulmonary embolisms. SPECT radioisotopes emit a single gamma beam as they decay. Every point on the gamma camera image corresponds to an entire line within the person being imaged. These projections can be reassembled to provide three-dimensional information about the distribution of radionuclides within the body. For pulmonary imaging, SPECT has been used to provide information about pulmonary physiology, i.e. ventilation and perfusion. Perfusion scanning is typically performed using 99m-technecium labelled macro-aggregated albumin (^{99m}Tc-MAA), which lodges in the pulmonary circulation after peripheral injection. Ventilation scanning requires the inhalation of gaseous radioisotopes (e.g. ^{81m}Kr and ^{133}Xe) and the gas distributes throughout the whole lung, and the differences in its regional distribution reflect differences in regional ventilation. These isotopes have been used to produce both perfusion[107] and ventilation[108,109] maps in subjects with obstructive lung disease. These studies have quantified perfusion defects and ventilation defects as the extent that is not perfused or ventilated, respectively.

In patients with asthma, the disease heterogeneity has been established using SPECT imaging.[110] Changes in regional perfusion and ventilation during bronchoconstriction,[111,112] bronchodilation,[113] exercise,[114] antigen challenge,[115] and histamine inhalation[116] have been evaluated in asthmatics using ^{99m}Tc-MAA and ^{81m}Kr. In patients with COPD, previous work has investigated the effects of baseline lobar perfusion on outcomes following endobronchial valve placement.[107] This study demonstrated that pulmonary function test measurements did not change pre- and post-endobronchial valve

placement. However, the patients with high baseline perfusion had significant shifts in perfusion with endobronchial valve placement, in comparison to patients with low baseline perfusion. Although SPECT has been used to assess the severity of airflow limitation in subjects with COPD,[117,118] intrabullous ventilation in patients with emphysema,[119] and ventilation-perfusion mismatch in COPD subjects,[120,121] it is limited by the risk of cumulative radiation exposure for longitudinal monitoring and offers poor spatial resolution. As a result so far there have been no published studies using SPECT to assess treatment responses aimed at improving ventilation patterns in asthma or COPD.

Positron Emission Tomography

PET utilises radioisotopes that emit positrons as they decay through the process of beta decay. As the positron is ejected from the nucleus and encounters an electron, these particles annihilate resulting in two photons emitted at approximately 180 degrees. These photons are detected at or very near the same time and are considered to be "coincident" and the location of the source particle can therefore be determined geometrically from the coincident beams—being located on the straight line between the two detectors. Flourine-18 (^{18}F) is the most commonly used radioisotope in PET and when it is bound to fluorodeoxyglucose (FDG) it can be taken up by metabolically active tissue. In COPD, ^{18}F-FDG has been used to assess inflammation. Studies have highlighted the challenges of quantifying inflammation given the variability of lung density in diseased patients.[122] For example, visually, a patient with emphysema would unlikely show an increased signal even when there is a high degree of inflammation, simply because there is so little tissue in each image voxel. However, the finding that COPD patients have greater ^{18}F-FDG uptake than healthy controls,[122,123] paves the road for future work that may assess treatment response with ^{18}F-FDG uptake as an endpoint. Regional ventilation has also been assessed using PET by using the ^{13}N isotope.[124] This marker is injected and enters the lung via pulmonary arterial circulation. Due to its low tissue solubility, the ^{13}N diffuses across the alveolar membrane and allows for the measurement of ventilation and perfusion. As such, unventilated lung regions, termed ventilation defects, retain the tracer due to gas-trapping whereas the tracer is quickly washed out of ventilated lung regions.

In patients with asthma, ^{18}F-FDG PET has been used to evaluate inflammation[125] and ^{13}N PET has been used to evaluate bronchoconstriction.[126] Studies have evaluated perfusion and ventilation using ^{13}N PET as a vascular biomarker in COPD, demonstrating that perfusion is significantly heterogeneous in COPD patients compared to healthy volunteers[127] and this may suggest that regional changes in pulmonary blood flow may precede lung parenchymal changes in COPD. Ventilation-perfusion ratios have also been assessed in COPD patients, where emphysema dominant COPD patients had higher ventilation-perfusion ratios compared to COPD patients with airways disease.[128]

PET has evolved over the years to allow for the measurement of ventilation and perfusion in patients with lung disease. However, the limitations that accompany PET include the need for a cyclotron for the production of isotopes, for short term repeated studies time is required for the radioisotope to decay enough to avoid signal contamination, cumulative radiation exposure limits longitudinal monitoring of patients, and low spatial resolution (due to physical effects) does not allow imaging of individual gas exchange units.

1.6 Pulmonary Magnetic Resonance Imaging

Unlike x-ray and nuclear imaging methods, magnetic resonance imaging (MRI) uses radiofrequency (RF) waves to manipulate nuclear spins (typically of hydrogen atoms) to generate images. The MRI signal is generated from the protons in water molecules and unfortunately, the lung contains only 800g of tissue which is distributed over 4-6L.[129] The resulting signal-intensity of the lung is low compared to the rest of the body. Although pulmonary MRI remains clinically challenging due to the unique characteristics of lung tissue, in the last several decades, MRI using hyperpolarized noble gases and conventional methods has revolutionized the field of pulmonary imaging. There have been a series of new technologies developed to qualitatively and quantitatively evaluate lung abnormalities. These techniques provide unique biomarkers and insights into the pathophysiology of obstructive pulmonary diseases. Before these biomarkers can be used in clinic, their structural determinants and clinical consequences must first be better understood.

1.6.1 Inhaled Noble Gas Magnetic Resonance Imaging

The development of inhaled gas contrast MRI has allowed for the visualization of lung function and structure. The first lung ventilation images acquired using hyperpolarized ^{129}Xe were captured in 1994.[130] Shortly after the first lung ventilation images were acquired using ^{129}Xe MRI, the field shifted towards hyperpolarized ^{3}He. The main reason for this stems from the inherent properties of these two gases. The gyromagnetic ratio of ^{129}Xe (γ=-11.8MHz/T) is three times smaller than that of ^{3}He (γ=-32.3MHz/T) and the achievable polarization of ^{129}Xe is lower (^{129}Xe: 8-25%; ^{3}He: 30-40%)[131]—which consequently leads to a lower signal-to-noise ratio. With improvements in hardware, however, similar signal-to-noise ratio is becoming more attainable.[132]

Unlike clinically available MR methods, hyperpolarized inhaled gas MRI requires specialized equipment and personnel to prepare and image the gas. This is because both ^{129}Xe and ^{3}He have low spin density in the gaseous state. The spin densities of these gases are typically about four orders of magnitude less than the density of protons in water.[133] Since MR signal is determined by the difference in the number of spins aligned in either direction, the most ideal case to produce signal would involve spins being aligned completely in one direction (i.e. 100% polarized). In practice, not all spins will align in one direction and this is determined by the Boltzmann distribution, therefore, there is a reduction in the polarization which is proportional to the signal. The polarization of dilute gases like ^{3}He and ^{129}Xe is not sufficient for imaging and results in a very low signal for *in-vivo* imaging. Angular momentum can be added to the system to align all nuclear spins in one direction and overcome the lack of polarization.

Classically, hyperpolarization involves the addition of angular momentum to the system. Optical pumping and spin exchange are typically used to polarize the gas. A circularly polarized laser serves as the carrier of the angular momentum. This laser (where the wavelength of laser photons matches the electronic orbital transmission of the alkali atom) is used to excite the electrons of an alkali metal (e.g. rubidium). The angular momentum that the electrons obtain from the laser is transferred to the noble gas nuclei through collisions. Once there is enough rubidium vapour (at temperatures >>40°C which is the

melting point of rubidium) for the gas to interact with, the temperature has a minimal effect on the spin exchange. It should be noted, that the pressure is well controlled in this system. This method increases the nuclear polarization of the unpaired nuclear proton in these atoms up to five orders of magnitude compared to thermal polarization.[134] This increase in polarization is needed to compensate for the low density of noble gas nuclei within the lung (compared to the protons from the lung tissue) and provides ventilation images with resolution on the order of millimetres. The polarization for ^{3}He and ^{129}Xe lasts up to days if there are no external sources of relaxation (such as oxygen, magnetic field gradients, and surface-to-volume relaxation).[131]

Ventilation Imaging

Hyperpolarized noble gas MRI using ^{3}He and ^{129}Xe provides a method to visualize those regions of the lung that are ventilated and those that are not. This type of imaging is based on the spin density of the hyperpolarized gas. In a healthy young subject, as shown in cyan in **Figure 1-12**, the hyperpolarized gas is distributed homogeneously in the lung. In older never-smokers or patients with obstructive lung disease (**Figure 1-12**), the distribution of the hyperpolarized gas is more heterogeneous. There are apparent regions of signal void known as ventilation defects. These regions of signal void can be quantified as the ventilation defect percent (VDP) by normalizing the ventilation defect volume (VDV) to the thoracic cavity volume (TCV).[135] The imaging biomarker, VDP, has been shown to be reproducible,[136] related to lung function,[137] and sensitive to disease severity and treatment response.[138,139]

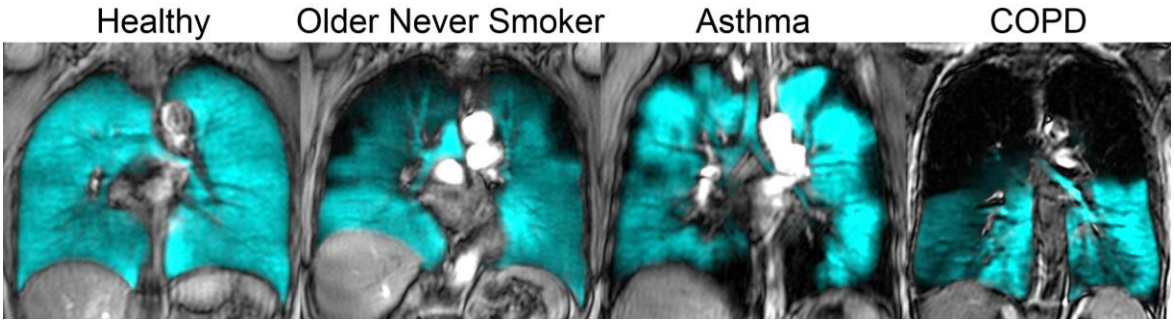

Figure 1-12 Representative coronal centre slice of healthy young and older never-smokers and patients with OLD.

Hyperpolarized ^{3}He MRI gas distribution (in cyan) registered to the ^{1}H MRI of the thorax (in grey-scale). Unlike the representative healthy young never-smoker, the older never-smoker and obstructive lung disease subjects have visually obvious ventilation defects.

Studies using ventilation MR imaging have revealed that COPD and asthma are regionally heterogeneous diseases[140,141] and that there are significant ventilation improvements post-therapy even in the absence of pulmonary function test measurement improvements.[138] As can be seen in **Figure 1-12**, the distribution of ventilation defects varies for those subjects who are older never-smokers or have asthma or COPD. Although the aged subject and subjects with obstructive lung disease have ventilation defects, they are distributed in different patterns. This suggests that there are different looks to ventilation patterns in obstructive lung disease patients and this information could potentially be used for phenotyping. But before these biomarkers can be used for phenotyping, as stated before, their structural determinants and clinical consequences need to be better understood.

In order to better understand the clinical consequences of this imaging biomarker in patients with obstructive lung disease, studies have evaluated aging,[142] asthma,[139,143-145] and patients with COPD.[138,140,146] Ventilation defects have been shown to correlate with age.[142] The clinical consequences of ventilation defects in aging have yet to be determined. In asthma, ventilation defects have been shown to be related to worse airflow obstruction, greater airways resistance, and airway inflammation.[145] Ventilation defects in severe asthmatics have also been reported to be related to asthma control.[147] In COPD, ventilation defects have been shown to represent a mixed airways disease-emphysema phenotype[148] and have been shown to be correlated with COPD exacerbations.[146]

Collectively, these studies suggest that in obstructive lung disease the biomarker VDP is related to airways disease and emphysema, these defects are heterogeneously distributed, and are responsive to therapy. Hyperpolarized noble gas MRI for evaluating lung ventilation has thus become an accepted tool for visualizing lung function. With the increased costs related to noble gas ventilation MR imaging, the field's future transition appears to be geared towards non-contrast enhanced MR methods, such as proton MRI. However, obstructive lung disease has yet to be evaluated using these more clinically available approaches. Although it can be hypothesized that the knowledge gained from

pulmonary non-contrast enhanced MRI studies will be complementary, direct comparisons with noble gas MRI are required.

Diffusion Weighted Imaging

In addition to the visualization of gas distribution, there is the potential to evaluate lung microstructure using hyperpolarized noble gas MRI. ^{3}He is a highly diffusive gas due to its low atomic weight (self-diffusion coefficient of 2cm^2/s at 37°C).[131] The diffusion coefficient can be measured using diffusion-weighted MR methods that are sensitive to the gas' self-diffusion based on the random Brownian motion of the atoms, as opposed to transmembrane gas diffusion. The ^{3}He apparent diffusion coefficient (ADC) reflects diffusion of the gas when restricted by the airways and airspaces. ^{129}Xe also provides measurements of lung structure, but ^{3}He ADC measurements have been more extensively reported. An increased ADC value reflects a greater mean square displacement of the gas molecule which is consistent with an increased measure of lung microstructure.

In healthy volunteers, diffusion weighted ^{3}He MRI has been used to demonstrate that structural changes occur with an annual increase in ADC of 0.0015cm^2/s for subjects between the ages of 20 and 70 years.[149] The limited work that has used ^{3}He ADC to evaluate asthma has revealed to be inconsistent. Some work has shown that ^{3}He ADC values are elevated in asthma (suggesting gas-trapping),[150] while others have reported no differences in ADC values between asthmatics and healthy volunteers.[151,152] In terms of evaluating treatment response, ^{3}He ADC values are elevated after bronchoconstriction (suggesting gas-trapping) and decreased following the administration of a bronchodilator.[153] In patients with COPD, ^{3}He and ^{129}Xe ADC values are elevated compared to age matched healthy volunteers.[154] Previous work has revealed the association of ^{3}He ADC measurements with pulmonary function test measurements,[155] histology,[156] age,[149] smoking history,[149] and gas-trapping.[148] ^{3}He ADC has also been evaluated pre- and post-bronchodilator administration and the newly ventilated regions of the lung did not have elevated ADC compared to the regions participating in ventilation before bronchodilator administration.[157]

Hyperpolarized noble gas MRI has yet to find wide-ranging acceptance in the clinic. Advances in CT, limited availability of the necessary hardware for polarizing and imaging hyperpolarized noble gases, and the identification of clinical applications that will benefit from this have made clinical translation difficult. With this, there has been growing motivation for the development and implementation of non-contrast enhanced pulmonary MRI to overcome the challenges of ionization radiation and resource accessibility.

1.6.2 Non-Contrast Enhanced ^{1}H Magnetic Resonance Imaging

As mentioned above, the lung is more challenging to image using conventional proton (^{1}H) MR pulse sequences than MRI of most other organs due the combined effects of low proton density, magnetic susceptibility, and to a lesser extent because of the effects of cardiac and respiratory motion.[158,159] Because the alveolar ducts and sacs make up most of the lung volume and are air-filled, there is very little lung tissue and consequently the mass density of the lung is lower than any other organ in the body, and is approximately 0.15g/mL.[159] Since MR signal is proportional to the proton density of the tissue, the resulting signal from the lung is much lower than all other body tissues.

The lung parenchyma also has a short transverse magnetization relaxation time (arising from natural interactions at the atomic or molecular levels), known as T_2. This is the time it takes the excited protons to lose phase coherence due to the interaction between spins resulting in a reduction in transverse magnetization. The decay of the MR signal due to T_2 is because of the natural interactions of spins at the atomic and molecular levels within the tissue. The resulting T_2* at 3T, which is the sum of T_2 and the relaxation due to the field inhomogeneities across a voxel ($\gamma\Delta B_0$), of the lung is also short (i.e. 0.4-0.9ms):[160,161]

Equation 1-2

$$\frac{1}{T_2 *} = \frac{1}{T_2} + \Delta B_0 \gamma$$

Taken together, these MR properties of the lung result in a much faster MR signal decay for the lung parenchyma in comparison to other tissues. In addition to the short T_2, another problem for MRI of the lung relates to the fact that air and tissue have very different

magnetic susceptibilities. The adult human lung is composed of approximately 480 million alveoli and it is the co-distribution of airspaces/tissue/gas/blood that leads to local magnetic field inhomogeneities[158,159] that are problematic for high spatial resolution MRI. The differences in the magnetic susceptibilities between different materials (i.e. air and alveolar wall tissue) lead to variations in the local magnetic field and this leads to faster spin dephasing (i.e. shorter T_2*). With an increased voxel size, there is a greater number of air-tissue interfaces and this may result in a greater T_2* decay. A larger voxel size is also susceptible to the main magnetic field inhomogeneities. Furthermore, since the local magnetic field determines the angular speed of magnetic spin rotation, the magnetic field inhomogeneity at the interface causes the spins to precess at different angular velocities and this leads to an increased dephasing of the measureable magnetization. The dephasing effect leads to a signal loss or field inhomogeneity artifacts which further degrade the ^{1}H signal and distort the image. Consequently, as shown in **Figure 1-13**, the lungs appear as black holes with no information that can be obtained about lung structure. Furthermore, the lungs of health and disease in these cases are indistinguishable.

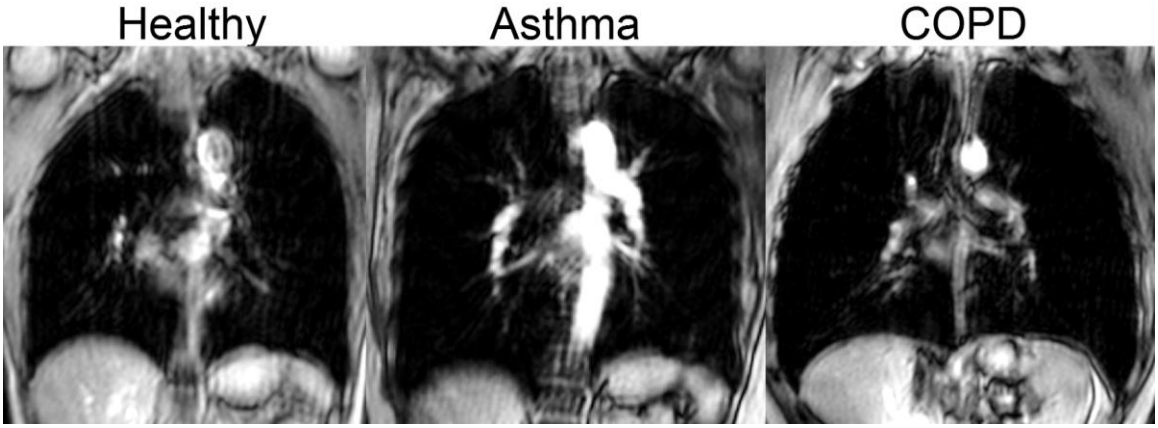

Figure 1-13 Representative coronal centre slice of healthy young never-smoker and patients with obstructive lung disease.
Due to low ^{1}H and tissue density within the lung there is no signal inside the lung and thus structural abnormalities are not visually apparent. Coronal ^{1}H MRI acquired using the whole-body RF coil and ^{1}H fast-spoiled, gradient-recalled echo sequence using a partial echo (16s total data acquisition, repetition time (TR)/echo time (TE)/flip angle = 4.7ms/1.2ms/30°, field-of-view (FOV)=40×40cm, bandwidth=24.4 kHz, matrix=128×80, 15-17 slices, 15mm slice thickness, 0 gap).

Making this situation even more complex is the respiratory motion that occurs during tidal breathing because the change in lung volume causes blurring of pulmonary structures. To overcome this limitation, the lung can be imaged under rapid breath hold conditions or using prospective or retrospective respiratory gating. The periodic motion of the heart also causes motion artifacts in MR images making the visualization of the lung parenchyma near the heart more complex.

Several techniques have been proposed to overcome these challenges and have been discussed above (i.e. hyperpolarized noble gas MRI). It should be noted, however, that these techniques require a certain amount of additional hardware such as special RF coils tuned to the Larmor frequency of the gas being imaged and hardware to prepare the hyperpolarized gases. Alternative methods that are based on the visualization of the enhanced proton signal of the lung tissue have been developed and will be discussed.

Ultra-Short Echo Time MRI

Although hampered by low signal-intensity due to low ^{1}H density and the multitude of lung air-tissue interfaces, ^{1}H MRI of the lung can be performed on every scanner without additional hardware (such as a polarizer or an MR system with multi-nuclear imaging capabilities). To maximize the potential to provide high spatial resolution quantitative images of lung parenchyma in MR images, pulse sequences need to provide maximal signal and minimal degradation in the presence of susceptibility dephasing. This can be achieved by minimizing the echo time (TE) which is the time between excitation and acquisition of the signal.[159] With recent technical advancements, MRI using ultra-short echo time (UTE) acquisition methods have emerged. These methods were first proposed as a way to address the inherent challenges of pulmonary imaging stemming from low tissue and ^{1}H density.[162] UTE MRI combines fast RF excitation pulses and efficient k-space sampling trajectories to minimize MR signal decay and motion artefacts.[162] The length of TE, however, depends on how quickly the RF electronics (hardware) can switch from transmit to receive.[163]

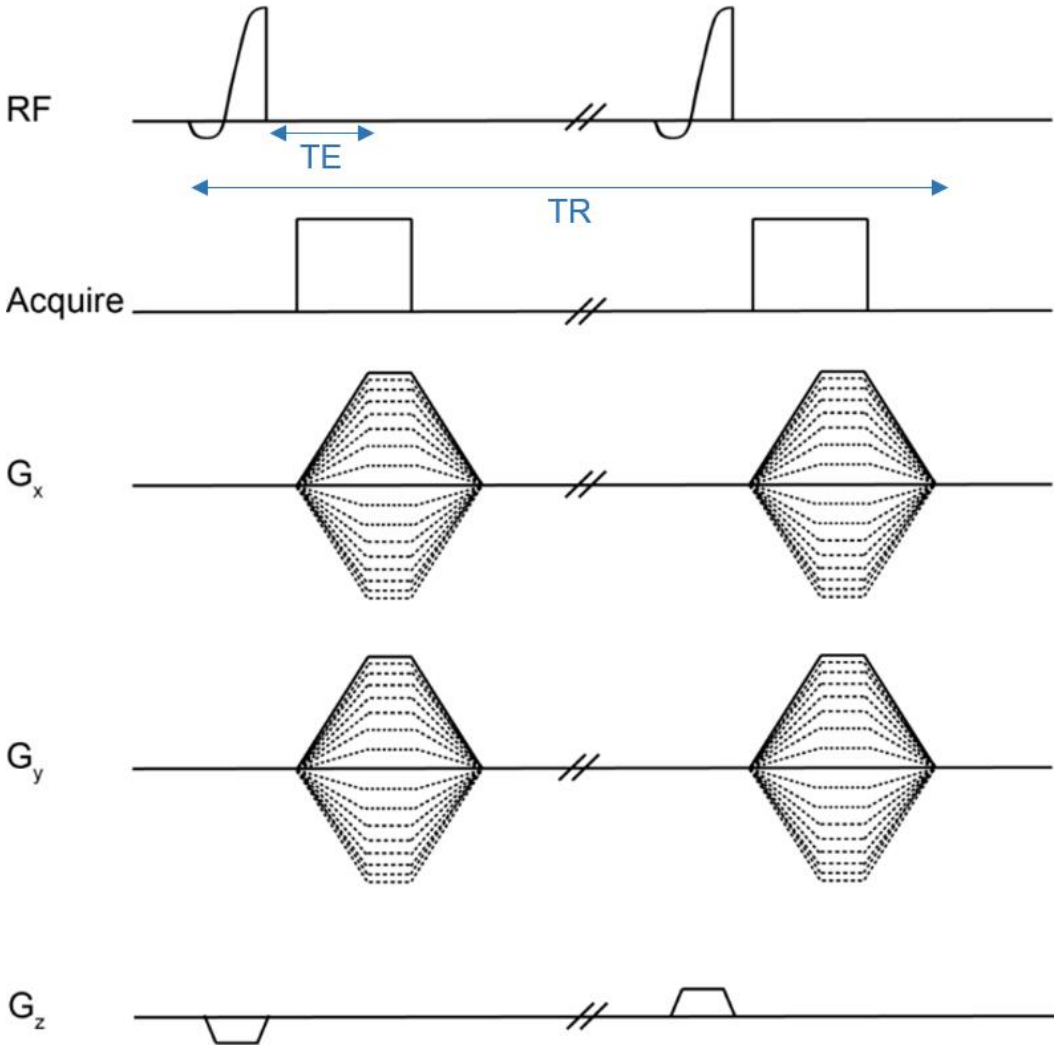

Figure 1-14 Conventional two-dimensional UTE pulse sequence diagram.
The half radiofrequency (RF) pulses are applied with a negative slice-selection gradient (G_z) in the first half and a positive gradient in the second half. The RF pulse is truncated and followed by a radial acquisition which is when G_x and G_y are applied. These gradients ramp up to a plateau during data acquisition.

Briefly, as shown in **Figure 1-14**, a typical two-dimensional UTE sequence starts with a half-sinc pulse RF excitation followed by a centre out radial acquisition, where the free induction decay will be acquired. To remove the out-of-slice signal and correct the phase resulting from the half-pulse excitation, a second excitation will be implemented simultaneously with the inverted slice select gradient. This acquisition will be added to the first acquisition to remove the phase variation across the slice and out-of-slice signal.

Figure 1-15 shows UTE MR images of a healthy never-smoker and patients with obstructive lung disease. There are visually apparent regions of low signal-intensity in the patients with obstructive lung disease which may reflect regions of low tissue density due to gas-trapping or emphysema. As can be seen when comparing **Figure 1-14** and **Figure 1-15**, UTE MRI methods result in higher pulmonary signal intensities than clinically available MR methods. The biomarkers stemming from UTE MRI include mean whole lung T_2*, mean whole lung signal-intensity, and threshold based indices quantifying volumes of low signal-intensity[164] which have been all used to evaluate lung parenchyma. It should be noted that the resulting MR signal is not only influenced by T_1, T_2*, and proton density, but also hardware factors such as the positioning of the RF coils, which introduce inter-scan variability. Because of this, it is difficult to ascertain the physiological meaning of ^{1}H MR signal-intensity and thus translate across multiple sites.

Thus far, in asthma, limited work has been done using UTE MR methods. However, conventional and clinically available ^{1}H MRI pulse sequences have been used to monitor inflammatory responses to allergen challenges in animal models[165] and asthmatics.[166] With recent advancements in pulmonary ^{1}H MRI, the first studies employing UTE methods imaged mice and reported that the MR signal and T_2* of the lung parenchyma were higher at end-expiratory phase than at end-inspiratory phase.[167] This work also reported that these values were reduced in the mouse model of emphysematous lungs compared to normal mouse lungs at end-expiratory phase suggesting that higher signal-intensity and T_2* values are related to increased lung density. More recently, UTE MRI measurements, implemented in a mouse model of emphysematous lungs, were correlated with histology measurements of the mean chord length of the alveoli.[168] These results are consistent with the notion that smoking exposure results in alveolar enlargement and increases the air-tissue ratio and susceptibility driven local field inhomogeneity.

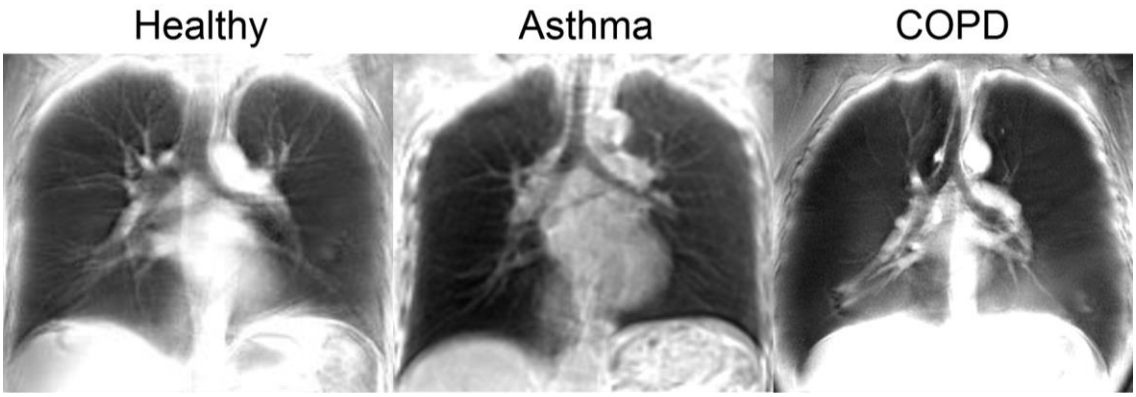

Figure 1-15 Representative coronal centre slices of healthy young never-smoker and patients with obstructive lung disease acquired using UTE MRI.
Regions of low signal-intensity are visually obvious in the obstructive lung disease subjects compared to the healthy never-smoker. Images of healthy volunteer and COPD subject acquired using a 2D UTE MR method using a 32-channel torso coil (GEHC) (13s acquisition time, TR/TE/flip angle=13.0ms/0.05ms/10°, FOV=40×40cm, matrix 256×511, NEX=2, 15mm slice thickness). Image of asthmatic acquired using a 3D UTE MR method using a 32-channel torso coil (GEHC) (15s acquisition time, TE/TR/flip angle=0.03ms/3.5ms/5°, FOV=40×40cm, matrix=200×200, NEX=1, and reconstructed to a 10mm slice thickness).

Fourier Decomposition MRI

Fourier decomposition (FD) MRI has also been proposed for non-contrast enhanced functional lung MRI to obtain regional ventilation and perfusion information about the lung. This approach exploits fast MRI acquisition of the lung with respiratory motion compensation using non-rigid image registration. Spectral analysis of the images allows for identification of peaks of the respiratory and cardiac frequencies; these peaks are related to ^{1}H density change caused by compression and expansion of the lung parenchyma and pulmonary blood flow.[169,170] Ventilation and perfusion maps of the lung can then be created using this information. Currently, FD techniques utilize a short echo dynamic steady state free precession lung image acquisition.[170] The limited work that has investigated the use of FDMRI in patients with asthma has shown similar information to hyperpolarized noble gas MRI after a bronchoconstriction challenge.[171] The first study to have used FDMRI to quantify pulmonary abnormalities in subjects with COPD demonstrated that the FDMRI derived ventilation measurements were associated with noble gas MRI ventilation abnormalities and CT derived measurements of emphysema.[172] Although FDMRI requires sophisticated post-processing methods, it is a promising method

for serial lung function measurements without the dependence of inhaled gases. Non-contrast enhanced ^{1}H MR methods such as UTE and FDMRI open up the opportunity for structural and functional lung imaging on clinically available MR systems for longitudinal monitoring of subjects with obstructive lung disease.

1.7 Thesis Hypotheses and Objectives

Pulmonary function tests are clinically used for the diagnosis, monitoring, and evaluation of response to therapy in patients with obstructive lung disease. These measurements, while important, conceal the regional contributions of underlying pathologies. Accordingly, a necessary goal of obstructive lung disease research is to develop ways to identify patients with specific underlying pathological phenotypes to further personalize medicine with the hopes to improve patient care and outcomes. Imaging methods such as thoracic CT and MRI have the potential to provide regional and quantitative biomarkers of obstructive lung disease. Before identifying patients with specific underlying pathological phenotypes, it is important to understand the physiological and clinical consequences of MR-derived measurements. Thus, the overarching objective of this thesis was to develop and evaluate lung structure and function measurements using multi-nuclear pulmonary MRI in older never-smokers and obstructive lung disease to provide an understanding of the physiological and clinical etiology of these MR-derived measurements. In **Chapter 2**, an understanding of healthy aging was first developed using hyperpolarized noble gas MRI. Following this, a non-contrast enhanced UTE MR method was developed and its reproducibility was evaluated. This method was then used to evaluate patients with COPD (**Chapter 3**) and asthma (**Chapter 4**) to determine the physiological and clinical consequences of UTE-derived measurements. The objectives and hypotheses specific to each chapter are described below.

In Chapter 2, our objective was to determine the physiological consequences and potential relevance of ventilation abnormalities in older never-smokers. We evaluated the response of bronchodilation (i.e. deep inspiration and salbutamol) on these defects and the relationship of ventilation defects with occupational exposures, pulmonary function, and exercise capacity. Based on previous work in young healthy volunteers where ventilation

defects resolved after deep inspiration, we hypothesized that in older never-smokers, narrowed or collapsed airways were responsible for persistent ventilation defects, and these would be responsive to and improve following deep inspiration.

In Chapter 3, our objective was to develop a UTE MR method, evaluate its reproducibility, and use this method to evaluate pulmonary abnormalities in COPD patients with and without bronchiectasis. We also evaluated the relationship between UTE-derived measurements with CT scan measurements and pulmonary function tests to better understand the underlying determinants of signal-intensity measurements in COPD and bronchiectasis. We hypothesized that pulmonary UTE MRI signal-intensity would have high short-term reproducibility and be related to CT radiodensity and pulmonary function test measurements in COPD patients with and without bronchiectasis.

In Chapter 4, our objective was to determine the underlying structural and clinical determinants of UTE-derived signal-intensity measurements in asthma by evaluating well-established clinical and emerging imaging (hyperpolarized noble gas MRI and CT) measurements in asthmatics. These patients shared some airway and inflammatory features common in COPD and bronchiectasis. We hypothesized that UTE-derived biomarkers that merge information acquired at different lung volumes could be generated to capture evidence of regional ventilation heterogeneity and these measurements would be related to gas-trapping and/or airway flow obstruction in patients with asthma.

In Chapter 5, an overview and summary of the important findings and conclusions of Chapters 2-4 is provided. The study specific and general limitations of these studies will be discussed and some potential solutions. The thesis concludes with an outline of future studies that can build on the work presented in this thesis.

1.8 References

(1) Vestbo, J. *et al.* Global strategy for the diagnosis, management, and prevention of chronic obstructive pulmonary disease: GOLD executive summary. *Am J Respir Crit Care Med* 2013; 187: 347-365.

(2) Global Initiative for Asthma. *Global Initiative for Asthma: Global Strategy for Asthma Management and Prevention*, <http://www.ginasthma.org/> (2015).

(3) World Health Organization. Global Burden of Disease: Disease Incidence, Prevalence, and Disability. (2004). <http://www.who.int/healthinfo/global_burden_disease/GBD_report_2004update_part3.pdf>.

(4) Global Alliance against Chronic Respiratory Diseases. *World Health Organization Asthma Fact Sheet N 307*, <http://www.who.int/mediacentre/factsheets/fs307/en/> (2013).

(5) World Health Organization. Global Health Estimates 2014 Summary Tables: Death by Cause, Age and Sex, 2000-2012. (2014). <http://www.who.int/healthinfo/global_burden_disease/en/>.

(6) Statistics Canada. (ed CANSIM) (Statistics Canada, Ottawa, Ontario, 2015).

(7) Gershon, A. S., Wang, C., Wilton, A. S., Raut, R. & To, T. Trends in chronic obstructive pulmonary disease prevalence, incidence, and mortality in Ontario, Canada, 1996 to 2007: a population-based study. *Archives of internal medicine* 2010; 170: 560-565.

(8) Gershon, A. S., Warner, L., Cascagnette, P., Victor, J. C. & To, T. Lifetime risk of developing chronic obstructive pulmonary disease: a longitudinal population study. *The Lancet* 2011; 378: 991-996.

(9) Canadian Institute for Health Information. Emergency Department Visits in 2014-2015. (2015). <https://secure.cihi.ca/free_products/NACRS_ED_QuickStats_Infosheet_2014-15_ENweb.pdf>.

(10) Canadian Institute for Health Information. Health Indicators 2008. (CIHI, Ottawa, 2008).

(11) Crighton, E. J., Ragetlie, R., Luo, J., To, T. & Gershon, A. A spatial analysis of COPD prevalence, incidence, mortality and health service use in Ontario. *Health Rep* 2015; 26: 10-18.

(12) OASIS. *OASIS: Asthma Infographic*, <http://lab.research.sickkids.ca/oasis/oasis-statistics/> (2015).

(13) To, T. *et al.* Progression from Asthma to Chronic Obstructive Pulmonary Disease. Is Air Pollution a Risk Factor? *Am J Respir Crit Care Med* 2016; 194: 429-438.

(14) Larsen, K. *et al.* The Annual September Peak in Asthma Exacerbation Rates. Still a Reality? *Ann Am Thorac Soc* 2016; 13: 231-239.

(15) Smetanin, P. *et al.* Life and economic impact of lung disease in Ontario: 2011 to 2041. *Risk Analytica on Behalf of the Ontario Lung Association* 2011.

(16) West, J. B. *Respiratory Physiology the Essentials*. Ninth edn, (Lippincott Williams & Wilkins, 2012).

(17) Silverthorn, D. U. *Human Physiology An Integrated Approach 6th Edition*. (Pearson, 2013).

(18) Ochs, M. *et al.* The number of alveoli in the human lung. *Am J Respir Crit Care Med* 2004; 169: 120-124.

(19) Eric P. Widmaier, H. R., and Kevin T. Strang. *Human Physiology The Mechanisms of Body Function*. Ninth edn, (McGraw Hill, 2004).

(20) Weibel, E. R. *Geometry and dimensions of airways of conductive and transitory zones*. (Springer, 1963).

(21) Fick, A. V. On liquid diffusion. *The London, Edinburgh, and Dublin Philosophical Magazine and Journal of Science* 1855; 10: 30-39.

(22) Verbeken, E. *et al.* The senile lung. Comparison with normal and emphysematous lungs. 1. Structural aspects. *CHEST Journal* 1992; 101: 793-799.

(23) Sobin, S. S., Fung, Y. C. & Tremer, H. M. Collagen and elastin fibers in human pulmonary alveolar walls. *J Appl Physiol (1985)* 1988; 64: 1659-1675.

(24) Toshima, M., Ohtani, Y. & Ohtani, O. Three-dimensional architecture of elastin and collagen fiber networks in the human and rat lung. *Arch Histol Cytol* 2004; 67: 31-40.

(25) Mahler, D. A., Rosiello, R. A. & Loke, J. The aging lung. *Clin Geriatr Med* 1986; 2: 215-225.

(26) Janssens, J. P., Pache, J. C. & Nicod, L. P. Physiological changes in respiratory function associated with ageing. *Eur Respir J* 1999; 13: 197-205.

(27) Gillooly, M. & Lamb, D. Airspace size in lungs of lifelong non-smokers: effect of age and sex. *Thorax* 1993; 48: 39-43.

(28) Sharma, G. & Goodwin, J. Effect of aging on respiratory system physiology and immunology. *Clin Interv Aging* 2006; 1: 253-260.

(29) Enright, P. L., Kronmal, R. A., Manolio, T. A., Schenker, M. B. & Hyatt, R. E. Respiratory muscle strength in the elderly. Correlates and reference values. Cardiovascular Health Study Research Group. *Am J Respir Crit Care Med* 1994; 149: 430-438.

(30) Tolep, K., Higgins, N., Muza, S., Criner, G. & Kelsen, S. G. Comparison of diaphragm strength between healthy adult elderly and young men. *Am J Respir Crit Care Med* 1995; 152: 677-682.

(31) Yunginger, J. W. *et al.* A community-based study of the epidemiology of asthma. Incidence rates, 1964-1983. *Am Rev Respir Dis* 1992; 146: 888-894.

(32) Anderson, H. R., Pottier, A. C. & Strachan, D. P. Asthma from birth to age 23: incidence and relation to prior and concurrent atopic disease. *Thorax* 1992; 47: 537-542.

(33) Martinez, F. D. & Vercelli, D. Asthma. *Lancet* 2013; 382: 1360-1372.

(34) Mallol, J. *et al.* Heightened bronchial hyperresponsiveness in the absence of heightened atopy in children with current wheezing and low income status. *Thorax* 2008; 63: 167-171.

(35) Becklake, M. R. Occupational exposures: evidence for a causal association with chronic obstructive pulmonary disease. *Am Rev Respir Dis* 1989; 140: S85-91.

(36) Higgins, M. W. *et al.* An index of risk for obstructive airways disease. *Am Rev Respir Dis* 1982; 125: 144-151.

(37) Health, U. D. o. & Services, H. The health consequences of smoking: a report of the Surgeon General. *Atlanta, GA: US Department of Health and Human Services, Centers for Disease Control and Prevention, National Center for Chronic Disease Prevention and Health Promotion, Office on Smoking and Health* 2004; 62.

(38) Fletcher, C. & Peto, R. The natural history of chronic airflow obstruction. *Br Med J* 1977; 1: 1645-1648.

(39) Hamid, Q. *et al.* Inflammation of small airways in asthma. *J Allergy Clin Immunol* 1997; 100: 44-51.

(40) Saetta, M. & Turato, G. Airway pathology in asthma. *Eur Respir J Suppl* 2001; 34: 18s-23s.

(41) Tulic, M. K., Christodoulopoulos, P. & Hamid, Q. Small airway inflammation in asthma. *Respir Res* 2001; 2: 333-339.

(42) Mullen, J. B., Wright, J. L., Wiggs, B. R., Pare, P. D. & Hogg, J. C. Reassessment of inflammation of airways in chronic bronchitis. *Br Med J (Clin Res Ed)* 1985; 291: 1235-1239.

(43) Hogg, J. C. Pathophysiology of airflow limitation in chronic obstructive pulmonary disease. *Lancet* 2004; 364: 709-721.

(44) Saetta, M. *et al.* Inflammatory cells in the bronchial glands of smokers with chronic bronchitis. *Am J Respir Crit Care Med* 1997; 156: 1633-1639.

(45) Mead, J. The lung's "quiet zone". *N Engl J Med* 1970; 282: 1318-1319.

(46) Dayman, H. Mechanics of airflow in health and in emphysema. *J Clin Invest* 1951; 30: 1175-1190.

(47) Butler, J., Caro, C. G., Alcala, R. & Dubois, A. B. Physiological factors affecting airway resistance in normal subjects and in patients with obstructive respiratory disease. *J Clin Invest* 1960; 39: 584-591.

(48) Mead, J., Turner, J. M., Macklem, P. T. & Little, J. B. Significance of the relationship between lung recoil and maximum expiratory flow. *J Appl Physiol* 1967; 22: 95-108.

(49) Matsuba, K. & Thurlbeck, W. M. The number and dimensions of small airways in emphysematous lungs. *Am J Pathol* 1972; 67: 265-275.

(50) Snider, G. The definition of emphysema; report of a National Heart, Lung and Blood Institute. Division of Lung Diseases. Workshop. *Am Rev Respir Dis* 1985; 132: 182-185.

(51) Thurlbeck, W. M. & Muller, N. L. Emphysema: definition, imaging, and quantification. *AJR Am J Roentgenol* 1994; 163: 1017-1025.

(52) Thurlbeck, W. M. & Simon, G. Radiographic appearance of the chest in emphysema. *AJR Am J Roentgenol* 1978; 130: 429-440.

(53) Tetley, T. D. Inflammatory cells and chronic obstructive pulmonary disease. *Curr Drug Targets Inflamm Allergy* 2005; 4: 607-618.

(54) Saetta, M. Airway inflammation in chronic obstructive pulmonary disease. *Am J Respir Crit Care Med* 1999; 160: S17-20.

(55) Saetta, M. *et al.* CD8+ T-lymphocytes in peripheral airways of smokers with chronic obstructive pulmonary disease. *Am J Respir Crit Care Med* 1998; 157: 822-826.

(56) Miller, M. R. *et al.* Standardisation of spirometry. *Eur respir J* 2005; 26: 319-338.

(57) Wanger, J. *et al.* Standardisation of the measurement of lung volumes. *European Respiratory Journal* 2005; 26: 511.

(58) Macintyre, N. *et al.* Standardisation of the single-breath determination of carbon monoxide uptake in the lung. *European Respiratory Journal* 2005; 26: 720-735.

(59) Clayton, N. Review Series: Lung function made easy: Assessing lung size. *Chronic respiratory disease* 2007; 4: 151-157.

(60) Turner, J. M., Mead, J. & Wohl, M. E. Elasticity of human lungs in relation to age. *J Appl Physiol* 1968; 25: 664-671.

(61) Mayer, E., Blazsik, C. & Rappaport, I. Emphysema and the lungs of the aged: a clinical study; preliminary report. *Dis Chest* 1958; 34: 247-256.

(62) Lokke, A., Lange, P., Scharling, H., Fabricius, P. & Vestbo, J. Developing COPD: a 25 year follow up study of the general population. *Thorax* 2006; 61: 935-939.

(63) West, J. B. *Pulmonary pathophysiology: the essentials*. (Lippincott Williams & Wilkins, 2011).

(64) ATS/ACCP Statement on cardiopulmonary exercise testing. *Am J Respir Crit Care Med* 2003; 167: 211-277.

(65) Albouaini, K., Egred, M., Alahmar, A. & Wright, D. J. Cardiopulmonary exercise testing and its application. *Postgrad Med J* 2007; 83: 675-682.

(66) Celli, B. R. *et al.* The body-mass index, airflow obstruction, dyspnea, and exercise capacity index in chronic obstructive pulmonary disease. *N Engl J Med* 2004; 350: 1005-1012.

(67) Vestbo, J. *et al.* Evaluation of COPD Longitudinally to Identify Predictive Surrogate End-points (ECLIPSE). *Eur Respir J* 2008; 31: 869-873.

(68) Brenner, D. J. & Hall, E. J. Computed tomography--an increasing source of radiation exposure. *N Engl J Med* 2007; 357: 2277-2284.

(69) Hodson, M. E., Simon, G. & Batten, J. C. Radiology of uncomplicated asthma. *Thorax* 1974; 29: 296-303.

(70) Rebuck, A. S. Radiological aspects of severe asthma. *Australas Radiol* 1970; 14: 264-268.

(71) Kerley, P. Emphysema: (Section of Radiology). *Proc R Soc Med* 1936; 29: 1307-1324.

(72) Petheram, I. S., Kerr, I. & Collins, J. Value of chest radiographs in severe acute asthma. *Clinical radiology* 1981; 32: 281-282.

(73) Hodson, C. & Trickey, S. Bronchial wall thickening in asthma. *Clinical Radiology* 1960; 11: 182-191.

(74) DiMango, E. A., Lubetsky, H. & Austin, J. H. Assessment of bronchial wall thickening on posteroanterior chest radiographs in acute asthma. *J Asthma* 2002; 39: 255-261.

(75) Andersen, P. E., Jr., Andersen, L. H. & Jest, P. The chest radiograph in chronic obstructive lung disease compared with measurements of single-breath nitrogen washout and spirometry. *Clin Radiol* 1982; 33: 51-55.

(76) Rosenblum, L. J. *et al.* Density patterns in the normal lung as determined by computed tomography. *Radiology* 1980; 137: 409-416.

(77) Haaga, J. R. & Boll, D. *Computed tomography & magnetic resonance imaging of the whole body*. (Elsevier Health Sciences, 2008).

(78) Litmanovich, D. E., Hartwick, K., Silva, M. & Bankier, A. A. Multidetector computed tomographic imaging in chronic obstructive pulmonary disease: emphysema and airways assessment. *Radiol Clin North Am* 2014; 52: 137-154.

(79) Dendy, P. P. & Heaton, B. *Physics for diagnostic radiology*. (CRC Press, 2011).

(80) Mettler, F. A., Jr., Huda, W., Yoshizumi, T. T. & Mahesh, M. Effective doses in radiology and diagnostic nuclear medicine: a catalog. *Radiology* 2008; 248: 254-263.

(81) Lambert, L., Banerjee, R., Votruba, J., El-Lababidi, N. & Zeman, J. Ultra-low-dose CT Imaging of the Thorax: Decreasing the Radiation Dose by One Order of Magnitude. *Indian J Pediatr* 2016.

(82) Willemink, M. J. *et al.* Iterative reconstruction techniques for computed tomography part 2: initial results in dose reduction and image quality. *Eur Radiol* 2013; 23: 1632-1642.

(83) Busacker, A. *et al.* A multivariate analysis of risk factors for the air-trapping asthmatic phenotype as measured by quantitative CT analysis. *Chest* 2009; 135: 48-56.

(84) Okazawa, M. *et al.* Human airway narrowing measured using high resolution computed tomography. *Am J Respir Crit Care Med* 1996; 154: 1557-1562.

(85) Little, S. A. *et al.* High resolution computed tomographic assessment of airway wall thickness in chronic asthma: reproducibility and relationship with lung function and severity. *Thorax* 2002; 57: 247-253.

(86) Awadh, N., Muller, N. L., Park, C. S., Abboud, R. T. & FitzGerald, J. M. Airway wall thickness in patients with near fatal asthma and control groups: assessment with high resolution computed tomographic scanning. *Thorax* 1998; 53: 248-253.

(87) Mitsunobu, F. *et al.* Decreased computed tomographic lung density during exacerbation of asthma. *Eur Respir J* 2003; 22: 106-112.

(88) Gono, H., Fujimoto, K., Kawakami, S. & Kubo, K. Evaluation of airway wall thickness and air trapping by HRCT in asymptomatic asthma. *Eur Respir J* 2003; 22: 965-971.

(89) Nakano, Y. *et al.* The prediction of small airway dimensions using computed tomography. *Am J Respir Crit Care Med* 2005; 171: 142-146.

(90) Han, M. K. *et al.* Chronic obstructive pulmonary disease exacerbations in the COPDGene study: associated radiologic phenotypes. *Radiology* 2011; 261: 274-282.

(91) Grydeland, T. B. *et al.* Quantitative computed tomography measures of emphysema and airway wall thickness are related to respiratory symptoms. *Am J Respir Crit Care Med* 2010; 181: 353-359.

(92) Nakano, Y. *et al.* Computed tomographic measurements of airway dimensions and emphysema in smokers. Correlation with lung function. *Am J Respir Crit Care Med* 2000; 162: 1102-1108.

(93) Orlandi, I. *et al.* Chronic obstructive pulmonary disease: thin-section CT measurement of airway wall thickness and lung attenuation. *Radiology* 2005; 234: 604-610.

(94) Kim, V. *et al.* Airway wall thickness is increased in COPD patients with bronchodilator responsiveness. *Respir Res* 2014; 15: 84.

(95) Hayhurst, M. D. *et al.* Diagnosis of pulmonary emphysema by computerised tomography. *Lancet* 1984; 2: 320-322.

(96) Barnes, P. J., Drazen, J. M., Rennard, S. I. & Thomson, N. C. *Asthma and COPD: basic mechanisms and clinical management*. (Elsevier, 2009).

(97) Sakai, N., Mishima, M., Nishimura, K., Itoh, H. & Kuno, K. An automated method to assess the distribution of low attenuation areas on chest CT scans in chronic pulmonary emphysema patients. *Chest* 1994; 106: 1319-1325.

(98) Bankier, A. A., De Maertelaer, V., Keyzer, C. & Gevenois, P. A. Pulmonary emphysema: subjective visual grading versus objective quantification with macroscopic morphometry and thin-section CT densitometry. *Radiology* 1999; 211: 851-858.

(99) Park, K. J., Bergin, C. J. & Clausen, J. L. Quantitation of emphysema with three-dimensional CT densitometry: comparison with two-dimensional analysis, visual emphysema scores, and pulmonary function test results. *Radiology* 1999; 211: 541-547.

(100) Gevenois, P. A., de Maertelaer, V., De Vuyst, P., Zanen, J. & Yernault, J. C. Comparison of computed density and macroscopic morphometry in pulmonary emphysema. *Am J Respir Crit Care Med* 1995; 152: 653-657.

(101) Muller, N. L., Staples, C. A., Miller, R. R. & Abboud, R. T. "Density mask". An objective method to quantitate emphysema using computed tomography. *Chest* 1988; 94: 782-787.

(102) Coxson, H. O. *et al.* A quantification of the lung surface area in emphysema using computed tomography. *Am J Respir Crit Care Med* 1999; 159: 851-856.

(103) Owrangi, A. M., Etemad-Rezai, R., McCormack, D. G., Cunningham, I. A. & Parraga, G. Computed tomography density histogram analysis to evaluate pulmonary emphysema in ex-smokers. *Acad Radiol* 2013; 20: 537-545.

(104) Cerveri, I. *et al.* Assessment of emphysema in COPD: a functional and radiologic study. *Chest* 2004; 125: 1714-1718.

(105) Martinez, C. H. *et al.* Relationship between quantitative CT metrics and health status and BODE in chronic obstructive pulmonary disease. *Thorax* 2012; 67: 399-406.

(106) Smith-Bindman, R. *et al.* Use of diagnostic imaging studies and associated radiation exposure for patients enrolled in large integrated health care systems, 1996-2010. *JAMA* 2012; 307: 2400-2409.

(107) Argula, R. G., Strange, C., Ramakrishnan, V. & Goldin, J. Baseline regional perfusion impacts exercise response to endobronchial valve therapy in advanced pulmonary emphysema. *Chest* 2013; 144: 1578-1586.

(108) Stavngaard, T. *et al.* Hyperpolarized 3He MRI and 81mKr SPECT in chronic obstructive pulmonary disease. *Eur J Nucl Med Mol Imaging* 2005; 32: 448-457.

(109) Suga, K. *et al.* Dynamic pulmonary SPECT of xenon-133 gas washout. *J Nucl Med* 1996; 37: 807-814.

(110) King, G. G., Eberl, S., Salome, C. M., Meikle, S. R. & Woolcock, A. J. Airway closure measured by a technegas bolus and SPECT. *Am J Respir Crit Care Med* 1997; 155: 682-688.

(111) Mishkin, F. & Wagner, H. N., Jr. Regional abnormalities in pulmonary arterial blood flow during acute asthmatic attacks. *Radiology* 1967; 88: 142-144.

(112) Farrow, C. E. *et al.* Airway closure on imaging relates to airway hyperresponsiveness and peripheral airway disease in asthma. *J Appl Physiol (1985)* 2012; 113: 958-966.

(113) Sovijarvi, A. R., Poyhonen, L., Kellomaki, L. & Muittari, A. Effects of acute and long-term bronchodilator treatment on regional lung function in asthma assessed with krypton-81m and technetium-99m-labelled macroaggregates. *Thorax* 1982; 37: 516-520.

(114) Munkner, T. & Bundgaard, A. Regional V/Q changes in asthmatics after exercise. *Eur J Respir Dis Suppl* 1986; 143: 62-66.

(115) Munkner, T. & Bundgaard, A. Regional V/Q changes in asthmatics after antigen inhalation. *Eur J Respir Dis Suppl* 1986; 143: 44-47.

(116) Munkner, T. & Bundgaard, A. Regional V/Q changes in asthmatics after histamine inhalation. *Eur J Respir Dis Suppl* 1986; 143: 22-27.

(117) Bajc, M. *et al.* Grading obstructive lung disease using tomographic pulmonary scintigraphy in patients with chronic obstructive pulmonary disease (COPD) and long-term smokers. *Ann Nucl Med* 2015; 29: 91-99.

(118) Norberg, P. *et al.* Quantitative lung SPECT applied on simulated early COPD and humans with advanced COPD. *EJNMMI Res* 2013; 3: 28.

(119) Suga, K., Iwanaga, H., Tokuda, O., Okada, M. & Matsunaga, N. Intrabullous ventilation in pulmonary emphysema: assessment with dynamic xenon-133 gas SPECT. *Nucl Med Commun* 2012; 33: 371-378.

(120) Jogi, J., Ekberg, M., Jonson, B., Bozovic, G. & Bajc, M. Ventilation/perfusion SPECT in chronic obstructive pulmonary disease: an evaluation by reference to symptoms, spirometric lung function and emphysema, as assessed with HRCT. *Eur J Nucl Med Mol Imaging* 2011; 38: 1344-1352.

(121) Suga, K. *et al.* Lung ventilation-perfusion imbalance in pulmonary emphysema: assessment with automated V/Q quotient SPECT. *Ann Nucl Med* 2010; 24: 269-277.

(122) Jones, H. A., Marino, P. S., Shakur, B. H. & Morrell, N. W. In vivo assessment of lung inflammatory cell activity in patients with COPD and asthma. *Eur Respir J* 2003; 21: 567-573.

(123) Jones, H. A. *et al.* In vivo measurement of neutrophil activity in experimental lung inflammation. *Am J Respir Crit Care Med* 1994; 149: 1635-1639.

(124) Senda, M., Murata, K., Itoh, H., Yonekura, Y. & Torizuka, K. Quantitative evaluation of regional pulmonary ventilation using PET and nitrogen-13 gas. *J Nucl Med* 1986; 27: 268-273.

(125) Harris, R. S. *et al.* 18F-FDG uptake rate is a biomarker of eosinophilic inflammation and airway response in asthma. *J Nucl Med* 2011; 52: 1713-1720.

(126) Venegas, J. G. *et al.* Self-organized patchiness in asthma as a prelude to catastrophic shifts. *Nature* 2005; 434: 777-782.

(127) Vidal Melo, M. F. *et al.* Spatial heterogeneity of lung perfusion assessed with (13)N PET as a vascular biomarker in chronic obstructive pulmonary disease. *J Nucl Med* 2010; 51: 57-65.

(128) Brudin, L. H. *et al.* Regional structure-function correlations in chronic obstructive lung disease measured with positron emission tomography. *Thorax* 1992; 47: 914-921.

(129) Albertine, K. Structural organization and quantitative morphology of the lung. *Application of magnetic resonance to the study of lung. Futura, Armonk, New York, USA* 1996; 73-114.

(130) Albert, M. S. *et al.* Biological magnetic resonance imaging using laser-polarized 129Xe. *Nature* 1994; 370: 199-201.

(131) Kauczor, H.-U. *MRI of the Lung*. (2009).

(132) Neil James Stewart, H.-F. C., Guilhem Jean Collier, Felix Clemens Horn, Graham Norquay, Juan Parra-Robles, Denise Yates, Paul Collini, Rod Lawson, Helen Marshall, and Jim Michael Wild. in *International Society of Magnetic Resonance in Medicine 24th Annual Meeting.*

(133) Roos, J. E., McAdams, H. P., Kaushik, S. S. & Driehuys, B. Hyperpolarized Gas MR Imaging: Technique and Applications. *Magn Reson Imaging Clin N Am* 2015; 23: 217-229.

(134) Saam, B. T. Magnetic resonance imaging with laser-polarized noble gases. *Nat Med* 1996; 2: 358-359.

(135) Kirby, M. *et al.* Hyperpolarized 3He magnetic resonance functional imaging semiautomated segmentation. *Acad Radiol* 2012; 19: 141-152.

(136) Mathew, L. *et al.* Hyperpolarized 3He magnetic resonance imaging of chronic obstructive pulmonary disease: reproducibility at 3.0 tesla. *Acad Radiol* 2008; 15: 1298-1311.

(137) Kirby, M. *et al.* Quantitative evaluation of hyperpolarized helium-3 magnetic resonance imaging of lung function variability in cystic fibrosis. *Acad Radiol* 2011; 18: 1006-1013.

(138) Kirby, M. *et al.* Chronic obstructive pulmonary disease: quantification of bronchodilator effects by using hyperpolarized (3)He MR imaging. *Radiology* 2011; 261: 283-292.

(139) Svenningsen, S. *et al.* Hyperpolarized He and Xe MRI: Differences in asthma before bronchodilation. *J Magn Reson Imaging* 2013.

(140) Kirby, M. *et al.* Chronic obstructive pulmonary disease: longitudinal hyperpolarized (3)He MR imaging. *Radiology* 2010; 256: 280-289.

(141) Svenningsen, S. *et al.* Pulmonary functional magnetic resonance imaging: asthma temporal-spatial maps. *Acad Radiol* 2014; 21: 1402-1410.

(142) Parraga, G., Mathew, L., Etemad-Rezai, R., McCormack, D. G. & Santyr, G. E. Hyperpolarized 3He magnetic resonance imaging of ventilation defects in healthy elderly volunteers: initial findings at 3.0 Tesla. *Acad Radiol* 2008; 15: 776-785.

(143) Aysola, R., de Lange, E. E., Castro, M. & Altes, T. A. Demonstration of the heterogeneous distribution of asthma in the lungs using CT and hyperpolarized helium-3 MRI. *J Magn Reson Imaging* 2010; 32: 1379-1387.

(144) de Lange, E. E. *et al.* Evaluation of asthma with hyperpolarized helium-3 MRI: correlation with clinical severity and spirometry. *Chest* 2006; 130: 1055-1062.

(145) Svenningsen, S. *et al.* What are ventilation defects in asthma? *Thorax* 2014; 69: 63-71.

(146) Kirby, M., Kanhere, N., Etemad-Rezai, R., McCormack, D. G. & Parraga, G. Hyperpolarized helium-3 magnetic resonance imaging of chronic obstructive pulmonary disease exacerbation. *J Magn Reson Imaging* 2013; 37: 1223-1227.

(147) Svenningsen, S., Nair, P., Guo, F., McCormack, D. G. & Parraga, G. Is ventilation heterogeneity related to asthma control? *Eur Respir J* 2016.

(148) Capaldi, D. P. *et al.* Pulmonary Imaging Biomarkers of Gas Trapping and Emphysema in COPD: (3)He MR Imaging and CT Parametric Response Maps. *Radiology* 2016; 279: 597-608.

(149) Fain, S. B. *et al.* Detection of age-dependent changes in healthy adult lungs with diffusion-weighted 3He MRI. *Acad Radiol* 2005; 12: 1385-1393.

(150) Wang, C. *et al.* Assessment of the lung microstructure in patients with asthma using hyperpolarized 3He diffusion MRI at two time scales: comparison with healthy subjects and patients with COPD. *J Magn Reson Imaging* 2008; 28: 80-88.

(151) Trampel, R. *et al.* Diffusional kurtosis imaging in the lung using hyperpolarized 3He. *Magn Reson Med* 2006; 56: 733-737.

(152) Fain, S. *et al.* in *Proc Intl Soc Mag Reson Med.* 335.

(153) Costella, S. *et al.* Regional pulmonary response to a methacholine challenge using hyperpolarized (3)He magnetic resonance imaging. *Respirology* 2012; 17: 1237-1246.

(154) Kirby, M. *et al.* Hyperpolarized 3He and 129Xe MR imaging in healthy volunteers and patients with chronic obstructive pulmonary disease. *Radiology* 2012; 265: 600-610.

(155) Salerno, M. *et al.* Emphysema: Hyperpolarized Helium 3 Diffusion MR Imaging of the Lungs Compared with Spirometric Indexes—Initial Experience 1. *Radiology* 2002; 222: 252-260.

(156) Woods, J. C. *et al.* Hyperpolarized 3He diffusion MRI and histology in pulmonary emphysema. *Magn Reson Med* 2006; 56: 1293-1300.

(157) Kirby, M., Heydarian, M., Wheatley, A., McCormack, D. G. & Parraga, G. Evaluating bronchodilator effects in chronic obstructive pulmonary disease using diffusion-weighted hyperpolarized helium-3 magnetic resonance imaging. *J Appl Physiol* 2012; 112: 651-657.

(158) Bergin, C. J., Noll, D. C., Pauly, J. M., Glover, G. H. & Macovski, A. MR imaging of lung parenchyma: a solution to susceptibility. *Radiology* 1992; 183: 673-676.

(159) Bergin, C. J., Glover, G. M. & Pauly, J. Magnetic resonance imaging of lung parenchyma. *J Thorac Imaging* 1993; 8: 12-17.

(160) Ohno, Y. *et al.* T2* measurements of 3-T MRI with ultrashort TEs: capabilities of pulmonary function assessment and clinical stage classification in smokers. *AJR Am J Roentgenol* 2011; 197: W279-285.

(161) Ohno, Y. *et al.* Pulmonary MR imaging with ultra-short TEs: utility for disease severity assessment of connective tissue disease patients. *Eur J Radiol* 2013; 82: 1359-1365.

(162) Bergin, C. J., Pauly, J. M. & Macovski, A. Lung parenchyma: projection reconstruction MR imaging. *Radiology* 1991; 179: 777-781.

(163) Gatehouse, P. D. & Bydder, G. M. Magnetic Resonance Imaging of Short T2 Components in Tissue. *Clinical Radiology* 2003; 58: 1-19.

(164) Roach, D. J. *et al.* Morphological and quantitative evaluation of emphysema in chronic obstructive pulmonary disease patients: A comparative study of MRI with CT. *J Magn Reson Imaging* 2016.

(165) Ble, F. X. *et al.* Allergen-induced lung inflammation in actively sensitized mice assessed with MR imaging. *Radiology* 2008; 248: 834-843.

(166) Vogel-Claussen, J. *et al.* Quantification of pulmonary inflammation after segmental allergen challenge using turbo-inversion recovery-magnitude magnetic resonance imaging. *Am J Respir Crit Care Med* 2014; 189: 650-657.

(167) Takahashi, M. *et al.* Ultra-short echo time (UTE) MR imaging of the lung: comparison between normal and emphysematous lungs in mutant mice. *J Magn Reson Imaging* 2010; 32: 326-333.

(168) Zurek, M., Boyer, L., Caramelle, P., Boczkowski, J. & Crémillieux, Y. Longitudinal and noninvasive assessment of emphysema evolution in a murine model using proton MRI. *Magnetic Resonance in Medicine* 2012; 68: 898-904.

(169) Bauman, G. *et al.* Non-contrast-enhanced perfusion and ventilation assessment of the human lung by means of fourier decomposition in proton MRI. *Magn Reson Med* 2009; 62: 656-664.

(170) Lederlin, M. *et al.* Functional MRI using Fourier decomposition of lung signal: reproducibility of ventilation- and perfusion-weighted imaging in healthy volunteers. *Eur J Radiol* 2013; 82: 1015-1022.

(171) Capaldi, D. P. *et al.* in *A19. GETTING POLARIZED: MR IMAGING IN OBSTRUCTIVE LUNG DISEASE* A1055-A1055 (Am Thoracic Soc, 2016).

(172) Capaldi, D. P. *et al.* Free-breathing pulmonary 1H and Hyperpolarized 3He MRI: comparison in COPD and bronchiectasis. *Acad Radiol* 2015; 22: 320-329.

CHAPTER 2

2 PULMONARY VENTILATION DEFECTS IN OLDER NEVER-SMOKERS

To better understand the physiological consequences and potential relevance of ^{3}He MRI ventilation defects in aging, we evaluated ^{3}He MRI ventilation defects in older never-smokers before and after bronchodilation administration. To identify the potential determinants of ventilation defects, we also evaluated dyspnea, pulmonary function, and exercise test measurements.

The contents of this chapter were previously published in the Journal of Applied Physiology: K Sheikh, GA Paulin, S Svenningsen, M Kirby, NAM Paterson, DG McCormack, and G Parraga. Pulmonary Ventilation Defects in Older Never-Smokers. J Appl Physiol 2014; 117(3):297-306. Permission to reproduce this article was granted by The American Physiological Society and is provided in Appendix A.

2.1 Introduction

Pulmonary aging is concomitant with changes in elastic recoil,[1-3] chest wall compliance,[1,3] and respiratory muscle strength.[4,5] In concert with these physiological changes, functional residual capacity (FRC), residual volume (RV), and airways resistance (Raw) also increase,[4] whereas the forced expiratory volume in one second (FEV_1), forced vital capacity (FVC)[6] and inspiratory capacity (IC) decrease.[7]

Healthy older adults may experience breathlessness during everyday activities[8-12] and this is related to mortality risk.[8,9,12] In addition, in older adults, cardiopulmonary exercise test (CPET) measurements[13] correlate more strongly with overall health status than do measurements of resting lung function.[14-16] Moreover, CPET measurements show that in "normal" healthy aging, there is lower exercise-related oxygen uptake (VO_2) as well as greater minute ventilation (V_E), and increased respiratory exchange ratio (RER).[17-19] Recent studies have also shown that during exercise, significant ventilatory impairment is possible without increased dyspnea or premature exercise limitation.[20]

The role of occupational and second-hand tobacco smoke exposure is important to acknowledge and understand in both normal and accelerated lung aging. In this context, the Burden of Obstructive Lung Disease (BOLD) study[21] showed that in never-smokers,

the prevalence of airflow limitation consistent with chronic obstructive pulmonary disease (COPD) was as high as 30%. The BOLD study also revealed the critical relationships in never-smokers between airflow limitation and age, history of occupational exposure and childhood respiratory disease.[22]

^{3}He ventilation magnetic resonance imaging (MRI) provides high resolution, non-invasive measurements of lung function,[23,24] and identifies those regions of the lung that participate in ventilation and those that do not.[24,25] In healthy young subjects, a single inhalation of hyperpolarized ^{3}He gas results in homogeneous lung filling, but in older never-smokers, characteristic "focal" ventilation defects are observed, corresponding to poorly ventilated lung regions.[23,25] In older never-smokers, ventilation defects are commonly observed on the lung periphery and the dependent lung regions, and this is in contrast with COPD and asthma, where numerous and large defects are heterogeneously distributed throughout the lung.[23,24,26]

The finding of spatially and temporally-persistent ^{3}He MRI ventilation defects in older never-smokers with normal spirometry[23,25] raises questions about the physiological meaning of ventilation defects in all subjects. For example, as previously shown, ^{3}He MRI ventilation abnormalities induced by methacholine challenge in young healthy volunteers were reversed by deep inspiration (DI).[27] In young asthmatics, salbutamol inhalation reduced ventilation defects observed with ^{3}He MRI after methacholine challenge,[28] but the effect of DI was not investigated. Airway resistance measurements determined that asthmatic subjects cannot maximally dilate their airways and that the dilation that does occur after DI constricts back to baseline much faster than in healthy subjects.[29] This suggested that in asthma, ventilation defects were related to salbutamol-responsive airway abnormalities, whereas in healthy volunteers, ventilation defects may reflect "normal" airway smooth muscle behaviour that is reversible using DI.

We hypothesized that in older never-smokers, narrowed or collapsed airways were responsible for the persistent ventilation defects observed and these would be responsive to, and improve following DI. To test this hypothesis, we evaluated the effect of both DI and salbutamol on ^{3}He ventilation defects in a relatively large group of older never-smokers

with no history of respiratory disease. We also evaluated the relationship of ventilation defects with occupational exposures, pulmonary function and cardiopulmonary exercise test measurements.

2.2 Materials and Methods

2.2.1 Study Subjects and Logistics

All subjects provided written informed consent to a study protocol approved by a local research ethics board and Health Canada. Subjects were enrolled between the ages of 60 and 90 years with a smoking history of < 0.5 pack-years and no history of chronic respiratory or cardiovascular disease. After providing consent, all subjects made a single 2-3 hour visit and underwent the following evaluations in the same order: 1) Burden of Obstructive Lung Disease (BOLD) occupational questionnaire,[5] 2) spirometry, 3) plethysmography and the diffusing capacity of carbon monoxide (DL_{CO}), 4) CPET including dyspnea score, and, 5) MRI. Pulmonary function tests were completed in approximately 45 minutes followed by CPET that was completed in 10-15 minutes. MRI was performed following CPET and for subjects who did not have ventilation defects and those with defects that responded to DI, MRI was completed within 10-15 minutes. For subjects who were administered salbutamol, MRI was performed 25-30 minutes post salbutamol inhalation.

2.2.2 Questionnaires

All subjects completed the BOLD occupational questionnaire[21] with exposures defined as previously described[22] including: 1) organic dust (farming; flour, feed or grain milling and cotton or jute processing), 2) inorganic dust (working with asbestos; hard-rock mining; coal mining; sandblasting and foundry or steel milling), and, 3) irritant gases (welding; firefighting; chemical or plastics manufacturing). We also directly queried subjects about spousal and/or life-partner smoking history and recorded potential household 2nd hand-smoke exposure.

2.2.3 Pulmonary Function and Cardiopulmonary Exercise Tests

Spirometry was performed using an ndd EasyOne spirometer (ndd Medizintechnik, Zurich) according to American Thoracic Society (ATS) guidelines. Body plethysmography was performed for the measurement of lung volumes and DL_{CO} was measured using the gas analyser (Medgraphics Corporation, St. Paul, MN). Inspiratory capacity (IC), defined as the volume change recorded at the mouth when taking a slow full inspiration from a position of passive end-expiration, was measured using body plethysmography[31] as was airways resistance (Raw), defined as the pressure difference per unit flow. Post-DI pulmonary function tests were not performed but for subjects administered salbutamol, FEV_1 and FVC were recorded 35-40 minutes post-inhalation and upon completion of MRI.

After completion of pulmonary function tests, all subjects performed CPET using a cycle ergometer (MedGraphics Ultima PFX, MedGraphics Corporation) according to ATS guidelines 14 with a two minute warm-up with no resistance, followed by a 20 watt incremental increase in work rate. Subjects were required to pedal at a frequency of 60 rpm with increasing work rate until the ventilatory anaerobic threshold was reached. Ventilatory anaerobic threshold was defined as the time when CO_2 production increased disproportionately in relation to O_2 consumption. The ventilatory anaerobic threshold was determined by onboard software for the CPET unit which used an iterative regression and analysis of slope. Subjects continued exercise until fatigue was reported. Oxygen uptake (VO_2), respiratory exchange ratio (RER), work rate (i.e. power) as well as minute ventilation (V_E) were measured at rest, at the ventilatory anaerobic threshold, and when maximum pulmonary O_2 uptake was reached. The time taken to reach VO_2max was also recorded. CPET measurements including VO_2, power, and V_E were adjusted for age, sex, and height using percent predicted values previously reported.[17,18,30] Borg dyspnea and leg discomfort scales were used before and after exercise.

2.2.4 Image Acquisition

MRI was performed after completion of all pulmonary function and cardiopulmonary exercise tests on a 3.0 Tesla MR750 (General Electric Health Care (GEHC), Milwaukee, WI) system as previously described[23] using a whole-body gradient set with maximum

gradient amplitude of 1.94 G/cm and a single-channel rigid elliptical transmit/receive chest coil (Rapid Biomedical GmbH, Germany). For both ^{1}H and ^{3}He MRI, subjects were instructed to inhale a gas mixture from a 1.0-liter Tedlar bag (Jensen Inert Products, Coral Springs, FL) from FRC, and image acquisition was performed during a 16 second breath-hold. Coronal (anatomical) ^{1}H MRI was performed using the whole-body RF coil and ^{1}H fast-spoiled, gradient-recalled echo sequence using a partial echo (16s total data acquisition, repetition time (TR)/echo time (TE)/flip angle = 4.7ms/1.2ms/30°, field-of-view (FOV)=40×40cm, bandwidth=24.4 kHz, matrix=128×80, 15-17 slices, 15mm slice thickness, 0 gap), as previously described.[23] ^{3}He MRI static ventilation images were acquired using a fast gradient-echo method using a partial echo (14s total data acquisition; TR/TE/flip angle = 4.3ms/1.4ms/7°, FOV = 40×40cm, bandwidth=48.8 kHz, matrix= 128×80, 15-17 slices, 15mm slice thickness, 0 gap).

Immediately after image acquisition, at the scanner while the subject was still in position, ^{3}He static ventilation images were qualitatively evaluated for ventilation abnormalities by a single trained observer. If ^{3}He gas was homogeneously distributed throughout the lung and there were no visible ventilation defects, the subjects were classified as belonging to the no defect group and the session was deemed complete. In contrast, if ^{3}He gas was heterogeneously distributed throughout the lung and/or there were visually obvious ventilation defects, the subject was classified as having ventilation defect(s). Upon qualitative inspection, subjects with visually obvious ventilation defects were instructed to perform DI. They were instructed to sit up whilst remaining on the scanner bed and take four deep breaths in through their nose and out through their mouth. Imaging was performed immediately following DI. If defects persisted following DI, the subject inhaled four puffs (400 µg) of salbutamol while seated upright, and 25 minutes later imaging was performed on a final occasion.

2.2.5 Image Analysis

Based on visual inspection at the scanner, subjects were classified as: 1) no defects—those subjects without visually obvious ventilation defects, 2) subjects with ventilation defects that responded to DI or salbutamol, and, 3) subjects with ventilation defects that did not

respond to DI or salbutamol. ^{3}He MRI semi-automated segmentation was performed, as previously described,[31] to generate ventilation defect percent (VDP) – the ventilation defect volume (VDV) normalized to ^{1}H MRI thoracic cavity volume (TCV). Briefly, ^{3}He static ventilation images were segmented using a k-means approach that classified voxel intensity values into five clusters ranging from signal void (cluster 1[C1] or VDV) and hypo-intense (cluster 2 [C2]) to hyper-intense signal (cluster 5 [C5]), therefore, generating a gas distribution cluster-map. For delineation of the ventilation defect boundaries, a seeded region-growing algorithm was used to segment the ^{1}H MRI thoracic cavity for registration to the cluster-map, as previously described.[31]

Ventilation heterogeneity was estimated according to a previously described method[27] using the coefficient of variation (COV). A local COV, rather than a global COV, was generated[27] to ensure local ventilation heterogeneity was not ignored. Briefly, for each voxel in a region of interest (ROI) a local ventilation heterogeneity value was calculated by computing the COV of the signal intensity in a 5×5 voxel neighbourhood which corresponded to a 244 mm^2 area centred on that voxel. To ensure that the 5×5 voxel neighbourhood did not include voxels that were outside of the lungs, a signal-to-noise threshold of five was established. For example, any voxels that were in a neighbourhood with an overall signal-to-noise ratio of less than five were excluded from the COV computation. COV of the lung was calculated for each subject as in **Equation 2-1**:

Equation 2-1

$$COV = \frac{\sqrt{\sum_{i=1}^{i=N} \frac{\sigma_i^2}{N}}}{\frac{\sum_{i=1}^{i=N} \mu_i}{N}}$$

where σ_i is the standard deviation of the signal intensity of the 5×5 voxel neighbourhood, μ_i is the mean signal intensity of the 5×5 voxel neighbourhood, and N is the number of ventilation ROIs in the lung. The ventilated lung ROI was defined as gas distribution cluster-map clusters C2-C5.

We also measured regional differences in VDP for the centre nine 15mm thick slices using several different measurements as shown in **Figure 2-1**. The VDP gradient in the posterior-anterior direction was defined as the slope of the line that described the change in VDP from the most posterior slice in centimeters over the nine central slices (with a slice thickness of 15mm each). The centre nine slices were used to ensure the static ventilation slices across subjects had adequate signal-to-noise ratios (i.e. SNR>10) for VDP calculations as well as to maintain an equal number of slices among all subjects. To calculate the gradient in the superior-inferior (SI) direction, the centre nine coronal slices were reformatted into 15mm axial slices. The VDP SI gradient was defined as the slope of the line that described the change in VDP over the axial superior-inferior slices. In addition, the VDP difference between the most posterior and anterior slices (VDP ΔPA) was calculated as was the VDP difference between the most superior and inferior slices (VDP ΔSI) of the central nine slices. The ventilation defect percent located on the peripheral boundary of the lung (relative peripheral VDP) was estimated as the ratio of the ventilation defect volume for the outermost 10 voxels of each slice (not including boundary voxels defined as SNR <2) to the ^{1}H MRI thoracic cavity volume. The proportion of ventilation defects located on the peripheral boundary was quantified as the ratio of peripheral lung VDV to whole lung VDV (i.e. VDV_{Per}/VDV_{WL}).

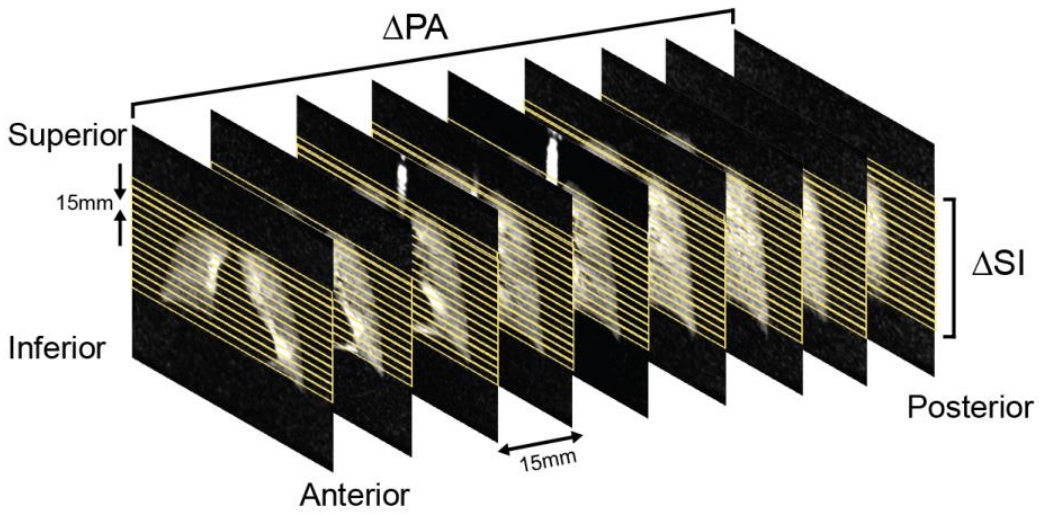

Figure 2-1 Schematic for regional evaluation of ^{3}He MRI ventilation-defect percent (VDP) The central coronal static ventilation image slices (9 × 15 mm) were evaluated. The lung was also divided into 15-mm slices in the axial direction. The VDP ΔSI was defined as the

difference between the most superior slice and the most inferior slice. The VDP ΔPA was defined as the difference between the most posterior slice and the most anterior slice.

2.2.6 Statistical Analysis

Analysis of variance (ANOVA), multivariate regression and post-hoc analysis using the Holm Bonferroni correction 32 were performed using SPSS 20.0 (IBM, Armonk, NY). Paired sample t-tests were performed to determine the differences in VDP ΔPA and VDP ΔSI using SPSS 20.0. We used the NHANES III reference standards[33] for percent predicted values. Univariate relationships were determined using regression (r^2) and Pearson correlation coefficients (r) for all subjects with GraphPad Prism V.6.00 (GraphPad Software Inc, La Jolla, CA). Stepwise multivariate regression was used to identify the predictors of VDP. The variables considered for modelling were chosen based on statistically significant univariate relationships with VDP. Results were considered statistically significant when the probability of making a Type I error was less than 5% ($p<0.05$).

2.3 Results

2.3.1 Subject Data

As summarized in **Table 2-1** (and a detailed subject listing in **Table 2-2**), 52 never-smokers (71±6 years) completed all measurements during a single visit. In total there were 13/52 (25%) subjects without ^{3}He MRI ventilation defects and 39/52 (75%) with ventilation defects. Of those subjects with ventilation defects, six (6/39, 15%) showed a VDP response (i.e. visually obvious and quantitative decrease in VDP) to DI (n=4) or salbutamol (n=2).

Table 2-1 Baseline subject demographic and other measurements.

		Ventilation Defects (n = 39)		Significance of Difference
	No Defects	Imaging Response	No Imaging Response	(p-value)*
	(n=13)	(n=6)	(n=33)	ND-IR-NIR
Demographics				
Age yrs (±SD)	71 (8)	72 (4)	71 (6)	0.90
Male n	6	3	12	
BMI kg/m^2 (±SD)	26 (4)	27 (3)	26 (3)	0.90
Occupational Exposures				
Organic Dust n	3	1	4	
Inorganic Dust n	0	2	2	
Irritant Gases n	0	0	1	
Pulmonary Function				
FEV_1 $\%_{pred}$ (±SD)	113 (11)	93 (29)	106 (20)	0.09
FVC $\%_{pred}$ (±SD)	107 (15)	96 (26)	103 (17)	0.40
FEV_1/FVC % (±SD)	80 (5)	71 (4) **	77 (5)	**0.004**
FRC $\%_{pred}$ (±SD)	105 (24)	114 (15)	107 (17)	0.60
IC $\%_{pred}$ (±SD)	112 (20)	94 (26)	106 (19)	0.20
RV/TLC % (±SD)	41 (7)	43 (15)	41 (7)	0.50
DL_{CO} $\%_{pred}$ (±SD)	96 (7)	75 (13)	92 (19)	0.07
Raw $\%_{pred}$ (±SD)	71 (25)	100 (82)	72 (31)	0.20
CPET				
VO_2max $\%_{pred}$ (±SD)	83 (18)	86 (11)	87 (19)	0.80
RER (±SD)	1.17 (0.15)	1.19 (0.11)	1.21 (0.12)	0.90
Power $\%_{pred}$ (±SD)	126 (38)	118 (9)	121 (31)	0.70
V_{Emax} $\%_{pred}$ (±SD)	50 (17)	54 (19)	51 (16)	0.90
Post Exercise Dyspnea (±SD)	2.1 (1.4)	2.0 (1.0)	2.3 (1.6)	0.80
Post Exercise Leg discomfort (±SD)	11.5 (2.4)	11.0 (3.7)	10.9 (3.3)	0.90
Time to VO_2max s (±SD)	478 (89)	532 (111)	494 (82)	0.50
MRI				
VDP % (±SD)	1.6 (0.7)	5.8 (3.8) **	2.6 (1.2)	**<0.001**
^{3}He COV (±SD)	0.19 (0.01)	0.24 (0.04) **	0.21 (0.02)	**0.001**
VDP ΔPA % (±SD)	0.7 (2.7)	11.2 (13.5) **	1.5 (4.0)	**0.001**
PA VDP Gradient %/cm (±SD)	-0.02 (0.17)	-0.69 (0.93) **	-0.05 (0.21)	**<0.001**
VDP ΔSI % (±SD)	-1.9 (1.3)	-3.4 (9.6)	-2.8 (2.3)	0.67
SI VDP Gradient %/cm (±SD)	0.14 (0.1)	0.26 (0.72)	0.21 (0.17)	0.67
Relative Peripheral VDP % (±SD)	1.3 (0.6)	3.3 (1.8) **	1.9 (0.8)	**0.001**
VDV_{Per}/VDV_{WL} % (±SD)	80 (10)	68 (13)	78 (10)	0.05

Imaging response refers to subjects with change in VDP after DI or salbutamol. No Imaging Response refers to subjects with no VDP change after salbutamol; IR=imaging response; NIR=imaging non-responders; NR=non responders. *Significance of difference ($p<.05$) determined using multivariate analysis of variance. **Post-hoc analysis conducted using Holm-Bonferroni demonstrating significant difference between groups. SD=standard deviation; BMI=body mass index; FEV_1=forced expiratory in 1 s; FVC=forced vital capacity; FRC=functional residual capacity; IC=inspiratory capacity; TLC=total lung capacity; DL_{CO}=diffusing capacity of carbon monoxide; Raw=airways resistance; RV=residual volume; VO_2max=maximal oxygen capacity; RER=respiratory exchange ratio at VO_2max; V_{Emax}=minute ventilation at VO_2max;VCO_2=volume of carbon dioxide at VO_2max; Time to VO_2max is time taken to reach VO_2max during CPET; VDP=ventilation defect percent; ^{3}He COV=ventilation coefficient of variation; PA ΔVDP=change in posterior and anterior VDP; SI ΔVDP=change in superior and inferior VDP; VDV_{Per}=ventilation defect volume in the periphery of the lung; VDV_{WL}=ventilation defect volume in the whole lung.

Table 2-2 Subject listing and demographics, pulmonary function tests, cardiopulmonary exercise testing, and imaging measurements

Subject	Age (yrs)	Sex	BMI kg^2/m	FEV_1 $\%_{pred}$	FVC $\%_{pred}$	FEV_1 /FVC %	FRC $\%_{pred}$	IC $\%_{pred}$	TLC $\%_{pred}$	RV $\%_{pred}$	RV/TLC %	DL_{CO} $\%_{pred}$	Raw $\%_{pred}$	VO_2 max $\%_{pred}$	RER	Power $\%_{pred}$	V_E $\%_{pred}$	Post Dyspnea	Post Exertion	VDP %	^{3}He COV	Occupational Exposure
001	74	F	22	89	91	73	92	112	95	95	43	99	130	103	1.22	159	64	3	11	1.37	0.200	
002	68	F	27	101	97	79	102	125	112	124	47	79	81	86	1.39	123	56	4	12	2.39	0.206	
003**	76	F	27	70	78	67	127	92	112	149	62	52	181	66	1.14	109	38	2	11	9.17	0.274	
004	69	M	25	94	84	83	86	111	98	109	38	116	84	87	1.27	96	56	3	13	4.70	0.238	
005	77	M	24	133	128	74	135	83	110	107	37	153	62	113	1.25	136	83	0.5	7	1.34	0.200	
006	66	M	23	88	94	70	90	92	91	90	33	90	99	67	1.25	85	43	2	11	2.96	0.227	Construction
007	65	F	31	86	76	86	81	90	85	87	43	78	52	72	1.11	97	34	0.5	7	1.45	0.201	
012	71	M	29	84	83	75	134	72	105	131	44	80	80	100	1.68	49	108	3	11	3.91	0.230	
013	83	M	27	151	141	75	92	125	107	64	23	62	58	122	1.24	148	87	0.5	7	2.05	0.203	
015	65	F	20	91	86	81	136	76	110	121	45	81	56	82	1.17	110	45	7	12	2.69	0.195	
016	67	F	30	120	116	77	123	124	123	132	37	114	39	49	1.29	105	28	0.5	12	2.22	0.205	
017**	69	F	27	59	65	68	107	81	96	134	61	68	216	84	1.07	129	34	1	14	10.6	0.294	
018	61	F	22	111	107	80	102	112	106	83	31	95	62	98	1.27	128	46	3	13	5.55	0.223	
019	67	M	26	131	129	75	118	138	128	122	33	84	44	86	1.36	107	83	2	13	1.08	0.199	Organic dust
020*	78	M	23	101	105	68	133	60	99	100	38	78	30	99	1.22	121	63	2	6	7.49	0.235	Inorganic
021	74	M	34	82	85	70	102	90	96	109	42	97	189	95	1.38	124	68	2	15	5.99	0.260	Welding
022	81	F	20	123	116	78	122	143	131	134	50	75	69	83	1.14	129	41	0.5	13	3.01	0.221	
023	68	F	30	93	90	79	92	99	95	95	43	90	102	115	1.18	116	55	3	9	1.60	0.215	
024	62	F	21	121	109	86	108	97	103	78	31	78	64	83	1.24	120	48	2	9	1.17	0.195	
025	66	M	24	95	98	72	139	88	115	160	46	114	29	92	1.16	102	54	2	11	3.10	0.234	Farming
029	84	M	24	102	80	87	79	114	67	58	35	92	65	53	1.03	64	36	5	14	2.74	0.229	
030	77	M	32	98	91	77	87	104	95	98	38	89	73	80	1.00	109	42	0	7	2.70	0.221	
031*	71	M	30	103	109	69	107	90	99	80	29	77	45	94	1.20	56	71	0.5	12	2.22	0.216	Fire Fighting
032	69	F	29	106	103	78	91	130	108	99	39	81	39	107	1.17	169	49	2	13	1.83	0.215	
033*	80	M	26	89	94	68	93	93	93	101	40	74	82	82	1.11	113	40	3	12	4.63	0.222	
034	69	M	28	122	120	75	113	103	108	92	29	78	28	93	1.26	118	63	4	15	2.46	0.196	
035	74	F	31	107	103	77	152	137	145	179	56	76	107	96	1.06	179	44	3	13	1.67	0.187	
036*	78	M	24	106	109	69	124	77	103	106	39	75	51	92	1.30	122	67	1	8	2.73	0.206	Farming
038	79	F	29	108	111	71	116	102	110	96	43	73	106	81	1.00	145	52	2	11	1.25	0.196	Farming
039	71	F	32	122	115	80	86	153	115	101	39	89	102	96	1.25	161	56	3	14	0.65	0.210	
041	71	F	31	89	87	78	110	116	112	134	51	101	99	99	1.18	184	56	3	13	3.62	0.216	
042	61	F	26	98	94	81	123	103	114	137	47	87	64	89	1.07	117	39	3	15	1.38	0.200	
044	65	F	28	95	88	82	92	109	99	105	44	81	61	68	1.15	110	30	4	13	1.82	0.194	
045	77	F	31	116	109	80	98	135	113	110	45	90	82	100	1.25	140	65	4	13	1.49	0.194	
046	73	F	27	102	90	85	92	93	92	81	40	81	73	100	1.00	80	100	0	6	2.29	0.218	
047	63	F	23	114	109	80	111	120	115	104	37	99	78	69	1.14	94	37	1	8	2.68	0.203	Farming
049	63	F	23	126	137	71	88	71	123	87	29	96	92	71	1.48	114	47	0.5	11	0.85	0.183	
050	66	F	22	123	117	80	132	105	121	2	38	91	48	68	1.29	101	39	0.5	7	0.72	0.188	
052	68	F	30	122	110	84	108	128	117	116	43	119	63	120	1.12	177	59	3	9	1.83	0.197	
053	75	F	33	111	107	78	73	128	96	78	37	86	41	103	1.14	181	51	1	9	1.58	0.243	Farming
054	65	F	27	102	111	70	98	121	108	86	33	119	44	68	1.07	98	34	3	13	2.30	0.192	

055	66	M	24	114	96	88	92	121	106	127	41	90	34	55	1.11	66	35	0.5	13	2.08	0.190	
056	61	F	25	108	102	81	105	127	115	122	41	72	58	76	1.20	105	41	6	18	2.10	0.206	
057	78	F	29	114	117	72	84	134	105	98	44	87	79	82	1.07	159	40	3	15	1.60	0.205	
059	79	M	26	116	98	83	78	91	84	87	41	74	85	62	1.06	93	40	0	9	2.83	0.221	Farming
060	77	F	24	120	112	80	104	107	105	106	47	91	89	84	1.14	135	47	2	14	1.27	0.195	
061#	74	F	24	72	71	77	126	83	108	153	64	90	34	65	1.03	92	30	3	7	3.26	0.231	
062	82	M	26	164	135	84	127	101	115	110	39	91	51	101	1.20	125	74	3	9	3.48	0.209	
063#	67	M	31	72	77	70	90	87	88	93	36	89	100	90	1.10	125	41	1	7	4.17	0.232	Foundry and Steel Milling
064	69	M	25	130	123	78	134	111	123	134	37	90	50	96	1.30	120	61	2	10	1.79	0.193	Farming
065	69	F	26	109	113	73	127	99	115	111	41	80	68	59	1.24	79	37	2	13	1.59	0.193	
066	73	M	28	110	104	76	101	112	106	99	34	82	55	111	1.34	156	99	3	12	2.10	0.207	

#: GOLD-Unclassified, *: Stage I COPD, **:Stage II COPD

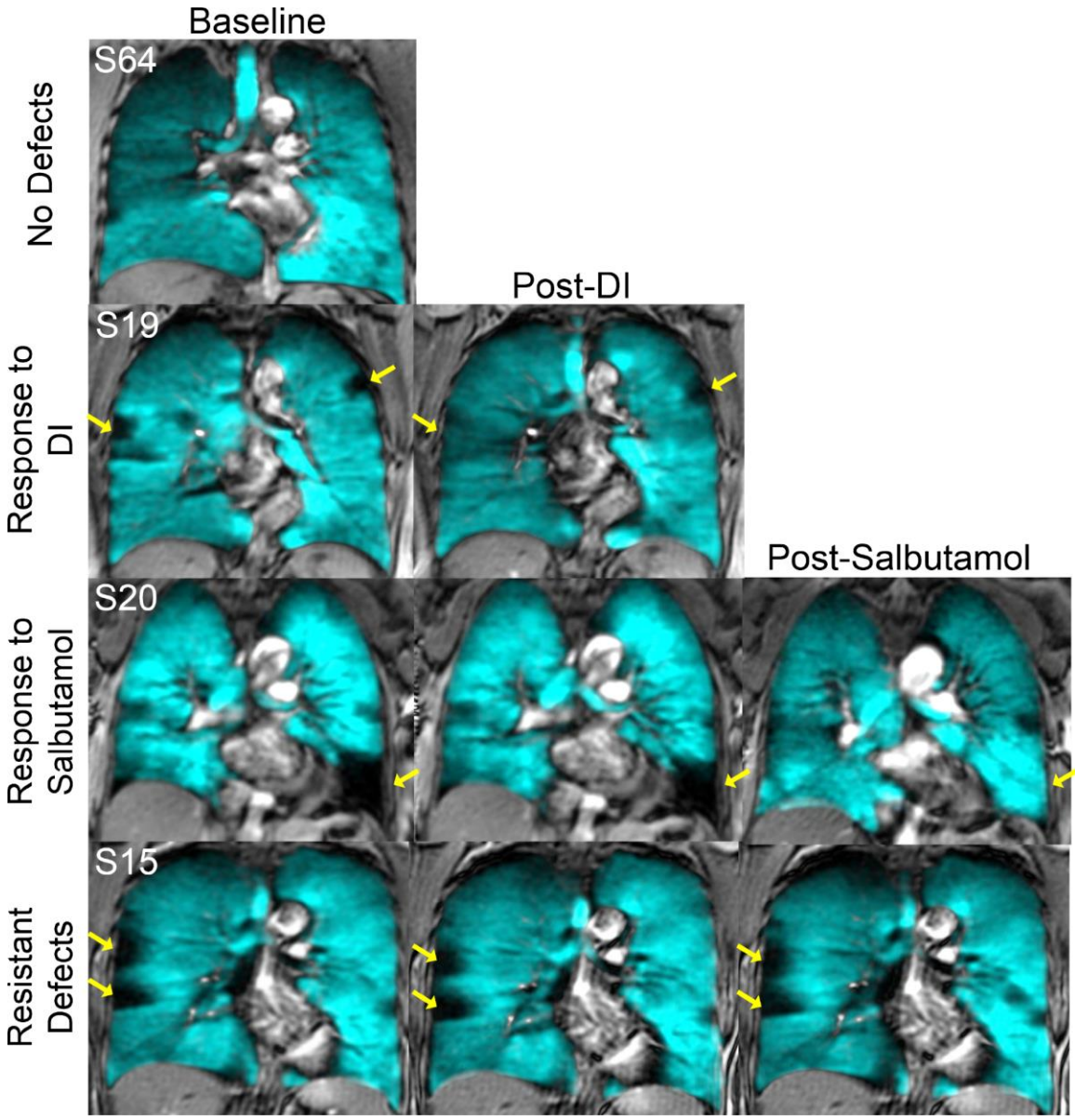

Figure 2-2 ^{3}He MRI for four representative subjects
^{3}He MRI ventilation (in blue) co-registered with anatomical ^{1}H MRI (grey-scale) of the centre coronal slice. Subject 64 (S64) is a 69 year old male: FEV_1=130%, FEV_1/FVC=78%, slice number shown: 7. Subject 19 (S19) is a 67 year old male: FEV_1=131%, FEV_1/FVC=75%, slice number shown: 8. Subject 20 (S20) is a 78 year old male: FEV_1=101%, FEV_1/FVC=68%, slice number shown: 9. Subject 15 (S15) is a 65 year old female: FEV_1=91%, FEV_1/FVC=81%, slice number shown: 8. Yellow arrows identify the position of ventilation defects. DI = Deep Inspiration.

Figure 2-2 shows ^{3}He MRI coronal slices at baseline, post-DI, and post-salbutamol for four representative subjects. For the subject shown without ventilation defects, there was homogeneous signal intensity over the entire lung with no obvious ventilation defects in the centre MR slice or any of the anterior to posterior slices. For two representative subjects that showed an imaging response to DI or salbutamol, there were ventilation defects peripherally located in the central and posterior slices that resolved (arrows) in response to DI or bronchodilation. For the representative subject with ventilation defects that did not appear to respond to DI or salbutamol, a number of small peripheral ventilation defects (arrows) remained spatially persistent post-DI and 25 minutes after salbutamol inhalation.

For the three comparator groups (**Table 2-1**) there was no significant difference for age, sex or BMI. However, there was a significant difference for FEV_1/FVC ($p=0.004$), VDP, ^{3}He COV, VDP ΔPA and PA gradient ($p<0.001$) as well as relative peripheral VDP ($p=0.001$). There was no significant difference for any CPET or other pulmonary function measurements for the three subgroups. Post-hoc analysis showed that the imaging responder group had significantly lower FEV_1/FVC and significantly higher VDP, ^{3}He COV, PA ΔVDP, and relative peripheral VDP than the no defect and no imaging response groups. **Figure 2-3** shows scatter plots for VDP, relative peripheral VDP, VDP ΔPA, VDP ΔSI, PA VDP gradient, SI VDP gradient and ^{3}He COV.

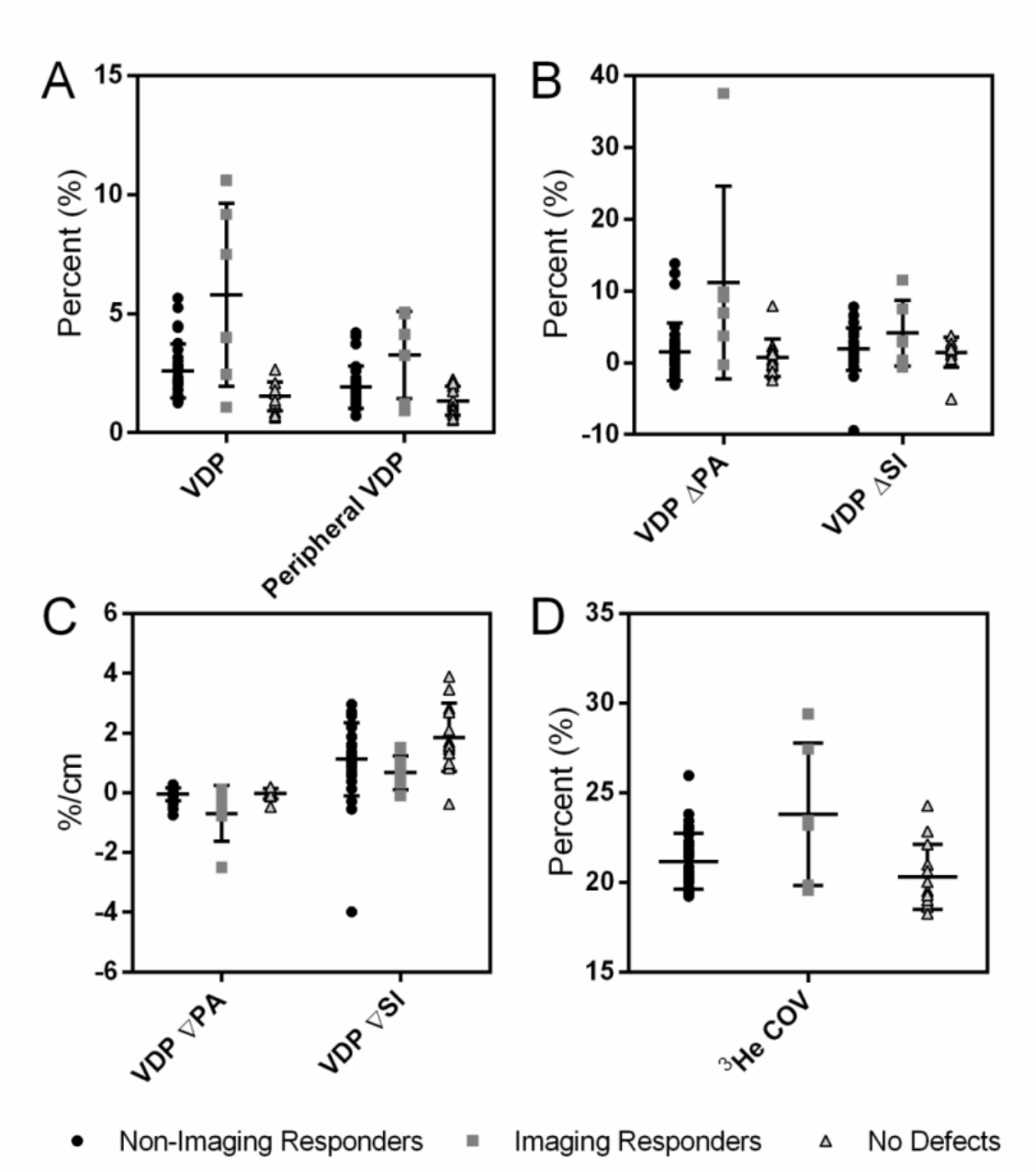

Figure 2-3 Scatter plots of MRI metrics
Plots showing all MRI metrics for three subgroups (non-imaging responders, imaging responders, and no defects). A) VDP and relative peripheral VDP, B) VDP ΔPA and VDP ΔSI, C) PA and SI gradients, and, D) ^{3}He COV. Error bars are the standard deviation of the mean.

Table 2-2 shows that 13 subjects reported significant exposure, 10 of whom (77%) had ventilation defects. Of those 10 subjects, three showed an imaging response to DI or salbutamol. **Table 2-2** also shows that eight never-smokers had spirometry evidence of

airway obstruction[34] (GOLD Unclassified (U) (n=2), GOLD 1 (n=4), GOLD 2 (n=2)). Five of these eight subjects reported second-hand smoke or occupational exposures and two subjects responded to salbutamol. In addition, 10 never-smokers had $0.70 \leq FEV1/FVC \leq 0.73$, where the 0.73 threshold was used to compensate for the variability in FEV1 and FVC.[35,36] The eight never-smokers with spirometry evidence of COPD had significantly greater VDP (5.5±3.1%, $p<0.001$) than the never smokers with (VDP=2.5±1.2%) or without (VDP=1.6±0.7%) ventilation defects. When the subjects with spirometry evidence of COPD (n=8) were removed in a sub analysis, only VDP remained significantly different across all three subgroups ($p=0.03$). Post-hoc analysis showed that the no imaging response group had greater baseline VDP than the no defect group, but was not significantly different from the imaging response group.

2.3.2 Pre- and Post-DI/Salbutamol Analysis

Table 2-3 shows a subject listing for pre- and post-salbutamol FEV_1, VDP, and ^{3}He COV for all subjects administered salbutamol (n=35). Three subgroups were identified for those subjects administered salbutamol: imaging-responders, FEV_1-responders, and non-responders. Twenty-eight of 35 subjects did not show an imaging response or an FEV_1 response to salbutamol. There were five subjects who responded to salbutamol ($\Delta FEV_1 > 200ml$), but did not have an imaging (VDP or cluster 1) response to salbutamol. In addition, for these five subjects, there was no significant change in any of ventilation clusters 2-5 or any combination of ventilation clusters (i.e. C1+C2) post-salbutamol. It is worth noting that one of the five FEV_1-responders reported 30 years of occupational exposure working in the steel mill industry (S63) while two were lifelong farmers (S25 and S59). Finally, for those subjects administered salbutamol, there were no relationships for the change in FEV_1 post-salbutamol with change in VDP ($r^2=0.04$, $p=0.50$) or change in ^{3}He COV ($r^2=0.08$, $p=0.10$).

Table 2-3 Subject Listing for FEV_1, VDP and ^3He COV for all subjects administered salbutamol (n=35)

Subject		Pre-Salbutamol				Post-Salbutamol						
	Age (yrs)	FEV_1 (L)	FEV_1 ($\%_{pred}$)	VDP (%)	^3He COV	FEV_1 (L)	FEV_1 $\%_{pred}$	VDP (%)	^3He COV	Δ FEV_1 (L)	Δ FEV_1 $\%_{pred}$	Δ VDP %
001	74	1.68	89	1.35	0.20	1.70	91	0.84	0.20	0.02	2	-0.51
002#	***68***	***2.52***	***101***	***2.34***	***0.21***	***2.72***	***109***	***1.65***	***0.20***	***0.20***	***8***	***-0.69***
003	76	1.30	70	9.17	0.27	1.34	72	8.15	0.28	0.04	2	-1.02
004	69	3.33	94	4.49	0.24	3.31	94	4.02	0.24	-0.02	0	-0.47
005	77	3.36	133	1.32	0.20	3.06	122	1.55	0.21	-0.30	-11	0.23
006	66	3.30	88	2.87	0.23	3.29	88	2.73	0.22	-0.01	0	-0.14
007	65	2.01	86	1.43	0.20	2.08	89	2.11	0.22	0.07	3	0.68
012	71	2.78	84	3.76	0.23	2.66	81	2.87	0.23	-0.12	-3	-0.90
015	65	2.38	91	2.61	0.20	2.52	96	2.29	0.21	0.14	5	-0.33
016	67	3.80	120	2.22	0.21	3.88	123	1.65	0.22	0.08	3	-0.57
017*	**69**	**1.24**	**59**	**10.6**	**0.29**	**1.35**	**64**	**7.91**	**0.27**	**0.11**	**5**	**-2.70**
018	61	3.06	111	5.26	0.22	3.14	114	5.62	0.24	0.08	3	0.36
020*	**78**	**2.76**	**101**	**7.49**	**0.24**	**3.02**	**110**	**3.47**	**0.24**	**0.26**	**9**	**-4.02**
021	74	2.32	82	5.65	0.26	2.41	85	3.25	0.25	0.09	3	-2.40
022#	***81***	***2.18***	***123***	***2.92***	***0.22***	***2.43***	***137***	***5.37***	***0.23***	***0.25***	***14***	***2.45***
023	68	1.96	93	1.57	0.22	2.09	99	1.25	0.21	0.13	6	-0.32
025#	***66***	***3.54***	***95***	***3.01***	***0.23***	***3.78***	***102***	***2.33***	***0.22***	***0.24***	***7***	***-0.68***
031	71	3.14	103	2.17	0.22	3.15	103	1.93	0.22	0.01	0	-0.24
032	69	2.75	106	1.79	0.22	2.82	109	1.56	0.21	0.07	3	-0.24
033	80	2.86	89	4.42	0.22	2.76	86	6.13	0.23	-0.10	-3	1.71
036	78	2.88	106	2.73	0.21	3.06	112	1.92	0.20	0.18	6	-0.81
041	71	2.19	89	3.49	0.22	2.31	94	3.38	0.22	0.12	5	-0.11
044	65	2.24	95	1.79	0.19	2.14	90	1.84	0.22	-0.10	-5	0.05
045	77	2.44	116	1.46	0.19	2.31	109	2.02	0.21	-0.13	-7	0.55
046	73	2.06	102	2.35	0.22	1.90	94	2.14	0.22	-0.16	-8	-0.21
047	63	2.52	114	2.61	0.20	2.53	116	3.09	0.20	0.01	2	0.48
052	68	2.55	122	1.83	0.20	2.63	125	1.58	0.19	0.08	3	-0.25
054	65	2.42	102	2.24	0.19	2.49	105	3.33	0.20	0.07	3	1.08
056	61	3.12	108	2.10	0.21	3.19	110	1.90	0.21	0.07	2	-0.20
057	78	2.23	114	1.58	0.21	2.27	116	1.29	0.21	0.04	2	-0.28
059#	***79***	***2.53***	***116***	***2.83***	***0.22***	***2.73***	***125***	***2.90***	***0.22***	***0.20***	***9***	***0.07***
060	77	2.36	120	1.26	0.20	2.37	121	1.55	0.20	0.01	1	0.29
061	74	1.53	72	3.15	0.23	1.59	75	5.21	0.24	0.06	3	2.03
063#	***67***	***2.46***	***72***	***4.00***	***0.23***	***2.94***	***86***	***3.72***	***0.22***	***0.48***	***14***	***-0.28***
065	69	2.57	109	1.59	0.19	2.70	114	1.79	0.20	0.13	5	0.20
Imaging Responders*	74	2.0	80	9.0	0.27	2.2	87	5.7	0.26	0.2	7.0	-3.4
Mean (SD) n=2	(6)	(1.1)	(30)	(2.2)	(0.04)	(1.2)	(33)	(3.0)	(0.02)	(0.1)	(2.8)	(0.9)
FEV_1 Responders#	74	2.7	102	3.1	0.22	3.0	112	3.3	0.22	0.3	10.0	0.2
Mean (SD) n=5	(7)	(0.5)	(20)	(0.5)	(0.01)	(0.5)	(20)	(1.3)	(0.01)	(0.1)	(3.8)	(1.3)
Non-responders	71	2.5	100	2.8	0.21	2.5	101	2.7	0.22	0.00	1.0	-0.04
Mean (SD) n=28	(5)	(0.6)	(16)	(1.7)	(0.02)	(0.6)	(15)	(1.7)	(0.02)	(0.1)	(4.4)	(0.8)

Table 2-4 shows VDP and ^3He COV measurements for all three time points for imaging responders (DI or salbutamol responders). There were no statistically significant differences in ^3He COV or VDP across time points for the imaging responders.

Table 2-4 VDP and ^{3}He COV measurements for imaging responders

	Baseline	Post-DI	Post-Salbutamol
Imaging Responders (n=6)			
VDP % (±SD)	5.8 (3.8)	4.7 (2.6)	5.7 (3.1)
^{3}He COV (±SD)	0.24 (0.04)	0.24 (0.04)	0.25 (0.02)
DI Responders (n=4)			
VDP % (±SD)	4.2 (3.5)	3.5 (2.3)	--
^{3}He COV (±SD)	0.23 (0.04)	0.23 (0.04)	--
Salbutamol-Responders (n=2)			
VDP % (±SD)	9.0 (2.2)	7.0 (1.0)	5.7 (3.1)
^{3}He COV (±SD)	0.26 (0.04)	0.25 (0.03)	0.25 (0.02)

2.3.3 Relationships between Imaging and other Measurements

Table 2-5 shows the results of a forward stepwise multivariate regression model using ^{3}He VDP as the dependent variable and all significant pulmonary function test measurements (obtained from the univariate analysis) as the independent variables. $FEV_1\%_{pred}$, $IC\%_{pred}$, and $Raw\%_{pred}$ were shown to predict 45% of the variability in VDP (p=0.001), with $FEV_1\%_{pred}$ making the greatest contribution. The univariate relationships are shown in **Figure 2-4** including $FEV_1\%_{pred}$ (r^2=0.29, p<0.0001), $Raw\%_{pred}$ (r^2=0.29, p<0.0001), and $IC\%_{pred}$ (r^2=0.17, p=0.003). There were no statistically significant relationships for VDP with CPET, dyspnea, or occupational exposure measurements. It is important to note that three subjects had VDP ≥ 3SD of the mean and when these data were removed from the regression analysis, $FEV_1\%_{pred}$ (r^2=0.13, p=0.009) and $IC\%_{pred}$ (r^2=0.17, p=0.003) was significantly related to VDP, and $Raw\%_{pred}$ was not.

Table 2-5 Univariate and Multivariate relationships for ^{3}He MRI VDP with pulmonary function measurements

Parameters	Univariate Relationship VDP r^2 (p value)	Multivariate Model VDP β, r^2, Δr^2 (p-value)
$FEV_1\%_{pred}$	**0.29 (<0.001)**	**-0.541, 0.292, 0.292 (<0.001)**
$Raw\%_{pred}$	**0.29 (<0.001)**	**0.359, 0.391, 0.099 (<0.001)**
$IC\%_{pred}$	**0.17 (0.003)**	**-0.265, 0.449, 0.058 (<0.001)**
FEV_1/FVC %	**0.17 (0.002)**	-0.147, 0.449, 0 (0.23)
$FVC\%_{pred}$	**0.24 (<0.002)**	0.114, 0.449, 0 (0.68)
RV/TLC %	**0.15 (0.005)**	0.105, 0.449, 0 (0.44)

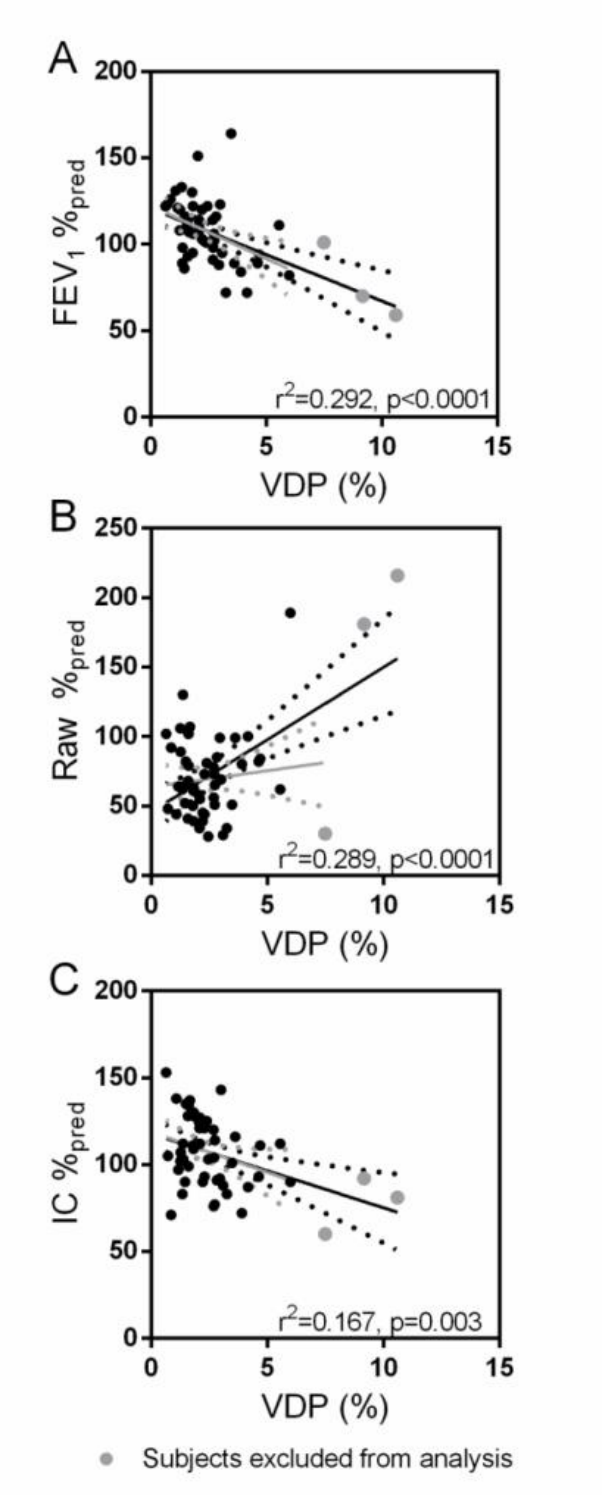

Figure 2-4 Univariate Relationships for ^{3}He MRI VDP
Univariate correlations for VDP with: A) FEV_1 $\%_{pred}$ for all subjects (r^2=0.29, r=-0.54, p<0.0001), B) Raw $\%_{pred}$ for all subjects (r^2=0.29, r=0.54, p<0.0001), and, C) IC $\%_{pred}$ for all subjects (r^2=0.17, r=-0.41, p=0.003). Grey circles show the subjects with VDP >3SD of

the mean. Grey regression line shows the alternate regression line that resulted from when these subjects were excluded.

2.4 Discussion

To better understand the determinants and physiological consequences of ventilation defects in older never-smokers, we evaluated pulmonary function and CPET measurements, as well as occupational/second-hand smoke exposure in 52 older adults. We made a number of key observations including: 1) three quarters of older never-smokers had ventilation defects, the majority of whom showed no VDP response to either DI or salbutamol, 2) ventilation heterogeneity and VDP were significantly greater, and FEV_1/FVC was significantly lower ($p<0.05$) for subjects with ventilation-defects responsive to DI/salbutamol compared to subjects without ventilation defects and subjects with ventilation-defects with no response to DI/salbutamol and, 3) in a multivariate model, FEV_1, IC and Raw explained nearly 50% of the variability in ^{3}He VDP in these older never-smokers.

2.4.1 Ventilation Abnormalities in Older Never-Smokers

In the 39 subjects with visually obvious ventilation defects, VDP was modest and lower than previously reported in COPD and asthma subjects; furthermore, only four subjects showed a change in VDP in response to DI. This is consistent with previous findings that showed that the bronchodilatory effects of DI decrease with age,[37] which may explain the low number of DI responders in this study. Similar to previous observations in COPD[38] and asthma,[26,28] two subjects showed an imaging response to salbutamol and this supports previous findings that reversible airflow limitation may be underappreciated in the elderly. Unexpectedly, the majority of older never-smokers with visually obvious ventilation defects (n=33/39, 85%) did not respond to DI or salbutamol. This is consistent with the notion that in older never-smokers, small ventilation defects are related to irreversible airway narrowing or collapse, loss of elastic recoil and/or small peripheral regions that are slow filling.

The majority of defects were observed along the periphery of the lung suggesting that terminal airway closure or narrowing may be a “normal” age-related pulmonary finding.

Relative peripheral VDP, ^{3}He COV, VDP ΔPA, and VDP PA gradient were significantly greater in the imaging responders compared to the non-responder and no defect groups. Together these findings suggest that subjects who responded to DI or salbutamol also had greater ventilation heterogeneity (or patchiness) and greater posterior/peripheral ventilation defects. The difference in ventilation heterogeneity between groups may reflect differences in lung filling related to airway lumen morphology, but this is yet to be determined. Other potential mechanisms for ventilation heterogeneity have been suggested including the loss of parenchymal tethering forces due to alveolar collapse that alters airway diameters, differences in regional lung expansion due to diaphragm and ribcage motions, or gravity-dependent differences in lung expansion contributing to airway constriction in the gravity-dependent regions.[39] Nevertheless, in these older never-smokers there appears to be a small, yet irreversible VDP component. Finally, as might be expected based on the BOLD study,[22] eight subjects showed spirometry evidence of COPD and another ten subjects exhibited $0.70<FEV_1/FVC\leq0.73$ (0.73 accounts for FEV_1 and FVC variability of 2-3%).[35,36] Therefore, here, the proportion of subjects with undiagnosed airflow limitation was 35%, which is in agreement with the results of the BOLD study.[22] It is interesting to note that when the eight subjects with spirometry evidence of COPD were removed from the analysis, FEV_1/FVC was no longer different across the three sub-groups, however, VDP remained different. For five subjects with an FEV_1 response to salbutamol > 200ml, there were no significant changes in VDP, ^{3}He COV or any of the ventilation clusters (C2-C5) post-salbutamol. The discrepancy between FEV_1 response and ^{3}He MRI response may have been due to the effort-dependence of spirometry. It is also important to note that all ventilation defects were peripherally located, near the distal airways, and this may also explain why salbutamol did not influence the size or magnitude of these ventilation defects.

2.4.2 Relationships: Ventilation Defects with Exercise Capacity and Dyspnea

In this study, the range of dyspnea scores and magnitude of ventilation defects observed were small as compared with recent findings in COPD and asthmatic subjects.[24,26,28,38] For these reasons, we were not surprised that there were no differences in CPET or dyspnea

measurements between subjects with and without ventilation defects. Further supporting this finding, O'Donnell and colleagues have shown that it is possible to have substantial ventilatory impairment during exercise without a corresponding effect on dyspnea.[20] This is consistent with the notion that in healthy subjects, cardiovascular, and not respiratory factors provide the dominant contributions to exercise limitation.[40,41] Furthermore, unlike previous work,[7] there were no relationships between dyspnea and other pulmonary function or CPET measurements which could be due to the limited range of dyspnea scores reported. Subjects with ventilation defects had normal lung function and exercise capacity measurements for their age. [6,7,42]

2.4.3 Relationships: Ventilation Defects with Pulmonary Function and Volumes

There were significant but weak univariate relationships for VDP with $FEV_1\%_{pred}$, $IC\%_{pred}$ and $Raw\%_{pred}$, although the relationship between VDP and $Raw\%_{pred}$ was dominated by three subjects with relatively large VDP values (S3, S17, and S21). S21 had occupational and environmental exposures, and both S3 and S17 had spirometry evidence of GOLD II COPD. In a multivariate regression model, $IC\%_{pred}$, $Raw\%_{pred}$, and $FEV_1\%_{pred}$ all provided significant contributions to VDP, with $FEV_1\%_{pred}$ being the strongest predictor. The negative correlation of $IC\%_{pred}$ with VDP is concordant with previous results in COPD ex-smokers which showed that abnormal IC is a marker of expiratory flow-limitation and a predictor of dynamic hyperinflation during exercise.[43] An increase in dynamic hyperinflation results in an increased elastic load on the inspiratory muscles, thus increasing the work and cost of breathing. This mechanical constraint can predispose individuals to fatigue and it has been shown that dynamic hyperinflation contributes to perceived exertional dyspnea in subjects with COPD.[43-45] It is also interesting to note that resting IC can predict the peak symptom-limited VO_2 in patients with expiratory flow-limitation at rest.[45]

2.4.4 Limitations

We recognize a number of limitations that restrict the general applicability of our results. First, subjects were classified by viewing the grayscale images while the patients were still

in the scanner. Offline, once the ventilation images were co-registered to the anatomical ^{1}H images, in two cases, previously classified ventilation defects could be directly related to anatomical bony structures and were unlikely to be ventilation abnormalities. As a result, two subjects who were classified at the scanner as having ventilation defects, did not appear to have these once a full analysis was completed, although both completed DI and salbutamol inhalation. One subject had ventilation defects that responded to DI (but not salbutamol) whereas the other subject had no ventilation defects and did not respond to DI or salbutamol. We did not remove these subjects from the analysis and their inclusion did not alter the final overall results. It should also be noted that since all subjects were imaged approximately 30 minutes after completion of CPET, ventilation defects and ventilation heterogeneity may have been influenced by exercise. Previous studies have shown that during exercise athletes experience ventilation-perfusion mismatch and diffusion limitation.[46] Other studies have evaluated the progression of ventilation-perfusion mismatch after exercise and showed that some subjects don't recover fully from ventilation-perfusion mismatch until 20 minutes post-exercise.[47] Because of the time delay between imaging and CPET and the fact that in this study, VDP did not correlate with any CPET measurements, it is unlikely that prior exercise influenced the presence or absence of ^{3}He MRI ventilation defects.

2.4.5 Conclusions

In summary, we evaluated hyperpolarized ^{3}He MRI ventilation defects—a surrogate measurement of airway function—in the first, large imaging study of healthy older never-smokers with no history of chronic heart or lung disease. While a minority of subjects reported occupational exposures, most subjects had visually obvious ventilation defects that did not change after DI or salbutamol administration suggesting that terminal airway closure or narrowing may be a normal age-related lung finding. While there were no differences in CPET or conventional pulmonary function measurements between subjects with and without ventilation defects, $FEV_1\%_{pred}$ in combination with $IC\%_{pred}$ and $Raw\%_{pred}$ predicted VDP in a multivariate regression model. Taken together, these findings provide a better understanding of the nature of ventilation defects in healthy older never-smokers.

2.5 References

(1) Frank, N. R., Mead, J. & Ferris, B. G., Jr. The mechanical behavior of the lungs in healthy elderly persons. *J Clin Invest* 1957;36:1680-1687.

(2) Thurlbeck, W. M. Internal surface area and other measurements in emphysema. *Thorax* 1967; 22: 483-496.

(3) Turner, J. M., Mead, J. & Wohl, M. E. Elasticity of human lungs in relation to age. *J Appl Physiol* 1968; 25: 664-671.

(4) Janssens, J. P., Pache, J. C. & Nicod, L. P. Physiological changes in respiratory function associated with ageing. *Eur Respir J* 1999; 13: 197-205.

(5) Enright, P. L., Kronmal, R. A., Manolio, T. A., Schenker, M. B. & Hyatt, R. E. Respiratory muscle strength in the elderly. Correlates and reference values. Cardiovascular Health Study Research Group. *Am J Respir Crit Care Med* 1994; 149: 430-438.

(6) Fletcher, C. & Peto, R. The natural history of chronic airflow obstruction. *Br Med J* 1977; 1: 1645-1648.

(7) Ofir, D., Laveneziana, P., Webb, K. A., Lam, Y. M. & O'Donnell, D. E. Sex differences in the perceived intensity of breathlessness during exercise with advancing age. *J Appl Physiol* 2008; 104: 1583-1593.

(8) Tessier, J. F. et al. Dyspnea and 8-year mortality among elderly men and women: the PAQUID cohort study. *Eur J Epidemiol* 2001; 17: 223-229.

(9) Ahmed, T., Steward, J. A. & O'Mahony, M. S. Dyspnoea and mortality in older people in the community: a 10-year follow-up. *Age Ageing* 2014; 41: 545-549.

(10) Nejjari, C. et al. The relationship between dyspnoea and main lifetime occupation in the elderly. *Int J Epidemiol* 1993; 22: 848-854.

(11) Ho, S. F. et al. Dyspnoea and quality of life in older people at home. *Age Ageing* 2001; 30: 155-159.

(12) Huijnen, B. et al. Dyspnea in elderly family practice patients. Occurrence, severity, quality of life and mortality over an 8-year period. *Fam Pract* 2006; 23: 34-39.

(13) Albouaini, K., Egred, M., Alahmar, A. & Wright, D. J. Cardiopulmonary exercise testing and its application. *Postgrad Med J* 2007; 83: 675-682.

(14) ATS/ACCP Statement on cardiopulmonary exercise testing. *Am J Respir Crit Care Med* 2003; 167: 211-277.

(15) Guenette, J. A., Chin, R. C., Cory, J. M., Webb, K. A. & O'Donnell, D. E. Inspiratory Capacity during Exercise: Measurement, Analysis, and Interpretation. *Pulmonary medicine* 2013; 956081.

(16) O'Donnell, D. E., O'Donnell, C. D., Webb, K. A. & Guenette, J. A. Respiratory Consequences of Mild-to-Moderate Obesity: Impact on Exercise Performance in Health and in Chronic Obstructive Pulmonary Disease. *Pulm Med* 2012; 818925.

(17) Kasch, F. W. et al. Cardiovascular changes with age and exercise. A 28-year longitudinal study. *Scand J Med Sci Sports* 1995; 5: 147-151.

(18) Heath, G. W., Hagberg, J. M., Ehsani, A. A. & Holloszy, J. O. A physiological comparison of young and older endurance athletes. *J Appl Physiol* 1981; 51: 634-640.

(19) Jensen, D., Ofir, D. & O'Donnell, D. E. Effects of pregnancy, obesity and aging on the intensity of perceived breathlessness during exercise in healthy humans. *Respir Physiol Neurobiol* 2009; 167: 87-100.

(20) Guenette, J. A., Diane Lougheed, M., Webb, K. A. & O'Donnell, D. E. Can an 86-year-old woman with advanced lung disease be a world class athlete? *Respir Physiol Neurobiol* 2012; 181: 162-166.

(21) Buist, A. S. et al. The Burden of Obstructive Lung Disease Initiative (BOLD): rationale and design. *COPD* 2005; 2: 277-283.

(22) Lamprecht, B. et al. COPD in never smokers: results from the population-based burden of obstructive lung disease study. *Chest* 2011; 139: 752-763.

(23) Parraga, G. et al. Hyperpolarized 3He ventilation defects and apparent diffusion coefficients in chronic obstructive pulmonary disease: preliminary results at 3.0 Tesla. *Invest Radiol* 2007; 42: 384-391.

(24) Kirby, M. et al. Chronic obstructive pulmonary disease: longitudinal hyperpolarized (3)He MR imaging. *Radiology* 2010; 256: 280-289.

(25) Parraga, G., Mathew, L., Etemad-Rezai, R., McCormack, D. G. & Santyr, G. E. Hyperpolarized 3He magnetic resonance imaging of ventilation defects in healthy elderly volunteers: initial findings at 3.0 Tesla. *Acad Radiol* 2008; 15: 776-785.

(26) Costella, S. et al. Regional pulmonary response to a methacholine challenge using hyperpolarized (3)He magnetic resonance imaging. *Respirology* 2012; 17: 1237-1246.

(27) Tzeng, Y. S., Lutchen, K. & Albert, M. The difference in ventilation heterogeneity between asthmatic and healthy subjects quantified using hyperpolarized 3He MRI. *J Appl Physiol* 2009; 106: 813-822.

(28) Svenningsen, S. et al. Hyperpolarized 3He and 129Xe MRI: Differences in asthma before bronchodilation. *J Magn Reson Imaging* 2013; 38: 1521-1530.

(29) Jensen, A., Atileh, H., Suki, B., Ingenito, E. P. & Lutchen, K. R. Selected contribution: airway caliber in healthy and asthmatic subjects: effects of bronchial challenge and deep inspirations. *J Appl Physiol* 2001; 91: 506-515; discussion 504-505.

(30) Guazzi, M. et al. EACPR/AHA Scientific Statement. Clinical recommendations for cardiopulmonary exercise testing data assessment in specific patient populations. *Circulation* 2012; 126: 2261-2274.

(31) Kirby, M. et al. Hyperpolarized 3He magnetic resonance functional imaging semiautomated segmentation. *Acad Radiol* 2012; 19: 141-152.

(32) VanBell G, F. L., Heagerty P, Lumley T. Multiple comparisons. In: Biostatistics: a methodology for the health sciences 2nd edn, (Wiley-Interscience, 2004).

(33) Hankinson, J. L., Odencrantz, J. R. & Fedan, K. B. Spirometric reference values from a sample of the general U.S. population. *Am J Respir Crit Care Med* 1999; 159: 179-187.

(34) Wan, E. S. et al. Clinical and radiographic predictors of GOLD-unclassified smokers in the COPDGene study. *Am J Respir Crit Care Med* 2011; 184: 57-63.

(35) Humerfelt, S., Eide, G. E., Kvale, G. & Gulsvik, A. Forced expiratory volume in 1 second (FEV1) and forced vital capacity (FVC) variability in asymptomatic never-smoking men. *Clin Physiol* 1998; 18: 387-396.

(36) Margaret R. Becklake, S. P. Evaluation of tests of lung function for screening for early detection of chronic obstructive lung disease. (Marcel Dekker, 1979).

(37) Scichilone, N. et al. The bronchodilatory effect of deep inspiration diminishes with aging. *Respir Med* 2004; 98: 838-843 (2004).

(38) Kirby, M. et al. Chronic obstructive pulmonary disease: quantification of bronchodilator effects by using hyperpolarized (3)He MR imaging. *Radiology* 2011; 261: 283-292.

(39) Venegas, J. G. et al. Self-organized patchiness in asthma as a prelude to catastrophic shifts. *Nature* 2005; 434: 777-782.

(40) Dempsey, J. A., Hanson, P. G. & Henderson, K. S. Exercise-induced arterial hypoxaemia in healthy human subjects at sea level. *J Appl Physiol* 1984; 355: 161-175.

(41) Harms, C. A., Wetter, T. J., St Croix, C. M., Pegelow, D. F. & Dempsey, J. A. Effects of respiratory muscle work on exercise performance. *J Appl Physiol* 2000; 89: 131-138.

(42) Astrand, I., Astrand, P. O., Hallback, I. & Kilbom, A. Reduction in maximal oxygen uptake with age. *J Appl Physiol* 1973; 35: 649-654.

(43) O'Donnell, D. E., Bertley, J. C., Chau, L. K. & Webb, K. A. Qualitative aspects of exertional breathlessness in chronic airflow limitation: pathophysiologic mechanisms. *Am J Respir Crit Care Med* 1997; 155: 109-115.

(44) O'Donnell, D. E. & Laveneziana, P. Dyspnea and activity limitation in COPD: mechanical factors. *COPD* 2007; 4: 225-236.

(45) O'Donnell, D. E., Revill, S. M. & Webb, K. A. Dynamic hyperinflation and exercise intolerance in chronic obstructive pulmonary disease. *Am J Respir Crit Care Med* 2001; 164: 770-777.

(46) Hopkins, S. R., McKenzie, D. C., Schoene, R. B., Glenny, R. W. & Robertson, H. T. Pulmonary gas exchange during exercise in athletes. I. Ventilation-perfusion mismatch and diffusion limitation. *J Appl Physiol* 1994; 77: 912-917.

(47) Schaffartzik, W. et al. VA/Q distribution during heavy exercise and recovery in humans: implications for pulmonary edema. *J Appl Physiol* 1992; 72: 1657-1667.

CHAPTER 3

3 ULTRA-SHORT ECHO TIME PULMONARY MAGNETIC RESONANCE IMAGING: EVALUATION AND REPRODUCIBILITY IN COPD SUBJECTS WITH AND WITHOUT BRONCHIECTASIS

To better understand the potential for ultra-short echo time MRI to provide quantitative COPD endpoints, we evaluated the reproducibility and consequences of signal-intensity in COPD subjects with and without bronchiectasis. We compared UTE MR measurements with CT measurements of radiodensity and pulmonary function test measurements.

The contents of this chapter were previously published in the Journal of Magnetic Resonance Imaging: W Ma, K Sheikh, S Svenningsen, D Pike, F Guo, R Etemad-Rezai, J Leipsic, HO Coxson, DG McCormack, and G Parraga. J Magn Reson Imaging 2015; 41(5):1465-1474. Permission to reproduce this article was granted by John Wiley & Sons and is provided in Appendix A.

3.1 Introduction

Computed tomography (CT) provides the main anatomical/morphological measurements for research and clinical investigations in patients with chronic obstructive pulmonary disease (COPD). Large multi-centre studies such as ECLIPSE,[1] COPDGene[2] and MESA[3] have highlighted the quantitative information that CT provides including structure-function phenotypes related to airway (including airway thickening and bronchiectasis) and parenchymal abnormalities that are regionally and heterogeneously distributed in obstructive lung disease.[4] Cumulative radiation exposure related to thoracic CT imaging remains a concern[5] and limits CT use in serial and longitudinal studies.

MRI using short and ultra-short echo time (UTE) acquisition methods, was first proposed as a way to address the inherent challenges of pulmonary imaging stemming from low tissue and proton density.[6] UTE MRI combines fast radiofrequency (RF) excitation pulses and efficient k-space sampling trajectories to minimize MR signal decay and motion artifacts.[6] Pulmonary UTE methods have been used to estimate pulmonary emphysema in COPD patients[7] lobar fissures and airways in pulmonary fibrosis[8] as well as inflammation and peribronchial abnormalities in animal models of asthma.[9]

Before UTE measurements can be used in longitudinal clinical studies of respiratory disease or for monitoring treatment effects, it is critical to understand the inherent variability that can be attributed to image acquisition methods, including those related to the scanner (e.g. field strength and coils used) and subject compliance (e.g. breath-hold, motion, and position). We hypothesized that rapid, single breath-hold UTE MRI could be optimized to reproducibly quantify abnormalities in COPD and that both low density parenchymal abnormalities and high density abnormalities such as airway thickening and mucous plugs could be quantified. Therefore, our objective was to evaluate rapid pulmonary MRI using UTE methods with comparison to quantitative CT scan measurements and pulmonary function tests of subjects with COPD.

3.2 Materials and Methods

3.2.1 Study Logistics

All subjects and healthy volunteers provided written informed consent to a protocol approved by a local research ethics board and Health Canada; the study was compliant with the Personal Information Protection and Electronic Documents Act (PIPEDA, Canada). MRI was performed 10 minutes after completion of spirometry and plethysmography that were performed using a MedGraphics Elite Series plethysmograph (MedGraphics, St. Paul, Minnesota, USA). For seven subjects with COPD, (n=3 with emphysema; n=4 with emphysema and bronchiectasis) there was a three-week follow-up visit to determine UTE signal intensity and ^{3}He apparent diffusion coefficients (ADC) reproducibility. ^{3}He ADC reproducibility analysis was conducted as an internal control of reproducibility comparisons with the ^{1}H UTE measurements.

CT evidence of bronchiectasis was established by an experienced chest radiologist with >20 years experience (RER) and defined by an enlarged bronchial diameter, the failure of larger airways to taper while progressing to the lung periphery, bronchial wall thickening, mucous in the dilated airways, and tree-in-bud nodularity.[10] All subjects had a clinical diagnosis of COPD with CT evidence of emphysema or both emphysema and bronchiectasis and were categorized according to the Global Initiative for Chronic Obstructive Lung Disease (GOLD) grades.[11]

3.2.2 Pulse Sequence

A research prototype two-dimensional pulse sequence (**Figure 3-1**) with interleaved half-pulse excitation and 2D radial k-space trajectories was used.[6] There was no dephasing lobe after the slice-select gradient and two half-sinc excitations were required per slice to remove inter-slice cross-talk. To decrease acquisition time, we adapted a compressed sensing algorithm that was previously described.[12]

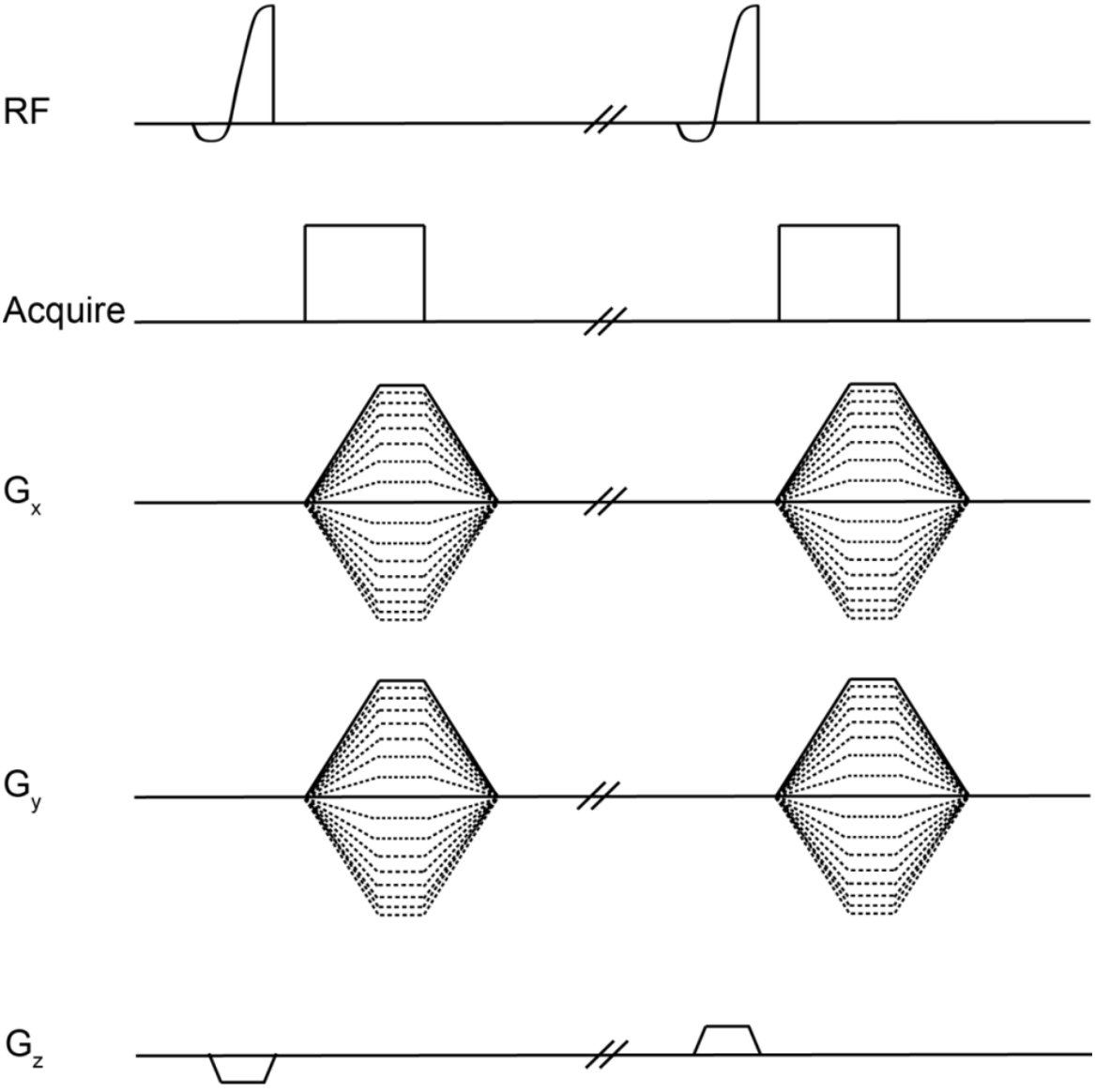

Figure 3-1 Pulse sequence diagram for 2D UTE with interleaved half-pulse excitation and 2D radial *k*-space trajectories

3.2.3 Image Acquisition

MRI was performed on a whole body 3T MR750 (General Electric Health Care [GEHC], Milwaukee, Wisconsin). To ensure that the same location was imaged at baseline and follow-up, we used the same fiducial landmarks and values for each of the three plane localizer scans performed. Briefly, using the sternum and spinal cord fiducials in the anterior-posterior direction, the scan space was divided into slices with slice thickness=15mm. In this manner, the same centre slice could be imaged which was typically the fifth coronal slice from the posterior direction and the slice that allowed for visualization of the carina. Centre slice ^{1}H UTE MRI was obtained in the coronal plane using a 32-channel torso coil and the single channel body coil for comparison (GEHC) (13s acquisition time, repetition time (TR) /echo time (TE)/flip angle=13.0ms/0.05ms/10°, field-of-view (FOV)=40×40cm, matrix 256×511, number of excitations (NEX)=2, 15mm slice thickness) at a lung volume of functional residual capacity (FRC)+1L. For comparison, coronal ^{1}H MRI was performed with a 32-channel torso coil using a fast-spoiled, gradient-recalled echo (FGRE) sequence (16s acquisition time, TR/TE/flip angle=4.7ms/1.2ms/30°, FOV=40×40cm, matrix 256×128, NEX=1, 14 slices, 15mm slice thickness). Diffusion-weighted hyperpolarized ^{3}He MRI was performed using a fast gradient-echo sequence with centric k-space sampling as previously described.[13] In healthy volunteers, UTE MRI was acquired in the coronal plane at four different lung volumes (23s acquisition time, TR/TE/flip angle=13.0ms/0.05ms/10°, FOV=40×40cm, matrix 256×439, NEX=4, 15mm slice thickness): full expiration (FE), FRC, FRC+1L, and full inhalation (FI). Thoracic CT was acquired in all COPD patients at FRC+1L, within 30 minutes of MRI, using a 64-slice Lightspeed VCT scanner (GEHC) using a detector configuration of 64×0.625mm, 120kVp, 100 effective mA, tube rotation time of 500ms, and a pitch of 1.0.

3.2.4 Image Analysis

We adapted definitions of the normalized contrast-to-noise ratio (C_R) and the apparent signal-to-noise ratio (S_R) as previously described[8] where SI_{lung} is the mean signal intensity of the lung, SI_{air} is the signal intensity of air outside of the subject, SI_{liver} is the mean signal intensity of the liver, SI_{vessel} is the mean signal intensity of the aorta:

Equation 3-1

$$C_R = \frac{SI_{lung} - SI_{air}}{SI_{vessel}}.$$

Equation 3-2

$$S_R = \frac{SI_{lung}}{SI_{air}}.$$

Absolute ^{1}H signal intensity was normalized to the liver in the same images ($SI/SI_{liver} \times 100\%$) to account for potential inter-scan variability in RF amplification and coil positioning. The ^{1}H SI coefficient of variation (COV) was calculated as the ratio of the standard deviation of the lung parenchyma signal intensity to the mean of the lung parenchyma signal intensity. The 15th percentile of the signal intensity histogram (SI_{15}) was compared with CT threshold measurements.

For healthy volunteers, manually segmented FRC+1L images were registered to the other three lung volumes as previously described.[14] ^{3}He MRI apparent diffusion coefficient (ADC) maps were generated using software, as previously described.[13] For CT image analysis, Pulmonary Workstation 2.0 (VIDA Diagnostics Inc., Iowa City, IA) was used to quantify tissue attenuation in Hounsfield units (HU) based on the relative area of the density histogram≤-950 HU (RA_{950}), 15th percentile of the density histogram (HU_{15}), mean radio-density, wall area percent (WA%), and lumen area (LA) for the segmental and subsegmental airways.[15] Signal intensity and CT density histograms were generated by combining all the pixel values of the corresponding subgroup or lung volume together. Histograms were normalized to the area beneath the curve.

3.2.5 Statistics

Independent t-tests, the Shapiro-Wilk test for normality, analysis of variance (ANOVA) and post-hoc analysis using the Holm-Bonferroni correction were performed using IBM SPSS Statistics 21.0 (SPSS Inc., Chicago, IL, USA). The data was normal and therefore parametric tests were used. Univariate relationships were determined using linear regression (r^2) and Pearson correlation coefficients (r) using Prism GraphPad version 6.00

(GraphPad Software, San Diego, CA). To evaluate three-week reproducibility, a repeated measures analysis of variance (ANOVA) was used for UTE signal intensity and ADC using IBM SPSS Statistics 21.0 (SPSS Inc., Chicago, IL, USA). Linear regression and Pearson correlation coefficients (r) were used to determine 3-week correlations and the relationship between UTE signal intensity and S_R using GraphPad Prism version 6.00 (GraphPad Software Inc, San Diego, CA). The COV which is the ratio of the standard deviation of all measurements and the mean of repeated measurements was used to evaluate repeat imaging reproducibility. A two-way mixed model intra-class correlation coefficient (ICC) analysis for absolute agreement was also used to determine reproducibility. Fisher z-transformation was used to determine the significance of difference between Pearson correlation coefficients. Results were considered significant when the probability of making a Type I error was less than 5% ($p<0.05$).

3.3 Results

3.3.1 Subject Demographics

Twenty subjects were evaluated including five healthy volunteers and 15 subjects (60±39 pack-years) with a clinical diagnosis of COPD, based on symptoms and GOLD criteria. For eight COPD subjects, there was qualitative CT evidence of emphysema only, whereas in seven COPD subjects, there was both emphysema and bronchiectasis. **Table 3-1** shows subject demographics and pulmonary function measurements for healthy volunteers, all COPD subjects and stratified into COPD subjects with emphysema, and subjects with both emphysema and bronchiectasis.

3.3.2 Relationship between Lung Density and Signal Intensity

Figure 3-2 shows the centre coronal slice for a healthy 22yr male using a conventional FGRE sequence and two different UTE imaging schemes. The normalized lung parenchyma signal intensity increased from 6% to 27% using 32-channel UTE MRI with compressed sensing. The bar graphs in the right panel show the significant improvements in signal intensity ($p<0.001$), S_R ($p=0.002$), and C_R ($p<0.001$) for the 32-channel UTE sequence as compared to the single-channel UTE and 32-channel FGRE approaches. **Figure 3-3** shows UTE images acquired for a representative healthy volunteer at four

different lung volumes and shows the qualitative differences in parenchymal signal intensity at full expiration compared to full inspiration. **Figure 3-3** also shows the strong and significant relationships of nominal lung mass-density with signal intensity using MRI-derived (r^2=0.98, r=0.99, p=0.007) and plethysmography-derived (r^2=0.89, r=0.94, p=0.06) lung volumes for all healthy volunteers. The relationship for signal intensity with MRI and plethysmography-derived volumes was not significantly different. The frequency distribution of mean signal intensity for all four lung volumes is also shown in **Figure 3-3C**, and shows a shift towards lower densities and narrowed distribution at higher lung volumes.

Table 3-1 Subject demographic and pulmonary function test measurements

		COPD (n=15)		GOLD Grade (n=15)			Significant Difference	
	Healthy	Emphysema	Emphysema +Bronchiectasis	GOLD I	GOLD II	GOLD III+IV	H/E/E+B	I/II/III+IV
Mean (±SD)	(n=5)	(n=8)	(n=7)	(n=3)	(n=6)	(n=6)	*p*	*p*
Age yrs	22(1)	67 (9)	65(8)	70 (9)	66 (8)	63 (9)	**<0.001**	0.6
Male Sex n	5	5	3	2	3	3		
BMI kg/m^2	26(1)	28(4)	26(4)	28 (4)	29 (3)	25 (5)	0.5	0.2
FEV_1 $\%_{pred}$	101(14)	62(24)	54(19)	89 (8)	65 (9)	37 (8)	**0.003**	**<0.001**
FVC $\%_{pred}$	99(14)	93(15)	82(26)	104 (7)	94 (22)	74 (17)	0.3	0.08
FEV_1/FVC %	85(3)	51(17)	49(12)	64 (11)	53 (11)	39 (10)	**<0.001**	**0.02**
TLC $\%_{pred}$	103(11)	123(11)	111(17)	118 (4)	109 (17)	126 (13)	0.05	0.4
RV $\%_{pred}$	117(1)	174(52)	151(44)	142 (15)	129 (27)	208 (38)	0.1	**0.002**
FRC $\%_{pred}$	101(16)	137(31)	134(36)	116 (13)	114 (24)	168 (15)	0.1	**0.001**
DL_{CO} $\%_{pred}$	132(18)	59(30)	58(19)	70 (38)	54 (4)	57 (32)	**<0.001**	0.7

Significance of difference ($p<0.05$) determined using an analysis of variance. H=healthy volunteer; E=CT evidence of emphysema only, E+B: CT evidence of emphysema and bronchiectasis; SD=standard deviation; BMI=body mass index; FEV_1=forced expiratory in 1s; $\%_{pred}$=percent predicted; FVC=forced vital capacity; FRC=functional residual capacity; TLC=total lung capacity; RV=residual volume; DL_{CO}=diffusing capacity of lung for carbon monoxide.

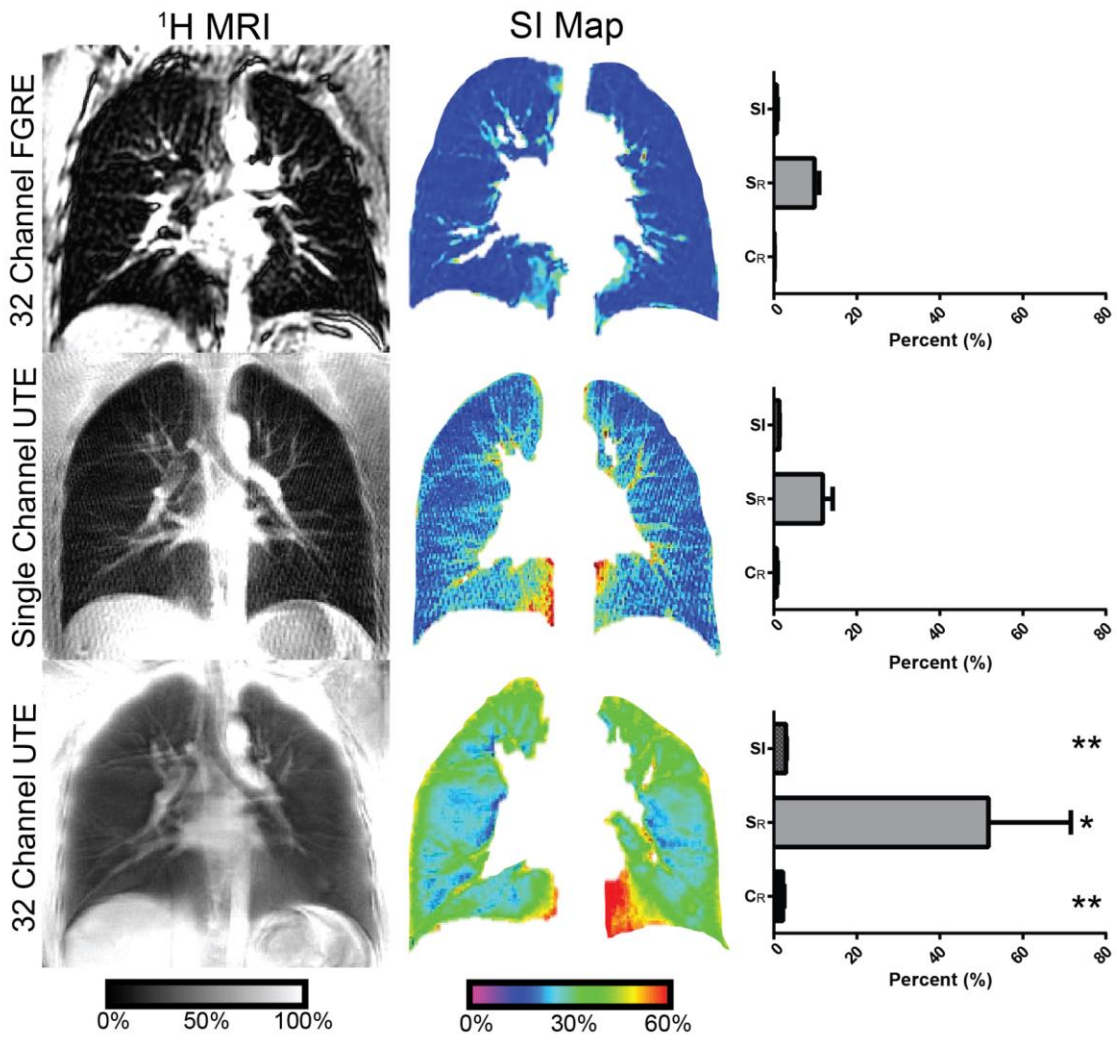

Figure 3-2 ^{1}H MRI of healthy volunteers
Top panel: 32-channel FGRE MRI with mean normalized ^{1}H SI=6%, S_R=1. Middle panel: single-channel UTE MRI with normalized mean ^{1}H SI=11%, S_R=3. Bottom panel: 32-channel UTE MRI using compressed sensing (CS) with mean normalized ^{1}H SI=27%, S_R=7. Right panel shows bar graphs with mean ^{1}H SI (normalized ^{1}H signal intensity), ^{1}H S_R (apparent signal-to-noise ratio), and ^{1}H C_R (normalized contrast-to-noise ratio) for all healthy volunteers (n=3 for signal channel UTE ^{1}H measurements). Significant differences between FGRE, signal-channel UTE, and 32-channel UTE MRI measurements shown by asterisks. *p<0.01, **p<0.001.

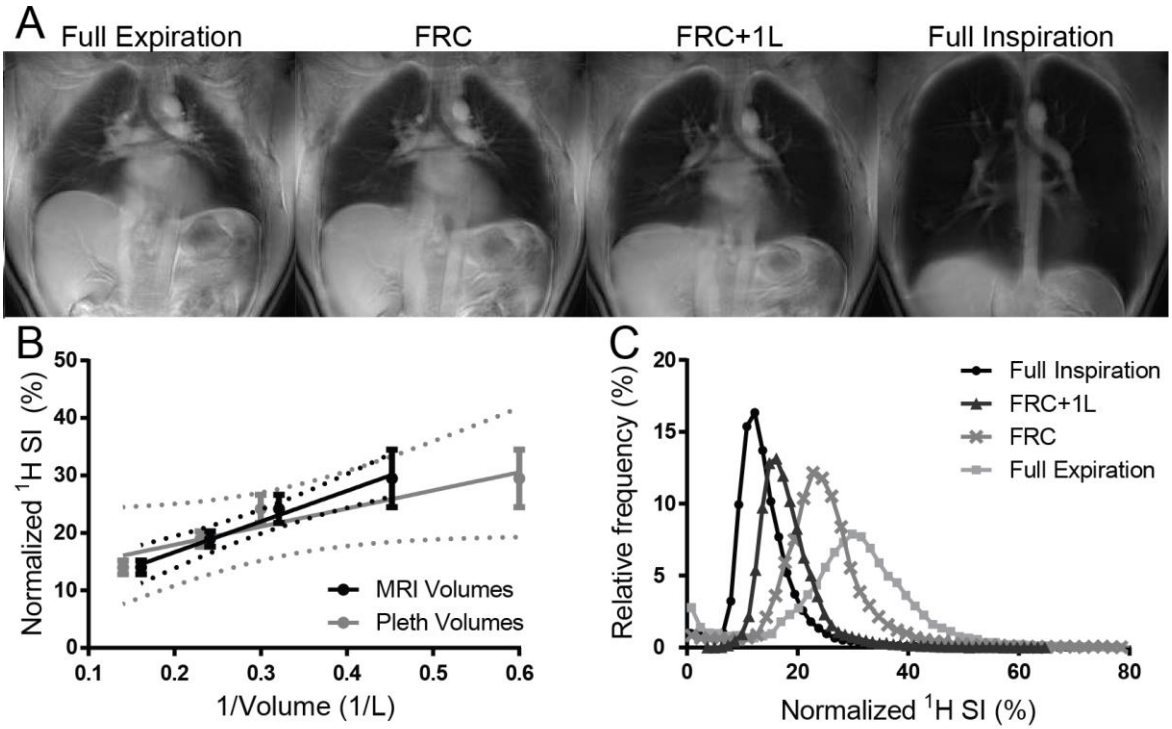

Figure 3-3 Centre coronal slice MRI of a representative healthy volunteer
A) UTE MR images of a 21 yr old male (FEV_1=89%$_{pred}$, FEV_1/FVC=88%, DL_{CO}=141%$_{pred}$) at full expiration (FE), functional residual capacity (FRC), FRC+1L, and, full inspiration (FI) (from left to right); B) Normalized UTE signal intensity compared to lung mass-density derived from FGRE volumes in black (y=5.3x10^3x+6, r^2=0.98, r=0.99, p=0.007) and with lung mass-density derived from plethysmography volumes in grey (y=3.2x10^3x+12, r^2=0.89, r=0.94, p=0.06); C) Normalized UTE signal intensity histograms for mean of all healthy volunteers at four different lung volumes.

3.3.3 Reproducibility

Seven subjects with COPD (emphysema, n=3; emphysema with bronchiectasis, n=4) underwent a three-week follow-up visit. Table 2 shows ^{1}H and ^{3}He MRI measurements at baseline and follow-up for seven subjects with COPD including COV, Pearson correlation coefficients, and ICC for 3-week re-scan measurements. ^{3}He ADC measurements were used as an internal control for reproducibility comparisons with the ^{1}H UTE measurements. There was no significant difference between baseline and 3-week ^{1}H UTE signal intensity (Δ^1H SI=0±2%, p=0.9), ^{1}H SI SD (Δ^1H SI SD=0±1%, p=0.2), ^{1}H SI COV (Δ^1H SI COV=2±4%, p=0.2), or ^{1}H SI_{15} (Δ^1H SI_{15}=0±1%, p=0.6). The COV for repeated measurements of ^{1}H signal intensity and SI_{15} was 4% and 8%, respectively. Reproducibility is also shown in **Figure 3-4** for a subject with emphysema and

bronchiectasis (**Figure 3-4A**) and for a subject with emphysema only (**Figure 3-4B**). The corresponding histograms are shown for the baseline and three-week histograms for UTE signal intensity and ADC maps. **Figures 3-4C-4E** show strong linear relationships for baseline and three-week normalized ^{1}H signal intensity (r^2=0.85, p=0.003), SI_{15} (r^2=0.67, p=0.02), and S_R (r^2=0.74, p=0.01), respectively. **Figure 3-4F** shows the strong linear relationship for baseline and three-week ADC measurements (r^2=0.95, p=0.002). There was no significant difference between ^{1}H signal intensity and ^{3}He ADC Pearson correlation coefficients (p=0.3). Finally, there was no significant correlation between ^{1}H signal intensity and S_R (r^2=0.08, p=0.5).

Table 3-2 Baseline and 3-week ^{1}H and ^{3}He measurements and reproducibility analysis

	COPD (n=7)*						
	^{1}H SI (%)	^{1}H SI SD (%)	^{1}H SI COV (%)	^{1}H SI_{15} (%)	^{1}H S_R	^{1}H C_R	ADC (cm^2/s)
Measurements							
Baseline (±SD)	27(4)	3(2)	27(6)	19(3)	7(5)	0.19(0.05)	0.42(0.14)
3-Week (±SD)	27(4)	3(1)	29(5)	19(2)	7(7)	0.17(0.07)	0.42(0.12)
Reproducibility							
COV (%)	4	13	4	8	36	9	6
Pearson r	0.87	0.84	0.85	0.82	0.85	0.09	0.97
ICC	0.87	0.80	0.84	0.81	0.79	0.08	0.96

*Including emphysema (n=3) and emphysema with bronchiectasis subjects (n=4). ^{1}H SI=normalized centre slice signal intensity, ^{1}H SI SD=standard deviation of the centre slice signal intensity, ^{1}H SI COV=centre slice signal intensity coefficient of variation, ^{1}H SI_{15}=15th percentile of the frequency distribution histogram of UTE signal intensities; ^{1}H S_R=centre slice apparent signal-to-noise ratio, ^{1}H C_R=centre slice normalized contrast-to-noise ratio, ADC=apparent diffusion coefficient, COV=coefficient of variation, ICC=intra-class correlation coefficient.

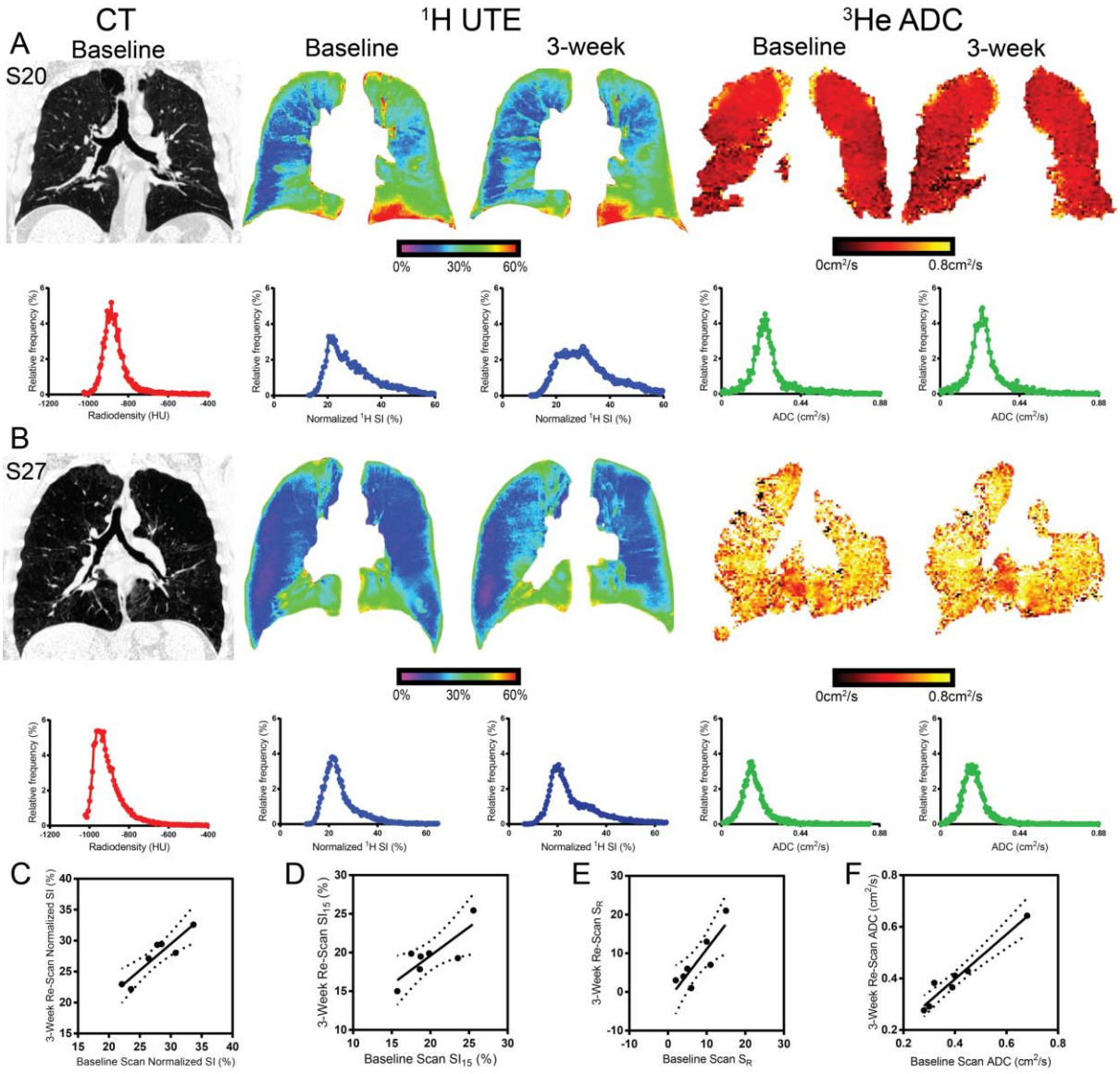

Figure 3-4 Baseline and 3-week images for two representative COPD subjects
Baseline CT, baseline and 3-week UTE MRI signal intensity maps and ^{3}He ADC maps with corresponding histograms. A) S20 is a 61 yr male with emphysema and bronchiectasis; B) S27 is a 51 yr male with emphysema. Shown below are linear regressions of inter-scan reproducibility for C) normalized ^{1}H signal intensity (r^2=0.85, r=0.87, p=0.003), D) SI_{15} (r^2=0.67, r=0.82, p=0.02), E) S_R (r^2=0.74, r=0.85, p=0.01), and, F) ADC (r^2=0.95, r=0.97, p=0.002).

3.3.4 Quantitative Analysis

Table 3-3 shows imaging measurements for healthy volunteers, COPD subjects with emphysema, and COPD subjects with both emphysema with bronchiectasis. Independent t-tests showed significant signal intensity differences ($p<0.05$) for healthy volunteers as

compared to subjects with emphysema and subjects with both emphysema with bronchiectasis. Healthy volunteers had significantly greater ^{1}H signal intensity and ^{1}H C_R than subjects with emphysema and subjects with both emphysema with bronchiectasis. Healthy volunteers also had significantly greater ^{1}H SI_{15} than the COPD subjects with emphysema, but this was not significantly different than subjects with both emphysema and bronchiectasis.

Table 3-3 Imaging measurements for all subjects

		COPD (n=15)		GOLD Grade (n=15)			Significant Difference	
	Healthy	**Emphysema**	**Emphysema +Bronchiectasis**	**GOLD I**	**GOLD II**	**GOLD III+IV**	**H/E/E+B**	**I/II/III+IV**
Mean (±SD)	**(n=5)**	**(n=8)**	**(n=7)**	**(n=3)**	**(n=6)**	**(n=6)**	***p***	***p***
^{1}H SI %	29(2)	23(3)*	24(4)*	27 (3)	23 (5)	22 (3)	0.07	0.3
^{1}H SI_{15} %	21(1)	18(3)*	18(4)	18 (4)	19 (4)	17 (2)	0.09	0.6
^{1}H S_R	5.17(1.99)	4.82(2.02)	3.04(1.57)	6.12 (2.17)	3.55 (1.59)	3.37 (1.80)	0.1	0.1
^{1}H C_R	0.22(0.03)	0.17(0.03)*	0.13(0.04)*	0.19 (0.03)	0.15 (0.04)	0.14 (0.03)	**0.001**	0.1
ADC cm^2/s	0.20(0.01)	0.46(0.14)	0.41(0.11)	0.39 (0.17)	0.41 (0.10)	0.48 (0.13)	**0.003**	0.4
Radiodensity HU	--	-855(35)	-849(43)	-831(26)	-839(47)	-874(27)	0.8	0.2
RA_{950} %	--	17(15)	11(9)	9 (12)	11 (9)	19 (15)	0.3	0.4
$HU_{15\%}$ HU	--	-942(37)	-927(41)	-921 (42)	-923 (47)	-950 (28)	0.5	0.3
WA %	--	60(4)	59(4)	63 (3)	58 (4)	60 (4)	0.7	0.1
LA mm^2	--	21(4)	27(14)	18 (6)	30 (13)	20 (4)	0.2	0.2
LA/BSA mm^2/m^2	--	11(3)	15(6)	10 (3)	16 (6)	12 (3)	0.1	0.6
Pi10 mm	--	4.23(0.15)	4.22(0.11)	4.31 (0.20)	4.24 (0.10)	4.17 (0.11)	0.9	0.3

Significance of difference ($p<0.05$) determined using an analysis of variance. H=healthy volunteer; E=CT evidence of emphysema only, E+B: CT evidence of emphysema and bronchiectasis; SD=standard deviation; SI=normalized ^{1}H signal intensity; SI_{15}=15th percentile of the frequency distribution histogram of UTE signal intensities; S_R=apparent signal-to-noise ratio; C_R=normalized contrast-to-noise ratio; ADC=apparent diffusion coefficients; RA_{950}=relative area of the lung with attenuation values < -950 HU; $HU_{15\%}$=15th percentile of the frequency distribution histogram in HU; LA=lumen area; BSA=body surface area; Pi10=airway wall thickness at an internal perimeter of 10mm. *Independent t-test shows significant difference between healthy volunteers ($p<0.05$).

Figure 3-5 shows the MRI signal intensity maps, CT images and frequency distribution for MRI signal intensity and CT radio-density for two representative subjects with emphysema and two representative subjects with both emphysema and bronchiectasis. The UTE signal intensity maps show regions of emphysema in blue and regions of inflammation, mucous, and other regions of increased lung density in yellow. For the UTE signal intensity and CT radio-density there is evidence of regionally consistent

identification of corresponding abnormalities. As shown in the signal intensity frequency distributions in **Figure 3-5**, there was a bi-modal distribution in S24 and with increasing COPD grade, the signal intensity distributions shifted towards lower signal intensities. This trend was also observed in the radio-density frequency distributions, where with increasing COPD grade, there was a shift towards the lower radio-densities.

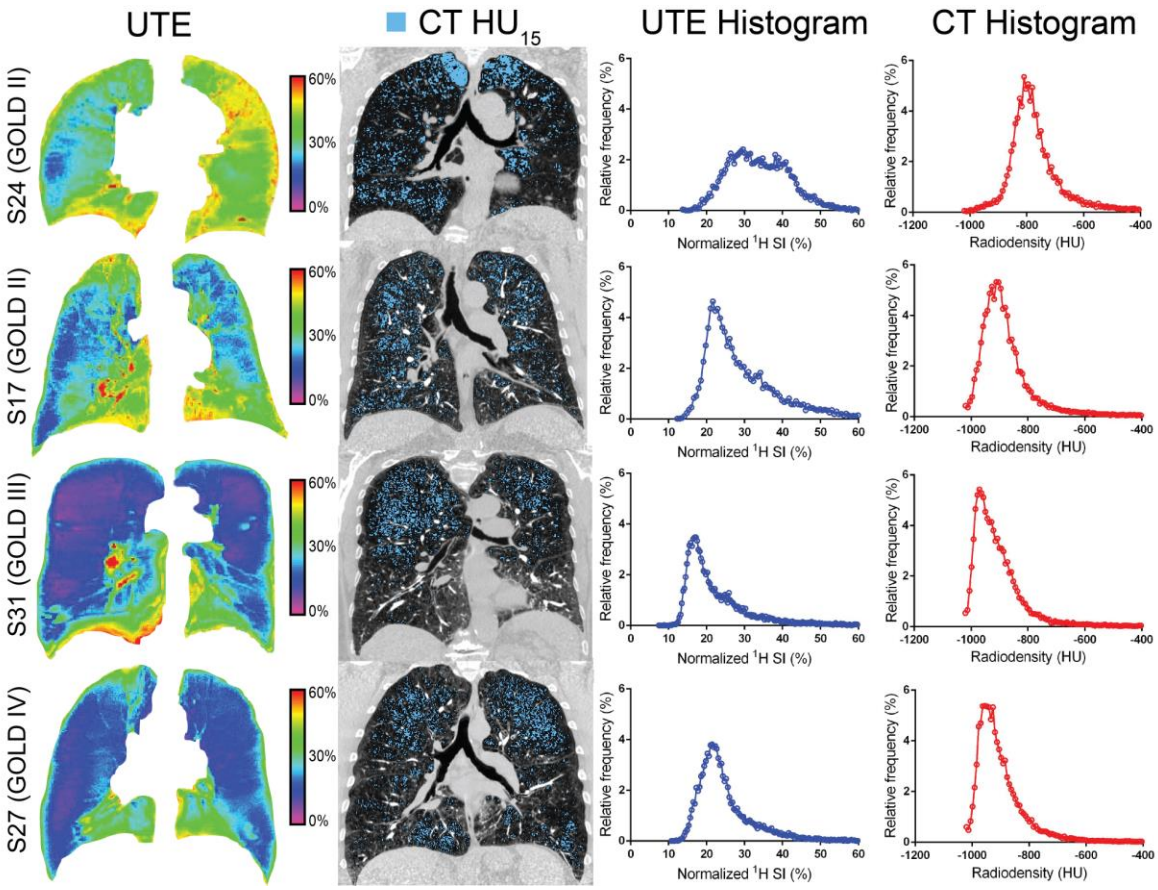

Figure 3-5 MRI and CT of COPD patients
Normalized UTE signal intensity maps, CT images with relative area (RA) emphysema mask for 15th percentile of the HU (HU_{15}, in blue), MRI signal intensity histograms, and CT radio-density histograms. S24 is a 59 yr female with emphysema and bronchiectasis, FEV_1=67%$_{pred}$, FEV_1/FVC=71%, DL_{CO}=54%$_{pred}$; S17 is a 77 yr male with emphysema and bronchiectasis and FEV_1=79%$_{pred}$, FEV_1/FVC=42%, DL_{CO}=50%$_{pred}$; S31 is a 75 yr female with GOLD III and FEV_1=46%$_{pred}$, FEV_1/FVC=39%, DL_{CO}=29%$_{pred}$; S27 is a 51 yr male with GOLD IV and FEV_1=28%$_{pred}$, FEV_1/FVC=22%, DL_{CO}=32%$_{pred}$.

3.3.5 Correlations with Pulmonary Function Measurements and CT

Table 3-4 summarizes the significant correlations for MRI signal intensity and pulmonary measurements for all COPD subjects. For all subjects, there were significant correlations

for signal intensity with RA_{950} (r^2=0.50, p=0.005), FEV_1/FVC (r^2=0.35, p=0.02), DL_{CO} (r^2=0.25, p=0.05), and mean radio-density (r^2=0.85, p<0.001). There was a significant but very modest correlation for SI_{15} and HU_{15} (r^2=0.38, p=0.01). For subjects with only emphysema, significant relationships were observed for signal intensity with RA_{950} (r^2=0.90, p=0.002), HU_{15} (r^2=0.83, p=0.005), and mean radio-density (r^2=0.90, p=0.001). For subjects with both emphysema and bronchiectasis, there were significant relationships were observed for signal intensity and RV (r^2=0.59, p=0.04), HU_{15} (r^2=0.76, p=0.01), Pi10 (r^2=0.62, p=0.04) and mean radio-density (r^2=0.85, p=0.04).

Table 3-4 UTE signal intensity correlations with ^{3}He MRI ADC, CT and pulmonary function test measurements

	COPD (n=15)				**GOLD Grade (n=15)**					
	Emphysema (n=8)		**Emphysema+ Bronchiectasis (n=7)**		**GOLD I (n=3)**		**GOLD II (n=6)**		**GOLD III+IV (n=6)**	
	r	**p**	**r**	**p**	**r**	**p**	**r**	**p**	**r**	**p**
FEV_1 $\%_{pred}$	0.50	NS	0.57	NS	0.78	NS	0.39	NS	0.30	NS
FEV_1/FVC %	0.50	NS	0.70	NS	0.91	NS	0.61	NS	0.37	NS
FRC $\%_{pred}$	-0.04	NS	-0.64	NS	-0.44	NS	-0.46	NS	-0.56	NS
TLC $\%_{pred}$	0.31	NS	-0.75	NS	0.99	NS	-0.57	NS	-0.16	NS
RV $\%_{pred}$	0.19	NS	**-0.77**	**0.04**	0.49	NS	-0.58	NS	0.31	NS
DL_{CO} $\%_{pred}$	0.62	NS	0.32	NS	0.67	NS	0.09	NS	**0.85**	**0.03**
ADC cm^2/s	-0.41	NS	-0.61	NS	-0.76	NS	-0.30	NS	-0.51	NS
Radiodensity HU	**0.95**	**0.001**	**0.92**	**0.004**	**0.99**	**0.04**	**0.93**	**0.02**	**0.82**	**0.04**
RA_{950} %	**-0.94**	**0.002**	-0.60	NS	-0.93	NS	-0.49	NS	-0.76	NS
$HU_{15\%}$ HU	**0.91**	**0.005**	**0.87**	**0.01**	0.87	NS	0.84	NS	**0.86**	**0.03**
WA %	0.45	NS	-0.09	NS	0.51	NS	0.19	NS	-0.19	NS
LA mm^2	-0.60	NS	0.20	NS	-0.75	NS	0.12	NS	-0.01	NS
LA/BSA mm^2/m^2	**-0.70**	**0.05**	-0.02	NS	-0.87	NS	0.04	NS	-0.57	NS
Pi10 mm	0.38	NS	**0.79**	**0.04**	0.19	NS	0.41	NS	**0.90**	**0.01**

r=Pearson correlation coefficient (p<0.05). FEV_1=forced expiratory in 1s; $\%_{pred}$=percent predicted; FVC=forced vital capacity; FRC=functional residual capacity; TLC=total lung capacity; RV=residual volume; DL_{CO}=diffusing capacity of lung for carbon monoxide; ADC=apparent diffusion coefficient; RA_{950}=relative area of the lung with attenuation values<-950 HU; $HU_{15\%}$=15th percentile of the frequency distribution histogram in HU; LA=lumen area; BSA=body surface area; Pi10=airway wall thickness at an internal perimeter of 10mm

3.4 Discussion

In recognition of some of the limitations of CT for longitudinal and serial evaluations of COPD, we are developing rapid pulmonary MRI methods to provide quantitative measurements of tissue density and airway abnormalities. By utilizing compressed sensing and parallel imaging in combination with an ultra-short echo time, we showed: 1) significantly improved C_R, S_R, and signal intensity, 2) a significant and strong relationship for MR signal intensity and tissue density, 3) high three-week reproducibility for UTE signal intensity measurements, and, 4) spatial correlations for signal intensity with CT-identified regions of emphysema, inflammation, and mucous plugging and quantitative correlations with pulmonary function and CT measurements.

First, there was significantly improved signal intensity, S_R, and C_R using the 32-channel UTE approach as compared to the single channel UTE and 32-channel FGRE approaches. The improved signal intensity and S_R was not surprising because of the geometry and number of elements in the 32-channel compared to the body coil. Improvements in signal intensity, S_R, and C_R using the 32-channel UTE sequence were also expected because of the shorter echo-time and radial sampling. Furthermore, for the UTE sequence, data acquisition began at the centre of *k*-space and extended radially, oversampling the centre of *k*-space and as a result, there was improved contrast at lower frequencies.

Second, in healthy volunteers, pulmonary signal intensity was strongly related to the inverse of lung volume and because total lung mass was constant, this reduced to a strong linear relationship for signal intensity and nominal lung density. Therefore, similar to CT,[16] signal intensity directly reflected lung density, which suggests that UTE signal intensity can be used to quantify parenchymal tissue destruction and inflammation. UTE signal intensity histograms shifted towards lower intensity values at higher lung volumes which is consistent with CT studies,[16] and this is important, given that CT is universally recognized as the clinical non-invasive gold standard for lung density measurements. The increased heterogeneity at full expiration may be explained by the changing vascular portion at different lung volumes.[16] UTE signal intensity maps showed similar regional information for both emphysema and inflammation/mucous deposition and these

preliminary qualitative results suggest that ^{1}H MRI may provide a way to characterize the heterogeneous pathological processes of COPD and offer an alternative to CT measurements.

We reported high UTE signal intensity reproducibility for three-week re-scan for COPD subjects which was consistent with high Pearson correlation coefficients, low COV and high ICC. To further understand the relationship of reproducibility with image quality, we investigated whether differences in S_R would influence UTE signal intensity, but did not find a significant relationship between them. This suggests that noise did not influence the UTE signal intensity measurements. Moreover, these results suggest that 2D UTE MRI provides a reproducible technique to monitor treatment response in longitudinal studies.

We reported significant and moderate correlations for UTE signal intensity with pulmonary function, and CT measurements for COPD subjects. These correlations are consistent with lung tissue destruction in emphysema leading to lung mass and density loss. It is interesting to note that in subjects with emphysema only, in addition to significant relationships between RA_{950}, HU_{15}, and mean radio-density there was a significant correlation with lumen area normalized to body surface area. It is also interesting to note that in subjects with both emphysema and bronchiectasis, there was a positive relationship between Pi10 and signal intensity, consistent with the notion that in bronchiectasis subjects, thickened airways resulted in increased signal intensity.

Although this study provides promising preliminary results, several limitations must be acknowledged. First, our analysis ignored the effect of pulmonary perfusion at different lung volumes in healthy volunteers. As lung perfusion is dictated by the relationship between alveolar, pulmonary arterial, and pulmonary venous pressures - all of which vary at different lung volumes, it is expected that different lung volumes will change perfusion and subsequently change the UTE signal. Several potential mechanisms may explain pulmonary perfusion changes at different lung volumes (hypoxic vasoconstriction of the alveolar vessels, vessel branching pattern change, and the cavity pressure change) and its impact on UTE signal intensity. Second, it is important to note that the impact of effective transverse decay time T2* on signal intensity at different lung volumes was ignored in

healthy volunteers for two reasons: 1) in human lungs, T2* variability was significantly smaller than other factors affecting SI across different lung volumes[17] 2) the echo-time of 50μs was significantly smaller than the parenchymal T2* (500-800μs),[7,17] which minimized the T2* weighting effect. Also, unlike CT, MRI signal intensity is influenced by hardware factors such as RF amplifications and the positioning of the RF coils, which introduce inter-scan variability. While we corrected for absolute signal intensity quantification by normalizing acquired images to the liver, this is influenced by the precision of liver measurements. In this regard, we note that the liver has minimal motion during the image acquisition and is relatively homogeneous despite inter-subject signal variability. Finally, we acknowledge that the histopathological relationship between MRI signal intensity and CT radio-density measurements has not yet been established. The quantification of emphysema using CT uses different threshold type analyses has been compared with histology,[18] this has not yet been undertaken with parenchymal MRI signal intensity. The comparison of mean MRI signal intensity to CT RA_{950} and HU_{15} is likely a conservative estimate of any direct relationships. For this reason, the comparison of MRI-derived SI_{15} with CT-derived HU_{15} is likely a better estimate of the direct relationships of MRI signal intensity and CT radio-density measurements.

Future studies will investigate three-dimensional UTE acquisition. The three-dimensional UTE method would allow for more efficient RF excitation, isotropic spatial resolution, and reduced sensitivity to motion artifacts compared to 2D UTE.[19]

In summary, we developed a 2D UTE MRI method to generate rapid measurements of pulmonary signal intensity that are strongly related to tissue density and in subjects with COPD is related to pulmonary function and CT measurements.

3.5 References

(1) Vestbo, J. et al. Evaluation of COPD Longitudinally to Identify Predictive Surrogate End-points (ECLIPSE). *Eur Respir J* 2008; 31: 869-873.

(2) Regan, E. A. et al. Genetic epidemiology of COPD (COPDGene) study design. *COPD* 2010; 7: 32-43.

(3) Bild, D. E. et al. Multi-ethnic study of atherosclerosis: objectives and design. *Am J Epidemiol* 2002; 156, 871-881.

(4) O'Brien, C., Guest, P. J., Hill, S. L. & Stockley, R. A. Physiological and radiological characterisation of patients diagnosed with chronic obstructive pulmonary disease in primary care. *Thorax* 2000; 55, 635-642.

(5) Smith-Bindman, R. et al. Use of diagnostic imaging studies and associated radiation exposure for patients enrolled in large integrated health care systems, 1996-2010. *JAMA* 2012; 307: 2400-2409.

(6) Bergin, C. J., Pauly, J. M. & Macovski, A. Lung parenchyma: projection reconstruction MR imaging. *Radiology* 1991; 179, 777-781.

(7) Ohno, Y. et al. T2* measurements of 3-T MRI with ultrashort TEs: capabilities of pulmonary function assessment and clinical stage classification in smokers. *AJR. Am J Roentgenol* 2011; 197: W279-285.

(8) Johnson, K. M., Fain, S. B., Schiebler, M. L. & Nagle, S. Optimized 3D ultrashort echo time pulmonary MRI. *Magn Reson Med* 2012; 70,1241-50.

(9) Bianchi, A., Ozier, A., Ousova, O., Raffard, G. & Cremillieux, Y. Ultrashort-TE MRI longitudinal study and characterization of a chronic model of asthma in mice: inflammation and bronchial remodeling assessment. *NMR Biomed* 2013; 26:1451-9.

(10) Rosen, M. J. Chronic cough due to bronchiectasis: ACCP evidence-based clinical practice guidelines. *Chest* 2006; 129: 122S-131S.

(11) Vestbo, J. et al. Global strategy for the diagnosis, management, and prevention of chronic obstructive pulmonary disease: GOLD executive summary. *Am J Respir Crit Care Med* 2013; 187: 347-365.

(12) Lustig, M. & Pauly, J. M. SPIRiT: Iterative self-consistent parallel imaging reconstruction from arbitrary k-space. *Magn Reson Med* 2010; 64: 457-471.

(13) Parraga, G. et al. Hyperpolarized 3He ventilation defects and apparent diffusion coefficients in chronic obstructive pulmonary disease: preliminary results at 3.0 Tesla. *Invest Radiol* 2007; 42: 384-391.

(14) Heinrich, M. P. et al. MIND: modality independent neighbourhood descriptor for multi-modal deformable registration. *Med Image Anal* 2012; 16: 1423-1435.

(15) Hasegawa, M. et al. Airflow limitation and airway dimensions in chronic obstructive pulmonary disease. *Am J Respir Crit Care Med* 2006; 173: 1309-1315.

(16) Wegener, O. H., Koeppe, P. & Oeser, H. Measurement of lung density by computed tomography. *J Comput Assist Tomogr* 1978; 2: 263-273.

(17) Yu, J., Xue, Y. & Song, H. K. Comparison of lung T2* during free-breathing at 1.5 T and 3.0 T with ultrashort echo time imaging. *Magn Reson Med* 2011; 66: 248-254.

(18) Gevenois, P. A. et al. Comparison of computed density and microscopic morphometry in pulmonary emphysema. *Am J Respir Crit Care Med* 1996; 154: 187-192.

(19) Barger, A. V., Block, W. F., Toropov, Y., Grist, T. M. & Mistretta, C. A. Time-resolved contrast-enhanced imaging with isotropic resolution and broad coverage using an undersampled 3D projection trajectory. *Magn Reson Med* 2002; 48: 297-305.

CHAPTER 4

4 THREE DIMENSIONAL ULTRA-SHORT ECHO TIME MAGNETIC RESONANCE IMAGING OF ASTHMA

To determine the underlying structural and clinical determinants of MRI signal-intensity in patients with asthma we generated novel ultra-short echo time (UTE) MRI biomarkers in asthmatics and directly compared these with structural CT and other clinical measurements.

The contents of this chapter have been submitted to the Journal of Magnetic Resonance in Medicine: K Sheikh, F Guo, DPI Capaldi, A Ouriadov, RL Eddy, S Svenningsen, and G Parraga. Accepted for publication in J Magn Reson Imaging 2016 (in press).

4.1 Introduction

Asthma is a chronic inflammatory disease involving both the large and small airways.[1,2] Complex airway abnormalities including airway smooth muscle remodeling[3,4] and inflammation[4] are thought to be the source of shortness of breath, wheeze and chest tightness. These are also associated with gas-trapping[5] and ventilation/perfusion abnormalities.[6] Currently, asthma is diagnosed and monitored based on spirometry measurements of airflow made at the mouth.[7] These measurements tend to over-estimate large airway constriction, under-estimate small airways disease[8] and cannot provide regional information.

Lung structural and functional abnormalities have also been measured in patients with asthma using chest computed tomography (CT),[9] single photon emission computed tomography,[10] positron emission tomography[11] and magnetic resonance imaging (MRI) using inhaled gases.[12,13] Because asthma often spans the lifetime of individual patients, the risk of cumulative radiation exposure certainly limits the use of x-ray based imaging for longitudinal and treatment response evaluations, especially in children.[14]

A number of research teams have pioneered the use of inhaled gas MRI in asthmatics;[12,15,16] this previous work showed that ventilation abnormalities were heterogeneously distributed,[17,18] reproducible,[19] related to asthma severity[12] and asthma control.[17] Recently, zero echo time and ultra-short echo time (UTE) MRI have emerged as methods to minimize

MRI signal decay for the quantification of lung proton density.[20-26] Previous UTE asthma studies showed the inflammatory response to allergen challenge in animal models[27] and patients.[28] This previous work demonstrated the potential and feasibility of ^{1}H MRI methods for measuring the therapeutic efficacy of new asthma treatments. Recent work also estimated regional ventilation deficits in asthmatics based on the change in signal-intensity measured at different lung volumes using conventional ^{1}H MR methods and echo-times.[29] However, it is well-understood that MRI signal-intensity is influenced by hardware factors such as RF amplification and RF coil positioning, which can introduce inter-scan variability. Because of this, it is difficult to ascertain the physiological meaning of ^{1}H MR signal-intensity changes especially in asthma where the underlying pathophysiology is complex.

In an effort to better understand pulmonary MRI measurements, two-dimensional UTE MRI was recently evaluated in participants with COPD and bronchiectasis,[30] patients that share some of the airway and inflammatory features common in asthmatics.[31] Based on some of this previous work, we hypothesized that UTE-derived biomarkers could be generated across different lung volumes to capture evidence of ventilation abnormalities in patients with asthma and these measurements would be related to pulmonary function test measurements of gas-trapping and/or airflow obstruction. Therefore, the objective of this proof-of-concept study was to generate novel UTE MRI biomarkers in asthmatics in whom CT structural and other clinical measurements could be directly compared.

4.2 Materials and Methods

4.2.1 Study Logistics

All participants provided written informed consent to a study protocol approved by a local research ethics board and compliant with the Health Insurance Portability and Accountability Act (HIPAA, USA). Healthy volunteers underwent pulmonary function tests and UTE MRI only. All subjects with a diagnosis of asthma underwent pre- and post-salbutamol pulmonary function tests, hyperpolarized noble gas MRI, UTE MRI and post-salbutamol thoracic CT. Methacholine challenge (MCh) was restricted to asthmatics according to ATS guidelines[32] with testing halted at the $\underline{PC}_{\underline{20}}$ which is the provocative

concentration resulting in a 20% decrease in forced expiratory volume in 1 second, or FEV_1.

Spirometry was used to measure FEV_1, forced vital capacity (FVC), and their ratio (FEV_1/FVC) according to American Thoracic Society (ATS) guidelines (MedGraphics Elite Series Plethysmograph, MedGraphics Corporation, St. Paul, Minnesota, USA).[33] Body plethysmography was also performed to measure lung volumes such as residual volume (RV), functional residual capacity (FRC), and total lung capacity (TLC).

4.2.2 Image Acquisition

MRI was acquired in the coronal plane using a whole body 3 Tesla Discovery MR750 (General Electric Health Care [GEHC], Milwaukee, WI, USA) system with broadband imaging capability. MRI was acquired pre- and post-salbutamol for all asthmatics and at PC_{20} in those asthmatics who underwent the methacholine challenge. UTE MRI was obtained using a 32-channel torso coil (GEHC) and 3D cones UTE sequence (GEHC). Whole lung UTE images were acquired in the coronal plane with the following parameters in breath-hold: 15s acquisition time, echo time (TE)/repetition time (TR)/flip angle=0.03ms/3.5ms/5°, field-of-view (FOV)=40×40cm, bandwidth (BW)=125kHz, matrix=200×200, number of excitations (NEX)=1, and reconstructed to a 10mm slice thickness. UTE MR images were acquired at four lung volumes including full expiration, FRC, FRC plus one liter, and full inspiration and this was completed in 5-10 minutes. Subjects were coached to achieve full expiration and full inspiration. FRC was achieved at the end of passive expiration and FRC+1L was achieved by the inhalation of a 1L bag of N_2. The B_1 field was mapped using a dual angle 3D Look-Locker pulse sequence (40s total data acquisition, TE/TR=0.3ms/1200ms, $\alpha/2\alpha$=5°/10°, FOV=48×48cm, BW=62.5kHz, matrix=32×32, 32 slices, 15mm slice thickness, 0 gap) using the 3T GE phantom model 2360049 (GEHC).[34]

Polarization of ^{3}He or ^{129}Xe gas was achieved using commercial polarizer systems (Polarean, Durham, NC, USA). Hyperpolarized ^{3}He was diluted with medical-grade N_2 gas (Spectra Gases, New Jersey, USA) and ^{129}Xe was diluted with ^{4}He and administered in 1.0-L Tedlar® bags (Jensen Inert Products, Florida, USA). Subjects were instructed to

inhale a gas mixture from the bag from FRC and image acquisition was performed under breath-hold conditions.[35] ^{1}H MRI was acquired with subjects in breath-hold using a whole-body radiofrequency coil and a ^{1}H fast spoiled gradient-recalled echo (FGRE) sequence with a partial echo (12s total data acquisition, TR/TE/flip angle=4.7ms/1.2ms/30°, FOV=40×40cm, BW=24.4kHz, matrix=128×80, number of slices=16, 15mm slice thickness, 0 gap), as previously described.[35] ^{3}He static ventilation MRI was acquired using a 2D multi-slice fast gradient-recalled echo sequence with a partial echo (total data acquisition time=10s, TR/TE/flip-angle=3.8ms/1.0ms/7°, FOV=40×40cm, BW=48.8kHz, matrix=128×80, NEX=1, number of slices=16, slice thickness=15mm) during breath-hold.[35] ^{129}Xe static ventilation MRI was also acquired in three subjects using methods previously described.[36]

Thoracic CT was acquired post-salbutamol with subjects at inspiration (lung volume of FRC+1L) breath-hold (FRC+1L to allow for CT to MRI comparison) using a multi-detector, 64-slice Lightspeed VCT scanner (GEHC, Milwaukee, WI) (64×0.625mm collimation, 120 kVp, 100 mA, tube rotation time=500ms, pitch=0.98).[37] All subjects were coached prior to scanning with a practice bag; subjects were instructed to breath in and out through their nose and after a passive expiration the N_2 gas was inhaled through the mouth from a 1 litre bag. A spiral acquisition was used and images were reconstructed using a Standard reconstruction algorithm and reconstructed slice thickness of 1.25mm.[37]

4.2.3 Image Analysis

A B_1 map was first applied to all UTE MR images to correct for flip angle inhomogeneities, which were then subsequently segmented using a multi-regional segmentation approach, previously described.[38,39] Briefly, a single observer (F.G.) placed seeds on the left lung, right lung and the background. These seeds were used to generate the probability distribution of signal intensities, which was used to generate the cost for assigning a corresponding label to a voxel. The segmentation optimization problem was solved using primal-dual analysis and convex optimization techniques, resulting in the segmented lung. The mean UTE MRI signal-intensity for the whole lung was determined and normalized to the mean liver signal-intensity, as previously described.[30] To determine signal-intensity

differences across the four different lung volumes, the images acquired at full-expiration, FRC, and full-inspiration were segmented and the extracted lung was registered to the lung acquired at FRC+1L (to ensure consistency with the noble gas and CT acquisitions) using an affine followed by a deformable registration approach provide by NiftyReg.[40] **Figure 4-1** shows a schematic that summarizes how dynamic proton-density maps were generated. Dynamic proton-density maps reflect the change from full inspiration to full expiration of UTE signal intensity for each lung voxel in the map. Each dynamic proton-density map required 15 minutes to generate (including the segmentation and registration time). Briefly, UTE MRI was acquired at four different lung volumes, and the magnitude of the slope of the line that described the signal intensity change across lung volumes was calculated on a voxel-by-voxel basis to generate the dynamic proton-density map. UTE images were qualitatively evaluated based on visual evidence of diminished signal-intensity at baseline, PC_{20}, and post-salbutamol. Dynamic proton-density maps with mainly warmer colours (e.g. orange, red) were classified as having diminished differences between full inspiration and full expiration signal-intensity. Dynamic proton-density maps with mainly cool colours (e.g. blue, green) were classified as having greater differences between full inspiration and full expiration signal-intensity.

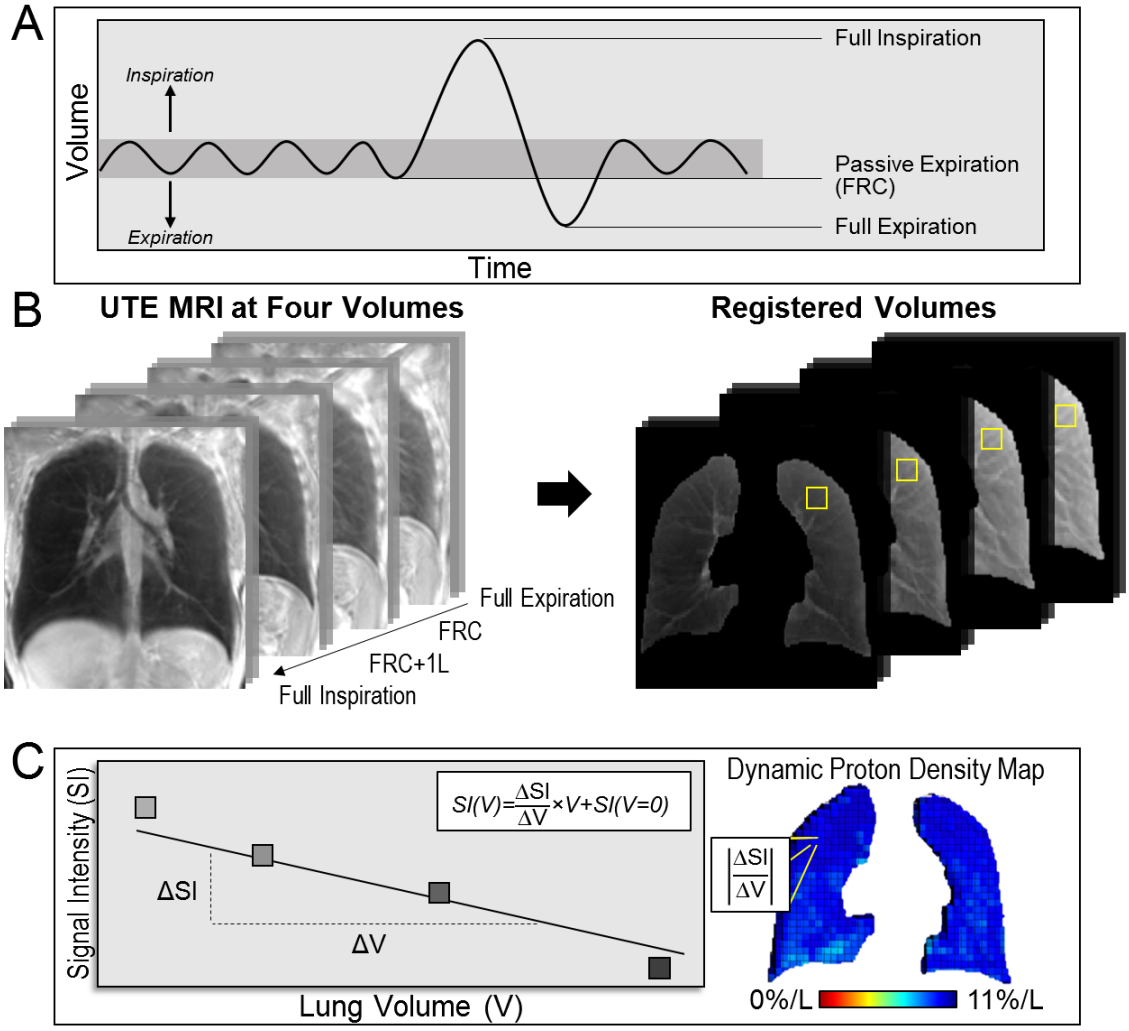

Figure 4-1 Schematic for generating Dynamic Proton-Density Maps
A) Volume-time plot that shows lung volumes at which MRI was acquired: full expiration, passive expiration (functional residual capacity [FRC]), FRC+1L, and full inspiration, B) Centre slice UTE images in greyscale at four lung volumes with corresponding segmented and registered images. Yellow box represents region-of-interest (ROI) and, C) Plot of ROI signal-intensity versus lung volume, where the slope of the line represents the dynamic proton-density value for each ROI or voxel that is used to generate a dynamic proton-density map.

Static ventilation images were segmented and co-registered with ^{1}H FGRE MRI using custom software generated using MATLAB R2014a (Mathworks, Natick, Massachusetts, USA).[41] Ventilation abnormalities were quantified using the ventilation defect percent (VDP) which represents the volume of ventilation defects (VDV) normalized to the thoracic cavity volume. Briefly, static ventilation images were segmented by a single

observer (K.S.) using a k-means approach that classified voxel intensity values into five clusters ranging from signal void (cluster 1[C1] or VDV) and hypo-intense (cluster 2 [C2]) to hyper-intense signal (cluster 5 [C5]) to generate a gas distribution cluster-map. For delineation of the ventilation defect boundaries, a seeded region-growing algorithm was used to segment the ^{1}H FGRE MRI thoracic cavity for registration to the cluster-map, as previously described.[41] Hyperpolarized noble gas images were qualitatively evaluated based on visual evidence of ventilation defects defined as any lung region of diminished signal-intensity but not including those areas of signal loss associated with the pulmonary vascular structures, heart, hilum, and mediastinum. Homogeneous distribution of hyperpolarized noble gas was defined as static ventilation images without focal areas of diminished signal-intensity. When ventilation defects were visibly improved (signal-intensity was greater) after the administration of salbutamol, they were deemed qualitatively diminished or improved.

Pulmonary Workstation 2.0 (VIDA Diagnostics Inc., Coralville, Iowa, USA) was used to segment whole lung and pulmonary lobes from the CT images. As previously described,[30] mean CT radio-density was determined using the CT pulmonary mask generated using VIDA. A threshold of -856HU[5] was not used to evaluate gas-trapping because images were not acquired at full expiration and instead, mean CT radio-density was used for direct comparison with mean UTE values across the entire lung and for individual lobes. Using the CT pulmonary lobe masks, CT radio-density, UTE signal-intensity and VDP (by registering CT to hyperpolarized noble gas MRI[42]) were determined for each pulmonary lobe. CT images were qualitatively evaluated and decreased lung density was described as a pulmonary hyperlucency or regions of hypoattenuation (i.e. low radio-density).

4.2.4 Statistics

Data were tested for normality using the Shapiro-Wilk normality test using SPSS 23.0 (IBM, Armonk, NY, USA) and parametric tests were performed when the data satisfied normal distribution. Univariate relationships were evaluated using linear regressions (r^2) and Pearson correlations (r), and Spearman correlations (r_s) (adjusted with Holm-Bonferroni correction). One-way analysis of variance (ANOVA) with a Holm-Bonferroni correction for multiple comparisons was used to compare measurements between healthy

volunteers and asthmatics. Repeated measures ANOVA was performed to evaluate the difference between baseline, PC_{20}, and post-salbutamol measurements. All statistical tests were performed using SPSS 23.0 (IBM, Armonk, NY). Results were considered significant when the probability of making a Type I error was less than 5% ($p<.05$).

4.3 Results

4.3.1 Study Subjects

Thirty subjects were evaluated including 13 healthy volunteers (7M/6F, 25±5 years) with no history of chronic or acute respiratory disease and 17 asthmatics (7M/10F, 47±11 years). Fourteen asthmatics were clinically diagnosed with severe, uncontrolled disease, while three patients had mild-to-moderate asthma. **Table 4-1** shows subject demographics and pulmonary function test measurements for all participants pre-salbutamol. Healthy volunteers were significantly younger and reported significantly greater FEV_1 and FEV_1/FVC as well as significantly lower RV/TLC than the asthmatics ($p<.001$).

Table 4-1 Participant demographics

Mean (±SD)	**Healthy Volunteers n=13**	**Asthma n=17**	**Significance of Difference p-value**
Male n	7	7	--
Age yrs	25 (5)	47 (11)	**<.001**
BMI kg/m^2	24 (4)	28 (5)	.09
FEV_1 $\%_{pred}$	102 (11)	69 (23)	**<.001**
FVC $\%_{pred}$	102 (11)	89 (17)	.1
FEV_1/FVC %	85 (6)	78 (17)	**<.001**
RV $\%_{pred}$	128 (29)	148 (43)	.7
TLC $\%_{pred}$	110 (12)	110 (11)	~1
RV/TLC %	28 (5)	42 (11)	**.002**
FRC $\%_{pred}$	112 (14)	116 (25)	~1
IC $\%_{pred}$	104 (17)	103 (22)	.9

*Significance of difference ($p<.05$) was determined using a one-way ANOVA with Holm-Bonferroni correction to correct for multiple comparisons. SD=standard deviation; BMI=body mass index; FEV_1=forced expiratory in 1s; FVC=forced vital capacity; TLC=total lung capacity; RV=residual volume, FRC=functional residual capacity; IC=inspiratory capacity.

4.3.2 UTE Signal Intensity and Dynamic Proton-density maps

Figure 4-2 shows multi-volume UTE MRI and dynamic proton-density maps for a representative healthy volunteer and an asthmatic participant as well as the normalized signal-intensity values for the two subgroups at each lung volume. For the healthy volunteer, there was qualitative evidence of homogeneously distributed low signal-intensity at all lung volumes and a homogeneous dynamic proton-density map that reflected an approximate 10%/L difference in mean signal-intensity across lung volumes (with greater signal-intensity at smaller lung volumes). For the representative asthmatic subject, there was qualitative evidence of low signal-intensity regions at all lung volumes, and a greater regional variability in the dynamic proton-density map reflecting regional heterogeneity in signal-intensity differences across the four lung volumes. The dynamic proton-density map for the asthma patient was not only more heterogeneous but also reflected smaller differences in signal-intensity. Quantitatively, there were significant differences between the healthy and asthmatic subgroup for signal-intensity at full expiration (healthy volunteers: 58±7%, asthmatics: 43±10%, $p<.001$) and FRC (healthy volunteers: 50±7%, asthmatics: 40±8%, $p=.003$). Whole lung dynamic proton-density measurements were also significantly different ($p<.001$) for healthy volunteers (7.4±2.0%/L) and asthmatics (4.5±1.9%/L).

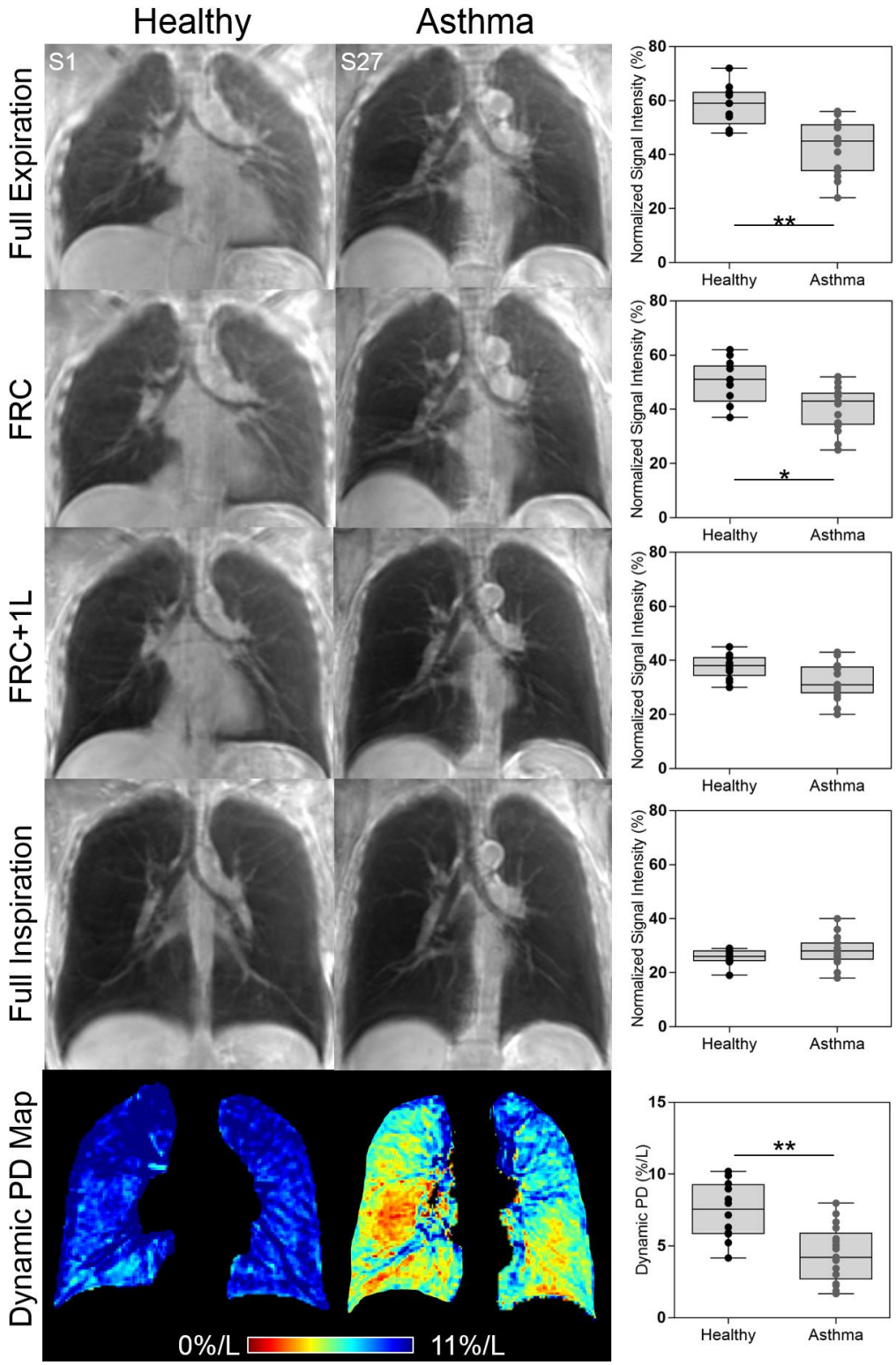

Figure 4-2 UTE MRI for Healthy Volunteers and Asthmatics
Coronal UTE MRI at full expiration, FRC, FRC+1L, and full inspiration with corresponding dynamic proton-density maps for a representative healthy volunteer and asthmatic. The far right panel shows normalized signal intensity and dynamic proton-

density values for the healthy volunteer and asthmatic subgroups. P-value determined using a one-way ANOVA with Holm-Bonferroni correction for multiple comparisons (*:$p \leq .05$, **:$p \leq .01$).

For participants with asthma, we also evaluated qualitative and quantitative relationships for UTE signal-intensity and dynamic proton-density maps with biomarkers derived from CT, ^{3}He MRI and pulmonary function tests. As shown in **Figure 4-3**, for subject S19, there was a homogeneous distribution of hyperpolarized ^{3}He gas and there were no visually obvious CT low attenuating regions or lucency. For asthmatic subject S27, there were ventilation defects in the lower lobes which corresponded to regional CT lucency and smaller signal-intensity/volume differences in the dynamic proton-density maps. In a similar manner for asthmatic subject S15, ventilation defects corresponded to regional CT lucency and small signal-intensity changes in the dynamic proton-density maps.

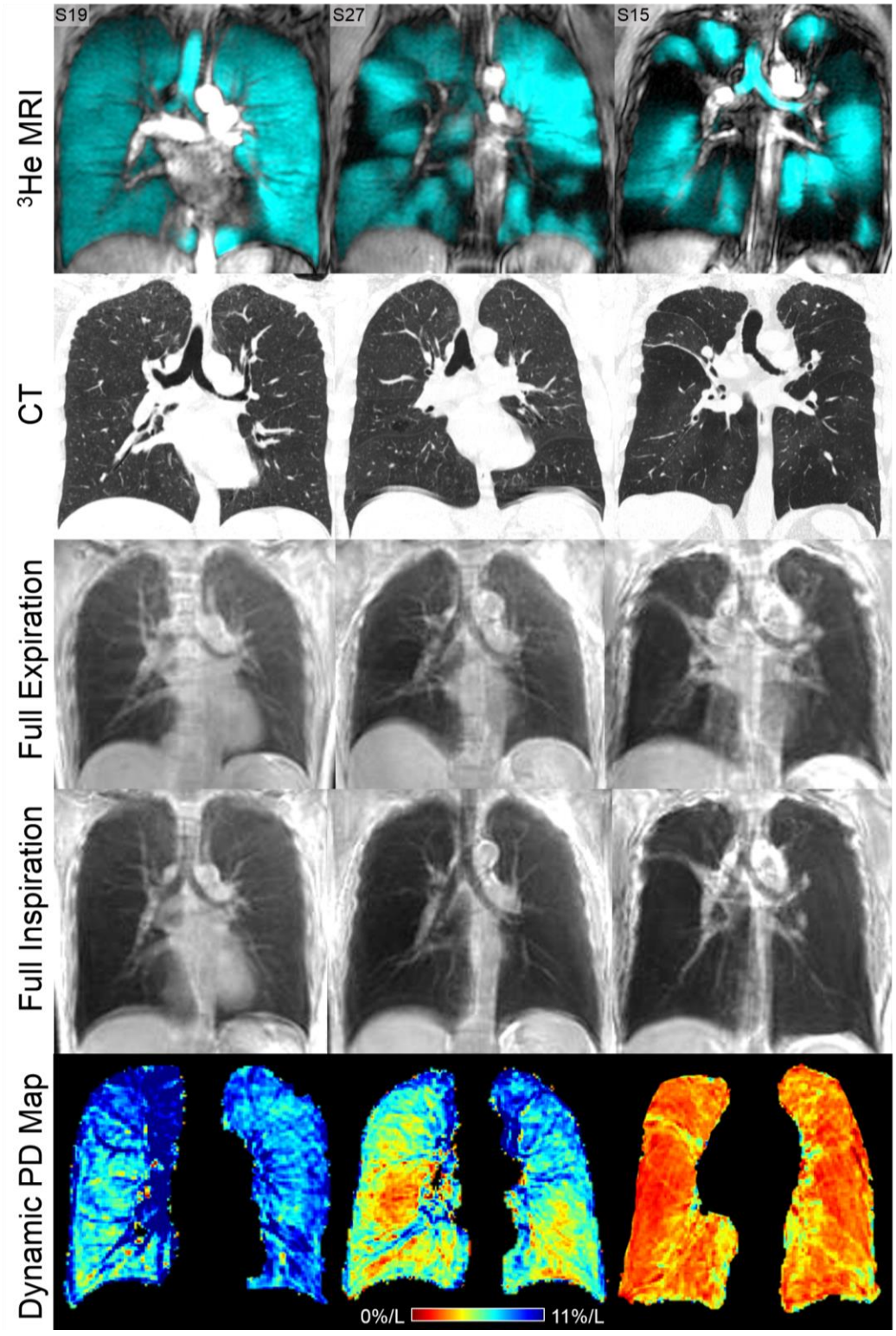

Figure 4-3 Pulmonary MRI and CT for Participants with Asthma
Coronal centre slice ^{3}He MRI, CT, UTE MRI at full expiration and full inspiration and dynamic proton-density maps for three representative asthmatic subjects. S19: 39 year old female, FEV_1=71%$_{pred}$, RV/TLC=45%, mean whole lung CT radio-density=-792HU, full

expiration/full inspiration signal-intensity=46%/31%, VDP=2%, whole lung mean dynamic proton-density=5.06%/L; S27: 60 year old female, FEV_1=52%$_{pred}$, RV/TLC=54%, mean whole lung CT radio-density=-814HU, full expiration/full inspiration signal-intensity=34%/23%, VDP=10% whole lung mean dynamic proton-density=4.80%/L; S15: 57 year old male, FEV_1=36%$_{pred}$, RV/TLC=48%, mean whole lung CT radio-density=-865HU, full expiration/full inspiration signal-intensity=31%/20%, VDP=32%, whole lung mean dynamic proton-density=2.65%/L.

Quantitative results for asthmatics are provided in **Figure 4-4** shows significant quantitative whole lung relationships for lung tissue CT radio-density with UTE signal-intensity at full expiration (r^2=0.67, r=0.82, p=.004) and FRC+1L (r^2=0.69, r=0.83, p=.006). There were similar findings for lobar relationships between CT radio-density and MRI signal-intensity at full expiration (r^2=0.30, r=0.55, p=.003) and FRC+1L (r^2=0.48, r=0.69, p=.004). Whole lung dynamic proton-density was also correlated with whole lung CT radio-density (r^2=0.51, r=0.71, p=.01) and lobar results were very similar (r^2=0.66, r=0.81, p=.003). Finally, there were significant whole lung relationships for UTE signal-intensity at full expiration with VDP (r^2=0.45, r=-0.67, p=.006) and as well for UTE signal intensity at FRC+1L with VDP (r^2=0.31, r=-0.56, p=.03). The relationship of whole lung dynamic proton-density with whole lung VDP was on the threshold of significance (r^2=0.26, r=-0.51, p=.05) while lobar signal-intensity at FRC+1L (r^2=0.13, r_s=-0.33, p=.02) and lobar dynamic proton-density (r^2=0.14, r_s=-0.47, p=.01) were both related to lobar VDP. We note that in this evaluation, data for three subjects were based on ^{129}Xe MRI VDP measurements. Because previous work demonstrated ^{129}Xe VDP was significantly greater than ^{3}He VDP [43] in asthmatics, we evaluated all correlations without ^{129}Xe VDP data and the relationships remained significant. Previous work showed that lung inflation volume and CT lung density [44-47] are strongly related and that UTE signal-intensity also scales with lung volume [30], which is exactly what the dynamic proton-density maps show.

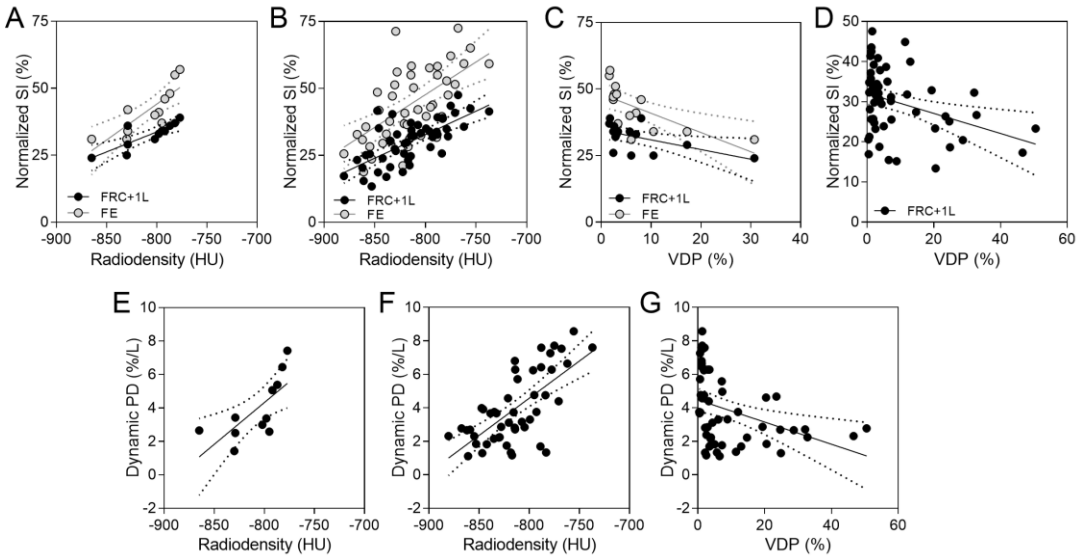

Figure 4-4 Relationships for UTE MRI Signal intensity and imaging measurements in asthmatics

Linear correlations for A) whole lung radio-density with whole lung UTE signal intensity (SI) at full expiration (r^2=0.67, r=0.82, p=.004) and FRC+1L (r^2=0.69, r=0.83, p=.006), B) lobar radio-density and lobar UTE signal intensity at full expiration (r^2=0.30, r=0.55, p=.003) and FRC+1L (r^2=0.48, r=0.69, p=.004), C) whole lung VDP with whole lung UTE signal intensity at full expiration (r^2=0.45, r=-0.67, p=.006) and FRC+1L (r^2=0.31, r=-0.56, p=.03), D) lobar VDP with lobar UTE signal intensity at FRC+1L (r^2=0.13, r_s=-0.33, p=.02), E) whole lung radio-density and whole lung dynamic proton-density (r^2=0.51, r=0.71, p=.01), F) lobar radio-density and lobar dynamic proton-density (r^2=0.66, r=0.81, p=.003), and G) lobar VDP with lobar dynamic proton-density (r^2=0.14, r_s=-0.47, p=.01).

Associations with pulmonary function test measurements and lung volumes are shown in **Figure 4-5** for all subjects by subgroup. In healthy volunteers, FEV_1 $\%_{pred}$ was significantly correlated with whole lung UTE signal-intensity at full expiration (r^2=0.50, r=0.71, p=.03), while for the asthmatic subgroup, there were significant relationships for FEV_1 $\%_{pred}$ (r^2=0.50, r=0.71, p=.006), FEV_1/FVC (r^2=0.53, r=0.73, p=.002) and RV/TLC (r^2=0.32, r=-0.57, p=.02) with whole lung signal-intensity. In asthma patients only, mean whole lung dynamic proton-density was related to FEV_1 $\%_{pred}$ (r^2=0.37, r=0.61, p=.02), FEV_1/FVC (r^2=0.56, r=0.75, p=.003), and RV $\%_{pred}$ (r^2=0.38, r=-0.62, p=.02). Based on previous work,[47] we performed linear regression analysis while controlling for TLC and the relationships for UTE and pulmonary function test measurements remained significant.

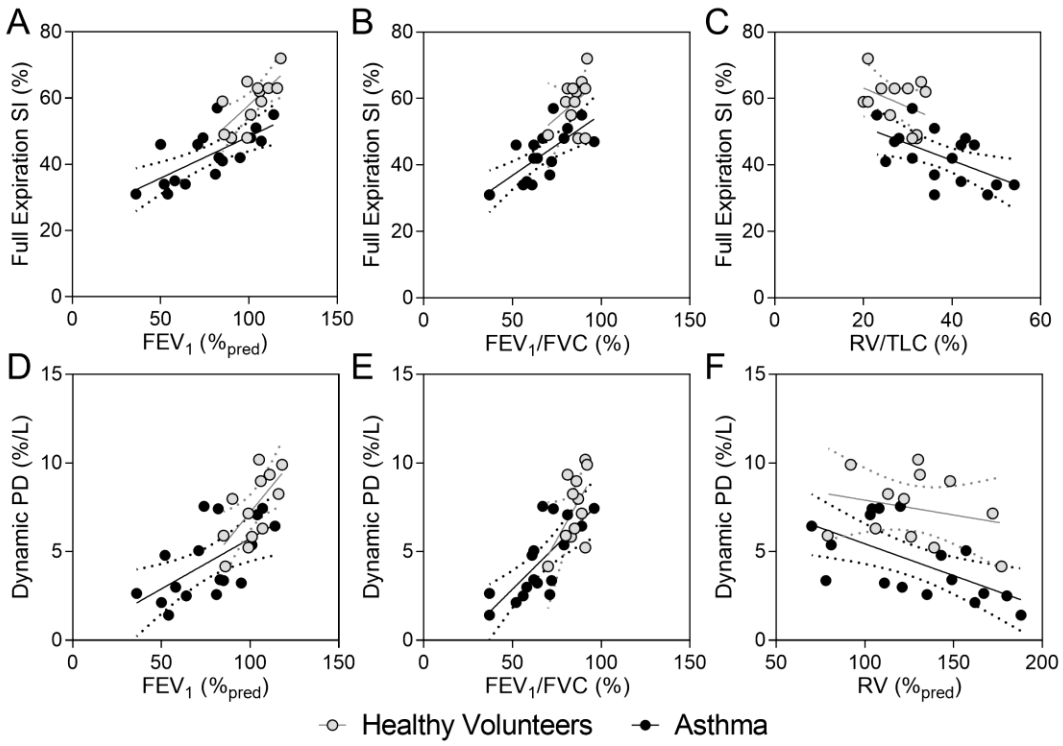

Figure 4-5 Relationships for UTE MRI and pulmonary function measurements
Signal intensity (SI) at full expiration associations with A) FEV_1 (Healthy: r^2=0.50, r=0.71, p=.03; Asthma: r^2=0.50, r=0.71, p=.006), B) FEV_1/FVC (Healthy: r^2=0.14, r=0.37, p=.2; Asthma: r^2=0.53, r=0.73, p=.002), C) RV/TLC (Healthy: r^2=0.25, r=0.50, p=.2; Asthma: r^2=0.32, r=-0.57, p=.02).
Dynamic proton-density associations with D) FEV_1 (Healthy: r^2=0.45, r=0.67, p=.4; Asthma: r^2=0.37, r=0.61, p=.02), E) FEV_1/FVC (Healthy: r^2=0.31, r=0.56, p=.2; Asthma: r^2=0.56, r=0.75, p=.003) F) RV (Healthy: r^2=0.06, r=-0.24, p=.4; Asthma: r^2=0.38, r=-0.62, p=.02).

4.3.3 Response to Bronchoconstriction and Bronchodilation

Because of the quantitative relationships observed in **Figures 4-4** and **4-5**, we also qualitatively investigated the potential for UTE MRI biomarkers to reflect well-understood changes in asthma lung function that occur during methacholine challenge and after bronchodilator inhalation. We note that based on international guidelines,[32] the vast majority of asthmatics in this study were too severe to undertake a methacholine challenge and therefore results were limited to three subjects in whom methacholine challenge and therapy withholding could be safely undertaken. **Table 4-2** summarizes pulmonary function test and imaging results from the bronchodilator and bronchoconstrictor challenge. There were significant differences in FEV_1 and RV/TLC pre- and post-

salbutamol in all asthmatics. There were no significant differences in imaging measurements in those subjects who only underwent tests pre- and post-salbutamol (n=14). In the three subjects that underwent the methacholine challenge, there were significant differences in signal-intensity at full expiration (p=.03).

Table 4-2 Pre- and post-salbutamol pulmonary function test and imaging measurements for all asthmatics.

Mean (±SD)	**Baseline n=14**		**Post-Salbutamol n=14**	**Significant Difference* p-value**
FEV_1 $\%_{pred}$	64 (22)		72 (21)	**<.001**
FEV_1/FVC %	58 (15)		63 (16)	**.001**
RV $\%_{pred}$	157 (41)		139 (29)	.05
RV/TLC %	44 (11)		40 (8)	**.03**
VDP %	10 (10)		8 (8)	.1
Full Expiration Signal-Intensity %	42 (10)		42 (8)	.9
Dynamic Proton Density %/L	4.4 (2.1)		4.3 (2.2)	.8
	Baseline n=3	**PC_{20} n=3**	**Post-Salbutamol n=3**	
FEV_1 $\%_{pred}$	92 (13)	-	100 (15)	**.04**
FEV_1/FVC %	74 (5)	-	80 (9)	.1
RV $\%_{pred}$	103 (12)	-	76 (6)	**.03**
RV/TLC %	33 (4)	-	25 (3)	**.008**
VDP %	4 (2)	9 (6)	4 (3)	.3
Full Expiration Signal-Intensity %	49 (6)	40 (3)	48 (7)	**.03**
Dynamic Proton Density %/L	4.8 (0.6)	3.6 (0.2)	5.1 (1.6)	.2

*Significance of difference (p<.05) was determined using a repeated measures ANOVA.

Figure 4-6 shows the results of a methacholine challenge and pre-to-post-salbutamol changes in two different representative asthmatics. At PC_{20}, for participant S14, MRI signal-intensity was qualitatively diminished and there were numerous ^{3}He MRI ventilation defects, most of which resolved post-salbutamol. In addition, dynamic proton-density maps reflected diminished differences between full inspiration and full expiration signal-intensity as represented by the regions of warm colours. After salbutamol administration, the lung signal-intensity was visually higher than at PC_{20} and the dynamic proton-density maps reflected greater differences between full inspiration and full expiration as represented by the regions of cool colours. These images were visually similar to what was observed in the healthy volunteers. For the individual patient S28 who was evaluated pre- and post-salbutamol, MRI signal-intensity was increased post-

salbutamol and there was a concomitant reduction in ^{3}He MRI ventilation defects. Concomitant with these post-salbutamol changes, dynamic proton-density maps showed that the difference between full inspiration and full expiration signal-intensity was greater and this is represented by the regions of cool colours.

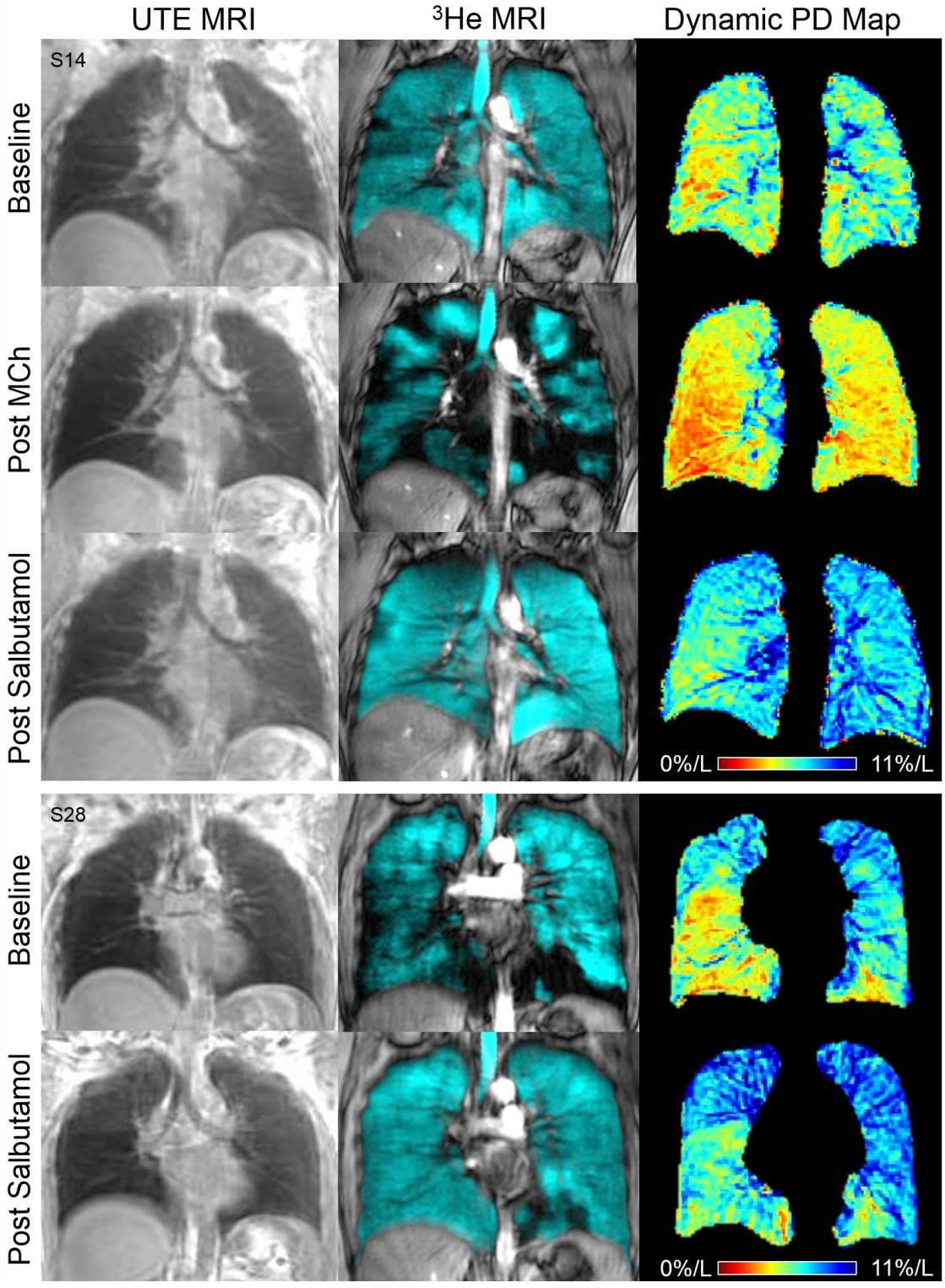

Figure 4-6 Asthma Response to Bronchodilator

MRI at baseline, PC_{20}, and post-salbutamol. For all subjects that underwent MCh (n=3), the mean VDP was: pre-/post-MCh=4±2%/9±6%, mean full expiration UTE signal-intensity was: pre-/post-MCh=49±6%/40±3%, and UTE dynamic proton-density was: pre-/post-MCh=4.8±0.5%/L/3.6±0.2%/L. S14: Asthmatic subject is 45 year old female with

pre-/post-salbutamol FEV_1=103%$_{pred}$/114%$_{pred}$, RV/TLC=29%/23%. Baseline UTE at full expiration signal-intensity/VDP/Dynamic proton-density=56%/2%/4.8%/L, post-MCh UTE at full expiration signal-intensity/VDP/Dynamic proton-density=43%/16%/3.7%/L, post-salbutamol UTE at full expiration signal-intensity/VDP/Dynamic proton-density=55%/2%/6.4%/L. For subjects that underwent pre-/post-salbutamol only (n=14), the mean VDP pre-/post-Salbutamol was 10±10%/8±8%, the mean full expiration UTE signal-intensity pre-/post-Salbutamol was 42±10%/42±8%, and the mean dynamic proton-density pre-/post-Salbutamol was 4.4±2.0/4.3±2.2%/L. S28: Asthmatic subject is 47 year old female with pre-/post-salbutamol FEV_1=55%$_{pred}$/74%$_{pred}$, RV/TLC=50%/43%. Baseline UTE at full expiration signal-intensity/VDP/Dynamic proton-density=46%/4%/6.7%/L, post-salbutamol UTE at full expiration signal-intensity/VDP/Dynamic proton-density=48%/3%/7.6%/L.

4.4 Discussion

Inhaled gas MRI biomarkers of asthma lung function have been developed over the past decade and have disrupted our understanding about the regional heterogeneity of lung functional abnormalities in asthmatics. While it has not been straightforward to replicate these findings using conventional ^{1}H MRI, we sought to establish such an approach by developing multi-volume UTE lung biomarkers. Therefore, in this proof-of-concept study in 30 participants, we investigated the potential of 3D UTE MRI as a practical way to measure and understand regional asthma lung function and observed: 1) UTE dynamic proton-density and signal-intensity measurements at full expiration and FRC were greater in healthy volunteers as compared to asthmatics, 2) in asthmatics, UTE biomarkers were significantly correlated with pulmonary function, CT radio-density and MRI VDP, and, 3) subsequent to methacholine inhalation, there were qualitative changes in signal-intensity and dynamic proton-density that resolved post-salbutamol.

First, we observed significantly greater normalized signal-intensity measurements in healthy volunteers as compared to asthmatics. These findings were similar to previously published work using CT that showed significantly lower radio-density in asthmatics than in healthy volunteers.[48] Diminished signal-intensity in the asthmatic lung may reflect gas-trapping which is certainly plausible given that in these patients there is often premature closure of peripheral airways toward the end of full expiration. In asthmatic lungs, small airways also close at higher lung volumes than in healthy subjects -a result of increased smooth muscle tone, edema, and or inflammation of the airway walls. In addition to

diminished signal-intensity, there was also diminished dynamic proton-density in the asthmatic subgroup. This was consistent with previous work using conventional ^{1}H MR that showed there was a larger change in signal-intensity across lung volumes in healthy volunteers than in asthmatics[29] which may be reflective of reduced lung compliance or decreased compressibility due to gas-trapping in asthmatics.

Second, in the participants with asthma, we observed moderate-to-strong correlations for UTE measurements with pulmonary function and CT measurements. Signal-intensity at full expiration and dynamic proton-density were both significantly correlated with FEV_1 and FEV_1/FVC suggesting relationships with airflow obstruction. Signal-intensity at full expiration was also correlated with RV/TLC which is consistent with the notion that gas-trapping is responsible for signal-intensity differences in asthmatics. Similar findings were previously reported using CT, where gas-trapping score was related to pulmonary function tests.[49]

Whole lung and regional UTE signal-intensity and dynamic proton-density measurements were also related to whole lung and regional CT radio-density. These findings are in agreement with previous work in COPD patients.[30] Similar to previous work in asthmatics in which focal lucency was spatially correlated with ^{3}He MRI ventilation defects,[16] here we also observed significant correlations for regional VDP and regional UTE measurements. These relationships were weak-to-modest, perhaps reflective of asthma heterogeneity and the relatively small sample size or that UTE measurements necessarily include signal from the vasculature.

Finally, we also observed visually obvious changes in UTE images after methacholine and salbutamol administration. To provide context, these results are similar to previous work using diffusion-weighted ^{3}He MRI to evaluate gas-trapping post-MCh.[50] This previous work demonstrated larger apparent diffusion coefficients (ADC) post-methacholine, suggesting an increase in airspace size or gas-trapping. Here, using UTE methods, the decrease in signal-intensity at PC_{20} suggests an increase in airspace size due to retained air (i.e. gas-trapping) resulting in lower proton density per voxel. These results hold promise for future studies attempting to evaluate treatment response in patients with asthma because

these regions of low signal-intensity and low magnitude of dynamic proton-density may provide potential targets for therapy.

Although this study provides promising preliminary results, we must point out a number of study limitations. We acknowledge that CT was not acquired at full expiration and this limited our ability to ascertain the etiology of CT lucency. Therefore, while we observed a relationship for UTE signal-intensity and CT radio-density, this was not in itself definitive for regional gas-trapping. However, signal-intensity at full expiration and dynamic proton-density measurements were related to RV and to RV/TLC (both reflective of gas-trapping) and to MRI ventilation defects. Previous studies have demonstrated the relationship of expiratory CT lucency and ^{3}He MRI ventilation abnormalities which is also supportive of a relationship between gas-trapping and ventilation defects in asthma.[16] There was a significant age difference between healthy volunteers and asthmatics which may have biased some of the results. We should also stress that for three asthmatics, only ^{129}Xe MRI was performed, which based on previous work, would be expected to be greater than ^{3}He VDP.[43] Importantly however, when these data were removed from the analysis, the correlations with VDP were not significantly different which may also be attributed to a small sample size. Finally, it should be noted that three subjects underwent the methacholine challenge. Although there were significant differences in signal-intensity at full expiration, caution must be taken when extrapolating these results to a larger sample size.

In conclusion, we developed UTE MRI signal-intensity and dynamic proton-density biomarkers of asthma that were related to pulmonary function and hyperpolarized noble gas MR measurements of ventilation defects. These MRI measurements made using conventional equipment suggested that UTE MRI may reflect ventilation heterogeneity and/or gas-trapping in asthmatics, making this approach amenable for clinical use.

4.5 References

(1) Carroll, N., Elliot, J., Morton, A. & James, A. The structure of large and small airways in nonfatal and fatal asthma. *Am Rev Respir Dis* 1993; 147: 405-410.

(2) Farah, C. S. *et al.* The role of the small airways in the clinical expression of asthma in adults. *J Allergy Clin Immunol* 2012; 129: 381-387, 387 e381.

(3) Sköld, C. M. Remodeling in asthma and COPD–differences and similarities. *The clinical respiratory journal* 2010; 4: 20-27.

(4) James, A. L., Paré, P. D. & Hogg, J. C. The mechanics of airway narrowing in asthma. *American Review of Respiratory Disease* 1989; 139: 242-246.

(5) Busacker, A. *et al.* A multivariate analysis of risk factors for the air-trapping asthmatic phenotype as measured by quantitative CT analysis. *Chest* 2009; 135: 48-56.

(6) Harris, R. S. *et al.* Regional pulmonary perfusion, inflation, and ventilation defects in bronchoconstricted patients with asthma. *American journal of respiratory and critical care medicine* 2006; 174: 245-253.

(7) Busse, W. W. Asthma diagnosis and treatment: filling in the information gaps. *J Allergy Clin Immunol* 2011; 128: 740-750.

(8) Perez, T., Chanez, P., Dusser, D. & Devillier, P. Small airway impairment in moderate to severe asthmatics without significant proximal airway obstruction. *Respir Med* 2013; 107: 1667-1674.

(9) King, G. G. *et al.* Heterogeneity of narrowing in normal and asthmatic airways measured by HRCT. *Eur Respir J* 2004; 24: 211-218.

(10) King, G. G., Eberl, S., Salome, C. M., Young, I. H. & Woolcock, A. J. Differences in airway closure between normal and asthmatic subjects measured with single-photon emission computed tomography and technegas. *Am J Respir Crit Care Med* 1998; 158: 1900-1906.

(11) Venegas, J. G. *et al.* Self-organized patchiness in asthma as a prelude to catastrophic shifts. *Nature* 2005; 434: 777-782.

(12) de Lange, E. E. *et al.* Evaluation of asthma with hyperpolarized helium-3 MRI: correlation with clinical severity and spirometry. *Chest* 2006; 130: 1055-1062.

(13) de Lange, E. E. *et al.* The variability of regional airflow obstruction within the lungs of patients with asthma: assessment with hyperpolarized helium-3 magnetic resonance imaging. *J Allergy Clin Immunol* 2007; 119: 1072-1078.

(14) Smith-Bindman, R. *et al.* Use of diagnostic imaging studies and associated radiation exposure for patients enrolled in large integrated health care systems, 1996-2010. *JAMA* 2012; 307: 2400-2409.

(15) Wang, C. *et al.* Assessment of the lung microstructure in patients with asthma using hyperpolarized 3He diffusion MRI at two time scales: comparison with healthy subjects and patients with COPD. *J Magn Reson Imaging* 2008; 28: 80-88.

(16) Fain, S. B. *et al.* Evaluation of structure-function relationships in asthma using multidetector CT and hyperpolarized He-3 MRI. *Acad Radiol* 2008; 15: 753-762.

(17) Svenningsen, S., Nair, P., Guo, F., McCormack, D. G. & Parraga, G. Is ventilation heterogeneity related to asthma control? *Eur Respir J* 2016.

(18) Svenningsen, S. *et al.* What are ventilation defects in asthma? *Thorax* 2014; 69: 63-71.

(19) Wheatley, A. *et al.* in *Medical Imaging.* 69161X-69161X-69168 (International Society for Optics and Photonics).

(20) Bergin, C. J., Glover, G. M. & Pauly, J. Magnetic resonance imaging of lung parenchyma. *J Thorac Imaging* 1993; 8: 12-17.

(21) Bergin, C. J., Pauly, J. M. & Macovski, A. Lung parenchyma: projection reconstruction MR imaging. *Radiology* 1991; 179: 777-781.

(22) Bieri, O. Ultra-fast steady state free precession and its application to in vivo (1)H morphological and functional lung imaging at 1.5 tesla. *Magn Reson Med* 2013; 70: 657-663.

(23) Grodzki, D. M., Jakob, P. M. & Heismann, B. Ultrashort echo time imaging using pointwise encoding time reduction with radial acquisition (PETRA). *Magn Reson Med* 2012; 67: 510-518.

(24) Johnson, K. M., Fain, S. B., Schiebler, M. L. & Nagle, S. Optimized 3D ultrashort echo time pulmonary MRI. *Magn Reson Med* 2012.

(25) Miller, G. W. *et al.* Advances in functional and structural imaging of the human lung using proton MRI. *NMR Biomed* 2014; 27: 1542-1556.

(26) Weiger, M., Pruessmann, K. P. & Hennel, F. MRI with zero echo time: hard versus sweep pulse excitation. *Magn Reson Med* 2011; 66: 379-389.

(27) Ble, F. X. *et al.* Allergen-induced lung inflammation in actively sensitized mice assessed with MR imaging. *Radiology* 2008; 248: 834-843.

(28) Vogel-Claussen, J. *et al.* Quantification of pulmonary inflammation after segmental allergen challenge using turbo-inversion recovery-magnitude magnetic resonance imaging. *Am J Respir Crit Care Med* 2014; 189: 650-657.

(29) Pennati, F. *et al.* Assessment of regional lung function with multivolume (1)H MR imaging in health and obstructive lung disease: comparison with (3)He MR imaging. *Radiology* 2014; 273: 580-590.

(30) Ma, W. *et al.* Ultra-short echo-time pulmonary MRI: Evaluation and reproducibility in COPD subjects with and without bronchiectasis. *J Magn Reson Imaging* 2014.

(31) Mauad, T. & Dolhnikoff, M. Pathologic similarities and differences between asthma and chronic obstructive pulmonary disease. *Curr Opin Pulm Med* 2008; 14: 31-38.

(32) Crapo, R. O. *et al.* Guidelines for methacholine and exercise challenge testing-1999. This official statement of the American Thoracic Society was adopted by the ATS Board of Directors, July 1999. *Am J Respir Crit Care Med* 2000; 161: 309-329.

(33) Miller, M. R. *et al.* Standardisation of spirometry. *Eur Respir J* 2005; 26: 319-338.

(34) Wade, T., McKenzie, C. A. & Rutt, B. K. Flip angle mapping with the accelerated 3D look-locker sequence. *Magn Reson Med* 2014; 71: 591-598.

(35) Parraga, G. *et al.* Hyperpolarized 3He ventilation defects and apparent diffusion coefficients in chronic obstructive pulmonary disease: preliminary results at 3.0 Tesla. *Invest Radiol* 2007; 42: 384-391.

(36) Kirby, M. *et al.* Pulmonary ventilation visualized using hyperpolarized helium-3 and xenon-129 magnetic resonance imaging: differences in COPD and relationship to emphysema. *J Appl Physiol* 2013; 114: 707-715.

(37) Kirby, M. *et al.* On the role of abnormal DLCO in ex-smokers without airflow limitation: symptoms, exercise capacity and hyperpolarised helium-3 MRI. *Thorax* 2013; 68: 752-759.

(38) Potts, R. B. in *Mathematical proceedings of the cambridge philosophical society*. 106-109 (Cambridge Univ Press).

(39) Guo, F. *et al.* Anatomical pulmonary magnetic resonance imaging segmentation for regional structure-function measurements of asthma. *Medical Physics* 2016; 43: 2911-2926.

(40) Modat, M. *et al.* Fast free-form deformation using graphics processing units. *Comput Methods Programs Biomed* 2010; 98: 278-284.

(41) Kirby, M. *et al.* Hyperpolarized 3He magnetic resonance functional imaging semiautomated segmentation. *Acad Radiol* 2012; 19: 141-152.

(42) Guo, F. *et al.* in *SPIE Medical Imaging 2015.* 941717-941717-941719 (International Society for Optics and Photonics).

(43) Svenningsen, S. *et al.* Hyperpolarized He and Xe MRI: Differences in asthma before bronchodilation. *J Magn Reson Imaging* 2013.

(44) Wegener OH, K. P., Oeser H. Measurement of lung density by computed tomography. *J Comput Assist Tomogr* 1978; 2: 263-273.

(45) Yamashiro, T. *et al.* Collapsibility of lung volume by paired inspiratory and expiratory CT scans: correlations with lung function and mean lung density. *Acad Radiol* 2010; 17: 489-495.

(46) Coxson, H. O. *et al.* Measurement of lung expansion with computed tomography and comparison with quantitative histology. *J Appl Physiol (1985)* 1995; 79: 1525-1530.

(47) Brown, R. H., Wise, R. A., Kirk, G., Drummond, M. B. & Mitzner, W. Lung density changes with growth and inflation. *Chest* 2015.

(48) Newman, K. B., Lynch, D. A., Newman, L. S., Ellegood, D. & Newell, J. D., Jr. Quantitative computed tomography detects air trapping due to asthma. *Chest* 1994; 106: 105-109.

(49) Laurent, F., Latrabe, V., Raherison, C., Marthan, R. & Tunon-de-Lara, J. M. Functional significance of air trapping detected in moderate asthma. *Eur Radiol* 2000; 10: 1404-1410.

(50) Costella, S. *et al.* Regional pulmonary response to a methacholine challenge using hyperpolarized (3)He magnetic resonance imaging. *Respirology* 2012; 17: 1237-1246.

CHAPTER 5

5 CONCLUSIONS AND FUTURE DIRECTIONS

In this final chapter, an overview and summary are provided in addition to the important findings and conclusions of Chapters 2-4. The study specific limitations and general limitations are also provided with some potential solutions. Finally, based on these findings, an outline is provided for future pulmonary MRI studies.

5.1 Overview and Research Questions

Obstructive lung diseases, including COPD and asthma, affect over six million Canadians. By 2030, it is projected that the current economic burden will double if no further improvements (including drug development) are made in dealing with obstructive lung disease.[1] Despite decades of research, therapies that modify obstructive lung disease progression and control are lacking.[2,3] This is in part because the diagnosis and monitoring of these patients and their response to therapy are currently made using airflow measurements. These measurements, while important, cannot account for inter-subject variability or be used to regionally evaluate pathologies. One goal of obstructive lung disease research is to develop ways to identify patients with specific underlying pathological phenotypes with the hope that this will improve patient care and outcomes. In this regard, imaging methods such as thoracic CT and MRI have the potential to provide regional and quantitative biomarkers of obstructive lung disease. As the first step to identify patients with specific underlying pathological phenotypes, it is important to understand the physiological and clinical consequences of these imaging derived measurements.

In response to the need for a better understanding of imaging-derived biomarkers, studies have evaluated the clinical significance of hyperpolarized noble gas MR biomarkers in obstructive lung disease.[4-6] Work using hyperpolarized noble gas MRI in aging has shown that with increasing age there is a relationship with increased ventilation defects[7] and increased lung microstructure measured using ^{3}He ADC.[8] But this work did not ascertain the clinical consequences of these biomarkers in older never-smokers. This understanding is important to appreciate the pulmonary consequences associated with obstructive lung

disease. Furthermore, hyperpolarized noble gas MRI has yet to find acceptance in the clinic. Dose limiting advances in CT, limited availability of the necessary hardware for polarizing and imaging hyperpolarized noble gases, and the identification of clinical applications that will benefit from this have made clinical translation difficult. With this in mind, there has been growing motivation for the development and implementation of non-contrast enhanced pulmonary MRI to overcome the challenges of ionizing radiation and resource accessibility.

Non-contrast enhanced pulmonary UTE MRI has been proposed as a way to address the inherent challenges of pulmonary imaging that stem from low tissue and ^{1}H density without the use of specialized equipment or personnel. Recent studies using pulmonary UTE MRI have quantified parenchymal signal-intensity as a function of lung volume or gravity dependence in healthy volunteers.[9] In mouse models, UTE MRI has been used to evaluate inflammation and peribronchial abnormalities in animal models of asthma.[10] Studies have also used UTE MRI to produce T_2* maps in murine models[11] and healthy volunteers,[12] and have shown that this biomarker is related to smoking history in COPD.[13] Previous work using this technique provides a strong foundation for its use in obstructive lung disease research and patient care; however, a major drawback is that the reproducibility and clinical and physiological meaning of UTE-derived measurements in obstructive lung disease are poorly understood. Thus, a clear understanding of UTE-derived biomarkers (including reproducibility and clinical meaning) is necessary prior to widespread clinical translation.

The overarching objective of this thesis was to develop and evaluate lung structure and function measurements using multi-nuclear MRI in aging and obstructive lung disease to provide an understanding of the physiological and clinical consequences of these MR-derived measurements. The specific research questions addressed were: 1) What are the physiological and clinical consequences of MR-derived biomarkers in normal aging? (**CHAPTER 2**); 2) Can non-contrast enhanced UTE MRI measurements be developed to have high reproducibility (comparable to that of ^{3}He derived measurements), and are these measurements related to pulmonary function tests and CT measurements of emphysema in obstructive lung disease (i.e. COPD)? (**CHAPTER 3**); and, 3) Can we extend the method in Chapter 3 and merge different lung volume information to capture evidence of gas-

trapping and ventilation heterogeneity in patients with obstructive lung disease (i.e. asthma)? (**CHAPTER 4**)

5.2 Summary and Conclusions

In Chapter 2 we determined the physiological consequences and potential relevance of ventilation abnormalities in older never-smokers. We also evaluated the relationship of ventilation defects with occupational exposures, pulmonary function, and exercise capacity. We found that majority of older never-smokers (39/52) had ventilation defects and 33 of these subjects had ventilation defects that did not resolve after bronchodilation. The six older never-smokers that did respond to bronchodilation had significantly worse baseline pulmonary function test measurements. However, most of these older never-smokers had normal pulmonary function test measurements, but with peripheral ventilation defects that were not reversible by bronchodilation. Ventilation defects were related to pulmonary function tests, however, dyspnea and exercise capacity were not. This study builds the foundation of pulmonary abnormalities observed with aging. Obstructive lung disease, such as COPD, tends to occur in elderly individuals and thus it will be important in future studies to quantify lung function using MRI to differentiate between normal aging and both aging and obstructive lung disease in this elderly diseased population.

We then developed and evaluated reproducibility of a non-contrast enhanced UTE MR method in patients with COPD in Chapter 3. We tested the hypothesis that the signal-intensity derived from UTE MRI has high short-term reproducibility in COPD and is related to CT radio-density and pulmonary function test measurements. In healthy subjects, signal-intensity correlated with the inverse of lung volume ($r=0.99$, $p=.007$). The coefficient of variation for 3-week repeated measurements was 4%. There were significant correlations for signal-intensity with RA_{950} ($r=-0.71$, $p=.005$), FEV_1/FVC ($r=0.59$, $p=.02$), and for SI_{15} with HU_{15} ($r=0.62$, $p=.01$). We developed a UTE MRI method to generate measurements of pulmonary signal-intensity that are strongly related to tissue density and in subjects with COPD are related to pulmonary function and CT measurements.

In Chapter 4 of this thesis, we developed and utilized UTE MRI biomarkers of asthma lung function. The mean signal-intensity at four lung volumes (full expiration, FRC, FRC+1L,

and full inspiration) was quantified. The difference in MRI signal-intensity across four lung volumes was also determined on a voxel-by-voxel basis to generate dynamic proton-density maps. The mean whole lung signal-intensity at full expiration and magnitude of the dynamic proton density maps were significantly greater (p=.001) in healthy volunteers than asthmatics. Mean signal-intensity at full expiration (p<.01), FRC (p<.05) and dynamic proton-density (p<.01) were greater in healthy-volunteers compared to asthmatics. In asthmatics, UTE signal-intensity at full expiration and dynamic proton-density were correlated with $FEV_{1/}FVC$ (signal-intensity r=0.73/p=.002; dynamic proton-density r=0.75/p=.003), RV/TLC (signal-intensity r=-0.57/p=.02) or RV (dynamic proton-density r=-0.62/p=.02), CT radio-density (signal-intensity r=0.83/p=.006; dynamic proton-density r=0.71/p=.01) and lobar VDP (signal-intensity r_s=-0.33/p=.02; dynamic proton-density r_s=-0.47/p=.01). This work demonstrated that in patients with asthma, UTE MR signal-intensity measurements were correlated with pulmonary function test measurements of gas-trapping and airflow obstruction, provided information about regional ventilation deficits and provided similar information as CT. Taken together, UTE MR measurements may provide a surrogate measurement for ventilation heterogeneity and/or gas-trapping in patients with asthma.

In summary, we have provided: 1) evidence that in a majority of older never-smokers there are age-related changes in pulmonary ventilation that are not reversible by bronchodilation and are related to pulmonary function test measurements, but not dyspnea or exercise capacity; 2) a new and reproducible non-contrast enhanced MR method to evaluate pulmonary abnormalities in patients with obstructive lung disease; and, 3) evidence that the measurements derived from non-contrast enhanced MR are related to tissue density measurements (evaluated using CT) and pulmonary function test measurements.

5.3 Limitations

In this section the most significant limitations from Chapters 2-4 will be discussed. It should be noted that the study specific limitations are also presented in the Discussion section of each respective Chapter.

5.3.1 Study Specific Limitations

Pulmonary ventilation defects in older never-smokers (Chapter 2)

In Chapter 2, we sought to better understand the physiological consequences and potential relevance of ^{3}He MRI ventilation defects in older never-smokers. We did not acquire CT images which limited our understanding of age-related airway changes and their relationship to ventilation defects. Our results, therefore, could not be directly compared to more established CT measurements, such as the percentage of low attenuation pixels as a measurement of the extent of senile emphysema or WA% as a measurement of airway wall thickness. A direct comparison of CT and hyperpolarized ^{3}He MRI measurements in the same subjects would allow for a better understanding of the etiology of the ventilation defects observed in older never-smokers.

Another limitation of this study was that subjects were classified by viewing the gray-scale images, while the patients were still in the scanner. In two cases, once the ventilation images were co-registered to the anatomical ^{1}H images, offline, previously classified ventilation defects could be directly related to anatomical bony structures and were unlikely to be ventilation abnormalities. As a result, the two subjects, who were classified at the scanner as having ventilation defects did not appear to have these once a full analysis was completed. Ideally, all subjects should have undergone deep inspiration and salbutamol administration and image analysis should have been used to evaluate bronchodilator response.

Finally, ^{129}Xe and UTE MRI were not acquired in the older never-smokers. The high cost of ^{3}He gas has restricted translation of this imaging method beyond specialized MRI centres. As previously discussed, this shortage is forcing the noble gas MRI community to transition to ^{129}Xe gas, a less expensive and more readily available contrast agent, and non-contrast enhanced methods such as UTE MRI. One can hypothesize that ventilation defects may be more prominent and obvious using ^{129}Xe MRI since previous work has shown the increased sensitivity of ^{129}Xe gas compared to ^{3}He gas in OLD.[14,15] One can also hypothesize that UTE MR signal-intensity measurements would be lower in older individuals than younger individuals due to increased resting lung volumes in older

subjects. Regardless, future studies should aim to image older never-smokers using ^{129}Xe and UTE MRI to better understand the age-related changes in these imaging measurements.

Ultra-short echo-time pulmonary MRI: evaluation and reproducibility in COPD subjects with and without bronchiectasis (Chapter 3)

In the study presented in Chapter 3, a reproducible UTE MRI method was developed and an understanding of the physiological determinants of UTE signal-intensity in patients with COPD was determined. First, we acquired single slice images rather than whole-lung images. This limited our understanding of this measurement in the anterior and posterior regions of the lung.

Second, it is important to note that the impact of effective transverse decay time T_2* on signal-intensity at different lung volumes was ignored in healthy volunteers for two reasons: 1) in human lungs, T_2* variability was significantly smaller than other factors affecting signal-intensity across different lung volumes 2) the echo-time of 0.05ms was significantly smaller than the parenchymal T_2* (0.5-0.8ms), which minimized T_2* weighting. Also, unlike CT, MRI signal-intensity is influenced by hardware factors such as the positioning of the RF coils, which introduce inter-scan variability. While we corrected for absolute signal intensity quantification by normalizing acquired images to the liver, this is influenced by the precision of liver measurements. In this regard, we note that the liver has minimal motion during the image acquisition and is relatively homogeneous despite inter-subject signal variability.

Finally, we acknowledge that the histopathological relationship between UTE MRI signal-intensity and CT radio-density measurements has not yet been established. The quantification of emphysema using CT uses different threshold type analyses has been compared and validated with histology, yet this has not been undertaken with parenchymal MRI signal intensity. The comparison of mean MRI signal-intensity to CT RA_{950} and HU_{15} is likely a conservative estimate of any direct relationships. For this reason, the comparison of MRI-derived SI_{15} with CT-derived HU_{15} is likely a better estimate of the direct relationships of MRI signal-intensity and CT radio-density measurements.

Ultra-short Echo Time Magnetic Resonance Imaging Biomarkers of Asthma (Chapter 4)

In Chapter 4 we developed a whole lung breath-hold UTE MRI protocol and evaluated asthmatics and healthy volunteers. There was a significant age difference between healthy volunteers and asthmatics which may have biased our results.

Another limitation of this study was that CT was not acquired at full expiration. Chest CT at full expiration allows for the evaluation of gas-trapping. The extent of the gas-trapping can be evaluated using a threshold type measurements (i.e. the relative area under -856HU, RA_{856}).[16] Unfortunately, this threshold is only appropriate when CT is acquired at a lung volume of full expiration and this limited our understanding of regional gas-trapping. Consequently, the mean whole lung radio-density was used for direct comparison with mean whole lung signal-intensity. It should be noted that not only does the mean measurement not capture the extent of low signal-intensity, but the lack of expiratory CT limits our understanding of regional gas-trapping and our ability to ascertain the etiology of CT lucency. Although we can comment on the relationship of UTE signal-intensity and CT radio-density, it is difficult to conclude that the signal-intensity at full expiration was reflective of regional gas-trapping. We can conclude, however, that signal-intensity at full expiration and dynamic proton-density measurements are related to pulmonary function test measurements of gas-trapping such as residual volume and the ratio of residual volume to total lung capacity. It is also important to note that UTE signal-intensity measurements were related to hyperpolarized noble gas ventilation defects. Previous studies have demonstrated the relationship of CT lucency and ^{3}He MRI which suggest the relationship between gas-trapping and ventilation defects in asthma.[17]

Finally, for three asthmatics, only ^{129}Xe MRI was performed, which based on previous work, would be expected to be greater than ^{3}He VDP.[14] Importantly, however, when these data were removed from the analysis, the correlations with VDP were not significantly different. It should also be noted that three subjects underwent the methacholine challenge. Although there were significant differences in signal-intensity at full expiration, caution must be taken when extrapolating these results to a larger sample size.

5.3.2 General Limitations

In Chapters 2-4, we used mean whole lung measurements of ventilation defects and signal-intensity to evaluate the extent of pulmonary abnormalities. Mean measurements tend to disregard the heterogeneity of lung disease. Threshold based measurements, such as VDP and SI_{15}, also do not capture the heterogeneity of obstructive lung disease. Moreover, these measurements ignore the regions of signal hyper-intensity since VDP is dependent on the noble gas signal that is of the lowest intensity and SI_{15} is dependent on the low signal-intensity. Limitations with single threshold methods also include the over or under-estimation of the disease, where a lower threshold differentiates more severe diseased regions[18] disregarding regions of mild disease and a higher threshold identifies regions of mild disease.[19] As a result, methods that diverge from single threshold measurements (e.g. principal component analysis and texture analysis) have emerged[20-22] to evaluate lung disease. Automated evaluation of the CT density histogram using principal component analysis[21] has been used to generate a principal component score based on each frequency–HU pair.[21] The strength of this approach relates to the fact that a broad frequency distribution of pixel intensities across a wide range of Hounsfield unit values is evaluated to generate a single score. This measurement is strongly related to pulmonary function tests and expert radiologist emphysema scores.[21] In future studies, it will be important to investigate pulmonary MR measurements that incorporate all signal-intensities to evaluate obstructive lung disease.

An important limitation of this work is that we still do not understand the etiology of MR ventilation defects in aging or UTE signal-intensity in obstructive lung disease. To truly understand the cause of the MR-derived biomarkers presented in this thesis it is important to determine the relationship between MRI measurements and histology and inflammatory markers. Although it can be speculated that these pulmonary imaging abnormalities are related to airway narrowing or wall thickening in older never-smokers, and emphysema or gas-trapping in patients with obstructive lung disease, it is difficult to ascertain the cause without histological specimen or other clinical biomarkers. Studies in mouse models of asthma[10,23] and emphysema[11] have demonstrated the relationship between histology and ^{1}H MR-derived measurements. Studies have also shown differences in eosinophil

percentages of bronchoalveolar lavage fluid that correspond to proton MR measurements in patients with asthma that have undergone an allergy challenge.[24] However, future studies still need to investigate the etiology of MR-derived biomarkers for us to fully understand what these measurements represent in patients with obstructive lung disease.

Another important limitation to this work is the limited availability of ^{3}He gas. It should be noted that Chapters 2-4 used ^{3}He MRI to evaluate static ventilation and/or apparent diffusion coefficients. The high cost of ^{3}He gas has restricted translation of this imaging method beyond specialized MRI centres. As previously discussed, this shortage is forcing the noble gas MRI community to transition to ^{129}Xe gas, a less expensive and more readily available inhaled gas. Studies have shown increased sensitivity to ventilation defects in COPD and asthma using ^{129}Xe MRI.[14,15] If Chapters 2 and 4 were to be done using ^{129}Xe, one may hypothesize that the extent of ventilation defects may be of greater magnitude than the values reported. Regardless of this speculation, future ^{129}Xe MRI studies are required to validate the results presented here using ^{3}He MRI. Moreover, future research and potential clinical applications of noble gas MRI will most definitely utilize ^{129}Xe gas.

Finally, for clinical translation of the presented methods it is important to understand their reproducibility and feasibility across a number of centres and in a clinically relevant population. As stated before, MR measurements are influenced by hardware factors such as RF amplifications and the positioning of the RF coils, which introduce inter-scan variability. An important application for the MR methods presented is pediatric imaging (e.g. survivors of preterm birth and those with bronchopulmonary dysplasia) and those subjects who require longitudinal monitoring (e.g. those with hereditary disorders such as alpha-1 antitrypsin deficiency). These populations are vulnerable to the radiation burden associated with CT based methods. To better understand these biomarkers in pediatric populations, one might want to image a younger cohort. Thus, future studies should aim to evaluate these MR methods across several sites and in a pediatric cohort.

5.4 Future Directions

5.4.1 Ultra-short echo time MRI Measurements of Tissue Density using Principal Component Analysis

In Chapters 3 and 4, we evaluated obstructive lung disease using mean signal-intensity of the UTE images. Pulmonary emphysema has been quantified using mean signal-intensity and T_2* measurements enabled by UTE MRI.[25] Previous work also showed the utility of a single MRI signal-intensity threshold based on thoracic CT emphysema thresholds.[26] Thoracic CT threshold-based emphysema measurements are correlated to pulmonary function tests, [27] and both microscopic and macroscopic measurements of emphysema,[28,29] but there is no consensus regarding an optimal threshold. Recent work has used principal component analysis (PCA) of CT radio-density histograms to assess emphysema. This method uses a broad frequency distribution of pixel intensities across a wide range of density values to produce a single score and measurements derived from this method have been shown to correlate with pulmonary function tests and expert radiologist emphysema scores.[21]

We have performed preliminary analysis in a small proof-of-concept study in which PCA was used to evaluate the UTE signal-intensity histograms to generate principal components based on each frequency-signal intensity pair. We wanted to evaluate and compare the performance of the UTE signal-intensity PCA score with CT measurements.

Frequency histograms of MR signal-intensity and CT radio-density (Hounsfield Units, HU) were generated and PCA was performed on the relative area under the histogram curve for each signal-intensity and HU value. Principal components (PC) were generated based on the variation between input variables. The first two PCs with the highest eigenvalues were selected and the density histogram principal component score (D_HP_CS) and signal-intensity histogram principal component score (S_HP_CS) were determined, as previously described:[21]

Equation 5-1 $$S_HP_CS = \sum_0^{50} RA_iPC_i$$

Where RA is the relative area under the histogram curve for each signal-intensity value and PC is the principal component value calculated from PCA analysis.

In this preliminary work in 10 COPD ex-smokers (68±8yrs) with CT evidence of emphysema, UTE signal-intensity histogram PC scores were determined. **Figure 5-1** shows mean signal-intensity, CT radio-density histograms and corresponding principal components. S_HP_CS was significantly correlated with D_HP_CS (r^2=0.49, p=.02). As shown in **Figure 5-2**, S_HP_CS significantly correlated with RA_{950} (r^2=0.43, p=.04) and FEV_1/FVC (r^2=0.50, p=.02), but not HU_{15} (r^2=0.34, p=.08), DL_{CO} (r^2=0.08, p=.5) or six minute walk distance (6MWD) (r^2=0.14, p=.3). SI_{15} was not significantly correlated with RA_{950} (r^2=0.05, p=.5), HU_{15} (r^2=0.08, p=.4), FEV_1/FVC (r^2=0.09, p=.4), DL_{CO} (r^2=0.0004, p=.9) or 6MWD (r^2=0.34, p=.06). We speculate that in a larger population of COPD subjects, PCA can be used to derive a UTE MRI score that is related to CT measurements of emphysema and gas-trapping. Accordingly, the next steps require a similar but larger-scale validation study of UTE PCA in COPD.

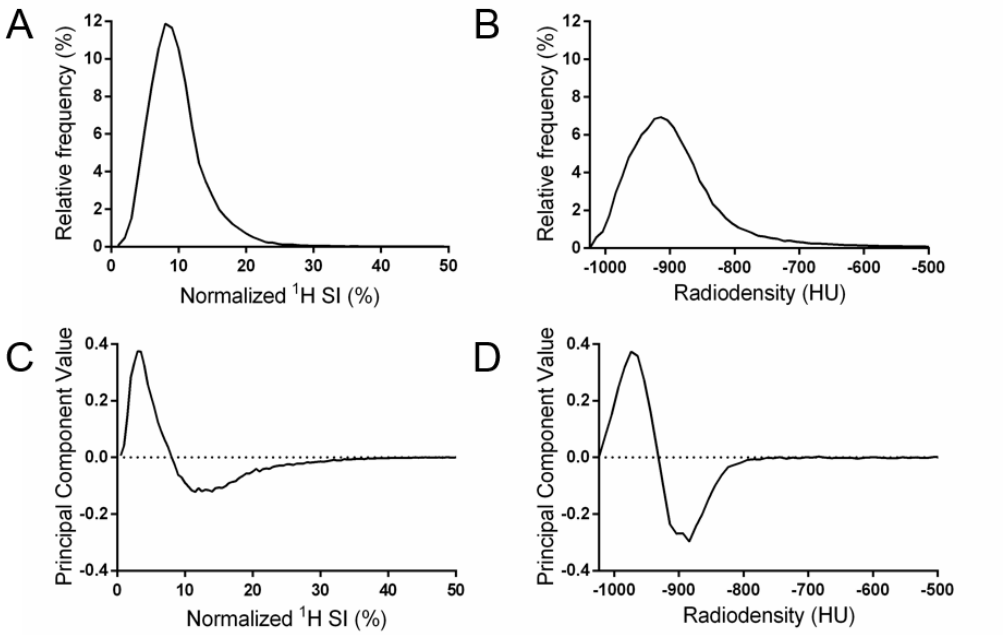

Figure 5-1 UTE signal-intensity and CT radio-density histograms and corresponding principal components generated by PCA with sum of the first and second principal components.

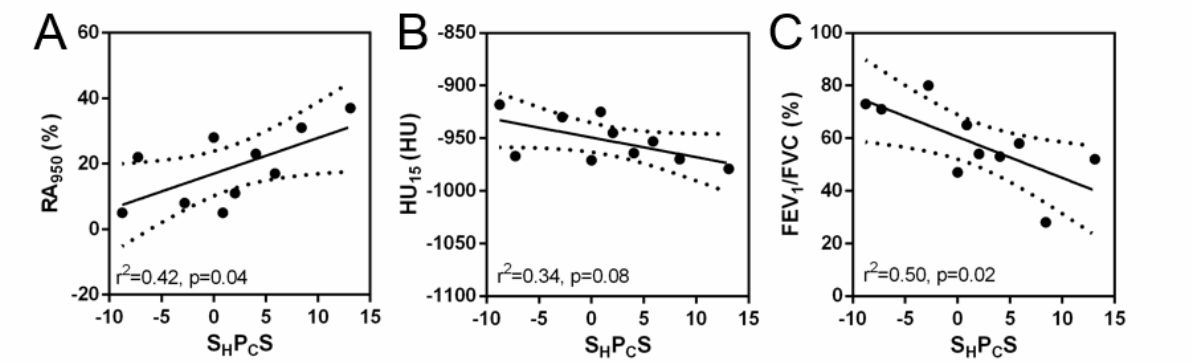

Figure 5-2 Relationships between UTE PCA score (S_HP_CS-defined as the summation of the relative frequency multiplied by the principal component value) and CT and pulmonary function test measurements.

5.4.2 The Etiology of Ultra-short echo time MRI Signal-Intensity

In this thesis, we demonstrated that UTE MR measurements are reproducible and related to CT measurements of tissue density. However, unlike CT measurements, MRI signal-intensity is dependent on four parameters that include the proton density, T_1 relaxation, T_2 relaxation, and flow. Briefly, proton density is the concentration of protons in the tissue in the form of water, fats, or proteins (i.e. macromolecules), T_1 and T_2 define the way the protons revert back to their resting states after excitation, and flow effects are due to the loss of signal due to arterial blood flow. UTE measurements of signal-intensity have the potential to be novel biomarkers of tissue density (e.g. parenchymal loss due to emphysema or regions of inflammation) in longitudinal studies of lung disease. But before this goal can be achieved, the etiology of regions of low UTE signal-intensity and high signal-intensity need to be determined.

To determine the etiology of UTE signal-intensity, there are various potential studies that could be performed. The most concrete evidence would be provided by histological evidence to determine the underlying pathology leading to regions of either high or low signal-intensity. Previous work in mouse models of asthma[10,23] and emphysema[11] have demonstrated the relationship between histology and ^{1}H MR-derived measurements. To evaluate the cause of these regions of low signal-intensity, a study following a similar protocol, but with a human population undergoing lung transplantation should be considered. Sampling the areas within the regions of low signal-intensity would allow for the evaluation of the parenchyma in the region of the low signal-intensity to determine

whether or not bullae or gas-trapping were present that may have contributed to the region of low signal. The area of the lungs that precede the ventilation defect should also be sampled to determine what lead to these regions of low signal.

In patients with asthma who have undergone an allergy challenge, studies have shown differences in eosinophil percentages of bronchoalveolar lavage fluid that correspond to increased regions of high signal-intensity.[24] Similar work could be done to evaluate the etiology of high signal-intensity regions where inflammation biomarkers are acquired to determine whether or not the high signal-intensity corresponds to inflammation, edema, or other pathologies that can potentially increase tissue density.

5.4.3 Ultra-short echo time MRI of Emphysema in Adults with Alpha-1-Antitrypsin Deficiency

Alpha-1-Antitrypsin Deficiency (AATD) is a hereditary disorder caused by a mutation in the SERPINA1 gene, which leads to a dysregulation in neutrophil elastase.[30] This disease affects approximately 1/5000 North Americans.[31,32] One of the hallmark findings of this chronic and progressive disease is panlobular emphysema which is mainly located in the lower lobes of the lung. This under-recognized genetic condition increases the risk of COPD.[33] Similar to smoking-related emphysema, AATD related emphysema has no cure. Therapies do exist, however, to slow the progression of alveolar destruction (e.g. exogenous alpha-1 antitrypsin augmentation therapy).

Current tools available to longitudinally monitor and evaluate therapy response in AATD include pulmonary function tests and imaging methods such as thoracic CT. However, pulmonary function tests do not provide regional information. Studies have shown the CT is more sensitive at monitoring emphysema progression in patients with AATD.[34-36] CT has also been used to monitor therapy response from augmentation therapy.[37] Unfortunately, x-ray based imaging methods pose radiation concerns especially in these patients where serial monitoring is important. Hyperpolarized noble gas MRI offers highly reproducible measurements of lung microstructure and may serve as a sensitive tool to evaluate disease progression. However, the translation of this method to clinic is limited due to advances in CT and limited availability of the necessary hardware for polarizing and

imaging hyperpolarized noble gases. UTE MRI provides a non-contrast enhanced and non-ionizing alternative to pulmonary imaging with reproducible measurements of tissue density (Chapter 3). UTE MR-derived measurements may serve as sensitive biomarkers to evaluate disease progression and response to potential AATD therapies.

Figure 5-3 shows coronal CT, UTE MR, and hyperpolarized noble gas images of three AATD patients with decreasing lung function. The signal intensity in the UTE images becomes visually lower from S1 to S3. In S2 (smoking history<0.5 pack-years) there are regions of visually obvious low signal intensity in the lower lobes of the UTE images that spatially correspond to the regions of ventilation defects and low radiodensity. Similarly, in S3 (smoking history=43 pack years), there are regions of low signal-intensity that visually correspond to regions of low radiodensity and ventilation defects. In this case, these regions are apparent in both the upper and lower lobes indicative of perhaps panlobular and centrilobular emphysema.

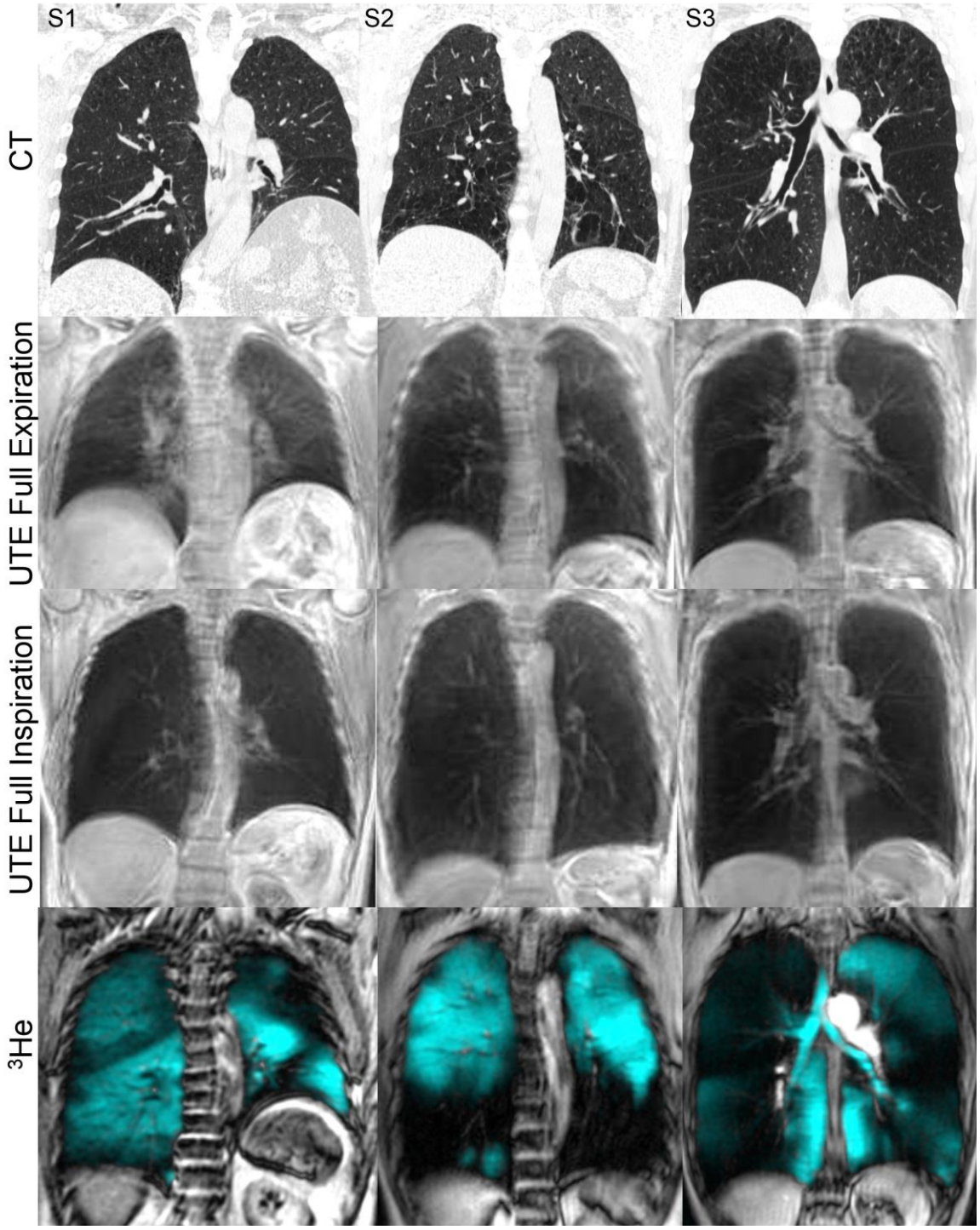

Figure 5-3 Pulmonary MR and CT of AATD.
Thoracic CT, UTE MRI at full expiration and FRC+1L, and ^{3}He MR static ventilation images shown for AATD subjects with decreasing lung function (S1: FEV_1=77%$_{pred}$, S2: FEV_1=55%$_{pred}$, S3: FEV_1=32%$_{pred}$).

Initial investigations should focus on qualitatively and quantitatively comparing CT and UTE MR images in a larger cohort of AATD. Future work should aim to answer the following research questions:

1) *Can UTE MRI provide similar information to that of CT in patients with AATD?*

2) *Are there regional structural and functional relationships between UTE MRI and hyperpolarized noble gas MRI?*

3) *What are the relationships between UTE MR signal-intensity measurements and pulmonary function test measurements in patients with AATD?*

4) *Can UTE MRI be used to monitor treatment response in AATD?*

5.4.4 From Neonatal Chronic Lung Disease to Early Onset Adult COPD: Ultra-short echo time MRI of Bronchopulmonary Dysplasia

Bronchopulmonary dysplasia (BPD) is a chronic lung disease resulting from oxygen therapy, mechanical-ventilation, and/or surfactant deficiency in premature infants who require oxygen 36 weeks post-menstrual age.[38] Studies in infants[39] with BPD have consistently demonstrated abnormalities in the peripheral lung, including failed alveolarization with a decreased number of large and simplified alveoli.[38] Although well-described in children, the long-term respiratory consequences of BPD in adults are not well-understood, although it is hypothesized that the risk of chronic lung disease and emphysema are increased.[40] Consequently, there is growing interest in risk factors beyond smoking given the development of emphysema and COPD in non-smokers.[41] Equipped with the knowledge of how the normal lung ages (Chapter 2) and the pulmonary MRI abnormalities that result in obstructive lung disease (Chapters 3 and 4), we can evaluate patients who are at risk of developing COPD with age. More importantly, we can evaluate regional structural and functional information using MRI without the use of ionizing radiation.

Individuals born extremely preterm, especially with BPD, share many clinical features with COPD patients. Prematurity-related morbidities are quite substantial and impact on

patient's health status such as seen in COPD patients.[42] Airflow obstruction is only partially reversible following administration of bronchodilators.[43] In fact, studies have shown that over 70% of children with BPD do not respond to bronchodilators as demonstrated by lack of significant increase in FEV_1.[44] Not only is there is no cure for BPD,[45] there are no evidence-based or consensus-based guidelines for its treatment in adults.[45] Stem cell therapies aimed at regenerating damaged lung tissue are now being developed, yet there are few tools that allow for longitudinal measures of treatment efficacy.[46] Moreover, our understanding of the morphological alterations of lung structure in patients with BPD is limited due to the difficulty of obtaining lung tissue from living individuals. Proton and inhaled hyperpolarized noble gas MRI provide ways to visualize functional and structural pulmonary information.

We have performed preliminary analysis in a single young adult (a survivor of extreme prematurity of birth) with bronchopulmonary dysplasia. She was born at 27 weeks gestation and was mechanically ventilated and in the neonatal intensive care unit for six weeks without surfactant therapy. She underwent pulmonary function tests, chest x-ray, hyperpolarized ^{3}He and UTE MRI, both pre- and post-salbutamol. As shown in **Figure 5-4**, cyst-like regions of low UTE signal-intensity were similar to previous MRI findings in infants[47] and previous CT findings in adults.[48] These regions of low UTE signal-intensity likely reflected gas-trapping and/or emphysema and have been hypothesized to be associated with prolonged mechanical-ventilation[47] often injurious to immature, surfactant deficient lungs.[49] ^{3}He ventilation defects were clearly abnormal and irreversible and spatially related to regions of low signal-intensity and elevated lung microstructure measurements, reflective of enlarged airspaces. Abnormal ADC (whole-lung mean ADC=0.36cm^2/s) were also heterogeneously distributed throughout the lung. These results demonstrate the feasibility of pulmonary MRI in BPD patients and showed the potential for MRI biomarkers to provide a better understanding of underlying pathophysiology responsible for symptoms and disease worsening in BPD patients.

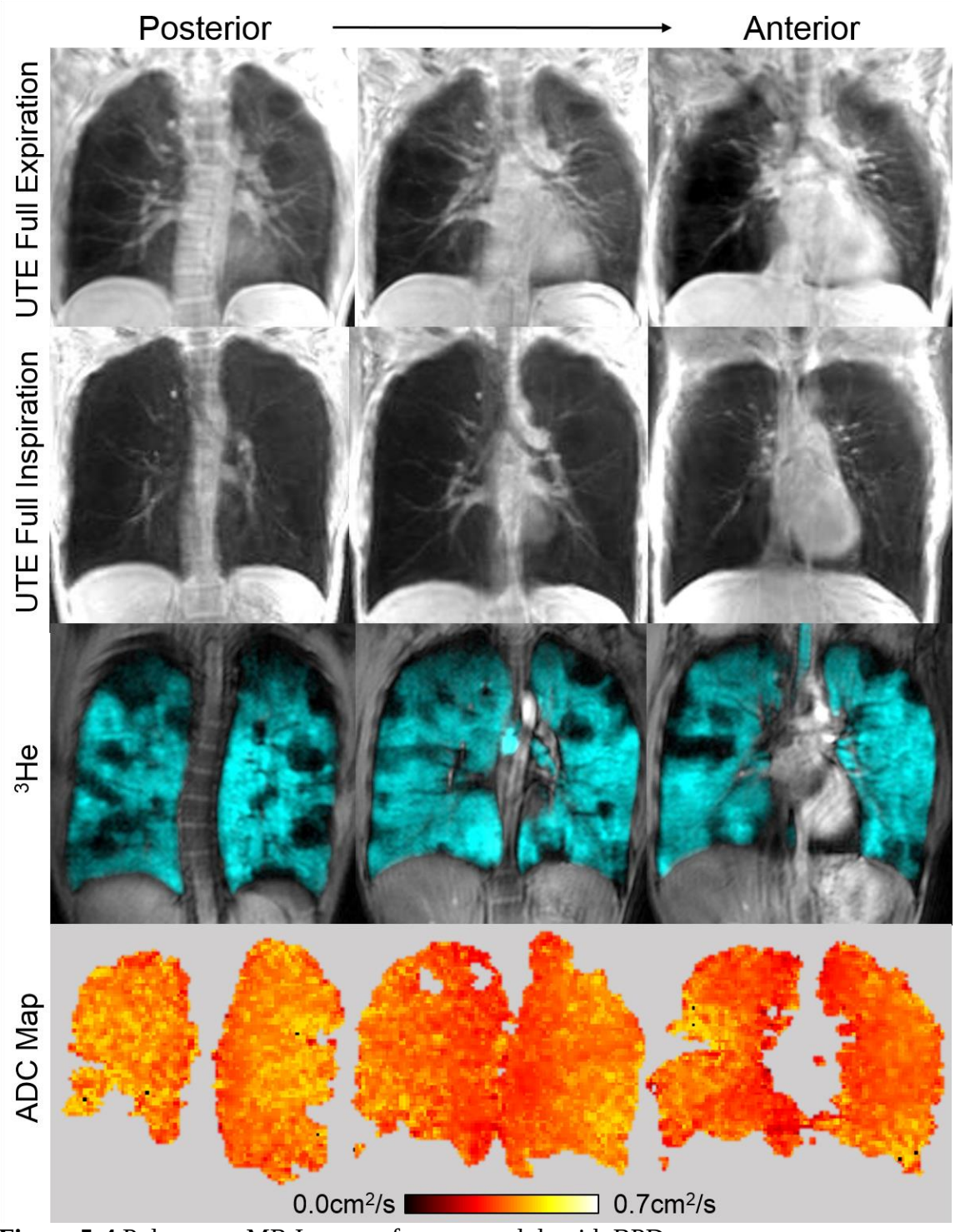

Figure 5-4 Pulmonary MR Images of a young adult with BPD.
Ultra-short echo time (UTE) MR images at full expiration and full inspiration shown for the posterior, centre, and anterior slices. Hyperpolarized ^{3}He static ventilation (cyan) images overlaid on FGRE anatomical images (greyscale) and ADC maps shown for posterior to anterior slices (from left to right).

In a study currently underway, we aim to use UTE and noble gas MRI to evaluate preterm young adults with and without BPD. We hypothesize that young adults born preterm have imaging abnormalities that can be used to evaluate the risk of developing COPD with age. This knowledge will help provide opportunities for early disease interventions. The overarching objective of this work is to characterize the structural and functional pulmonary changes following preterm birth in young adults. This study will address the following research questions:

1) *Are there differences in UTE MR images of young adults born preterm with and without BPD and term-born controls?*

2) *What are the relationships between UTE MR signal-intensity measurements and pulmonary function test measurements in young adults born preterm with and without BPD and term born controls?*

3) *Can UTE MRI be used to longitudinally evaluate young adults born preterm with and without BPD to better understand the natural history of BPD? Are longitudinal changes in UTE MRI measurements in young adults born preterm similar to those young adults born at term?*

5.5 Significance and Impact

Obstructive lung disease affects over six million Canadians and costs the economy $12 billion per year in direct and indirect expenditures. These diseases affect individuals of all ages and can start from birth lasting until the end of life. Despite years of research, obstructive lung disease continues to takes its toll on our healthcare system and economy. More importantly, the quality of life of patients and families facing a life-long battle with lung disease is severely burdened. For many patients, current therapies do not modify disease progression or control requiring the need for hospitalizations or emergency department visits which lead to days lost at school or work. Pulmonary function tests are the gold standard for the diagnosis, monitoring, and evaluation of response to therapy in patients with obstructive lung disease. These measurements, while important, conceal the regional contributions of underlying pathologies. Accordingly, a necessary goal of

obstructive lung disease research is to develop ways to identify patients with specific underlying pathological phenotypes to further personalize medicine with the hopes to improve patient care and outcomes. Imaging methods such as thoracic CT and MRI have the potential to provide regional and quantitative biomarkers of obstructive lung disease. Until now, pulmonary MRI has focused on hyperpolarized noble gas MRI. These inhaled gas MR methods have yet to find wide-ranging acceptance in the clinic. Advances in low dose CT, limited availability of the necessary hardware for polarizing and imaging hyperpolarized noble gases, and the determination of clinically-relevant applications have made clinical translation difficult. However for clinical trials, especially those including a placebo cohort, repeated exposure to ionizing radiation must be considered given that there may be no clinical benefit to monitoring these subjects.

In this thesis we have evaluated pulmonary MR biomarkers in aging and disease to better understand their physiological and clinical consequences. Not only have we provided a basis for imaging abnormalities associated with pulmonary aging, we have introduced a novel method for quantifying lung tissue density without the use of ionizing radiation or inhaled gas contrast. UTE signal-intensity measurements have high reproducibility and are related to pulmonary function test and CT measurements in obstructive lung disease. These methods can be used on clinically available MR scanners without additional specialized equipment or personnel and have the potential to longitudinally evaluate emphysema/gas-trapping for exploratory research or drug-development.

5.6 References

(1) Louis Theriault, G. H., Danielle Goldfarb, Carole Stonebridge, Fares Bounajm. Cost Risk Analysis for Chronic Lung Disease in Canada. (Ottawa, Canada, 2012).

(2) Vestbo, J. *et al.* Global strategy for the diagnosis, management, and prevention of chronic obstructive pulmonary disease: GOLD executive summary. *Am J Respir Crit Care Med* 2013; 187: 347-365.

(3) Reddel, H. K. *et al.* A summary of the new GINA strategy: a roadmap to asthma control. *Eur Respir J* 2015; 46: 622-639.

(4) Svenningsen, S. *et al.* What are ventilation defects in asthma? *Thorax* 2014; 69: 63-71.

(5) Svenningsen, S., Nair, P., Guo, F., McCormack, D. G. & Parraga, G. Is ventilation heterogeneity related to asthma control? *Eur Respir J* 2016.

(6) Kirby, M., Pike, D., Coxson, H. O., McCormack, D. G. & Parraga, G. Hyperpolarized He Ventilation Defects Used to Predict Pulmonary Exacerbations in Mild to Moderate Chronic Obstructive Pulmonary Disease. *Radiology* 2014; 140161.

(7) Parraga, G., Mathew, L., Etemad-Rezai, R., McCormack, D. G. & Santyr, G. E. Hyperpolarized 3He magnetic resonance imaging of ventilation defects in healthy elderly volunteers: initial findings at 3.0 Tesla. *Acad Radiol* 2008; 15: 776-785.

(8) Fain, S. B. *et al.* Detection of age-dependent changes in healthy adult lungs with diffusion-weighted 3He MRI. *Acad Radiol* 2005; 12: 1385-1393.

(9) Lederlin, M. & Cremillieux, Y. Three-dimensional assessment of lung tissue density using a clinical ultrashort echo time at 3 tesla: A feasibility study in healthy subjects. *J Magn Reson Imaging* 2013.

(10) Bianchi, A., Ozier, A., Ousova, O., Raffard, G. & Cremillieux, Y. Ultrashort-TE MRI longitudinal study and characterization of a chronic model of asthma in mice: inflammation and bronchial remodeling assessment. *NMR Biomed* 2013.

(11) Takahashi, M. *et al.* Ultra-short echo time (UTE) MR imaging of the lung: comparison between normal and emphysematous lungs in mutant mice. *J Magn Reson Imaging* 2010; 32: 326-333.

(12) Togao, O., Tsuji, R., Ohno, Y., Dimitrov, I. & Takahashi, M. Ultrashort echo time (UTE) MRI of the lung: assessment of tissue density in the lung parenchyma. *Magn Reson Med* 2010; 64: 1491-1498.

(13) Ohno, Y. *et al.* T2* measurements of 3-T MRI with ultrashort TEs: capabilities of pulmonary function assessment and clinical stage classification in smokers. *AJR Am J Roentgenol* 2011; 197: W279-285.

(14) Svenningsen, S. *et al.* Hyperpolarized He and Xe MRI: Differences in asthma before bronchodilation. *J Magn Reson Imaging* 2013.

(15) Kirby, M. *et al.* Pulmonary ventilation visualized using hyperpolarized helium-3 and xenon-129 magnetic resonance imaging: differences in COPD and relationship to emphysema. *J Appl Physiol* 2013; 114: 707-715.

(16) Busacker, A. *et al.* A multivariate analysis of risk factors for the air-trapping asthmatic phenotype as measured by quantitative CT analysis. *Chest* 2009; 135: 48-56.

(17) Fain, S. B. *et al.* Evaluation of structure-function relationships in asthma using multidetector CT and hyperpolarized He-3 MRI. *Acad Radiol* 2008; 15: 753-762.

(18) Muller, N. L., Staples, C. A., Miller, R. R. & Abboud, R. T. "Density mask". An objective method to quantitate emphysema using computed tomography. *Chest* 1988; 94: 782-787.

(19) Coxson, H. O. *et al.* A quantification of the lung surface area in emphysema using computed tomography. *Am J Respir Crit Care Med* 1999; 159: 851-856.

(20) Xu, Y., Sonka, M., McLennan, G., Guo, J. & Hoffman, E. A. MDCT-based 3-D texture classification of emphysema and early smoking related lung pathologies. *IEEE Trans Med Imaging* 2006; 25: 464-475.

(21) Owrangi, A. M., Etemad-Rezai, R., McCormack, D. G., Cunningham, I. A. & Parraga, G. Computed tomography density histogram analysis to evaluate pulmonary emphysema in ex-smokers. *Acad Radiol* 2013; 20: 537-545.

(22) Mohamed Hoesein, F. A. *et al.* Computed tomography-quantified emphysema distribution is associated with lung function decline. *Eur Respir J* 2012; 40: 844-850.

(23) Conti, G. *et al.* Evaluation of lung inflammation induced by intratracheal administration of LPS in mice: comparison between MRI and histology. *MAGMA* 2010; 23: 93-101.

(24) Vogel-Claussen, J. *et al.* Quantification of pulmonary inflammation after segmental allergen challenge using turbo-inversion recovery-magnitude magnetic resonance imaging. *Am J Respir Crit Care Med* 2014; 189: 650-657.

(25) Zurek, M., Boyer, L., Caramelle, P., Boczkowski, J. & Crémillieux, Y. Longitudinal and noninvasive assessment of emphysema evolution in a murine model using proton MRI. *Magnetic Resonance in Medicine* 2012; 68: 898-904.

(26) Ma, W. *et al.* Ultra-short echo-time pulmonary MRI: Evaluation and reproducibility in COPD subjects with and without bronchiectasis. *J Magn Reson Imaging* 2014.

(27) Park, K. J., Bergin, C. J. & Clausen, J. L. Quantitation of emphysema with three-dimensional CT densitometry: comparison with two-dimensional analysis, visual

emphysema scores, and pulmonary function test results. *Radiology* 1999; 211: 541-547.

(28) Gevenois, P. A., de Maertelaer, V., De Vuyst, P., Zanen, J. & Yernault, J. C. Comparison of computed density and macroscopic morphometry in pulmonary emphysema. *Am J Respir Crit Care Med* 1995; 152: 653-657.

(29) Gevenois, P. A. *et al.* Comparison of computed density and microscopic morphometry in pulmonary emphysema. *Am J Respir Crit Care Med* 1996; 154: 187-192.

(30) Stoller, J. K. Alpha-1 antitrypsin deficiency: An underrecognized, treatable cause of COPD. *Cleve Clin J Med* 2016; 83: 507-514.

(31) Marciniuk, D. *et al.* Alpha-1 antitrypsin deficiency targeted testing and augmentation therapy: A Canadian Thoracic Society clinical practice guideline. *Can Respir J* 2012; 19: 109-116.

(32) Stoller, J. K. & Aboussouan, L. S. A review of α1-antitrypsin deficiency. *American journal of respiratory and critical care medicine* 2012; 185: 246-259.

(33) Evald, T., Dirksen, A., Keittelmann, S., Viskum, K. & Kok-Jensen, A. Decline in pulmonary function in patients with alpha 1-antitrypsin deficiency. *Lung* 1990; 168 Suppl: 579-585.

(34) Dirksen, A. *et al.* A randomized clinical trial of alpha(1)-antitrypsin augmentation therapy. *Am J Respir Crit Care Med* 1999; 160: 1468-1472.

(35) Dawkins, P. A., Dowson, L. J., Guest, P. J. & Stockley, R. A. Predictors of mortality in alpha1-antitrypsin deficiency. *Thorax* 2003; 58: 1020-1026.

(36) Parr, D. G., Stoel, B. C., Stolk, J. & Stockley, R. A. Validation of computed tomographic lung densitometry for monitoring emphysema in alpha1-antitrypsin deficiency. *Thorax* 2006; 61: 485-490.

(37) Chapman, K. R. *et al.* Intravenous augmentation treatment and lung density in severe alpha1 antitrypsin deficiency (RAPID): a randomised, double-blind, placebo-controlled trial. *Lancet* 2015; 386: 360-368.

(38) Jobe, A. H. & Bancalari, E. Bronchopulmonary dysplasia. *Am J Respir Crit Care Med* 2001; 163: 1723-1729.

(39) Husain, A. N., Siddiqui, N. H. & Stocker, J. T. Pathology of arrested acinar development in postsurfactant bronchopulmonary dysplasia. *Hum Pathol* 1998; 29: 710-717.

(40) Saigal, S. & Doyle, L. W. An overview of mortality and sequelae of preterm birth from infancy to adulthood. *The Lancet* 2008; 371: 261-269.

(41) Eisner, M. D. *et al.* An official American Thoracic Society public policy statement: Novel risk factors and the global burden of chronic obstructive pulmonary disease. *Am J Respir Crit Care Med* 2010; 182: 693-718.

(42) Zwicker, J. G. & Harris, S. R. Quality of life of formerly preterm and very low birth weight infants from preschool age to adulthood: a systematic review. *Pediatrics* 2008; 121: e366-376.

(43) Fawke, J. *et al.* Lung function and respiratory symptoms at 11 years in children born extremely preterm: the EPICure study. *Am J Respir Crit Care Med* 2010; 182: 237-245.

(44) Baraldi, E., Bonetto, G., Zacchello, F. & Filippone, M. Low exhaled nitric oxide in school-age children with bronchopulmonary dysplasia and airflow limitation. *Am J Respir Crit Care Med* 2005; 171: 68-72.

(45) Kotecha, S. J. *et al.* Effect of bronchodilators on forced expiratory volume in 1 s in preterm-born participants aged 5 and over: a systematic review. *Neonatology* 2015; 107: 231-240.

(46) van Haaften, T. *et al.* Airway delivery of mesenchymal stem cells prevents arrested alveolar growth in neonatal lung injury in rats. *American journal of respiratory and critical care medicine* 2009; 180: 1131-1142.

(47) Adams, E. W. *et al.* Magnetic resonance imaging of lung water content and distribution in term and preterm infants. *Am J Respir Crit Care Med* 2002; 166: 397-402.

(48) Howling, S. J. *et al.* Pulmonary sequelae of bronchopulmonary dysplasia survivors: high-resolution CT findings. *AJR Am J Roentgenol* 2000; 174: 1323-1326.

(49) Dreyfuss, D. & Saumon, G. Ventilator-induced lung injury: lessons from experimental studies. *Am J Respir Crit Care Med* 1998; 157: 294-323.

APPENDIX

Appendix A – Permission for Reproduction of Scientific Articles

American Physiological Society LICENSE
TERMS AND CONDITIONS

Jan 05, 2016

This is a License Agreement between Khadija Sheikh ("You") and American Physiological Society ("American Physiological Society") provided by Copyright Clearance Center ("CCC"). The license consists of your order details, the terms and conditions provided by American Physiological Society, and the payment terms and conditions.

All payments must be made in full to CCC. For payment instructions, please see information listed at the bottom of this form.

License Number	3782550220405
License date	Jan 05, 2016
Licensed content publisher	American Physiological Society
Licensed content title	Journal of applied physiology
Licensed content date	Jan 1, 1985
Type of Use	Thesis/Dissertation
Requestor type	Author of requested content
Format	Electronic
Portion	chapter/article
Title or numeric reference of the portion(s)	Abstract, Introduction, Methods, Discussion and Conclusion, Table 1, Table 2, Table 3, Table 4, Figure 1, Figure 2, Figure 3, Figure 4
Title of the article or chapter the portion is from	Pulmonary ventilation defects in older never-smokers
Editor of portion(s)	N/A
Author of portion(s)	Khadija Sheikh
Volume of serial or monograph.	117
Issue, if republishing an article from a serial	N/A
Page range of the portion	None
Publication date of portion	Aug 1, 2014
Rights for	Main product
Duration of use	Current edition and up to 15 years
Creation of copies for the disabled	no
With minor editing privileges	no
For distribution to	Canada
In the following language(s)	Original language of publication

JOHN WILEY AND SONS LICENSE TERMS AND CONDITIONS

Jan 05, 2016

This Agreement between Khadija Sheikh ("You") and John Wiley and Sons ("John Wiley and Sons") consists of your license details and the terms and conditions provided by John Wiley and Sons and Copyright Clearance Center.

License Number	3782521118946
License date	Jan 05, 2016
Licensed Content Publisher	John Wiley and Sons
Licensed Content Publication	Journal of Magnetic Resonance Imaging
Licensed Content Title	Ultra-short echo-time pulmonary MRI: Evaluation and reproducibility in COPD subjects with and without bronchiectasis
Licensed Content Author	Weijing Ma,Khadija Sheikh,Sarah Svenningsen,Damien Pike,Fumin Guo,Roya Etemad-Rezai,Jonathan Leipsic,Harvey O. Coxson,David G. McCormack,Grace Parraga
Licensed Content Date	Jun 26, 2014
Pages	10
Type of use	Dissertation/Thesis
Requestor type	Author of this Wiley article
Format	Electronic
Portion	Full article
Will you be translating?	No
Title of your thesis / dissertation	Multi-Nuclear Magnetic Resonance Imaging to Phenotype Chronic Lung Disease
Expected completion date	Jul 2016
Expected size (number of pages)	250
Requestor Location	Khadija Sheikh

Billing Type

Billing Address

This Agreement between Khadija Sheikh ("You") and John Wiley and Sons ("John Wiley and Sons") consists of your license details and the terms and conditions provided by John Wiley and Sons and Copyright Clearance Center.

Your confirmation email will contain your order number for future reference.

Printable details.

License Number	3981501238326
License date	Nov 03, 2016
Licensed Content Publisher	John Wiley and Sons
Licensed Content Publication	Journal of Magnetic Resonance Imaging
Licensed Content Title	Ultrashort echo time MRI biomarkers of asthma
Licensed Content Author	Khadija Sheikh,Fumin Guo,Dante P.I. Capaldi,Alexei Ouriadov,Rachel L. Eddy,Sarah Svenningsen,Grace Parraga
Licensed Content Date	Oct 12, 2016
Licensed Content Pages	1
Type of use	Dissertation/Thesis
Requestor type	Author of this Wiley article
Format	Print and electronic
Portion	Full article
Will you be translating?	No
Title of your thesis / dissertation	Multi-Nuclear Magnetic Resonance Imaging to Phenotype Chronic Lung Disease
Expected completion date	Jul 2016
Expected size (number of pages)	250
Requestor Location	
Publisher Tax ID	EU826007151
Billing Type	Invoice
Billing address	
Total	0.00 CAD

Appendix B – Health Science Research Ethics Board Approval Notices

Office of Research Ethics

The University of Western Ontario

Website: www.uwo.ca/research/ethics

Use of Human Subjects - Ethics Approval Notice

Principal Investigator:	Dr. G. Parraga
Review Number:	17396 **Review Level:** Full Board
Review Date:	September 14, 2010 **Approved Local # of Participants:** 180
Protocol Title:	Longitudinal 3 He Magnetic Resonance Imaging of Health Lung
Department and Institution:	Imaging, Robarts Research Institute
Sponsor:	CIHR-CANADIAN INSTITUTE OF HEALTH RESEARCH
Ethics Approval Date:	November 09, 2010 **Expiry Date:** September 30, 2014
Documents Reviewed and Approved:	UWO Protocol (including instruments noted in Section 0.1), Letter of Information and Consent Form dated Sept. 27, 2010 version 2, and Advertisement.
Documents Received for Information:	Clinical Study Protocol Version #1 27 August 2010; IB NC1100182-Inhalation (Hyperpolarised 3HE) 5th edition 09 Sep 05; NC1100182 IB April 7, 2009 Product Monograph Ventolin HFA

This is to notify you that The University of Western Ontario Research Ethics Board for Health Sciences Research Involving Human Subjects (HSREB) which is organized and operates according to the Tri-Council Policy Statement: Ethical Conduct of Research Involving Humans and the Health Canada/ICH Good Clinical Practice Practices: Consolidated Guidelines; and the applicable laws and regulations of Ontario has reviewed and granted approval to the above referenced study on the approval date noted above. The membership of this REB also complies with the membership requirements for REB's as defined in Division 5 of the Food and Drug Regulations.

The ethics approval for this study shall remain valid until the expiry date noted above assuming timely and acceptable responses to the HSREB's periodic requests for surveillance and monitoring information. If you require an updated approval notice prior to that time you must request it using the UWO Updated Approval Request Form.

During the course of the research, no deviations from, or changes to, the protocol or consent form may be initiated without prior written approval from the HSREB except when necessary to eliminate immediate hazards to the subject or when the change(s) involve only logistical or administrative aspects of the study (e.g. change of monitor, telephone number). Expedited review of minor change(s) in ongoing studies will be considered. Subjects must receive a copy of the signed information/consent documentation.

Investigators must promptly also report to the HSREB:

a) changes increasing the risk to the participant(s) and/or affecting significantly the conduct of the study;
b) all adverse and unexpected experiences or events that are both serious and unexpected;
c) new information that may adversely affect the safety of the subjects or the conduct of the study.

If these changes/adverse events require a change to the information/consent documentation, and/or recruitment advertisement, the newly revised information/consent documentation, and/or advertisement, must be submitted to this office for approval.

Members of the HSREB who are named as investigators in research studies, or declare a conflict of interest, do not participate in discussion related to, nor vote on, such studies when they are presented to the HSREB.

Chair of HSREB: Dr. Joseph Gilbert
FDA Reg. #: IRB 00000941

Ethics Officer to Contact for Further Information

☐ Janice Sutherland ☐ Elizabeth Wambolt ☐ Grace Kelly

This is an official document. Please retain the original in your files.

cc: ORF File
HRI

UWO HSREB Ethics Approval - Initial
V:2009-07-01 (rptApprovalNoticeHSREB_Initial)

17396

Page 1 of 1

Western Research

Western University Health Science Research Ethics Board
HSREB Amendment Approval Notice

Principal Investigator: Dr. Grace Parraga
Department & Institution: Schulich School of Medicine and Dentistry/Imaging Robarts Research Institute

HSREB File Number: 7320
Study Title: Longitudinal ^{3}He Magnetic Resonance Imaging of Healthy Lung (REB #17396)
Sponsor: Canadian Institutes of Health Research

HSREB Amendment Approval Date: June 24, 2014
HSREB Expiry Date: September 30, 2016

Documents Approved and/or Received for Information

Document Name	Comments	Version Date
Revised Western University Protocol		2014/05/15
Revised Letter of Information & Consent	version 6	2014/05/15

The Western University Health Science Research Ethics Board (HSREB) has reviewed and approved the amendment to the above named study, as of the HSREB Initial Approval Date noted above.

HSREB approval for this study remains valid until the HSREB Expiry Date noted above, conditional to timely submission and acceptance of HSREB Continuing Ethics Review. If an Updated Approval Notice is required prior to the HSREB Expiry Date, the Principal Investigator is responsible for completing and submitting an HSREB Updated Approval Form in a timely fashion.

The Western University HSREB operates in accordance with the Tri-Council Policy Statement: Ethical Conduct for Research Involving Humans (TCPS2), the International Conference on Harmonization of Technical Requirements for Registration of Pharmaceuticals for Human Use Guideline for Good Clinical Practice Practices (ICH E6 R1), the Ontario Personal Health Information Protection Act (PHIPA, 2004), Part 1 of the Natural Health Product Regulations, Health Canada Medical Device Regulations and Part C, Division 5, of the Food and Drug Regulations of Health Canada.

Members of the HSREB who are named as Investigators in research studies do not participate in discussions related to, nor vote on, such studies when they are presented to the REB.

The HSREB is registered with the U.S. Department of Health & Human Services under the IRB registration number IRB 00000940.

Ethics Officer, on behalf of Dr. Joseph Gilbert, HSREB Chair

Ethics Officer to Contact for Further Information

☑ Grace Parraga	Dawn Kelly	Michelle Gill	Vikki Tran

This is an official document. Please retain the original in your file.

R06037

Research Ethics

Western Research

Use of Human Participants - Ethics Approval Notice

Principal Investigator: Dr. Grace Parraga
File Number:103959
Review Level: Full Board
Approved Local Adult Participants:30
Approved Local Minor Participants:0
Protocol Title: Evaluation of Oscillatory Positive Expiratory Pressure (oPEP) in Bronchiectasis and COPD
Department & Institution: Schulich School of Medicine and Dentistry\Imaging,Robarts Research Institute
Sponsor:
Ethics Approval Date: July 30, 2013
Ethics Expiry Date: September 30, 2014

Documents Reviewed & Approved & Documents Received for Information:

Document Name	Comments	Version Date
Protocol	Robarts Protocol - Received for information	2013/06/12
Other	Instructions for Aerobika device	
Response to Board Recommendations	Response to Board Recommendations	2013/07/10
Health Canada Correspondence	Health Canada MDL	
Letter of Information & Consent	Letter of Information V2 Clean	2013/07/10
Instruments	Study Diary,Patient Evaluation Questionnaire, St. George's Respiratory Questionnaire and BORG Scale	
Western University Protocol		

This is to notify you that the University of Western Ontario Health Sciences Research Ethics Board (HSREB) which is organized and operates according to the Tri-Council Policy Statement: Ethical Conduct of Research Involving Humans and the Health Canada/ICH Good Clinical Practice Practices: Consolidated Guidelines; and the applicable laws and regulations of Ontario has reviewed and granted approval to the above referenced study on the approval date noted above. The membership of this HSREB also complies with the membership requirements for REB's as defined in Division 5 of the Food and Drug Regulations.

The ethics approval for this study shall remain valid until the expiry date noted above assuming timely and acceptable responses to the HSREB's periodic requests for surveillance and monitoring information. If you require an updated approval notice prior to that time you must request it using the University of Western Ontario Updated Approval Request form.

Member of the HSREB that are named as investigators in research studies, or declare a conflict of interest, do not participate in discussions related to, nor vote on, such studies when they are presented to the HSREB.

The Chair of the HSREB is Dr. Joseph Gilbert. The HSREB is registered with the U.S. Department of Health & Human Services under the IRB registration number IRB 00000940.

Signature

Ethics Officer to Contact for Further Information

This is an official document. Please retain the original in your files.

RAB 2038 R2

Western Research

Research Ethics

Use of Human Participants - Revision Ethics Approval Notice

Principal Investigator: Dr. Grace Parraga
File Number:103989
Review Level: Delegated
Protocol Title: Evaluation of Oscillatory Positive Expiratory Pressure (oPEP) in Bronchiectasis and COPD
Department & Institution: Schulich School of Medicine and Dentistry\Imaging,Robarts Research Institute
Sponsor:
Ethics Approval Date: October 31, 2013 **Expiry Date:**September 30, 2014
Documents Reviewed & Approved & Documents Received for Information:

Document Name	Comments	Version Date
Revised Western University Protocol	Modification to sections 2.4 and 2.8: inclusion of Airwave Oscillometry testing for remainder of participants' final visits (Received Oct.21/13)	
Revised Letter of Information & Consent		2013/10/21

This is to notify you that The University of Western Ontario Research Ethics Board for Health Sciences Research Involving Human Subjects (HSREB) which is organized and operates according to the Tri-Council Policy Statement: Ethical Conduct of Research Involving Humans and the Health Canada/ICH Good Clinical Practice Practices: Consolidated Guidelines; and the applicable laws and regulations of Ontario has reviewed and granted approval to the above referenced revision(s) or amendment(s) on the approval date noted above. The membership of this REB also complies with the membership requirements for REB's as defined in Division 5 of the Food and Drug Regulations.

The ethics approval for this study shall remain valid until the expiry date noted above assuming timely and acceptable responses to the HSREB's periodic requests for surveillance and monitoring information. If you require an updated approval notice prior to that time you must request it using the University of Western Ontario Updated Approval Request Form.

Members of the HSREB who are named as investigators in research studies, or declare a conflict of interest, do not participate in discussion related to, nor vote on, such studies when they are presented to the HSREB.

The Chair of the HSREB is Dr. Joseph Gilbert. The HSREB is registered with the U.S. Department of Health & Human Services under the IRB registration number IRB 00000940.

Signature

Ethics Officer to Contact for Further Information

Erika Basile	Grace Kelly	Vikki Tran

This is an official document. Please retain the original in your files.

Western Research

Use of Human Participants - Ethics Approval Notice

Principal Investigator: Dr. Grace Parraga
File Number: 103516
Review Level: Full Board
Approved Local Adult Participants: 200
Approved Local Minor Participants: 0
Protocol Title: Structure and Function MRI of Asthma
Department & Institution: Schulich School of Medicine and Dentistry\Imaging,Roberts Research Institute
Sponsor:
Ethics Approval Date: April 08, 2013
Ethics Expiry Date: March 31, 2020

Documents Reviewed & Approved & Documents Received for Information:

Document Name	Comments	Version Date
Protocol	Roberts Protocol - Received for information only	2013/02/06
Instruments	Telephone Script	2013/03/14
Letter of Information & Consent	ROB0037 CF March 13 2013	2013/03/12
Western University Protocol	(including study instruments & questionnaires)	

This is to notify you that the University of Western Ontario Health Sciences Research Ethics Board (HSREB) which is organized and operates according to the Tri-Council Policy Statement: Ethical Conduct of Research Involving Humans and the Health Canada/ICH Good Clinical Practice Practices: Consolidated Guidelines; and the applicable laws and regulations of Ontario has reviewed and granted approval to the above referenced study on the approval date noted above. The membership of this HSREB also complies with the membership requirements for REB's as defined in Division 5 of the Food and Drug Regulations.

The ethics approval for this study shall remain valid until the expiry date noted above assuming timely and acceptable responses to the HSREB's periodic requests for surveillance and monitoring information. If you require an updated approval notice prior to that time you must request this using the University of Western Ontario Updated Approval Request form.

Member of the HSREB that are named as investigators in research studies, or declare a conflict of interest, do not participate in discussions related to, nor vote on, such studies when they are presented to the HSREB.

The Chair of the HSREB is Dr. Joseph Gilbert. The HSREB is registered with the U.S. Department of Health & Human Services under the IRB registration number IRB 00000940

Signature

Ethics Officer to Contact for Further Information

Janice Sutherland	Grace Kelly	Shantal Walcott

This is an official document. Please retain the original in your files.

Appendix C – Curriculum Vitae

EDUCATION

08/12-11/16	Doctor of Philosophy in Medical Biophysics (*Candidate*) Department of Medical Biophysics The University of Western Ontario, London, Ontario, Canada *Supervisor*: Dr. Grace Parraga *Thesis Title*: Multi-nuclear Magnetic Resonance Imaging of Obstructive Lung Disease
08/12-11/16	Clinical Master of Science in Medical Biophysics (CAMPEP-accredited) *(Candidate)* Department of Medical Biophysics The University of Western Ontario, London, Ontario, Canada *Supervisor*: Dr. Grace Parraga
09/08-08/12	Bachelor of Science Honours Physics and High Technology (Medical Physics) with Co-op Minor in Mathematics The University of Windsor, Windsor, Ontario, Canada

POSITIONS

09/12-present	Graduate Research Assistant Department of Medical Biophysics The University of Western Ontario, London, Ontario, Canada *Supervisor*: Dr. Grace Parraga
05/14-08/14, 09/15-12/15	Quality Assurance Internship London Regional Cancer Program London Health Science Centre, London, Ontario, Canada *Supervisor*: Dr. Slav Yartsev
09/11-12/11	Production Engineer Co-op Student Production Department Tokai Rika Quality Safety Systems Company, Tecumseh, Ontario, Canada
07/11-11/11	Student Research Assistant Department of Physics The University of Windsor, Windsor, Ontario, Canada *Supervisor*: Dr. Steven Rehse *Project*: Laser Based Identification of Bacteria using Discriminant Function Analysis

01/11-04/11 Student Research Assistant
Department of Physics
TRIUMF, Vancouver, British Columbia, Canada
Supervisor: Dr. Michael Hasinoff
Project: Time Reversal Experiment with Kaon Decay

05/10-09/10 X-ray Diffraction Technician
Department of Research and Design
Proto Manufacturing, Sandcastle, Ontario, Canada

ACADEMIC AWARDS, SCHOLARSHIPS, and DISTINCTIONS

09/16 Western University Doctoral Excellence Research Award
Awarded to a full time graduate student holding a national tri-agency (i.e. CIHR, NSERC, or SSHRC) doctoral scholarship.
Institutional
$10,000

05/16 International Society for Magnetic Resonance in Medicine Magna Cum Laude Award
Awarded to the top 15% of written abstracts at the annual international meeting within a major subject review category.
International

05/16 International Society for Magnetic Resonance in Medicine Educational Stipend Award
Awarded to support the attendance of students, postdoctoral and clinical trainees to present abstracts at the scientific meeting.
International
$475 USD

03/16 London Health Research Day Top Written Abstract in Circulatory Category
Awarded to the top written abstract within a major subject category.
Institutional
$100

05/15-05/16 Western University Ontario Graduate Scholarship
Queen Elizabeth II Graduate Scholarship in Science and Technology
Awarded to a full time graduate student for stipend support who has maintained an average of 80% or more and exhibits research ability, excellent communication skills, and interpersonal and leadership abilities.
Provincial
$15,000

Declined

05/15-05/17 Natural Sciences and Engineering Research Council of Canada (NSERC)
Alexander Graham Bell Canadian Graduate Scholarship (CGS) Doctoral
Award based on academic excellence, research ability, and communication, interpersonal, and leadership abilities.
National
$70,000

06/15 International Society for Magnetic Resonance in Medicine Educational Stipend Award
Awarded to support the attendance of students, postdoctoral and clinical trainees to present abstracts at the scientific meeting.
International
$360 USD

09/13-Present Canadian Institutes of Health Research Strategic Training Program in Vascular Research
Institutional
$20,000

05/13-05/14 Western University Ontario Graduate Scholarship
Queen Elizabeth II Graduate Scholarship in Science and Technology
Awarded to a full time graduate student for stipend support who has maintained an average of 80% or more and exhibits research ability, excellent communication skills, and interpersonal and leadership abilities.
Provincial
$15,000

09/12-09/13 Schulich Graduate Scholarship, The University of Western Ontario
Awarded to a full time graduate student for stipend support who has maintained an average of 80% or more.
Institutional
$4,500

04/12, 01/09 Dean's Honour Roll
Awarded to a full-time student who has maintained an 11.0 or more out of 13.0.
Institutional

09/10 Canadian Interuniversity Sport Academic All-Canadian
Awarded to a student-athlete who has maintained an 80% average while competing as a varsity athlete.

National

09/10 Recognition of Achievement Bursary
Awarded to students on OSAP assistance who have maintained an 80% or higher average
Provincial
$1000

09/10 Blue and Gold Scholarship, The University of Windsor
Awarded to a student-athlete who has excelled at his/her sport.
Institutional
$200

09/08-09/09 Outstanding Scholars Scholarship
Awarded upon admission to Windsor students who have an admission average of 85% or more.
Institutional
$1500

09/08 Interfaculty Physics Scholarship
Awarded upon admission to the top five Honours Physics students who have the highest admission average
Institutional
$1000

PUBLICATIONS and PRESENTATIONS

A. Refereed Journal Manuscripts (14 published, 4 submitted)

Published (14)

1. **K Sheikh**, F Guo, A Ouriadov, DPI Capaldi, RL Eddy, S Svenningsen, G Parraga. Ultra-short Echo Time Magnetic Resonance Imaging Biomarkers of Asthma. Submitted to *Journal of Magnetic Resonance Imaging (MS # JMRI-16-0866R1 in press).*

2. F Guo, S Svenningsen, RL Eddy, DPI Capaldi, **K Sheikh**, J Yuan, A Fenster, G Parraga. Anatomical Pulmonary Magnetic Resonance Imaging Segmentation for Regional Structure-Function Measurements of Asthma. *Medical Physics (MS #16-156R in press).*

3. C Davis, **K Sheikh**, D Pike, S Svenningsen, DG McCormack, D O'Donnell, JA Neder, G Parraga. Ventilation Heterogeneity in Never-Smokers and COPD: Comparison of Pulmonary Functional Magnetic Resonance Imaging with the Poorly Communicating Fraction Derived from Plethysmography. *Academic Radiology*. 2016 Apr;23(4):398-405.

4. GA Paulin, A Ouriadov, E Lessard, **K Sheikh**, NAM Paterson, DG McCormack, G Parraga. Non-Invasive Quantification of Alveolar Morphometry in Older Never-Smokers. *Physiological Reports* 2015 Oct; 3(10): e12583.

5. **K Sheikh**, HO Coxson, G Parraga. This is What COPD Looks Like. *Respirology* 2016 Feb; 21(2):224-236. **Cover of Journal**.

6. **K Sheikh**, DPI Capaldi, DA Hoover, DA Palma, BP Yaremko, G Parraga. Magnetic Resonance Imaging Biomarkers of Chronic Obstructive Pulmonary Disease prior to Radiation Therapy for Non-Small Cell Lung Cancer. *European Journal of Radiology Open.* 2015 May 26; 2: 81-89.

7. F Guo, J Yuan, M Rajchl, S Svenningsen, DPI Capaldi, **K Sheikh**, A Fenster, G Parraga. Globally optimal joint segmentation of three-dimensional pulmonary ^{1}H and hyperpolarized ^{3}He MRI with spatial consistence prior. *Medical Image Analysis*. 2015 Apr 17; 23(1):43-55.

8. S Svenningsen, GA Paulin, **K Sheikh**, F Guo, A Hasany, M Kirby, J Suggett, R Etemad-Rezai, G Parraga, DG McCormack. Oscillatory Positive Expiratory Pressure in Chronic Obstructive Pulmonary Disease. *Journal of Chronic Obstructive Pulmonary Disease*. 2016 Feb;13(1):66-74.

9. DA Hoover, DPI Capaldi, **K Sheikh**, DA Palma, GB Rodrigues, R Dar, E Yu, M Landis, B Dingle, W Kocha, MS Sanatani, MD Vincent, J Younus, S Kuruvilla, S Gaede, G Parraga, BP Yaremko. Functional lung avoidance for individualized radiotherapy (FLAIR): Study protocol for a randomized, double-blind clinical trial. *BMC Cancer*. 2014 Dec 11; 14:934.

10. DPI Capaldi, **K Sheikh**, F Guo, S Svenningsen, R Etemad-Rezai, HO Coxson. JA Leipsic, DG McCormack, G Parraga. Free-breathing pulmonary ^{1}H and hyperpolarized ^{3}He MRI: comparison in COPD and bronchiectasis. *Academic Radiology*. 2015 Mar; 22(3):320-329.

11. W Ma, **K Sheikh,** S Svenningsen, D Pike, F Guo, R Etemad-Rezai, J Leipsic, HO Coxson, DG McCormack, G Parraga. Ultra-short echo-time Pulmonary MRI: Evaluation and Reproducibility in COPD subjects with and without Bronchiectasis. *Journal of Magnetic Resonance Imaging.* 2015 May; 41(3):1465-1474.

12. D Pike, M Kirby, TJ Lindenmaier, **K Sheikh**, CE Neron, DG Hackam, JD Spence, A Fenster, NA Paterson, DD Sin, HO Coxson, DG McCormack, G Parraga. Pulmonary abnormalities and carotid atherosclerosis in ex-smokers without airflow limitation. *Journal of Chronic Obstructive Pulmonary Disease*. 2015 Feb; 12(1):62-70.

13. **K Sheikh**, GA Paulin, S Svenningsen, M Kirby, NA Paterson, DG McCormack, G Parraga. Pulmonary ventilation defects in older never-smokers. *Journal of Applied Physiology*. 2014; 117(3): 297-306.

14. QI Mohaidat, **K Sheikh**, S Palchaudhuri, SJ Rehse. Pathogen identification with laser-induced breakdown spectroscopy: the effect of bacterial and biofluid specimen contamination. *Applied Optics*. 2012; **51:** B99-B107.

Submitted (4)

1. A Bhalla, E Lessard, D Pike, **K Sheikh**, DG McCormack, A Ouriadov, G Parraga. Cross-sectional and Longitudinal Pulmonary Magnetic Resonance Imaging Biomarkers of Alpha-1 Antitrypsin Deficiency. Submitted to *Journal of Chronic Obstructive Pulmonary Disease*.

2. **K Sheikh**, A Ouriadov, HM Young, C Yamashita, TM Luu, SL Katz, G Parraga. Multi-Spectral Pulmonary Magnetic Resonance Imaging of Bronchopulmonary Dysplasia. Submitted to *Journal of Chronic Obstructive Pulmonary Disease*.

3. F Guo, S Svenningsen, M Kirby, DPI Capaldi, **K Sheikh**, A Fenster, G Parraga. CT-^{1}H/^{3}He MRI Co-Registration for Regional Pulmonary Structure-Function Measurements of Chronic Lung Disease. Submitted to *Medical Image Analysis*.

4. A Ouriadov, E Lessard, **K Sheikh**, A Bhalla, GA Paulin, M Kirby, G Parraga. Chronic Obstructive Pulmonary Disease and Alpha-one Antitrypsin Deficiency: Non-invasive MRI Biomarkers of Airspace Enlargement and Emphysema. Submitted to *Radiology*.

B. Published Refereed Conference Papers (1)

1. TJ Lindenmaier, **K Sheikh**, E Bluemke, I Gyacskov, M Mura, C Licskai, L Mielniczuk, A Fenster, IA Cunningham, G Parraga. Three-Dimensional Segmentation of Pulmonary Artery Volume from Thoracic Computed Tomography Imaging. *Proc SPIE* 2015 Vol. 8320, 9417-99.

C. Peer Reviewed Published Conference Abstracts (28)

1. **K Sheikh**, DPI Capaldi, DA Hoover, DA Palma, BP Yaremko, G Parraga, Pulmonary Functional imaging Biomarkers of NSCLC to Guide and Optimize Functional Lung Avoidance Radiotherapy. American Association of Physicists in Medicine Annual Meeting 2016 Washington, District of Columbia, July 31-August 4, 2016.

2. **K Sheikh**, F Guo, A Ouriadov, DPI Capaldi, S Svenningsen, M Kirby, DG McCormack, HO Coxson, G Parraga, Ventilation Estimates in Severe Uncontrolled Asthma using 3D Single breath-hold Ultra-short Echo Time MRI. International Society of Magnetic Resonance in Medicine Annual Scientific Meeting 2016 Singapore, Singapore May 7-13, 2016.

3. DPI Capaldi, A Lausch, **K Sheikh**, F Guo, DG McCormack, G Parraga, Pulmonary Imaging Biomarkers of COPD for Personalized Treatment and Better Outcomes.

International Society of Magnetic Resonance in Medicine Annual Scientific Meeting 2016 Singapore, Singapore May 7-13, 2016.

4. F Guo, **K Sheikh**, RL Eddy, DPI Capaldi, DG McCormack, A Fenster, G Parraga, A Segmentation Pipeline for Measuring Pulmonary Ventilation Suitable for Clinical Workflows and Decision-making. International Society of Magnetic Resonance in Medicine Annual Scientific Meeting 2016 Singapore, Singapore May 7-13, 2016.

5. M Fennema, N Zha, D Pike, **K Sheikh**, S Svenningsen, DG McCormack, G Parraga, MRI Ventilation Texture Measurements as an Intermediate Endpoint of Asthma. International Society of Magnetic Resonance in Medicine Annual Scientific Meeting 2016 Singapore, Singapore May 7-13, 2016.

6. **K Sheikh**, F Guo, S Svenningsen, A Ouriadov, DPI Capaldi, RL Eddy, DG McCormack, G Parraga, What does Magnetic Resonance Imaging Signal-Intensity mean in Asthma? American Thoracic Society Annual Scientific Meeting 2016 San Francisco, California May 13-18, 2016.

7. RL Eddy, D Pike, **K Sheikh**, GA Paulin, M Kirby, DG McCormack, G Parraga, Testing the Fletcher-Peto Assumptions using Pulmonary Imaging Biomarker Longitudinal Measurements. American Thoracic Society Annual Scientific Meeting 2016 San Francisco, California May 13-18, 2016.

8. M Fennema, DPI Capaldi, **K Sheikh**, S Svenningsen, RL Eddy, C Licskai, DG McCormack, G Parraga, The Abnormal Airways that Dominate Asthma Attack: New clues using ventilation MRI during Exercise- and Methacholine-Challenge. American Thoracic Society Annual Scientific Meeting 2016 San Francisco, California May 13-18, 2016.

9. DPI Capaldi, **K Sheikh**, S Svenningsen, M Kirby, HO Coxson, DG McCormack, G Parraga. Measurement of Asthma Treatment Response using Free-breathing ^{1}H Ventilation MRI. American Thoracic Society Annual Scientific Meeting 2016 San Francisco, California May 13-18, 2016.

10. B Yaremko, DA Palma, G Parraga, DPI Capaldi, **K Sheikh**, G Rodrigues, AR Dar, AV Louie, E Yu, S Gaede, D Hoover, Functional Lung Avoidance Radiation Therapy for Stage III Non-Small Cell Lung Cancer: A Double-Blind Randomized Phase 2 Trial. American Society for Radiation Oncology Annual Scientific Meeting 2015 San Antonio, Texas October 18-21, 2015.

11. **K Sheikh**, A Ouriadov, F Guo, DPI Capaldi, DG McCormack, G Parraga. Structure-Function Magnetic Resonance Imaging of Bronchopulmonary Dysplasia as an alternative to pulmonary CT. International Workshop for Pulmonary Functional Imaging Edinburgh, United Kingdom September 28-30, 2015.

12. DPI Capaldi, **K Sheikh**, DA Hoover, DA Palma, BP Yaremko, G Parraga. Fourier-decomposition Pulmonary Magnetic Resonance Imaging Ventilation and Perfusion

Defects in Non-Small Cell Lung Cancer Patients prior to Radiotherapy: Comparison with ^{3}He Ventilation Defects and Smoking History. International Workshop for Pulmonary Functional Imaging Edinburgh, United Kingdom September 28-30, 2015.

13. DPI Capaldi, **K Sheikh**, S Svenningsen, D Pike, D McCormack, G Parraga. MRI Measurements of Regional Ventilation Heterogeneity: Ventilation Defect Clusters. International Society of Magnetic Resonance in Medicine Meeting 2015, Toronto, Canada June 1-5, 2015.

14. DPI Capaldi, N Zha, D Pike, **K Sheikh**, D McCormack, G Parraga. ^{3}He MRI and CT Parametric Response Mapping of Small Airways Disease: The Battle-Ground for Ground Truth. International Society of Magnetic Resonance in Medicine Meeting 2015, Toronto, Canada June 1-5, 2015.

15. GA Paulin, A Ouriadov, **K Sheikh**, DG McCormack, G Parraga. What can multiple b-value ^{3}He MRI tell us about lung micro-structure in healthy elderly never-smokers? International Society of Magnetic Resonance in Medicine Meeting 2015, Toronto, Canada June 1-5, 2015.

16. **K Sheikh**, DPI Capaldi, S Svenningsen, DG McCormack, G Parraga. Ultra-short Echo Time MRI Measurements of Emphysema using Principal Component Analysis. International Society of Magnetic Resonance in Medicine Meeting 2015, Toronto, Canada June 1-5, 2015.

17. GA Paulin, **K Sheikh**, DG McCormack, G Parraga. Differences in Pulmonary Structure and Function in Healthy Elderly Never-smokers after Two Years. American Thoracic Society Annual Scientific Meeting 2015, Denver, Colorado May 16-20 2015.

18. E Bluemke, S Svenningsen, **K Sheikh**, GA Paulin, DG McCormack, G Parraga. Relationship of Ventilation Heterogeneity in the Conducting and Acinar Airway Zones with ^{3}He MRI in Elderly Never-Smokers. American Thoracic Society Annual Scientific Meeting 2015, Denver, Colorado May 16-20 2015.

19. S Svenningsen, DPI Capaldi, E Bluemke, GA Paulin, C Davis, **K Sheikh**, DG McCormack, G Parraga. Lung Clearance Index and Hyperpolarized ^{3}He MRI Ventilation Heterogeneity Measurements in non-CF Bronchiectasis and COPD. American Thoracic Society Annual Scientific Meeting 2015, Denver, Colorado May 16-20 2015.

20. **K Sheikh**, GA Paulin, S Svenningsen, DG McCormack, JA Neder, G Parraga. How do Exercise Responses Relate to ^{3}He Magnetic Resonance Imaging Apparent Diffusion Coefficients in Older Never-Smokers? American Thoracic Society Annual Scientific Meeting 2015, Denver, Colorado May 16-20 2015.

21. DPI Capaldi, **K Sheikh**, GA Paulin, S Svenningsen, HO Coxson, DG McCormack, G Parraga. Conventional non-contrast MRI of Ventilation Abnormalities in Bronchiectasis:

New Tools and Measurements for an Old Disease. American Thoracic Society Annual Scientific Meeting 2014, San Diego, California May 17-21 2015.

22. W Ma, **K Sheikh**, D Pike, S Svenningsen, HO Coxson, DG McCormack, G Parraga. Conventional Pulmonary MRI and CT of Bronchiectasis and Emphysema: Tissue density measurements and relationship to pulmonary function tests. American Thoracic Society Annual Scientific Meeting 2014, San Diego, California May 17-21 2015.

23. **K Sheikh**, W Ma, F Guo, S Svenningsen, TM Peters, HO Coxson, DG McCormack, R Etemad-Rezai, G Parraga. Two Dimensional Radial Pulmonary Ultra-short time ^{1}H MRI: Reproducibility in COPD and Bronchiectasis. International Society of Magnetic Resonance in Medicine Meeting 2014, Milan, Italy May 10-16, 2014.

24. DPI Capaldi, F Guo, S Svenningsen, W Ma, **K Sheikh**, R Etemad-Rezai, J Leipsic, HO Coxson, DG McCormack, G Parraga. Comparison of Pulmonary ^{1}H non-contrast and Hyperpolarized ^{3}He MRI Ventilation Abnormalities in Bronchiectasis and COPD. International Society of Magnetic Resonance in Medicine Meeting 2014, Milan, Italy May 10-16, 2014.

25. W Ma, **K Sheikh**, J Leipsic, HO Coxson, DG McCormack, R Etemad-Rezai, G Parraga. Pulmonary Ultra-short Echo-time (UTE) Two-dimensional Radial Acquisition with Compressed Sensing: Preliminary Quantitative Results with Comparison to Thoracic CT. International Society of Magnetic Resonance in Medicine Meeting 2014, Milan, Italy May 10-16, 2014.

26. D Pike, M Kirby, **K Sheikh**, D Buchanan, C Neron, JD Spence, NAM Paterson, HO Coxson, DG McCormack, G Parraga. Airways Disease in Asymptomatic Ex-smokers without Airflow Limitation: Relationship to Carotid Atherosclerosis. American Thoracic Society Annual Scientific Meeting 2013, Philadelphia, Pennsylvania May 18-22, 2013.

27. **K Sheikh**, S Svenningsen, M Kirby, NAM Paterson, A Wheatley, DG McCormack, G Parraga. What is the Relationship between Hyperpolarized ^{3}He MRI Measurements, Airborne Toxin Exposure, and Exercise Capacity in Healthy Elderly Never-Smokers? American Thoracic Society Annual Scientific Meeting 2013, Philadelphia, Pennsylvania May 18-22, 2013.

28. **K Sheikh**, S Svenningsen, M Kirby, DG McCormack, G Parraga. Hyperpolarized ^{3}He MRI Ventilation Defects in Healthy Elderly Never-Smokers: Response to Deep Inspiration and Salbutamol. American Thoracic Society Annual Scientific Meeting 2013, Philadelphia, Pennsylvania May 18-22, 2013.

29. **K Sheikh**, S Svenningsen, M Kirby, DG McCormack, G Parraga. Hyperpolarized ^{3}He Magnetic Resonance Imaging ADC Gradients in Healthy Elderly Never-Smokers. International Society of Magnetic Resonance in Medicine Meeting 2013, Salt Lake City, Utah April 20-26, 2013.

C. Peer Reviewed Oral Presentations (12)

1. **K Sheikh**, DPI Capaldi, DA Hoover, DA Palma, BP Yaremko, G Parraga, Pulmonary Functional imaging Biomarkers of NSCLC to Guide and Optimize Functional Lung Avoidance Radiotherapy. American Association of Physicists in Medicine Annual Meeting 2016 Washington, District of Columbia, (08/16).

2. **K Sheikh**, F Guo, A Ouriadov, DPI Capaldi, S Svenningsen, M Kirby, DG McCormack, HO Coxson, G Parraga, Ventilation Estimates in Severe Uncontrolled Asthma using 3D Single breath-hold Ultra-short Echo Time MRI. International Society of Magnetic Resonance in Medicine Annual Scientific Meeting 2016 Singapore, Singapore (05/16)

3. **K Sheikh**, F Guo, S Svenningsen, A Ouriadov, DPI Capaldi, RL Eddy, DG McCormack, G Parraga, What does Magnetic Resonance Imaging Signal-Intensity mean in Asthma? American Thoracic Society Annual Scientific Meeting 2016 San Francisco, California (05/16).

4. RL Eddy, D Pike, **K Sheikh**, GA Paulin, M Kirby, DG McCormack, G Parraga, Testing the Fletcher-Peto Assumptions using Pulmonary Imaging Biomarker Longitudinal Measurements. American Thoracic Society Annual Scientific Meeting 2016 San Francisco, California (05/16).

5. DPI Capaldi, **K Sheikh**, S Svenningsen, M Kirby, HO Coxson, DG McCormack, G Parraga. Measurement of Asthma Treatment Response using Free-breathing ^{1}H Ventilation MRI. American Thoracic Society Annual Scientific Meeting 2016 San Francisco, California May (05/16).

6. **K Sheikh**, F Guo, S Svenningsen, A Ouriadov, DPI Capaldi, RL Eddy, DG McCormack, G Parraga, What does Magnetic Resonance Imaging Signal-Intensity mean in Asthma? London Health Research Day (Top 32), London, Ontario (03/16).

7. B Yaremko, DA Palma, G Parraga, DPI Capaldi, **K Sheikh**, G Rodrigues, AR Dar, AV Louie, E Yu, S Gaede, D Hoover, Functional Lung Avoidance Radiation Therapy for Stage III Non-Small Cell Lung Cancer: A Double-Blind Randomized Phase 2 Trial. American Society for Radiation Oncology Annual Scientific Meeting 2015, San Antonio, Texas (10/15).

8. DPI Capaldi, N Zha, D Pike, **K Sheikh**, D McCormack, G Parraga. ^{3}He MRI and CT Parametric Response Mapping of Small Airways Disease: The Battle-Ground for Ground Truth. International Society of Magnetic Resonance in Medicine Annual Scientific Meeting, Toronto, Canada (05/15).

9. **K Sheikh**, GA Paulin, S Svenningsen, DG McCormack, JA Neder, G Parraga. How do Exercise Responses Relate to ^{3}He Magnetic Resonance Imaging Apparent Diffusion Coefficients in Older Never-Smokers? Imaging Network of Ontario Symposium, Toronto, Canada (03/15).

10. DPI Capaldi, **K Sheikh**, F Guo, S Svenningsen, DG McCormack, G Parraga. Fourier-decomposition Pulmonary Magnetic Resonance Imaging Ventilation Defects in Ex-smokers: Relationship to Emphysema and ^{3}He ventilation defects. Radiological Society of North America Conference, Chicago, Illinois (12/14).

11. W Ma, **K Sheikh**, J Leipsic, HO Coxson, DG McCormack, R Etemad-Rezai, G Parraga. Pulmonary Ultra-short Echo-time (UTE) Two-dimensional Radial Acquisition with Compressed Sensing: Preliminary Quantitative Results with Comparison to Thoracic CT. Imaging Network Ontario Symposium, Toronto, Canada (03/14).

12. **K Sheikh**, S Svenningsen, M Kirby, D.G. McCormack, G Parraga. Hyperpolarized ^{3}He MRI Ventilation Defects in Healthy Elderly Never-Smokers: Response to Deep Inspiration and Salbutamol. Imaging Network Ontario Symposium, Toronto, Canada (02/13).

D. Peer Reviewed Poster Presentations (23)

1. DPI Capaldi, A Lausch, **K Sheikh**, F Guo, DG McCormack, G Parraga, Pulmonary Imaging Biomarkers of COPD for Personalized Treatment and Better Outcomes. International Society of Magnetic Resonance in Medicine Annual Scientific Meeting 2016 Singapore, Singapore May 7-13, 2016. *(Accepted February 1, 2016)*

2. F Guo, **K Sheikh**, RL Eddy, DPI Capaldi, DG McCormack, A Fenster, G Parraga, A Segmentation Pipeline for Measuring Pulmonary Ventilation Suitable for Clinical Workflows and Decision-making. International Society of Magnetic Resonance in Medicine Annual Scientific Meeting 2016 Singapore, Singapore May 7-13, 2016. *(Accepted February 1, 2016)*

3. M Fennema, DPI Capaldi, **K Sheikh**, S Svenningsen, RL Eddy, C Licskai, DG McCormack, G Parraga, The Abnormal Airways that Dominate Asthma Attack: New clues using ventilation MRI during Exercise- and Methacholine-Challenge. American Thoracic Society Annual Scientific Meeting 2016 San Francisco, California May 13-18, 2016. *(Accepted January 20, 2016)*

4. **K Sheikh**, A Ouriadov, F Guo, DPI Capaldi, DG McCormack, G Parraga. Structure-Function Magnetic Resonance Imaging of Bronchopulmonary Dysplasia as an alternative to pulmonary CT. International Workshop for Pulmonary Functional Imaging Edinburgh, United Kingdom (09/15).

5. DPI Capaldi, **K Sheikh**, S Svenningsen, D Pike, D McCormack, G Parraga. *MRI* Measurements of Regional Ventilation Heterogeneity: Ventilation Defect Clusters. International Society of Magnetic Resonance in Medicine 2015, Toronto, Canada (05/15).

6. GA Paulin, A Ouriadov, **K Sheikh**, DG McCormack, G Parraga. What can multiple b-value ^{3}He MRI tell us about lung micro-structure in healthy elderly never-smokers? International Society for Magnetic Resonance in Medicine 2015, Toronto, Canada (05/15).

7. **K Sheikh**, DPI Capaldi, S Svenningsen, DG McCormack, G Parraga. Ultra-short Echo Time MRI Measurements of Emphysema using Principal Component Analysis. International Society for Magnetic Resonance in Medicine 2015, Toronto, Canada (05/15).

8. GA Paulin, **K Sheikh**, DG McCormack, G Parraga. Differences in Pulmonary Structure and Function in Healthy Elderly Never-smokers after Two Years. American Thoracic Society Annual Scientific Meeting 2015, Denver, Colorado (05/15).

9. E Bluemke, S Svenningsen, **K Sheikh**, GA Paulin, DG McCormack, G Parraga. Relationship of Ventilation Heterogeneity in the Conducting and Acinar Airway Zones with ^{3}He MRI in Elderly Never-Smokers. American Thoracic Society Annual Scientific Meeting 2015, Denver, Colorado (05/15).

10. S Svenningsen, DPI Capaldi, E Bluemke, GA Paulin, C Davis, **K Sheikh**, DG McCormack, G Parraga. Lung Clearance Index and Hyperpolarized ^{3}He MRI Ventilation Heterogeneity Measurements in non-CF Bronchiectasis and COPD. American Thoracic Society Annual Scientific Meeting, Denver, United States of America (05/15).

11. **K Sheikh**, GA Paulin, S Svenningsen, DG McCormack, JA Neder, G Parraga. How do Exercise Responses Relate to ^{3}He Magnetic Resonance Imaging Apparent Diffusion Coefficients in Older Never-Smokers? American Thoracic Society Annual Scientific Meeting, Denver, United States of America (05/15).

12. **K Sheikh**, W Ma, F Guo, S Svenningsen, TM Peters, HO Coxson, DG McCormack, R Etemad-Rezai, G Parraga. Two Dimensional Radial Pulmonary Ultra-short time ^{1}H MRI: Reproducibility in COPD and Bronchiectasis. International Society for Magnetic Resonance in Medicine Annual Meeting 2014, Milan, Italy (05/14).

13. DPI Capaldi, F Guo, S Svenningsen, W Ma, **K Sheikh**, R Etemad-Rezai, J Leipsic, HO Coxson, D.G. McCormack, G Parraga. Comparison of Pulmonary ^{1}H non-contrast and Hyperpolarized ^{3}He MRI Ventilation Abnormalities in Bronchiectasis and COPD. International Society for Magnetic Resonance in Medicine Annual Meeting 2014, Milan, Italy (05/14).

14. W Ma, **K Sheikh**, J Leipsic, HO Coxson, DG McCormack, R Etemad-Rezai, G Parraga. Pulmonary Ultra-short Echo-time (UTE) Two-dimensional Radial Acquisition with Compressed Sensing: Preliminary Quantitative Results with Comparison to Thoracic CT. International Society for Magnetic Resonance in Medicine Annual Meeting 2014, Milan, Italy (05/14).

15. DPI Capaldi, **K Sheikh**, GA Paulin, S Svenningsen, HO Coxson, DG McCormack, G Parraga. Conventional non-contrast MRI of Ventilation Abnormalities in Bronchiectasis: New Tools and Measurements for an Old Disease. American Thoracic Society Annual Scientific Meeting (05/14).

16. W Ma, **K Sheikh**, D Pike, S Svenningsen, HO Coxson, DG McCormack, G Parraga. Conventional Pulmonary MRI and CT of Bronchiectasis and Emphysema: Tissue density measurements and relationship to pulmonary function tests. American Thoracic Society Annual Scientific Meeting (05/14).

17. **K Sheikh**, S Svenningsen, M Kirby, NAM Paterson, A Wheatley, DG McCormack, G Parraga. What is the Relationship between Hyperpolarized ^{3}He MRI Measurements, Airborne Toxin Exposure, and Exercise Capacity in Healthy Elderly Never-Smokers? American Thoracic Society Annual Scientific Meeting (05/13).

18. **K Sheikh**, S Svenningsen, M Kirby, DG McCormack, G Parraga. Hyperpolarized ^{3}He MRI Ventilation Defects in Healthy Elderly Never-Smokers: Response to Deep Inspiration and Salbutamol. American Thoracic Society Annual Scientific Meeting (05/13).

19. **K Sheikh**, S Svenningsen, M Kirby, DG McCormack, G Parraga. Hyperpolarized ^{3}He Magnetic Resonance Imaging ADC Gradients in Healthy Elderly Never-Smokers. The International Society for Magnetic Resonance in Medicine (04/13).

20. **K Sheikh**, S Svenningsen, M Kirby, NAM Paterson, A Wheatley, DG McCormack, G Parraga. Relationship between Hyperpolarized ^{3}He MRI Measurements and Exercise Capacity in Healthy Elderly. Imaging Network Ontario Symposium (02/13).

21. D Pike, M Kirby, **K Sheikh**, D Buchanan, C Neron, JD Spence, NAM Paterson, HO Coxson, DG McCormack, G Parraga. Airways Disease in Asymptomatic Ex-smokers without Airflow Limitation: Relationship to Carotid Atherosclerosis. American Thoracic Society (05/13).

22. **K Sheikh**, A Daabous, R Putnam, SJ Rehse. Chemometric Data Analysis Strategies for Optimizing Pathogen Discrimination and Classification Using Laser-Induced Breakdown Spectroscopy (LIBS) Emission Spectra. Canadian Association of Physicists Congress, Calgary, Alberta, Canada (06/12).

23. QI Mohaidat, **K Sheikh**, S Palchaudhuri, SJ Rehse. Laser-Based Identification of Bacteria using Discriminant Function Analysis. Canadian Undergraduate Physics Conference, Saskatoon, Saskatchewan, Canada (10/11).

LEADERSHIP and VOLUNTEER ACTIVITIES

02/16	**Team Captain**, Fight for Air Climb-American Lung Association
05/15-5/16	**Member**, Medical Biophysics Graduate Recruitment Committee
09/12-present	**Member**, Network of Imaging Students extraordinaire (NOISe)
01/12-05/12	**Organizer**, Science Rendezvous Windsor
09/11-08/12	**Vice President**, University of Windsor Physics Club
09/10	**Member**, Ontario University Athletics Women's Track and Field Championship Team
06/09-09/09	**Volunteer**, Women's Enterprise of Skills and Training

09/08-09/10 **Member**, University of Windsor Varsity Track and Field Team
10/04-05/11 **Volunteer**, Lancer Alumni
10/04-04/11 **Member**, Windsor Legion Track and Field Club

PROFESSIONAL MEMBERSHIPS

2015-present American Association of Physicists in Medicine
Student Member

2013-present Canadian Organization of Medical Physicists
Student Member

2013-present International Society of Magnetic Resonance in Medicine
Student Member

2013-present Canadian Thoracic Society
Student Member

2013-present American Thoracic Society
Student Member

2011-2012 Canadian Association of Physicists
Student Member